Geological Survey of Finland

Bulletin 397

Evolution and 3D modelling of structural and metamorphic patterns of the Palaeoproterozoic crust in the Tampere-Vammala area, southern Finland

by Timo Kilpeläinen

Geological Survey of Finland
Espoo 1998

Geological Survey of Finland, Bulletin 397

EVOLUTION AND 3D MODELLING OF STRUCTURAL AND METAMORPHIC PATTERNS OF THE PALAEOPROTEROZOIC CRUST IN THE TAMPERE-VAMMALA AREA, SOUTHERN FINLAND

by

TIMO KILPELÄINEN

with 65 figures, one table and 2 appendices

ACADEMIC DISSERTATION

GEOLOGICAL SURVEY OF FINLAND
ESPOO 1998

Kilpeläinen, T. 1998. Evolution and 3D modelling of structural and metamorphic patterns of the Palaeoproterozoic crust in the Tampere-Vammala area, southern Finland. *Geological Survey of Finland, Bulletin 397.* 124 pages, 65 figures, one table and 2 appendices.

The study area is characterized by both the zonal and the high temperature/low pressure type of metamorphism, but the intensities and ages of the tectonic and metamorphic structures vary considerably in different parts of the area.

The central parts of the Tampere Schist Belt metamorphosed under greenschist facies, while the Vammala migmatite area is characterized by intensely migmatized greywackes metamorphosed under the equilibrium field of garnet and cordierite. The dominant schistosity in the Tampere Schist Belt is the axial plane schistosity of upright synclinal folding whereas the main schistosity of the migmatites was originally gently dipping. The relative ages of the dated intrusions and tectonometamorphic structures indicate, that tectonic and metamorphic evolution started earlier in the migmatite area than in the well-preserved schist belt.

The grade of oldest metamorphism (M_1) varied with depth and S_1 is the main schistosity in rocks that were below the brittle/ductile transition zone at the end of D_1. The variations in grade of M_1 on the present erosion level are mainly due to F_2 folding with gentle axis and steep axial planes. The M_1 metamorphic structures are cut by M_2 and M_3 metamorphisms concentrated on F_2 synforms, F_2/F_3 interference basins and D_3 shear zones.

The subhorizontal D_1 structures and M_1 metamorphism are estimated to be over 1889 Ma in age. M_1 isotherms folded during D_2 at 1889-1878 Ma ago and their stabilization caused prograde reactions on F_2 synforms and retrograde alterations on F_2 antiforms. M_3 is supposed to be a reflection of the metamorphism that culminated in southwesternmost Finland 1840-1830 Ma ago, but the evolution of D_3 structures started immediately after and partly even synchronously with D_2.

All the tectonic structures in the study area can be explained by north-south compression associated with simultaneous extension during D_1 stage. D_1 evolution includes subduction and the development of extensional structures in an arc and back arc environments.

Key words (GeoRef Thesaurus, AGI): crust, schist belts, migmatites, metasedimentary rocks, igneous rocks, structural geology, deformation, metamorphism, migmatization, tectonics, plate tectonics, three-dimensional models, Svecofennides, geotraverses, SVEKA, Proterozoic, Palaeoproterozoic, Tampere, Vammala, Finland

Timo Kilpeläinen, University of Turku, Department of Geology, FIN-20014 TURKU, FINLAND

E-mail: Timo.Kilpelainen@utu.fi

ISBN 951-690-701-6
ISSN 0367-522X

CONTENTS

INTRODUCTION

Infra-/suprastructure problem

The structural and metamorphic contrast between the Tampere Schist Belt and the Pori-Vammala-Mikkeli Migmatite Zone has been a subject of geological interest since the studies of Sederholm (1897). In the early years of the present century scholars discussed the possibility of a "great discordance" between migmatites and well-preserved areas (Mäkinen 1914, 1915, Sederholm 1931, 1932, Simonen 1948, 1952, 1953a, 1953b, Wahl 1936). Since the stratigraphic investigations of Simonen (1953b), however, it has been largely accepted that the areas are not exotic relative to each other in either age or palaeogeography (Simonen 1971, 1980, Matisto 1977, Nironen 1989a, Lahtinen 1994, Kilpeläinen et al. 1994, Kähkönen et al. 1994, Vaasjoki et al. 1994).

Problems have been caused by the observation that the migmatites representing deeper sections seem to have the signature of a more complex evolution than the layered metasedimentary rocks in the schist belt. Moreover, the strongest schistosity, particularly in the central parts of the Tampere synform area, is the axial plane schistosity of synclinal folding that has been vertical from the very beginning whereas the main schistosity of the migmatites was gently dipping to start with. Arguments have been presented suggesting synchronism between the gently and steeply dipping schistosities, and opinions have been voiced that tectonic and metamorphic evolution started earlier in the migmatite area (Simonen 1953b, Campbell 1980, Nironen 1989a, 1989b, Kilpeläinen et al. 1994).

Selection of study area

In 1987, the Committee of the International Lithosphere Programme (ILP) of Finland selected the deep seismic sounding line SVEKA, which runs in a NE-SW direction from Kuhmo to Keuruu, intersecting the central parts of the Fennoscandian Shield, as the transect of Finland's Global Geoscience Transect Project (GGT). Four years later, financed by the Academy of Finland, SVEKA was extended to Kustavi, in the southwest. As a result, the line known as SVEKA-SW crossed the western part of the Tampere Schist Belt as well as the Pori-Vammala-Mikkeli Migmatite Zone (Fig. 1). Finland's GGT project differed from those undertaken elsewhere in that not only were the available geodata collected but key areas along the transect were selected for field studies with a view to providing insight into the evolution and characteristics of the lithosphere.

One of the key sites was the Tampere-Vammala area (Fig. 2), which, although relatively small, showed many metamorphic and structural features typical of the Svecofennides in southern Finland. From previously published geochemical and isotope geological studies it was also known that, compared with present island arc environ-

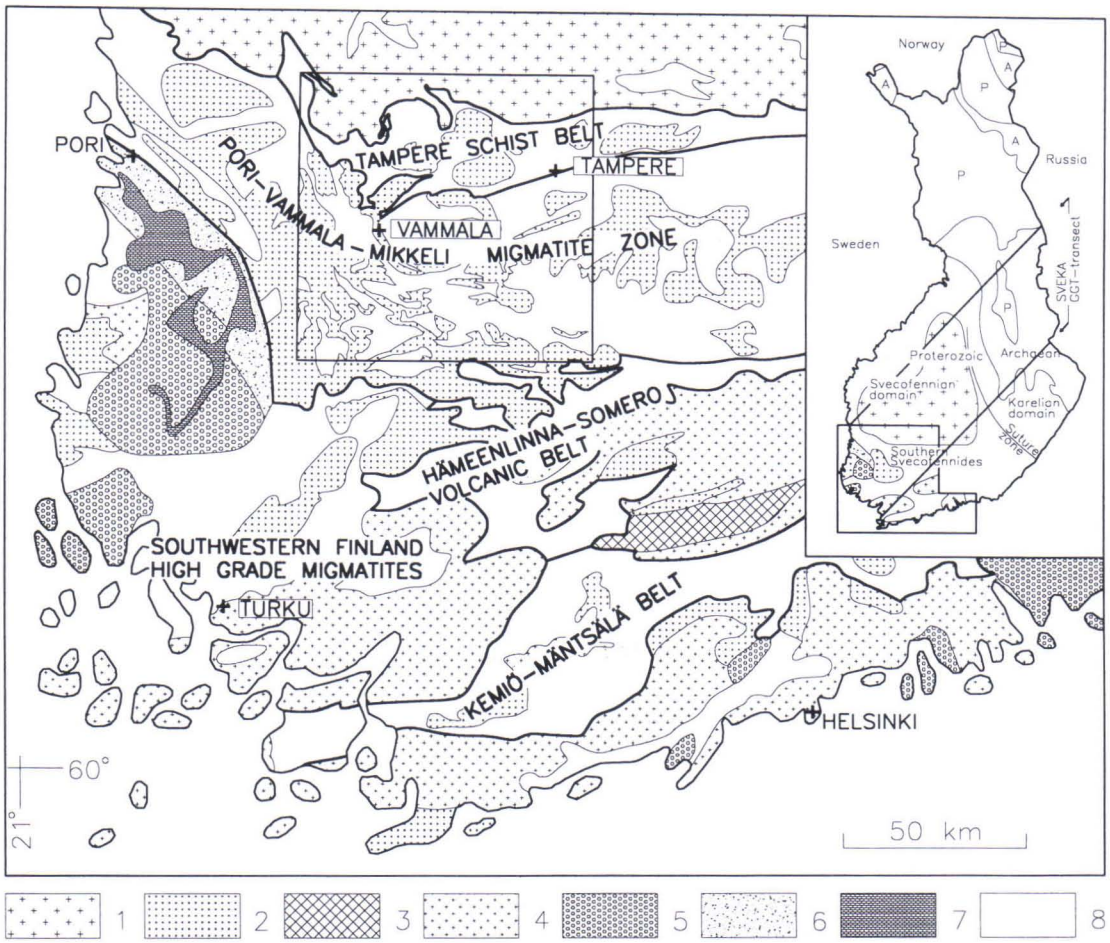

Fig. 1. Location of study area and general geology of South Finland's Svecofennides. Lithology simplified from Koistinen (1994). 1. Central Finland Granitoid Complex 2. Synorogenic granitoids 3. Synorogenic metadiorite/gabbro 4. Lateorogenic granite 5. Anorogenic rapakivi 6. Jotnian sandstone 7. Postjotnian diabase 8. Supracrustal rocks. Symbols in insert figure as in main figure, except: P = Proterozoic cover rocks, A = Archaean rocks.

ments, the area exhibited the rapid evolution of a Proterozoic orogeny (Huhma 1986, Gaál & Gorbatschev 1987, Kähkönen 1987, Claesson et al. 1991, Lahtinen 1994). As one of the targets of the GGT project was to establish the relation of mineralization to crustal evolution, the Vammala area, due to its nickel potentiality, was well suited for a key area.

Aims

The present work, which arose as part of the studies of the Tampere-Vammala GGT key area, concerns the tectonic and metamorphic structure of that area. The starting point was to find out why the intensities and ages of the tectonic and metamorphic structures vary so much within such a small area. The main objective was to construct a plate tectonic evolution model based on field observations and published models that would

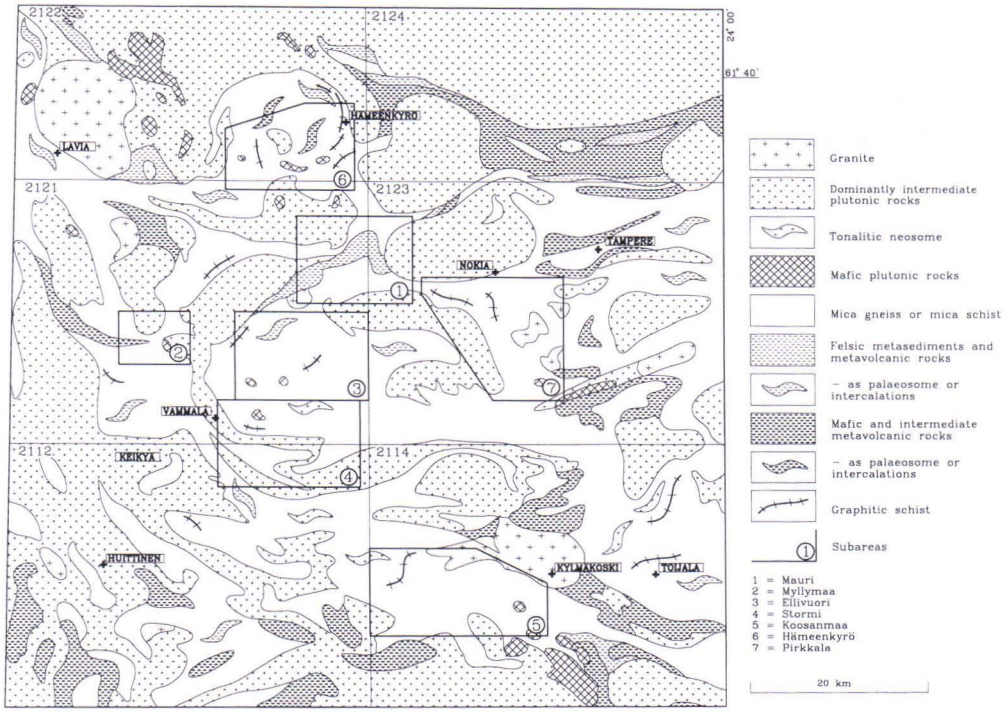

Fig. 2. Lithology of Tampere-Vammala area and location of subareas. Lithology modified from Koistinen (1994). Subareas: 1 = Mauri, 2 = Myllymaa, 3 = Ellivuori, 4 = Stormi, 5 = Koosanmaaa, 6 = Hämeenkyrö, 7 = Pirkkala. Map sheets: 2122 = Ikaalinen, 2124 = Viljakkala-Teisko, 2121 = Vammala, 2123 = Tampere, 2112 = Huittinen, 2114 = Toijala.

explain, as correctly as possible, the metamorphic and structural features and lithological variation visible on and characteristic of the present erosional level in the Tampere-Vammala area. It was also important to test the 3D geometry of the model to establish whether the evolution presented in 2D sections really does show the features on the erosion level revealed and presented by previous studies and the present work.

Methods

Field work in the Tampere-Vammala area began in 1991. Since the aim was to investigate the genetics of various metamorphic subareas and to correlate their tectono-metamorphic events, the emphasis was on metamorphism and structural geology. The field work was undertaken mainly as a joint effort by the Geological Survey of Finland (GSF) and the Department of Geology at the University of Turku. The Institute of Seismology at the University of Helsinki and the Institute of Geophysics at the University of Oulu were closely involved as the interpretation models of their deep sounding data guided the work not only in the Tampere-Vammala area but also elsewhere along the SVEKA transect. Understanding the general structure and evolution of the area also required cooperation with geophysicists at the GSF and researchers in many other sectors of geology. The age

determinations were undertaken at the unit for Isotope Geology, GSF.

The identification of deformation structures and the interpretation of age relations were based mainly on crosscutting relations, the morphology of the structures and the relation of metamorphic structures to tectonic structures (Hobbs et al. 1976, Vernon 1978, Williams & Schoneweld 1981, Bell 1985, Bell et al. 1986). The thrust of the field work was on the correlation of the structures with the change in metamorphic grade. In the study area the metamorphic contrast is strongest between the Tampere Schist Belt and the Vammala migmatite area. Although the schist belt is typically bordered in the south by a fault, in places it grades into the migmatite area, making correlation possible. In regional interpretation of the structures use was also made of the geophysical, especially aeromagnetic low-altitude, maps of the GSF. The 3D modelling of the structures was done with AutoCad software. The principles of the modelling technique are dealt with in the appropriate chapter.

In the course of the GGT project, about 1500 outcrop observations were recorded in the study area, about one fifth by the author. A third of the observations were made in the subareas to be described later. As the emphasis was on metamorphism and structure, an overwhelming number of the observations refer to supracrustal rocks, the bulk of them metasedimentary rocks. The relief of the study area is gentle and vertical sections are therefore rare in outcrops.

Samples for thin sections were taken almost invariably with a sampler drill and as oriented. Most of the thin sections were prepared in the section laboratory of the GSF but some at the Institute of Geology of the University of Turku. More than 300 thin sections were made and some of them were polished for electron microprobe analyses.

A total of 830 electron microprobe analyses were performed, mainly on samples from the Stormi subarea. The analytical data have also been summarized and interpreted in a report by Kilpeläinen & Rastas (1992). The analyses were made at the Materials Science Laboratory of Physics at the University of Turku using a Cambridge S 200 electron microscope fitted with an analyser.

MAIN GEOLOGICAL FEATURES OF THE FENNOSCANDIAN SHIELD ALONG THE SVEKA LINE

Archaean Karelian province

In Finland, the central areas of the Fennoscandian Shield have traditionally been divided into a western and an eastern part. The latter is an Archaean province, whilst the western one is an area of Palaeoproterozoic rocks divided into Karelian and Svecofennian provinces by a suture zone trending from northwest to southeast (Eskola 1963, Koistinen 1981, Simonen 1980, Gaál & Gorbatschev 1987) (Fig. 1). The eastern parts of the Karelian province are composed of autochthonous Sariolan and Jatulian sedimentary rocks that deposited discordantly on the Archaean craton 2.45-1.9 Ga ago, and of the mafic dykes crosscutting them. Above the Sariolan and Jatulian rocks are Kalevian metasedimentary rocks, which, due to the dissimilarity in their evolution, can be divided into eastern and western Kalevian metasedimentary rocks (Kohonen 1995). The autochthonous sedimentary rocks of the eastern Kalevian deposited in rift basins on the edge of the Archaean continent about 2.1 Ga ago (Huhma 1986, Ward 1987, Kohonen 1995). The island arc metapsammites of the western Kalevian are allochthonous and were over-

thrusted into their present position during the Svecofennian orogeny (Koistinen 1981, Ward 1987, Kohonen 1995). Sm-Nd isotope studies on the granitoids of the Karelian province demonstrate the existence of Archaean crust under the Svecofennian rocks everywhere east of the above suture zone (Huhma 1986). The Archaean province and the area of Karelian rocks are therefore called jointly the Archaean Karelian domain (Korsman et al. 1997, Korsman et al., in press).

Svecofennian domain

Age data

The Svecofennian domain is mainly composed of greywackes and island arc volcanic rocks that deposited in a marine environment 2.0-1.9 Ga ago (Gaál & Gorbatschev 1987) and of the granitoids of different ages cross-cutting them. According to the classification of Sederholm (1934), the bulk of the Svecofennian granitoids are synorogenic and intruded 1.90-1.83 Ga ago (Huhma 1986, Nurmi & Haapala 1986, Patchett & Kouvo 1986, Welin 1987). The Central Finland Granitoid Complex, which covers a substantial part of the total area of Finland's Svecofennides is mainly composed of granitoids of this age group. Gneissose tonalites and the associated acid volcanic rocks immediately at the western margin on the above mentioned suture, whose U-Pb ages on zircons vary in a range of 1.93-1.91 Ga, are older than the synorogenic granitoids and are, at the same time, the oldest Svecofennian formations in Finland (Helovuori 1979, Korsman et al. 1984, Vaasjoki & Sakko 1988, Kousa et al. 1994). The latest geochemical and isotope investigations have, however, revealed indications of a still older, $\geq$ 2.0 Ga, Palaeoproterozoic crust (Lahtinen & Huhma 1997).

Southwestwards along the GGT transect, magmatism gets younger and becomes richer in potassium. Thus, in southwestern Finland a substantial proportion of the granitoids belong to the late-orogenic (1.84-1.84 Ga) age group (Hopgood et al. 1983, Korsman et al. 1984, Huhma 1986, Hölttä 1986, Patchett & Kouvo 1986, Vaasjoki & Sakko 1988, Suominen 1991). Typical of southwesternmost Finland are not only 1.77-1.80-Ga postorogenic granites (Suominen 1991) but also 1.57-Ga rapakivi granite batholiths and the associated diabases and anorthosites (Vaasjoki 1977, Rämö et al. 1994).

Crustal structure

Great variation (42-65 km) in crustal thickness is a characteristic feature of the Svecofennides in Finland, mainly due to the variation in thickness of the high-velocity layer of the lower crust. The crust is at its thickest (56-65 km) in the central parts of the Svecofennian domain, thinning rapidly towards southwestern Finland (Luosto 1991). The crust became thicker during two collision stages (at 1.91-1.90 Ga and 1.89 Ga) and continued to thicken in the overthrust stage at 1.86-1.84 Ga (Lahtinen 1994). That the crust has remained exceptionally thick shows that the central part of the Svecofennian domain did not undergo a substantial post-collisional extension (Lahtinen & Huhma 1997). The thinner crust in southwesternmost Finland has been attributed to the extension that started at 1.84 Ga, during the final stages of which the rapakivi magmas that formed in the partial melting of the lower crust intruded with the associated diabases (Korja & Heikkinen 1995).

Metamorphism

The Svecofennides in Finland are characterized by both the zonality of metamorphism and an HT/LP type of metamorphism (Korsman 1977, Korsman et al. 1984, Schreurs 1984, Schreurs & Westra 1985, Hölttä 1986). As a rule, metamorphism took place above the equilibrium field of muscovite, usually in the upper amphibolite or granulite facies (Korsman 1977, Hölttä 1986, Korja et al. 1994). However, unmigmatized metasedimentary rocks occur in narrow zones between high-grade areas. Metamorphism regularly started in migmatized areas earlier than in muscovite-bearing schist belts (Kilpeläinen et al. 1994, Korsman et al., in press). On the basis of the age of the peak metamorphism, the Svecofennides in Finland can be divided into two groups. In the central and northern parts of the Svecofennian domain metamorphism reached its peak (670-800 °C, c. 5 kb) about 1885 Ma ago, after which the crust stabilized rapidly (Korsman et al. 1984). In southern Finland the temperature remained high (800 °C) and migmatization was intense until the intrusion of the late-orogenic granitoids (1840-1830 Ma) (Korsman et al. 1984, Schreurs & Westra 1986, van Duin 1992, Väisänen et al. 1994).

From north to south, the most important schist belts along the GGT transect in the Svecofennian domain are the Savo Schist Belt, the Tampere Schist Belt, the Pori-Vammala-Mikkeli Migmatite Zone, the Hämeenlinna-Somero Volcanic Belt, the Kemiö-Mäntsälä Belt and the high-grade migmatite area of southwestern Finland. All these belts differ from each other in both tectono-metamorphic evolution and lithology.

Savo Schist Belt

The volcanic-sedimentary Savo Schist Belt, at the eastern edge of the Svecofennian domain, is characterized by a structure caused by postmetamorphic block faulting (Korsman et al. 1984). Although the metamorphic grade varies on the present erosion level in different blocks from epidote-amphibolite facies to granulite facies the initial stages of metamorphic evolution have certain features in common. In the Savo Schist Belt, metamorphism reached its peak not later than 1885 Ma ago, after which the crust cooled very rapidly, the pyroxene granitoids, ca. 1885 Ma in age, having a distinct thermal aureoles to the country rocks (Korsman et al. 1984, Korsman et al. 1988, Haudenschild 1995, Hölttä, 1988, 1995). Block formation started not later than 1830 Ma ago and continued until 1700 Ma, as inferred from K-Ar ages on biotite and muscovite (Haudenschild 1988, Kilpeläinen 1988, Korsman et al. 1988).

Tampere Schist Belt

The Tampere volcanic-sedimentary schist belt (Fig. 1) is mainly composed of turbiditic metagreywackes and intermediate pyroclastic volcanic rocks of the island arc type (Ojakangas 1986, Kähkönen 1987, 1989). The central area of the schist belt, metamorphosed under greenschist facies conditions at its lowest, represents the least metamorphosed part of the Svecofennian domain. The relative age and grade of metamorphism vary within the schist belt but, as shown by mineral parageneses and thermobarometric determinations, metamorphism took place at 470-600 °C and 1.5-4 kb (Campbell 1978, Mäkelä 1980, Törnroos 1982, Kilpeläinen et al. 1994). According to Nironen (1989b), the synkinematic granitoids have a contact effect on country rocks, although, at least in some parts of the schist belt, peak metamorphism was not reached until after the intrusion of these granitoids (the present work).

Pori-Vammala-Mikkeli Migmatite Zone

The Pori-Vammala-Mikkeli Migmatite Zone (Fig. 1) is characterized by intensely migmatized turbiditic greywackes and the synkinematic granitoids crosscutting them. The metamorphic grade was already high (670 °C, 5-6 kb) at the initial stage of structural development, before the intrusion of synkinematic tonalites, and the high intensity of the hydration reactions at the retrograde stage is typical of porphyroblastic rocks in the zone (Kilpeläinen et al. 1994).

Hämeenlinna-Somero Volcanic Belt

The Hämeenlinna-Somero Volcanic Belt (Fig. 1), the largest continuous volcanic belt in Finland's Svecofennides, contains only minimal amounts of greywacky or pelitic metasedimentary rocks. The metamorphic grade increases in the belt from north to south. In the north, the mineral assemblage cordierite-andalusite-chlorite-muscovite is typical of pelitic rocks (Hakkarainen 1994) and even in central parts metamorphism still occurred at about 600 °C and 3-4 kb (Mäkelä 1980). In the south, however, metamorphism took place above the decomposition reaction of biotite, and the metasedimentary rocks are typically cordierite-potassium feldspar gneisses and garnet-cordierite gneisses (Stel et al. 1989). The age of the peak metamorphism is not well established but the dome of a late-orogenic granite (Huhma 1986) in the south of the belt (Tiainen & Viita 1994, Stel et al. 1989) deforms metamorphic structures (Stel et al. 1989).

Kemiö-Mäntsälä Belt

In the Kemiö-Mäntsälä Belt (Fig. 1), which is characterized by acid volcanic rocks and turbiditic metasedimentary rocks, the metamorphic grade increases from west to east. At the western end of the belt, metamorphism took place under amphibolite facies conditions (550-650 °C, 3-5 kb), but eastwards the metamorphic grade increases up to the granulite facies (750-825 °C, 3-5 kb) (Dietworst 1982, Schreurs & Westra 1986, Colley & Westra 1987). The granulite facies metamorphism crosscuts both the synkinematic granitoids and some of the late-orogenic microcline granite intrusions, although most of the latter are contemporaneous with the peak metamorphism (Parras 1958, Schreurs & Westra 1986).

Southwestern Finland High-Grade Migmatites

The high-grade migmatite area of southwestern Finland (Fig. 1) is mainly composed of migmatitic metasedimentary rocks, synorogenic granitoids and a great number of late-orogenic S-type granites. The metamorphic grade increases from the amphibolite facies at the western edge (650-670 °C, 5 kb) almost isobarically towards the granulite facies in the centre (750 °C) (Hölttä 1986, Väisänen et al. 1994). Metamorphic evolution started before the intrusion of synorogenic granitoids but at least some of the late-orogenic granites derive from in-situ melts of the peak metamorphism (Väisänen et al. 1994).

GENERAL GEOLOGICAL SETTING OF STUDY AREA

Southern Svecofennides

The study area of the present work, later to be referred to as the Tampere-Vammala area, extends in the north to the Central Finland Granitoid Complex and contains the central parts of both the Tampere Schist Belt and the Pori-Vammala-Mikkeli Migmatite Zone (Fig. 1). It covers the whole of 1:100 000 map sheets 2112 (Matisto 1976b, 1978),

2114 (Matisto 1973, 1976a), 2121 (Matisto 1967, 1971), 2123 (Matisto 1961, 1977) and the southern parts of sheets 2122 (Huhma et al. 1952a, 1952b, Virransalo & Vaarma 1993) and 2124 (Simonen 1952, 1953a). The SVEKA line runs through the northwestern part of the study area and thus the area is confined in its entirely within the 100-km wide GGT transect.

Supracrustal rocks typical of the Svecofennides of southern Finland are the metasedimentary rocks deposited in a marine environment and classified mainly as greywackes, and the belts of island arc volcanic rocks that occur in discrete zones. The zircon U-Pb ages of the Tampere island arc volcanic rocks vary in the range 1904-1889 Ma (Kähkönen et al. 1989), but some of the detrital zircons in the greywackes are Archaean (Huhma et al. 1991). In the north of the Svecofennides, the supracrustal rocks are cut by granitoids that were mainly classified as synorogenic by Sederholm (1934). The zircon ages of these granitoids, which cover most of the area of the Central Finland Granitoid Complex, are in the range 1890-1870 Ma (Patchett & Kouvo 1986, Nurmi & Haapala 1986, Huhma 1986, Front & Nurmi 1987, Nironen & Front 1992). Further south, 1840-1830-Ma-old (Patchett & Kouvo 1986, Suominen 1991), late-orogenic S-type, coarse-grained granites predominate.

The depositional base of the Svecofennides is unknown, but it has been suggested that the Vammala Migmatite Zone might contain relicts of Palaeoproterozoic crust over 1905 Ma in age (Nironen 1989a, Kähkönen 1996). In the southwestern part of the study area, the synorogenic (c. 1885 Ma) hornblende gabbro in the Keikyä intrusive breccia (Fig. 2) brecciates a quartz diorite containing mafic enclaves. The zircons in the quartz diorite constitute two populations, of which the older may represent Svecofennian protocrust over 1.9 Ga old (Vaasjoki et al. 1996). Lahtinen & Huhma (1997) have postulated that the latest geochemical and isotope data, together with the reinterpreted older data, demonstrate the existence of an evolved type of crust, over 2.0 Ga old, even in southernmost Finland.

Tampere-Vammala area

Southern edge of Central Finland Granitoid Complex

The northern part of the Tampere-Vammala area is bounded by the Central Finland Granitoid Complex, which is mainly composed of plutonic rocks varying in composition from gabbros to granites and of small areas of supracrustal rocks (Fig. 1). The majority of the plutonic rocks of the granitoid complex belong to the synorogenic age group, and represent the stage at which the bulk of the Svecofennian crust formed. However, in the southern part of the area, immediately north of the Tampere Schist Belt, there is a group of potassium-rich granitoids, 1870 Ma old (Rämö & Nironen 1996), that are felsic, nonfoliated rocks, usually K-feldspar porphyritic and post-tectonic in local character. According to Rämö and Nironen (1996), their geochemical similarity with the rapakivi granites indicates that the compressional stage came to an end in the northern part of the Svecofennides of southern Finland with the emplacement of granitoids of this age group.

Tampere Schist Belt

About 12 km wide at its greatest, the east-west-trending Tampere Schist Belt is composed predominantly of turbiditic metasedimentary rocks and arc type pyroclastic metavolcanic rocks (Ojakangas 1986, Kähkönen

1989). Lowermost in the stratigraphy of the schist belt are basalts of the Haveri formation, interpreted as having deposited either during the initial stage of island arc evolution (Mäkelä 1980) or as representing rifting stage of the older, pre-1910-Ma Palaeoproterozoic crust (Kähkönen & Nironen 1994, Lahtinen 1994). Next in stratigraphy is the Myllyniemi formation, which is dominated by turbiditic metasedimentary rocks geochemically clearly belonging to the island-arc environment (Kähkönen and Leveinen 1994).

The ages of clastic zircons of the Myllyniemi formation vary in the range 2000-1910 Ma, but some of them are Archaean (Huhma et al. 1991). Rounded clasts of the Ahvenlampi conglomerate, which is part of the Myllyniemi formation, have also yielded Archaean ages (Kähkönen & Huhma 1993). The formation is overlain by main island-arc volcanic rocks and they in turn by Veittijärvi-type conglomerates, the plutonic clasts of which show ages between 1890 and 1884 Ma (Nironen 1989b). Highest in the stratigraphy of the schist belt are mafic volcanic rocks of the Takamaa formation (Kähkönen et al. 1994). The age of the detrital zircon in the Mauri meta-arkose, 1.9 Ga (Matisto 1968), is interpreted as implying that the rock is located in the upper part of the schist belt stratigraphy.

Vammala Migmatite Area

The boundary between the Tampere Schist Belt and the Vammala Migmatite Area south of it, which is characterized by migmatitic metasedimentary rocks and synkinematic granitoids that are commonly conformable with migmatite structures, is gradual in places but locally also clearly controlled by faults. The metaturbidites in the north of the migmatite zone, at least, can be correlated with the metasedimentary rocks of the Tampere Schist Belt (Lahtinen 1994, 1996); graphite-bearing gneisses are, however, more common there than in the Tampere Schist Belt. Some of the conglomerates in the migmatite zone resemble the conglomerates in the schist belt (Kähkönen 1996). Volcanic rocks are rare in the migmatite zone.

Granitoids

Synkinematic granitoids are typically gneissose but in places they are unfoliated and K-feldspar porphyritic. As well as synkinematic plutonic rocks, the migmatite zone contains granites as dykes and small intrusions cutting the migmatite structures. There are also numerous mafic and ultramafic intrusions, some hosting economically viable Ni deposits. The contacts of the Ni intrusions with mica gneisses are subconformable (Häkli et al. 1979, Papunen 1980) and intrusions are interpreted as having participated in regional metamorphism (Kilpeläinen & Rastas 1992, Mancini 1996, Mancini et al. 1996a, 1996b, Marshall et al. 1995, Peltonen 1995a, 1995b).

Main structures

In the northeastern part of the study area, the Tampere Schist Belt forms an east-west-trending synform with a horizontal axis (Nironen 1989a). The Hämeenkyrö (1885 ± 2 Ma) and the Värmälä (1878 ± 3 Ma) synkinematic granitoid intrusions were emplaced during the evolution of this structure

(Nironen 1989b). A corresponding synclinal structure, although rotated into a northwest-southeast direction, has been described from the western continuation of the schist belt, from Suodenniemi (Perttula 1982). The axial plane schistosity of the synform folding is the earliest metamorphic feature recognizable in the Tampere synform area, which metamorphosed under greenschist and amphibolite facies conditions (Nironen 1989a).

Corresponding folding is recognizable in the migmatites of the Vammala area, where

the highest grade metamorphism took place in the garnet-cordierite-sillimanite-biotite equilibrium field, although metamorphism started earlier there in relation to the structures than in the Tampere Schist Belt. Metamorphic schistosity, the intensity of which increases with the metamorphic grade, is then the deforming feature (Kilpeläinen et al. 1994). For the same reason, the deformation structures were numbered differently in previous regional studies. Thus, metamorphism started in the Tampere-Vammala area before the emplacement of the synkinematic granitoids.

The lithological and metamorphic features on maps of the Tampere-Vammala area have also been affected by the highly plastic folding and shearing that occurred in a conjugate pair. In the east of the area folding has dextral asymmetry, with the axial planes usually striking from northeast to southwest, whereas in the west folding has sinistral asymmetry with axial planes striking from northwest to southeast (Kilpeläinen et al. 1994). Visible throughout the study area is also a zonal, late-metamorphic pulse, considered to reflect metamorphism of the high grade migmatites of SW Finland that culminated at 1850-1830 Ma (Kilpeläinen et al. 1994, Korja et al. 1994, Väisänen et al. 1994).

Migmatization and metamorphism

The migmatization of high-grade metasedimentary rocks at Vammala has been discussed by Campbell (1980), Aarnisalo (1988) and Kilpeläinen & Rastas (1992). It started simultaneously with the evolution of the earliest deformation structures and manifests itself in trondhjemitic veining and segregation parallel to the layering and S_1 schistosity. The grain size of the migmatizing veins and the width of the veins increase with younging of the relative age. At the same time the veins become richer in potassium feldspar and the youngest migmatization is shown by granite veins, a few centimetres or a few tens of centimetres wide, crosscutting D_1 and D_2 structures (the present work). It is, however, in most places difficult to determine the relative age of the neosome as the veins tend to imitate old primary and deformation structures; moreover, old veins may have been remobilized.

Hydration reactions following the progressive stage of metamorphism are typical of the Vammala migmatite area in particular, where they have altered the composition of garnet and cordierite, causing their biotitization and also local crystallization of andalusite.

Plate tectonics

As shown by Sm-Nd isotope studies, evolution of the Svecofennian crust in southern Finland is connected with subduction or a similar process (Huhma 1986, Patchett & Kouvo 1986). Geochemical and isotope-geological investigations, however, suggest that the Palaeoproterozoic island-arc complex did not simply collide with the Archaean craton; instead the Svecofennian orogeny is composed of at least two island arc systems and of their collisions and extensions during various stages of evolution (Korsman et al. 1988, Vaasjoki & Sakko 1988, Kähkönen 1989, Nironen 1989a, Kähkönen et al. 1994, Lahtinen 1994, Korja 1995, Lahtinen & Huhma 1997, Nironen 1997).

STRUCTURES AND METAMORPHISM OF SUBAREAS AND THE RELATIVE AGE OF IGNEOUS ROCKS

Introduction

Seven subareas (Figs 2 and 3) differing in metamorphic grade and mode of occurrence of deformation structures were chosen to facilitate the description of deformation structures and metamorphic features. The subareas, which vary in size and shape, were taken from different parts of the study area to enable us to obtain a correlatable, overall picture of the relations between the mode of occurrence of structures and metamorphism throughout the study area.

Although the subareas were selected to exhibit as wide a range of metamorphic and structural features as possible, a compromise often had to be reached on what to include. The aluminium-rich metasedimentary rocks

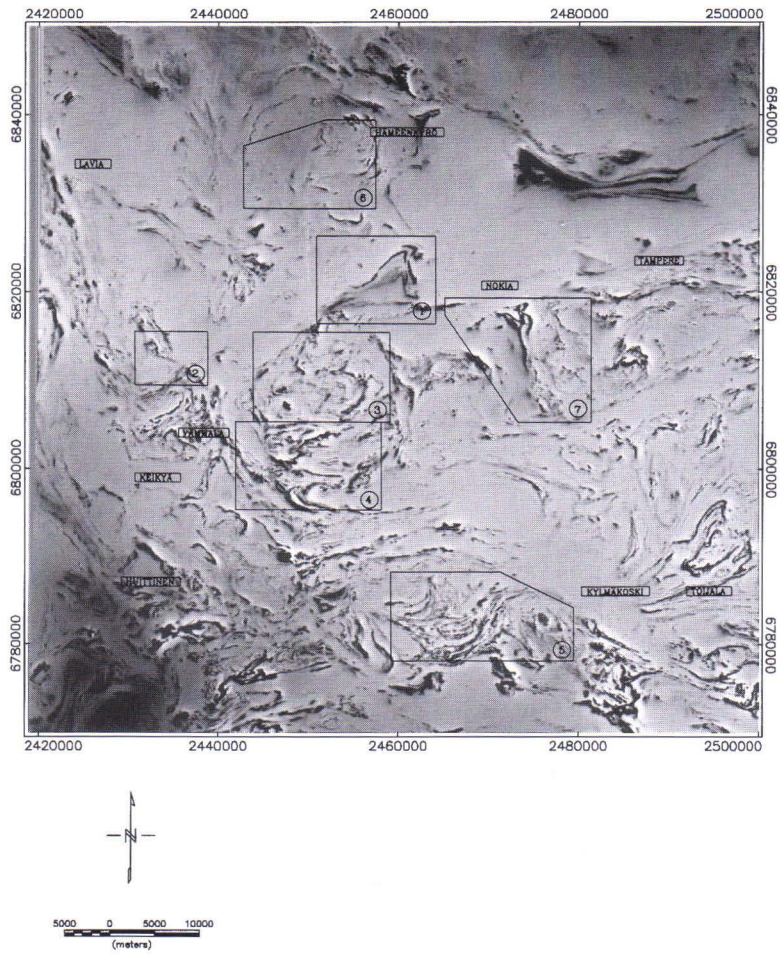

Fig. 3. Aeromagnetic low-altitude map of Tampere-Vammala area. The area is identical to the study area. Geological Survey of Finland, Espoo. Compiled by Maija Kurimo.

so useful for studies of metamorphism, for instance, are very rare in the study area, and thus the selection of subareas was largely based on the occurrence of porphyroblastic rocks. Even so, due to informative structural features, some of the selected subareas are virtually devoid of porphyroblasts.

In the following, the subareas are briefly described in terms of visible structures, metamorphism and the relation of intrusive rocks to structural evolution. For structures and metamorphism, the emphasis is on features significant to interpretation of the tectono-metamorphic evolution of the whole study area. For reasons to be discussed later, the numbering of the deformation events differs from the classification applied in earlier structural investigations in the Tampere-Vammala area (Campbell 1980, Nironen 1989a, 1989b, Aarnisalo 1988, Kilpeläinen & Rastas 1992). The first four descriptions of subareas (Mauri, Myllymaa, Ellivuori, Stormi) examine the gradual change in the relative and absolute ages of structures and metamorphism as the metamorphic grade increases from the lower amphibolite facies in the Tampere Schist Belt towards the high-grade metamorphic Vammala Migmatite Area. The next two subareas (Koosanmaa and Hämeenkyrö) are examples of the effect of the deformations following the peak metamorphism on present-day erosion level patterns. As well as all the features described earlier, the last subarea (Pirkkala) shows a rapid but gradual change in metamorphic grade from the Tampere Schist Belt to the Vammala migmatite area.

Kinematic analysis is not included in the description of the subareas, as this will be dealt with in the chapter on correlating deformation structures of the subareas and in conjunction with geometrical modelling. Neither are lineation data presented, there being too few lineations for reliable conclusions to be drawn concerning the directions of tectonic movements.

The terminology of the tectonic and tectono-metamorphic structures is after Powell (1979), Bell & Rubenach (1983), Bell (1985) and Ramsay & Huber (1989).

Mauri subarea

General geology

The Mauri subarea is located at the southern edge of the Tampere Schist Belt, about 20 km west of the synformal area described by Nironen (1989a) (Figs 2 and 4). The arcuate Mauri meta-arkose, so named by Sederholm (1897, 1913), is a formation a few kilometres wide in the middle of the subarea. It is bordered in the north by mica gneisses containing amphibole and plagioclase bands, and by conglomerates. The supracrustal rocks in the south are andalusite-bearing and in places garnet-bearing mica gneisses. Owing to the relatively low metamorphic grade, the primary structures of the supracrustal rocks are commonly preserved. According to Leveinen (1994), the meta-arkose (metasandstone) can be correlated stratigraphically with the central or upper part of the Tampere Schist Belt, as is also suggested by the age of detrital zircons (1.9 Ga, Matisto 1968), which is close to that of the granitoids, which were emplaced syntectonically in relation to Tampere synclinal folding (1885-1978 Ma, Nironen 1989b).

The primary structures of both the meta-arkose and the enveloping supracrustal rocks show that they deposited in shallow water (Leveinen 1994). Owing to the deformation of rocks and scarcity of contact observations, the mutual stratigraphy of the rocks is difficult to establish. However, at least in the western contact of the north-south-trending part of the meta-arkose, the facing of the meta-arkose and andalusite-mica schists is

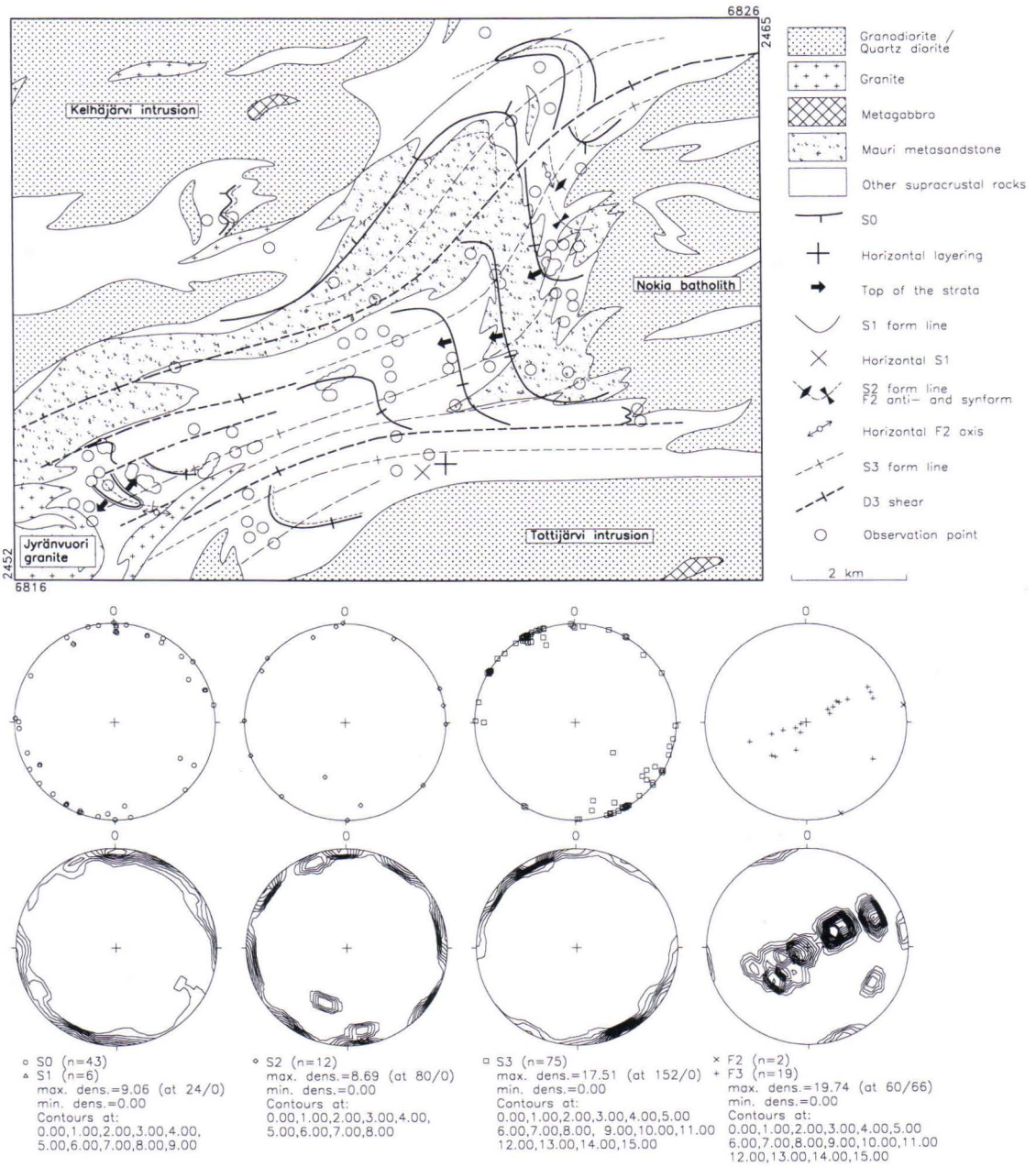

Fig. 4. Form line map of Mauri subarea and lower hemisphere projections of structures shown on it. Lithology modified from Matisto (1961, 1967).

invariably westwards, implying that the andalusite-mica schists deposited after the meta-arkose (Fig. 4).

Structurally, too, the Mauri subarea belongs to the continuations of the Tampere synclinal area even though the metamor-

phism of structures started earlier in the Mauri subarea than in the core of the Tampere synform area. Consequently, the earliest schistosities are stronger and the modes of occurrence of younger, synmetamorphic deformation events differ from those in the synform area (Kilpeläinen et al. 1994).

The metamorphic grade is at its lowest in the central part of the subarea, where the rocks are layered metapelites with well-preserved primary structures and in places large andalusite porphyroblasts. From there the metamorphic grade increases gradually in every direction, being at its highest in the southernmost part of the area, where the rocks are mica gneisses distinctly coarser due to metamorphism and in places containing sillimanite.

Deformation - D_1, D_2, D_3 and Equal area projections

D_1 - Penetrative schistosity (S_1) due to fine biotite scales is the earliest deformation structure in the subarea, particularly in fine-grained mica schist layers rich in biotite. S_1 is always parallel to the layering and no fold structures related to D_1 have been encountered. The intensity of S_1 seems to depend not only on the abundance of mica but also on the metamorphic grade of the rock, as it is lacking entirely in the best preserved rocks in the middle of the area (rocks without porphyroblasts and andalusite-mica schists) but is at its strongest in the south of the area. The present geometry of the structures in the subarea shows that after the first deformation stage the layering of the metasedimentary rocks was still subhorizontal.

Other structures related to D_1 are the shears parallel to S_0. These shears in graphite and sulphide-bearing layers weather easily and so are now mainly visible on road cuts only. Even there they are strongly weathered and highly fractured and do not have useful kinematic indicators.

D_2 - The horizontal structures were folded by F_2 with horizontal axis during the second deformation stage (Fig. 5a). The current intensity of folding varies, usually being fairly tight, as the layering in the outcrops on the limbs of F_2 folds is subvertical (Fig. 4). The axial planes of folding were - and still are - predominantly strictly vertical and the axial plane properties vary not only with the rock type (abundance of mica) but also such that where S_1 has intensified, S_2 is spaced or crenulation schistosity, depending on the scale of examination (Fig. 5b). Thus S_1 was not completely obliterated during D_2, but at those sites where S_1 cannot now be recognized, it probably never existed in the first place. Owing to the horizontal axis, the size of the F_2 folds is difficult to grasp. However, the mere fact that only one distinct synform and one antiform structure can be deduced for the area from the facing data (Leveinen 1994) suggests that the wavelength is of the order of kilometres.

In a few outcrops on the limb of the F_2 fold in the east of the Mauri subarea there is complex deformation of layering that, due to the unfavourable structural location of the outcrops, could not have been connected with any definite deformation stage. These outcrops show zones, usually a few metres wide, parallel to the layering, in which the adjacent well-preserved primary layering is completely mixed up (Fig. 5c). The structure is definitely older than D_3, for S_3 schistosity crosscuts the chaotically folded layering (Fig. 5c). The relation of the structure to D_2 cannot be deduced from the schistosities, because S_3 is the only macroscopic or microscopic schistosity both in this rock and in the adjacent host rock with preserved layering. Hence, the structure could even be synsedimentary.

D_3 - The current arcuate shape of the Mauri arkose formed when the dextral F_3, its axial plane striking roughly ENE-WSW, folded the east-west-trending vertical $S_0/S_1/S_2$ struc-

Fig. 5a. F_2 and F_3 folded pelitic metasedimentary rock in southwestern corner of Mauri subarea (Fig. 4). Northwest upwards. A horizontal section. X = 6817.70, Y = 2453.65. Code bar 6 cm.

Fig. 5b. Thin section cut perpendicular to an F_2 fold axis from hinge of an F_2 fold in outcrop of Fig. 5a. Mauri subarea (Fig. 4). One nicol. X = 6817.70, Y = 2453.65. Field of view 12 mm wide.

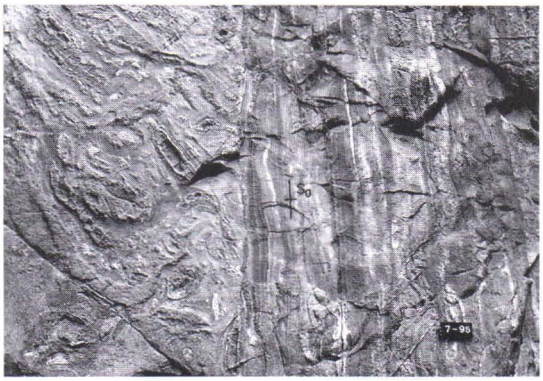

Fig. 5c. Complex deformational structures on limb of an F_2 fold in layered metasedimentary rock. Mauri subarea (Fig. 4). East upwards. X = 6821.95, Y = 2461.80. Code bar 6 cm.

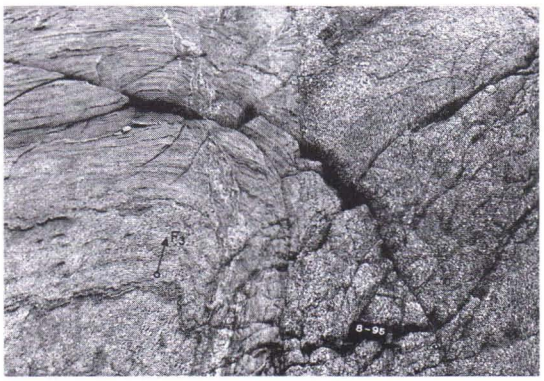

Fig. 6a. Porphyritic granodiorite dyke intruded in axial plane of F_3 folding in metasedimentary rock close to southeastern contact of Kelhäjärvi batholith. Mauri subarea (Fig. 4). East-northeast upwards. X = 6822.40, Y = 2455.40. Code bar 6 cm.

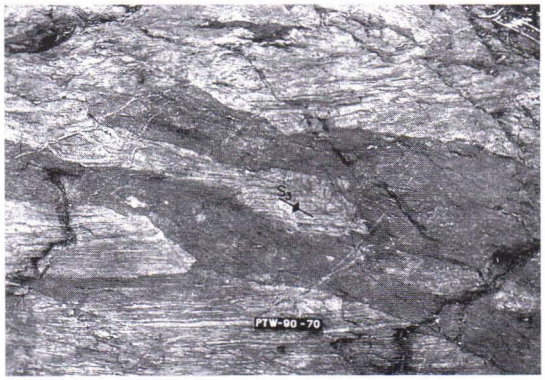

Fig. 6b. Syn-F_3 intruded plagioclase porphyritic dyke at contact of Mauri meta-arkose with andalusite-mica schist. Mauri subarea (Fig. 4). Northwest upwards. X = 6821.25, Y = 2460.45. Code bar 11 cm.

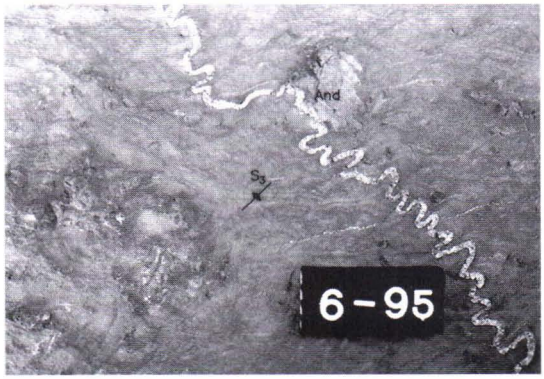

Fig. 6c. Quartz vein in andalulsite-staurolite mica schist formed as D_3 tension gashes and folded by F_3. Mauri subarea (Fig. 4). Note the unfolded nature of quartz vein at the pressure shadow of the andalusite porphyroblast. South upwards. X = 6819.80, Y = 2460.30. Code bar 6 cm.

tures created by F_2. The F_3 folds are fairly open both on map scale and in outcrops. However, shears developed in the axial plane of folding and some vertical movement took place along these in addition to dextral horizontal movement. This is suggested by the sudden increase in metamorphic grade from north to south at the eastern end of the southernmost shear (Fig. 4). In the southwest of the area, D_3 is so intense that the older structures have commonly been totally transposed into an ENE-WSW direction. Like that of S_2, the mode of occurrence of S_3 is controlled by the intensity of older structures. In the central part of the subarea, S_3 is the penetrative biotite schistosity, but northeastwards and southwestwards it changes into crenulation as the metamorphic grade increases. Thus, S_3 differs from S_2 in that, at its most intense, it overprints the older schistosities, rendering them indecipherable.

In the west of the area and south of the Nokia batholith the D_2 structures are cut by subvertical crenulation striking 120-150°. In places this feature also cuts D_3 but since in some outcrops the 60°-striking S_3 crenulation also shows a northwest-southeast conjugate, the feature clearly refers to different modes of occurrence of D_3 in each case.

Equal area projections - From the S_1 projection points in Fig. 4 can be deduce that the measurements were made on outcrops where the angle between S_0/S_1 and the dominant S_3 is high. The measurements were made on outcrops where the F_2 structure could be reliably identified and where the danger of misinterpreting the S_1/S_{1+n} composite structure as S_1 is therefore at a minimum. The S_0/S_1 directions in the hinges of horizontal F_2 folds were not plotted for the outcrop area shown in Fig. 5a, since due to the intensity of D_3 the points would have been distributed evenly over the whole lower hemisphere. For the same reason, the projection points of the F_2 fold axes only reflect the trends of the F_2 axes of two outcrop areas. Horizontal F_2 axes trending from northwest to southeast were measured at the southwestern edge of the subarea, northeast of the Jyrävuori granite. East-west axes were measured at the southern edge of the subarea, which is shown on the structural map as an area of horizontal S_0 and S_1. Although the intense D_3 causes the S_2 projection points to spread fairly evenly in all directions, S_2 has almost invariably remained subvertical, suggesting that the true axis of F_3 was subvertical despite a slight variation in the plunge of the F_3 axes measured.

Igneous rocks

The supracrustal rocks of the subarea are surrounded on almost all sides by granitoids, of which only the Nokia batholith in the east of the area has been dated. The batholith has two zircon populations differing in age (1898 ± 9 Ma and 1909 ± 12 Ma), of which even the younger is older than the typical Svecofennian synkinematic granitoids (Kouvo & Tilton 1966, Nironen 1989b). According to Nironen (1989b), this is probably either due to the intermixing of zircon generations or because even the younger zircons have inherited some old lead.

In places, the southern contact of the Nokia batholith cuts the S_0/S_1-structures of metasedimentary rocks at high angles, being conformable with S_2 (Fig. 4). The batholith also contains fragments of supracrustal rocks showing D_2 structures. Consequently, it must be contemporaneous with or younger than D_2. The Kelhäjärvi granodiorite/quartz diorite bordering on supracrustal rocks in the north is porphyritic at its southeastern end. A porphyritic variant also occurs as dykes in supracrustal rocks intruded along S_3 planes (Fig. 6a). The contact of the Tottijärvi granodiorite/quartz diorite in the south of the area with the supracrustal rocks is not exposed but the metasedimentary rocks near it are highly migmatic, the veining being contemporaneous with both D_2 and D_3. Clearly

then, the Tottijärvi massif had a distinct contact effect on the surrounding supracrustal rocks.

The dykes associated with the Jyrävuori granite stock in the southwestern corner of the area crosscut all the above structures.

Felsic, even-grained dykes, less than 1 m wide, are exposed in some andalusite-mica gneiss outcrops. Their age in relation to structural succession is ambiguous. They were clearly deformed by F_3 folding and show pre-D_3 schistosity. However, due to the lack of F_2 and D_1 structures in the surrounding supracrustal rocks their relative ages cannot be determined more precisely.

In the very centre of the subarea, at the southern contact of the Mauri arkose, there is an outcrop where, visually estimated, intermediate plagioclase porphyritic dykes have intruded along the axial plane of F_3 folding (Fig. 6b). Hence, these dykes demonstrate that magmatic activity continued in the subarea during D_3.

Quartz veins associated with D_3 occur particularly in the northeast and southwest of the area. Some of them are paralllel to the S_3 planes, some have formed as D_3 tension veins, which have subsequently deformed during D_3 (Fig. 6c).

Metamorphism and migmatization

The compositions of the metasedimentary rocks throughout the subarea are not very favourable to the crystallization of porphyroblasts. The Mauri meta-arkose, for example, lack aluminosilicates altogether as do almost all the mica gneisses north of the arkose. The abundance of porphyroblasts is

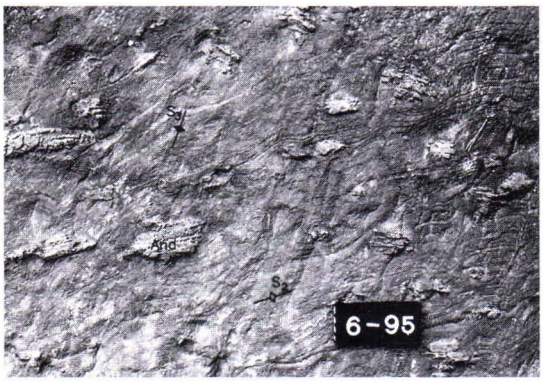

Fig. 7a. Andalusite porphyroblasts elongated in $S_0/S_1/S_2$ direction, with crystallization controlled by evolving S_2 schistosity. Mauri subarea (Fig. 4). Southwest upwards. X = 6819.80, Y = 2460.30. Code bar 6 cm.

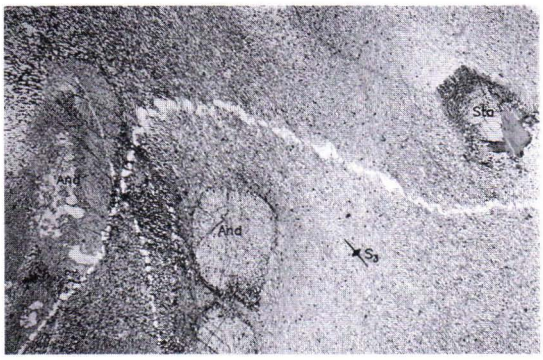

Fig. 7b. Photomicrograph of a sample from outcrop of Fig. 7a. Margins of andalusite porphyroblasts have crystallized after the development of S_3. S_3 is deflected around margins of staurolite grains. Note syn-D_3 quartz vein deformed by D_3 outside an andalusite grain. Mauri subarea (Fig. 4). One nicol. X = 6819.80, Y = 2460.30, Field of view 12 mm wide.

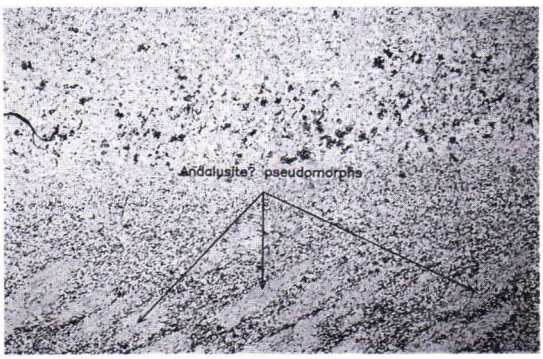

Fig. 7c.

Fig. 7c. Possible andalusite pseudomorphs in layered metasedimentary rock at southern contact of Nokia batholith. Pseudomorphs are elongated in S_2 direction and resemble those described by Nironen (1989b) from southern contact of Värmälä intrusion at eastern end of Tampere synclinal area. Mauri subarea (Fig. 4). One nicol. X = 6819.00, Y = 2462.75. Field of view 12 mm wide.

highest in the mica schists of the central part of the area, which, in addition to andalusite, commonly contain staurolite. Andalusite started to crystallize during D_2, with the consequence that S_2 schistosity has in places remained as the S_i structure of porphyroblasts when they grew into elongated grains, up to 20 cm long, controlled by the evolving S_2 (Figs 7a and 7b). Andalusite continued to crystallize over the syn-D_3 quartz veins at D_3. However, at the final stage of D_3 the edges of the porphyroblasts were already mechanically fractured.

Staurolites clearly crystallized at least before the peak of S_3 schistosity development, as S_3 is deflected around the edges of staurolite grains (Fig. 7b). The euhedral staurolite grains are virtually free of inclusions, and so their relative crystallization age cannot be dated more accurately.

At the southern contact of the Nokia batholith, the mica gneiss contains small muscovite aggregates that resemble porphyroblasts which have undergone retrograde metamorphism (Fig. 7c). Seitsaari (1951) and Nironen (1989b) have described corresponding aggregates from the Värmälä stock contact and interpreted them as pseudomorphs after andalusite. Nironen (1989b) suggested that they were crystallized due to the effect of contact metamorphism and subjected to retrograde alteration syntectonically in relation to the Tampere synform folding. Their mode of occurrence is entirely different from that of the above large andalusite grains. Migmatitic rocks have been only encountered near the contact of Tottijärvi intrusion (see above).

Myllymaa subarea

General geology

The Myllymaa subarea is located in the western continuation of the Tampere Schist Belt, about 20 km southwest of the Mauri subarea (Figs 2 and 8). The supracrustal rocks of this area, which is partly bordered by synkinematic granitoids, are mainly distinctly layered metasedimentary rocks that are best preserved in the eastern and central parts of the area. In the south and northwest the rocks are somewhat migmatitic, although layering is in places still discernible. The occurrence of sedimentary material varies, the most pelitic rocks being in the best preserved areas; moreover, the most intensely metamorphosed rocks are arenaceous in composition and their layers are clearly thicker than those in nonmigmatitic rocks.

In the well preserved metasedimentary rocks, sandy and silty or clayey layers, about 2 cm thick, alternate (Fig. 9a). In a few outcrops, however, the rocks are coarse meta-arenites or metagreywackes, commonly showing crossbedding (Fig. 9b). In this respect they resemble the above Mauri metaarkose, but they lack the red hue macroscopically typical of it. Owing to repetition caused by folding with subhorizontal axes and poor exposure, the stratigraphic position of the crossbedded rock in relation to the layered mica schist is unclear. For the same reason the original thicknesses of the various sediment associations in the subarea are difficult to estimate. In the western part of the area, the fold axis of the first folding stage later became more vertical, so that it is almost certain that the migmatitic, sandier metasedimentary rocks are stratigraphically below the better preserved metapelites (Fig. 8).

The metasedimentary rocks in the subarea are poor in porphyroblasts. Small amounts of andalusite and garnet occur in the mica schist of the central part but the more sandy rocks in the west are devoid of porphyroblasts. As shown by migmatization, however, the metamorphic grade at the western end of the area increases towards north and south.

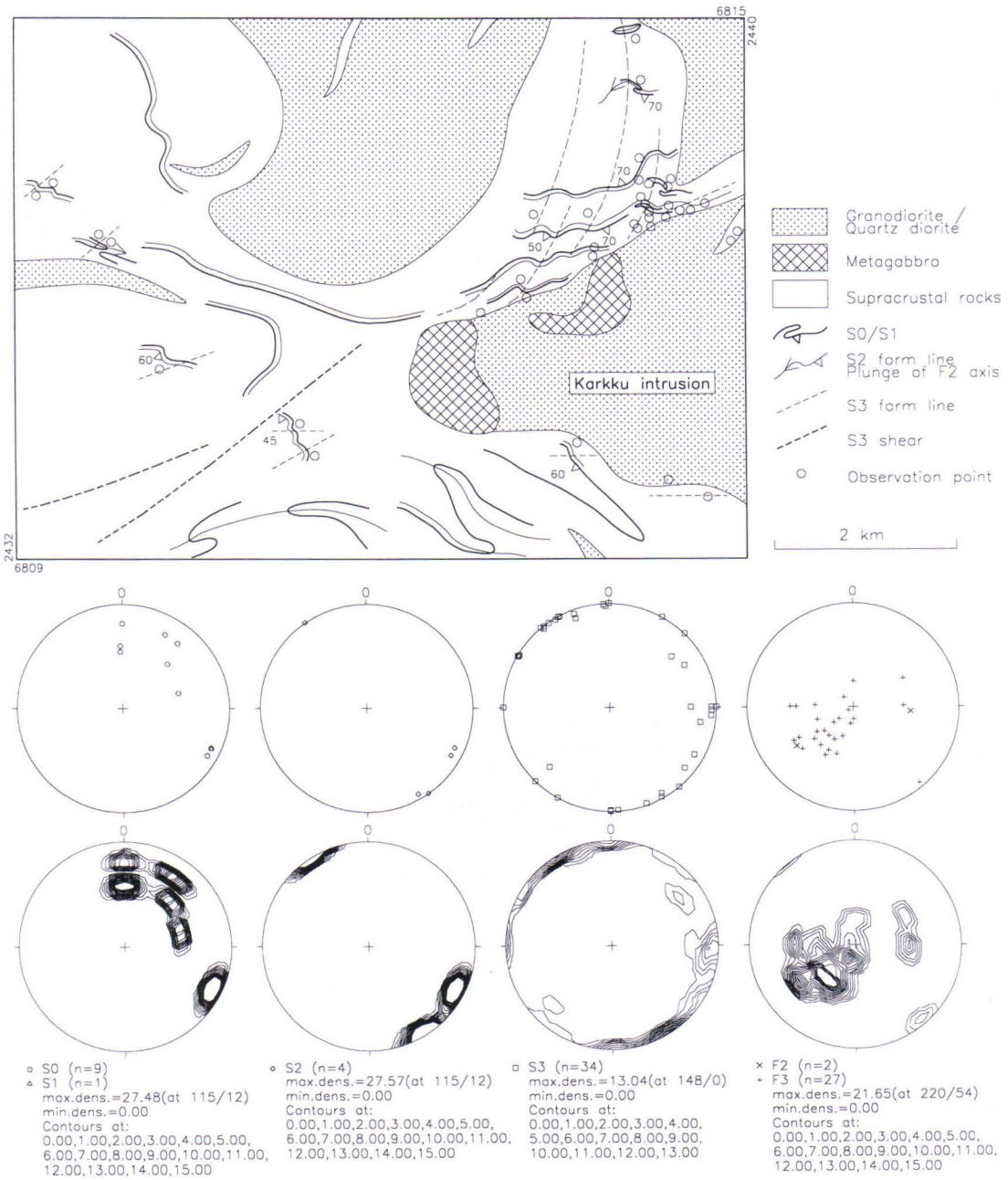

Fig. 8. Form line map of Myllymaa subarea and lower hemisphere projections of structures shown on it. Lithology modified from Matisto (1967).

Fig. 9a. F_2 and F_3 folded, thinly layered metasedimentary rock. Eastern part of Myllymaa subarea (Fig. 8). North upwards. X = 6812.85, Y = 2438.95. Code bar 6 cm.

Fig. 9b. Crossbedded metagreywacke in eastern part of Myllymaa subarea (Fig. 8). South upwards. X = 6812.80, Y = 2438.35. Code bar 6 cm.

Fig. 9c. Closing interference structures of F_2 and F_3 with subhorizontal axes in layered metasedimentary rock. Myllymaa subarea (Fig. 8). East upwards. X = 6814.85, Y = 2438.75. Code bar 6 cm.

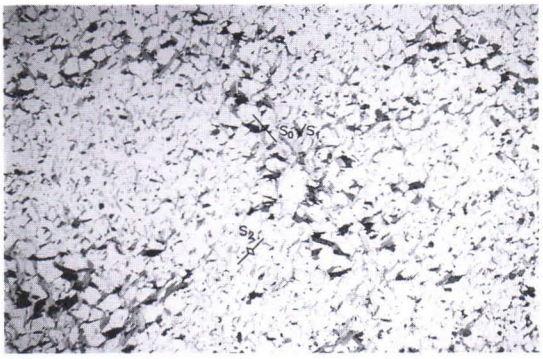

Fig. 9d. Thin section cut perpendicular to fold axis from hinge of an F_2 fold in layered metasedimentary rock. Western part of Myllymaa subarea (Fig. 8). X = 6812.40, Y = 2433.00. Field of view 12 mm wide.

Deformation - D_1, D_2, D_3 and Equal area projections

D_1 - The oldest tectonometamorphic feature in the area is the penetrative schistosity (S_1) parallel to layering and is defined by fine-grained biotite scales. It is, however, lacking in the best preserved mica schists in the central part of the area. Fold structures associated with the D_1 stage have not been encountered in the subarea, neither has the repetition of rock units or layers that would suggest the presence of F_1 folds. The geometry of the current structures in the subarea (gently plunging and, in places, horizontal F_2 axes, symmetrical F_2 folds) shows, in any case, that the layering was still subhorizontal before the F_2 folding.

D_2 - During the second deformation stage, the horizontal layering and the S_1 parallel to it folded tightly by F_2 with horizontal axis (Figs 9a and 9c). The compression was approximately north-south and horizontal, due to which the F_2 axial planes attained a subvertical and east-west-striking attitude. Although younger deformations have changed the plunges of the F_2 axes, these are still

fairly gently plunging in many outcrops (Fig. 9c). Owing to the minor variation in lithology, the size of the F_2 folds is difficult to assess. However, on magnetic maps the F_2 folds in the west of the subarea have wavelengths of the order of hundreds of metres, if not more.

The axial plane properties of the F_2 folds depend largely on the intensity of S_1. In the least metamorphosed rocks in the eastern and central parts of the area, which lack S_1, S_2 is penetrative but in more strongly metamorphosed rocks S_1 is clearly visible as is S_2 (Fig. 9d). Most of the outcrops do not, however, show F_2 folds and, due to the tightness of F_2, the main schistosity is commonly the $S_0/S_1/S_2$ composite.

D_3 - The axial planes of folds of the third deformation stage in the area usually strikes roughly from northeast to southwest, but varies considerably due to the local variation in the stress field in the pressure shadows of plutonite intrusions (Fig. 8). In places F_3 folding is not visible in outcrops but manifests itself as a variation in the plunge of F_2 axes (Fig. 9c).

In the well-preserved mica schists in the eastern and central parts of the area the axial planes of F_3 folds have spaced or crenulation cleavage, but the more intensely metamorphosed metasedimentary rocks in the west rarely exhibit any S_3 features as such. Throughout the area, however, zones of intense deformation are associated with the axial planes of F_3 folds, and from these zones structures older than D_3 have been almost totally obliterated. Owing to the poor exposures, it has not been possible to determine the kinematics of these zones.

At the eastern end of the subarea, close to the contact of the Karkku porphyritic granodiorite, folding with northwest-southeast-striking axial planes that deforms all the above structures, D_3 shears included, is visible in places. This structural feature is, however, local only and does not seem to have markedly affected the present total structure of the area.

Equal area projections - The projections in Fig. 8 show that most of the planal structures measured are S_3 schistosities. The measurements were made exclusively in the area of well-preserved rocks immediately north of the Karkku intrusion, where the F_3 axial planes strike from northeast to southwest and in the north also from north to south, and where S_3 structures dominate due to the weakly developed S_1 and S_2. The projections further show that the F_3 fold axes and S_0 correlate strongly, i.e. F_3 axes were measured on rocks that had preserved their layering.

In the projections, S_0 invariably dips to southwest. If the measurements of S_0 directions, of which there were only nine, were made on both limbs of F_2 folds, the axial planes of the F_2 folds also dip at a high angle to southwest. On the basis of these data it is impossible to say whether the attitudes of the folds are primary or whether they tilted into their present position later. The $S_0/S_1/S_2$ composite, which is commonly visible due to the tightness of the F_2 folding and which is referred to as pre-D_3 schistosity, is not shown in stereographic projections.

Igneous rocks

Two large, non-dated and partly porphyritic granodiorite intrusions extend into the subarea. Associated with the southern one, the Karkku porphyritic granodiorite, are dykes whose age in relation to structural elements can be established on outcrops.

These dykes occur particularly in the east of the area, close to the contact of the Karkku granodiorite. As a rule, the dykes, 1-5 m wide, have intruded along the axial planes of F_3 folds (Fig. 10a). The S_3 orientation shown by the dykes cuts the porphyritic structure, as demonstrated by the schistosity deflecting around potassium feldspar

Fig. 10a. Porphyritic granodiorite dyke intruded in F_3 axial plane of metasedimentary rock and further S_3 oriented. Myllymaa subarea (Fig. 8). East upwards. X = 6813.15, Y = 2439.20. Code bar 5 cm.

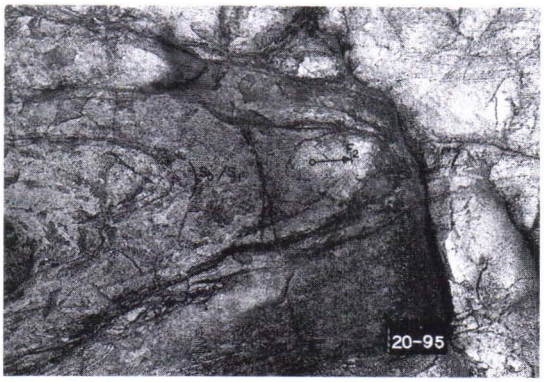

Fig. 10b. Supracrustal fragment containing S_1 and F_2 structures in porphyritic Karkku granodiorite. Structure of fragment implies that the intrusion is younger than F_2 folding. Myllymaa subarea (Fig. 8). South upwards. X = 6812.55, Y = 2439.95. Code bar 6 cm.

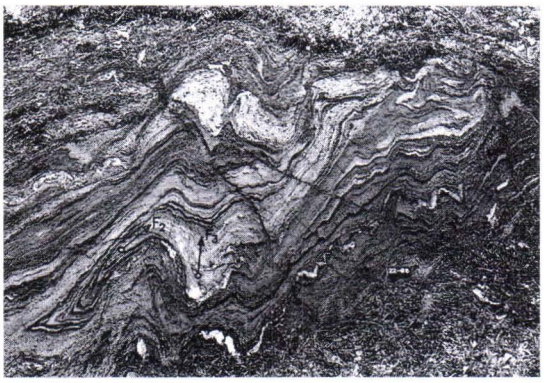

Fig. 10c. Quartz veins in metasedimentary rock formed as tension gashes that opened during F_3 folding deforming tight F_2 folding. Western part of Myllymaa subarea (Fig. 8). Northeast upwards. X = 6812.40, Y = 2433.00. Code bar 6 cm.

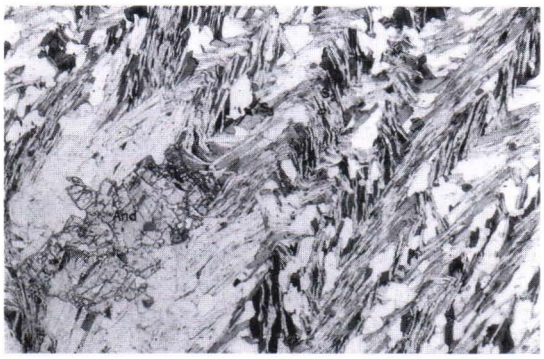

Fig. 11. Andalusite porphyroblast in metasedimentary rock crystallized after the development of S_3 crenulation. Myllymaa subarea (Fig. 8). One nicol. X = 6812.85, Y = 2438.95. Field of view 4 mm wide.

phenocrysts. The syn-D_3 character of the dykes is further suggested by the fact that the dykes, too, have been deformed by the above, youngest folding with a northwest-southeast-striking axial plane. The Karkku granodiorite also has fragments of supracrustal rocks exhibiting F_2 folds (Fig. 10b).

The best preserved supracrustal rocks in the subarea, particularly in the zones of intense D_3, have abundant quartz veins, a few centimetres wide, that have formed either along S_3 planes or tension gashes opened during F_3 (Fig. 10c).

Granite dykes less than a few tens of centimetres wide and commonly striking roughly from north to south are particularly common in the southwestern part of the area. There they cut all the above structures, with the possible exception of the youngest folding with a northwest-southeast-trending axial plane, whose relation to the granite dykes has not been established due to the lack of observations.

Metamorphism and migmatization

Metasedimentary rocks with porphyroblasts are extremely rare in the area. However, andalusite grains, a few millimetres across and crystallized on the S_3 crenulation, occur in samples taken from the well-preserved rocks in the east (Fig. 11). Other samples from the same outcrops contain small, euhedral garnet grains that crystallized at least later than S_2. Since they occur only in layers in which S_3 is poorly visible due to the low abundance of mica, the relation of the garnet to D_3 is unclear.

In the west of the area, porphyroblasts are lacking and the changes in metamorphic grade can be estimated only from the amount of migmatization. Such an estimation tends to be subjective, as the amount of veining is controlled by the primary composition of the migmatized rock as well as by pressure and temperature. Interpretation is further hampered by the fact that migmatization in the Vammala area is thought to be caused not only by increased temperature but also by H_2O-rich fluid activity (J. Karhu, pers. comm.). Since outcrops show only a few F_2 folds, the relative age of migmatization is difficult to establish. At any rate, the most intensely migmatized rocks occur in the south and southwest of the area, where the earliest veining in the $S_0/S_1/S_2$ plane seems to be more abundant than elsewhere. Veining also occurred during D_3, but only in the south and southwest of the area.

Ellivuori subarea

General geology

The Ellivuori subarea is located immediately south of the Mauri subarea (Figs 2 and 12) but it cannot be included in the continuations of the Tampere Schist Belt on the basis of either its metamorphic grade or the composition of the metasedimentary rocks. The supracrustal rocks are arenaceous metasedimentary rocks in which, due to the low variation in composition, the layering is not always visible, even if the metamorphic grade and deformation were not intense enough to obliterate the primary features. Consequently, fold structures are not clear in outcrops. Since, moreover, the abundance of micas in the arenaceous rocks is low, the metamorphic structures are not very conspicuous either. Nevertheless, there are some metasedimentary rocks with distinct layering, and in these the layers vary from a few centimetres to a few decimetres in thickness.

The lithology of the northwestern corner of the subarea differs from that elsewhere. There the rocks close to the contact with the Karkku granodiorite are not only unusually pelitic in their primary composition but they are also intensely sheared, and the sedimentary structures have been almost totally destroyed.

The Karkku porphyritic granodiorite described in the context of the Myllymaa subarea extends to the northwestern corner, and in the northeastern corner there is a part of the Tottijärvi quartz diorite-granodiorite intrusion described in the context of both the Mauri and Pirkkala subareas. There are also a large number of granite intrusions varying in size (Fig. 12).

In this subarea, too, estimates of the metamorphic grade depends on the few outcrops containing porphyroblasts. As suggested by these, metamorphism took place in the equilibrium field of potassium feldspar and sillimanite or potassium feldspar and cordierite, but in the south of the area the intense migmatization imply a southward increase in metamorphic grade. The change in sedimentary material as a function of metamorphic

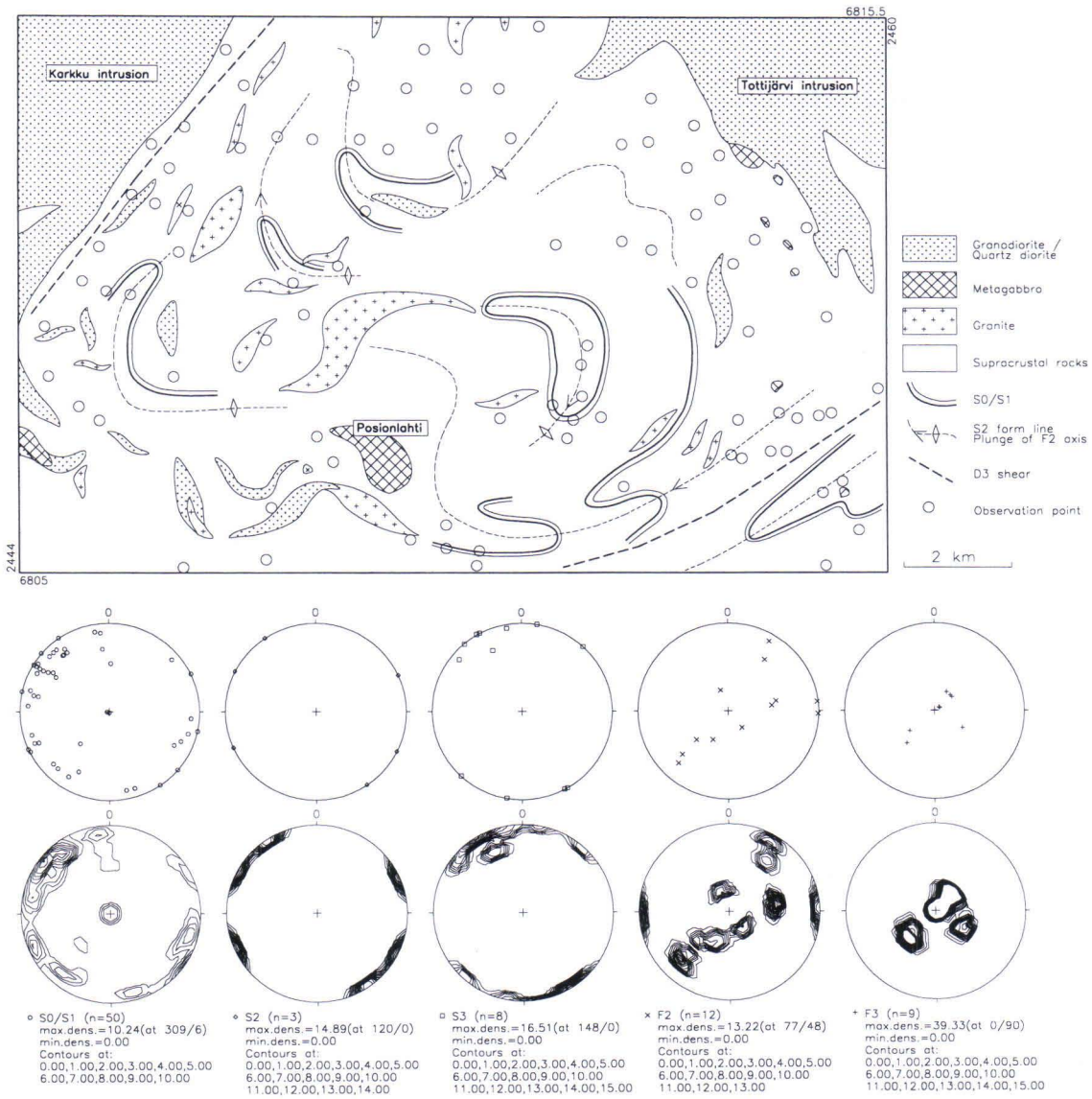

Fig. 12. Form line map of Ellivuori subarea and lower hemisphere projections of structures shown on it. Lithology modified from Matisto (1967).

grade as described in the context of the Myllymaa subarea, cannot be seen in the Ellivuori subarea.

Deformation - D_1, D_2, D_3 and Equal area projections

D_1 - The oldest tectono-metamorphic feature in the supracrustal rocks of the Ellivuori subarea is the penetrative biotite schistosity parallel to the layering, although, due to the arenaceous average composition of the rocks, it is visible only in the most fine-grained layers (Fig. 13a). Owing to the rarity of sufficiently pelitic rocks, it is impossible

to see the variation in the intensity of S_1. S_1 schistosity is nevertheless present throughout the Ellivuori subarea whenever the composition of the rock is appropriate. Fold structures associated with the same deformation as the evolution of this schistosity have not been identified. After D_1, the layering was still horizontal, implying that if folds developed in association with D_1 their axial planes must have been recumbent.

D_2 - During the second deformation stage, the above structures were folded in horizontal compression. The fold axes were then horizontal and the axial planes vertical. The unfolding of the present total structure of the subarea suggests compression from roughly north to south and an east-west primary strike for the axial planes of the F_2 folds. Owing to the low variation in lithology, it is difficult to visualize the sizes of the folds, but the F_2 folds shown by the magnetic map have a wavelength of at least several hundreds of metres. The tightness of the large folds, too, is difficult to estimate, but the fact that the S_0/S_1 structures in the subarea are now fairly vertical, the hinge of the F_2 folds excluded, implies that it was fairly tight. Although post-D_2 folding has reoriented the plunges of the F_2 axes, most of them are still subhorizontal (Fig. 13b).

The intensity of S_2 schistosity varies from one zone to the other, although its type also depends on the lithology. In the most sandy layers, S_2 may be the dominant or only visible schistosity, but in pelitic layers, in which S_1 was already intense, S_2 is crenulating in character. Thus, the properties of the axial plane of F_2 vary considerably, even between different parts of an outcrop-scale fold (Fig. 13a). As most of the outcrops are located on the limbs of large F_2 folds, the $S_0/S_1/S_2$ composite is the structure to be classified as the main schistosity.

D_3 - In the third deformation stage, the above structures underwent folding with an ENE-WSW-striking axial plane, which, as suggested by the style of folding, seems to have occurred when the rocks were still fairly plastic (Fig. 13c). Since the primary structures forced into a vertical position during D_2 folded during this stage, the D_3 structures are the most conspicuous both in outcrops and on geophysical maps. As suggested by magnetic maps, the F_3 folds are fairly open and large, with a wavelength of the order of kilometres. The axial planes are vertical, at least to the accuracy with which they can be measured on the open structures in outcrops.

The axial planes of F_3 folds in the Ellivuori subarea do not show schistosity. The intensity of S_3 is at its maximum in the pelitic layers of metasedimentary rocks, where it is crenulation without substantial new mineral growth. In contrast to the Mauri subarea, shears are not often associated with the axial planes of F_3 folds in the Ellivuori subarea. The exception is the northwest corner, where, close to the contact of the Karkku porphyritic granodiorite, there is a high-strain zone with mylonitic metasedimentary rocks related to D_3. Here all the structures have been transposed into a northeast-southwest direction, making it difficult to distinguish between F_2 and F_3 folds. However, some biotite recrystallized in the axial planes of folds suggested as F_3 by the vertical fold axes. The deep plunge of the F_3 axes in the high-strain zone indicates that movement in the zone was mainly horizontal. The metasedimentary rocks in the high-strain zone have been weathered so strongly, however, that no useful kinematic indicators have been found in them. According to geophysical maps, a similar shear zone occurs in the southeastern corner of the subarea, but nowhere is it exposed.

Equal area projections - The stereograms in Fig. 12 show that, as in the two previous subareas, the axial planes of all F_3 folds except two strike in a northeast-southwest direction. The same holds for D_2 structures, implying strong influence of D_3 on the total

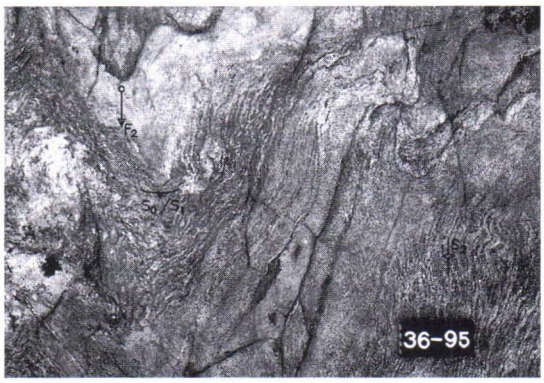

Fig. 13a. F_2 folds in layered metasedimentary rock. Northern part of Ellivuori subarea (Fig. 12). Depending on composition and grain size, the main schistosity is either S_1 or S_2. Northeast upwards. X = 6815.20, Y = 2453.40. Code bar 6 cm.

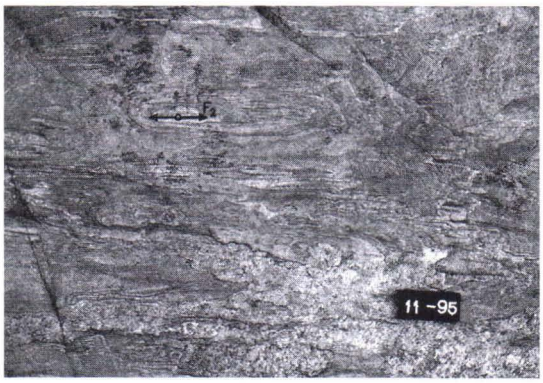

Fig. 13b. F_2 folding with horizontal axis in sandy and almost homogeneous metasedimentary rock typical of Ellivuori subarea (Fig. 12). East upwards. X = 6808.15, Y = 2453.80. Code bar 6 cm.

Fig. 13c. Plastic F_3 folding deforming F_2 structures in migmatized metasedimentary rock at southeastern edge of Ellivuori subarea (Fig. 12). Southeast upwards. X = 6807.30, Y = 2458.35. Code bar 6 cm.

Fig. 14a. S_2 oriented and F_3 folded granodiorite dyke intruded in migmatitic metasedimentary rock. Ellivuori subarea (Fig. 12). North upwards. X = 6809.50, Y = 2444.85. Diameter of coin 2.2 cm.

Fig. 14b. Fragmented and F_3 folded mafic dyke in migmatitic metasedimentary rock. Ellivuori subarea (Fig. 12). Northeast upwards. X = 6806.50, Y = 2459.20. Code bar 6 cm.

Fig. 14c. F_2 folded and S_2 oriented mafic dyke in psammitic metasedimentary rock. Ellivuori subarea (Fig. 12). North-northwest upwards. X = 6810.05, Y = 2444.50. Diameter of coin 2.2 cm.

Fig. 14d. Potassium feldspar porphyritic, syn-F_3 intruded granite dyke in migmatitic metasedimentary rock. Ellivuori subarea (Fig. 12). Northeast upwards. X = 6809.50, Y = 2444.85. Diameter of coin 2.2 cm.

Fig. 14e. North-south-striking granite dyke cutting F_3 folding of migmatitic metasedimentary rock. Ellivuori subarea (Fig. 12). Viewed towards north. X = 6807.35, Y = 2457.80. Code bar 17 cm.

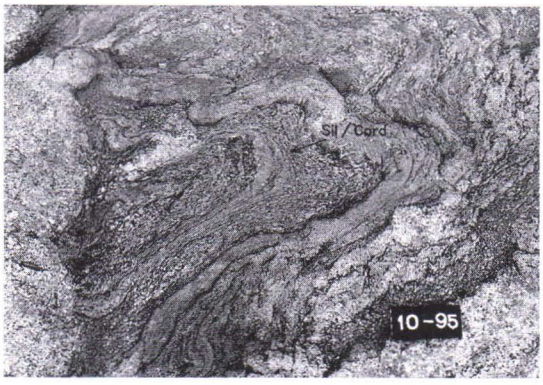

Fig. 15a. F_2 deformed sillimanites recrystallized into cordierite with increase in temperature. Note the cutting granite dyke similar as in Fig. 14e. Ellivuori subarea (Fig. 12). South upwards. X = 6807.85, Y = 2452.80. Code bar 6 cm.

Fig. 15b. Photomicrograph in which potassium feldspar porphyroblasts crystallized in decomposition reaction of muscovite have S_1 biotite schistosity as S_1 structure. Sample was taken from the outcrop shown in Fig. 13a. Ellivuori subarea (Fig. 12). One nicol. X = 6815.20, Y = 2453.40. Field of view 4 mm wide.

structures of the subarea. The majority of the measurements have, however, been interpreted as S_0/S_1 structures and, in view of the above, some of the projected structures are probably in fact $S_0/S_1/S_2$ composite structures. Owing to the high intensity of both D_2 and D_3, the S_0/S_1 points are projected evenly in every direction. The projection points clustering close to the periphery refer to the tightness of F_2 folding whereas the few points indicating subhorizontal S_0/S_1 imply F_2 with a gently plunging axis.

Igneous rocks

The Karkku porphyritic granodiorite intrusion described in conjunction with the Myllymaa subarea shows intense D_3 orientation at its contact in the Ellivuori subarea in the same way as do the adjacent supracrustal

rocks. Here too, the porphyritic texture of the rock predates D_3 schistosity, the schistosity being deflected around the margins of potassium feldspar grains. Right at the contact the plutonic rock contains supracrustal fragments, which have also been strongly deformed by D_3. On the basis of these structural features, it is evident that the granodiorite must have intruded before the end of D_3, although in the zone of intense D_3 it is not possible to establish the emplacement time more accurately. Felsic dykes indisputably associated with the Karkku granodiorite are not exposed in the supracrustal rocks of the subarea.

The Tottijärvi intrusion is a somewhat gneissose, equigranular quartz diorite/granodiorite body whose age in relation to the structures is not clear. Informative contacts are not exposed in the subarea, but the shape of the tonalite massif suggests either that it intruded before D_3 or a tension crack opened during D_3. The first alternative is supported by the fact that its contacts are at least approximately parallel to the S_2 planes in the supracrustal rocks adjacent to the contacts.

Synkinematic granitoids also occur in the subarea as minor intrusions. These are invariably tectonically oriented and at least where the orientation can be compared with the structures of supracrustal rocks, it is correlatable with the S_2 of metasedimentary rocks (Fig. 14a).

Mafic dykes are fairly abundant in the metasedimentary rocks of the subarea. D_3 typically deforms S_2-oriented mafic dykes parallel to S_2 (Fig. 14b). The relationship between the dykes and F_2 folding is rarely visible but at least some of the dykes are affected by F_2 folding (Fig. 14c).

Microcline granites occur in the area as small intrusions cutting all the above deformation structures and as dykes varying in width, of which a substantial number clearly intruded the axial planes of F_3 folds (Fig. 14d). Granite dykes of another type are the 0-30° striking, 10-cm to 1-m wide dykes cutting D_3 structures (Fig. 14e) that occur throughout the subarea. These dykes seem to have intruded a crust that was already fairly stable, as they are completely undeformed and, moreover, invariably strike from north to south. The above syn-D_3 dykes mainly occur in the western margin of the subarea, in particular close to the contact of the Karkku porphyric granodiorite. It is possible, then, that they are associated with this granodiorite, which means that there are at least two granite generations of different ages in the subarea.

There are also a few mafic-ultramafic intrusions in the subarea (e.g. Posionlahti), whose age relations to the structures of supracrustal rocks have not been established due to the lack of exposures.

Metamorphism and migmatization

Porphyroblastic metasedimentary rocks are rare in the Ellivuori subarea. Right at the northern edge of the area, potassium feldspar-sillimanite gneisses occur in a few outcrops. Fibrolitic sillimanite has grown into elongated grain aggregates parallel to S_0/S_1, which, in the hinges of F_2 folds, have undergone further deformation (Fig. 15a). Potassium feldspar occurs in them as poikiloblasts less than 1 mm across, with S_1 biotite schistosity as S_i (Fig. 15b). The structure implies that muscovite was decomposed in the area at least before the peak of D2.

Compared with those in the northern part of the area, the potassium feldspar porphyroblast in the central parts are large poikiloblastic grains, up to a few millimetres in diameter. Even if outcrops did not show F_2 structures, the S_i of potassium feldspars is commonly at a high angle with the main schistosity, which was earlier concluded to be the $S_0/S_1/S_2$ composite. In these cases, too, the S_i structure of potassium feldspars is unfolded. Provided then that the idea of Bell

(1985) about the nonrotation of porphyroblasts holds for the Ellivuori metasedimentary rocks, the above features are suggestive of pre-D_2 crystallization of the potassium feldspar porphyroblasts.

The S_1 schistosity in potassium feldspars is composed by markedly finer-grained biotite than are the S_1 biotites in matrix in the hinges of F_2 folds. This may be due to the coarsening of matrix S_1 after the crystallization of potassium feldspars (Vernon 1978). The coarsening may have happened either during D_1 or then not until D_2, by which time the S_1 biotites had recrystallized by imitating the existing structures (Vernon 1977). In the first alternative, muscovite would have decomposed syntectonically with D_1. In the second, potassium feldspar would also have been able to crystallize between D_1 and D_2. According to Ferguson & Hart (1975), the difference between the grain sizes of S_i and S_1 biotites can be attributed to the downsizing (dissolution) of inclusions during the crystallization of porphyroblasts.

Typical of the whole subarea is the high abundance of retrograde muscovite. Sillimanite grains are almost invariably at least partly muscovitized and large muscovite scales have crystallized elsewhere in the matrix, too. As muscovites crystallized they cut D_2 structures, but it has not been possible to estimate the time of their crystallization in relation to the structural elements more accurately. It is possible that the above granites reheated the retrograde rocks, as new sillimanite seems to have crystallized at the edges of muscovite scales, and plagioclase grains were recrystallized.

Except in the zone of intense D_3 adjacent to the Karkku granodiorite, the supracrustal rocks are migmatitic, at least to some extent, throughout the area. The earliest, trondhjemitic veining is parallel to the layering and thus also parallel to S_1. Migmatization continued during D_2, but a substantial portion of the veins are younger still (e.g. Fig. 13c). Although the amount of migmatization appears to be controlled by the primary composition of the rock, outcrop observations suggest that the pre-D_3 migmatization, at least, increases in the subarea both eastwards and southwards.

Stormi subarea

General geology

The Stormi subarea is located in the middle of the study area (Figs 2 and 16) and represents the zone of tonalitic migmatites extending from Pori to Mikkeli at its most typical. Several studies have been published from the subarea, most of them, however, dealing with the petrology and geochemistry of the Stormi Ni deposit (Häkli & Vormisto 1985, Peltonen 1995a, 1995b). Supracrustal rocks in the environment of the Ni deposit and their structures are described in reports of Aarnisalo (1988) and Kilpeläinen and Rastas (1992).

The subarea is mainly composed of intensely migmatized, arenaceous metasedimentary rocks and the synkinematic granodiorites and quartz diorites that cut them. Mafic and ultramafic intrusions occur evenly throughout the area, although the best-known of them are concentrated at Stormi. Mafic and ultramafic rocks also occur as dismembered dykes and fragments in migmatitic mica gneiss. Rocks that could be classified distinctly as extrusives on the basis of their structures are few; Heikkilä-Harinen (1975) has described agglomerates from the northern part of the area and, according to Peltonen (1995a), the Uusiniitty, Vammala and Komerolahti formations, earlier referred to as cortlandites, are in fact pic-

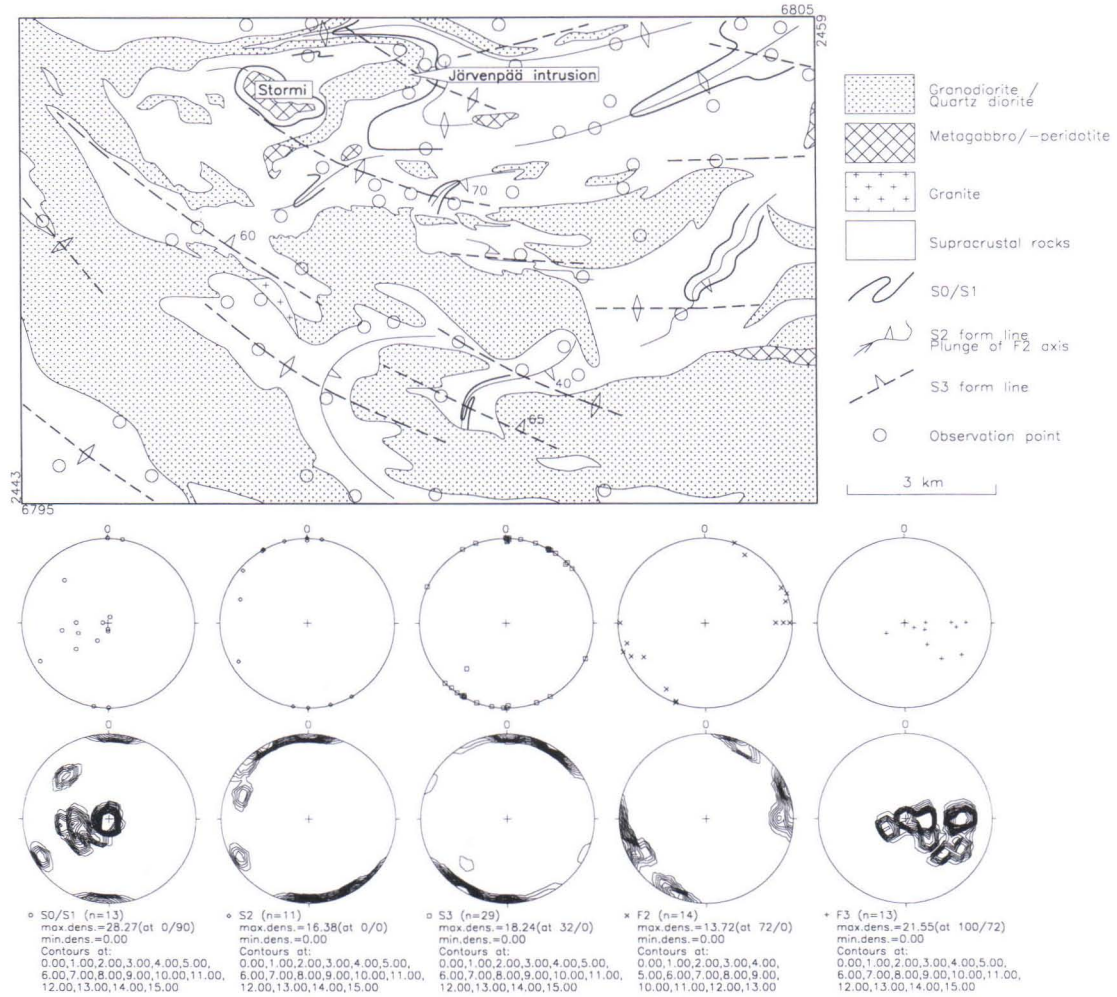

Fig. 16. Form line map of Stormi subarea and lower hemisphere projections of structures shown on it. Lithology modified from Heikkilä-Harinen (1975) and Matisto (1967).

ritic metalavas. Granites occur as small intrusions and as cutting dykes varying in width.

In migmatites, garnet, cordierite and sillimanite are in equilibrium although rocks containing all these porphyroblasts are relatively rare due to the psammitic composition of the metasedimentary rocks. The metamorphic grade varies in the equilibrium field of the above paragenesis and thus manifests itself in changes of composition of mineral assemblages only and cannot be recognized reliably in outcrops. The migmatization degree of the mica gneisses varies, especially in the youngest migmatization phases (Kilpeläinen & Rastas 1992).

Deformation - D_1, D_2, D_3 and Equal area projections

D_1 - The oldest and, at the same time, most intense metamorphic and tectonic feature in the metasedimentary rocks of the Stormi subarea is the penetrative biotite schistosity

Fig. 17a. Photomicrograph of intense S_1 in metasedimentary rock. All minerals elongated parallel to schistosity. Stormi subarea (Fig. 16). One nicol. X = 6797.20, Y = 2451.45. Field of view 4 mm wide.

Fig. 17b. F_3 deforming F_2 folds with subhorizontal axes in migmatized metasedimentary rock of Stormi subarea (Fig. 16). Note also migmatization associated with D_3. South upwards. X = 6804.20, Y = 2448.55. Code bar 6 cm.

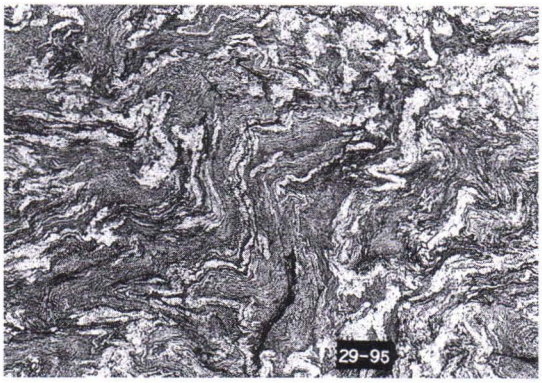

Fig. 17c. S_1, F_2 and F_3 structures in migmatitic metasedimentary rock in Stormi subarea (Fig. 16). South upwards. X = 6797.20, Y = 2451.45. Code bar 6 cm.

Fig. 17d. F_3 folding deforming $S_0/S_1/S_2$ composite and associated migmatization in metasedimentary rock. Stormi subarea (Fig. 16). Southeast upwards. X = 6797.20, Y = 2452.45. Field of view 50 cm wide.

(S_1) parallel to the layering. However intense deformation and metamorphism have commonly rendered the layering of the metasedimentary rocks unrecognizable, and it is not always possible to establish the parallelism between the layering and S_1. In particular, the originally most pelitic layers have shears parallel to S_1, and in this direction all syn- and pre-D_1 minerals have been strongly compressed (Fig. 17a).

Recognizable folds related to D_1 are not exposed in the subarea. Because intense schistosity developed in metasedimentary rocks during D_1, it is possible that the structures preceding the peak of S_1 (such as F_1) were obliterated in deformation, especially when high-temperature metamorphism was promoting the process. Even so, the metasedimentary rocks have preserved their layering in many places. If folding occurred in the subarea during D_1 it must have been recumbent, for the present total structure can best be explained by assuming that the structures at Stormi were still subhorizontal after

D_1.

D_2 - During the second deformation stage, the horizontal structures were compressed into folds with horizontal axes. Owing to the horizontal compression, the axial planes became vertical and, due to the tightness of the folding, the S_0/S_1 planes on the limbs of the F_2 folds also turned into a vertical position. Despite the intense post-D_2 deformation, the F_2 axes are still commonly gently plunging in the Stormi subarea (Fig. 17b). The size of the F_2 folds cannot be estimated on the outcrops, but magnetic maps show F_2 structures with wavelengths of the order of kilometres. Indirectly deduced, the amplitude of folding is also kilometres, the S_0/S_1 structures being vertical, for instance, on the limbs of the large F_2/F_3 interference structure of Stormi.

The trends of the axial planes of F_2 folds vary a great deal due to younger deformations, making reconstruction of their primary orientation difficult. Nevertheless, as shown by the magnetic map, the large F_2 fold with the east-west-striking axial plane at Stormi has been refolded mainly at its hinge (Figs 3 and 16). On outcrops, too, the strike of the axial plane of this fold is approximately constant despite the folds that cut it.

The character of the S_2 axial plane schistosity depends indirectly on the lithology of the rocks and on the part of the large F_2 fold in which the observation outcrop happens to be. In the most arenaceous layers of metasedimentary rocks, in which S_1 was not very intense, local penetrative schistosity developed in zones of intense S_2, whereas in the pelitic layers S_2 is a distinct crenulation without significant mineral growth. The latter situation is very clearly visible in the hinges of F_2 folds, where S_2 is least intense (Figs 17b and 17c). The tightness of F_2 folding is such that most of the outcrops exhibit only one schistosity, which, on the basis of the above descriptions, can be considered mainly as a $S_0/S_1/S_2$ composite.

D_3 - The structures described above are cut in the subarea by two sets of folds differing distinctly in their axial plane directions. The usually sinistral, asymmetric folds with a northwest-southeast-striking axial plane are dominant (Figs 17b and 17c) and, varying in intensity, are visible in almost every outcrop. Most of them are relatively open and the plunge of their axes is controlled by older structures. The other post-D_2 folding is very similar, but the axial planes strike about 60°. As no distinct cutting relation has been established for either of these two structures in the subarea and as their morphology and axial plane properties are similar, they will be treated later together under the rubric D_3.

Owing to the tightness of the F_2 folding, most of the outcrops in the subarea exhibit a structure in which the subvertical $S_0/S_1/S_2$ plane was compressed by F_3 into fairly open folds with a subvertical axis (Fig. 17d). The axial planes of F_3 commonly show weakly developed crenulation, but biotite of that age has not been crystallized. Granitic migmatization parallel to the axial planes and cutting the older trondhjemitic, thinly veined migmatization typical of migmatites in the Stormi subarea is also present, most noticeably in the zones of the most intense D_3.

Plastic folds, migmatization during deformation and the high grade syn-D_3 mineralogy to be described later imply that D_3 occurred at high temperature in the Stormi subarea. It is presumably for this reason that cataclastic D_3 structures, too, are lacking in the subarea, even though D_3 has affected the current geometry of tectonometamorphic patterns of Stormi more than in any of the above subareas. Hence, the zones of intense D_3 at the southwestern edge of the Stormi subarea show up mainly as zones of anomalously high migmatization, in which the host rock is commonly visible only as fragments in schlieren or schollen migmatites.

Equal area projections - The orientation of D3-structures in the Stromi subarea differs markedly from those described from El-

livuori subarea (see above). The projections in Fig. 16 show that in the Stormi subarea the axial traces of F_3-folding strike WNW-ESE. The F_3 axes are subvertical or plunge ESE. As shown by the diagrams, most of the F_3 measurements were made on the folded S_0/S_1 structure, which in some measurements, though, may be the $S_0/S_1/S_2$ composite.

The steep dip of F_2 axial planes and the gentle plunge of F_2 axes are also visible in the distribution of projection points. The latter imply that the S_0/S_1 structure, which is dominant in the subarea, is gentle dipping in many outcrops, a fact also indicated by the projecting of S_0/S_1 points at the centre of the circle.

Igneous rocks

Synkinematic intrusions varying in size and shape and being in composition mainly granodiorites or quartz diorites abound in the Stormi subarea. They tend to be equigranular, albeit distinctly gneissose, and invariably contain mafic enclaves elongated parallel to schistosity. The contacts of the intrusions with the supracrustal rocks are usually tectonically disturbed and always parallel to the $S_0/S_1/S_2$ schistosity of the metasedimentary rocks. Outcrops showing F_2 structures in supracrustal rocks and contacts at igneous rocks have not been encountered in the subarea. However, since not only the contacts of igneous rocks but also the gneissosity of these plutonic rocks are conformable with S_2 it can be assumed that the gneissosity developed either during or before D_2. During D_3 the gneissosity was crenulated like S_1/S_2 in the supracrustal rocks.

North and east of the Stormi Ni deposit, there is the long, arcuate Järvenpää quartz diorite intrusion (Fig. 18), which, unlike the rest of the syntectonic granitoids in the subarea, contains garnet. The rock is medium-grained, equigranular and intensely gneissose. The main minerals are plagioclase, quartz, biotite, hornblende and garnet. The abundance of garnet fluctuates but may be up to several per cent (modal composition) (Heikkilä-Harinen 1975).

The relation of this intrusion to the supracrustal structures is no different from that of the other syntectonic granitoids. North of Stormi, the intrusion trends east-west, parallel to the axial plane of F_2 folding. The contact of the intrusion with supracrustal rocks is visible in one outcrop on the northern limb of the large F_2/F_3 interference structure of Stormi. There, the contact of the intrusion with the arenaceous metasedimentary rock is tectonized and disturbed by migmatization. The gneissosity in quartz diorite corresponds to the S_1/S_2 schistosity of the metasedimentary rocks in the outcrop. East of Stormi the F_2 folds in mica gneiss have been deformed by F_3 folding with a northeast-southwest-striking axial plane. Corresponding F_3 folding of the gneissosity of the quartz diorite is visible in the adjacent outcrop (Fig. 18). The above features imply that the quartz diorite intruded the axial plane of the F_2 folds of the metasedimentary rocks in the course of folding, and thus the intense gneissosity of the plutonic rock can be correlated with the regional S_2 schistosity.

Dismembered by deformation, mafic and ultramafic rocks occur as abundant dykes in the migmatites of the Stormi subarea (Fig. 19a). The dykes, which are usually less than 1 m wide, are contemporaneous with D_2 at least but some of them formed boudins before F_2 folding, and so are clearly older than D_2.

The contacts of the mafic and ultramafic intrusions could not be observed in outcrops of the subarea. Moreover, only a few of them have been intersected in exploration drilling. Hence, the relative dating of their emplacement is here based on the best studied Stormi Ni-Cu-bearing body. The host rock of bowl-shaped Ni-Cu deposit of Stormi is composed of two, if not more, ultramafic magma pulses

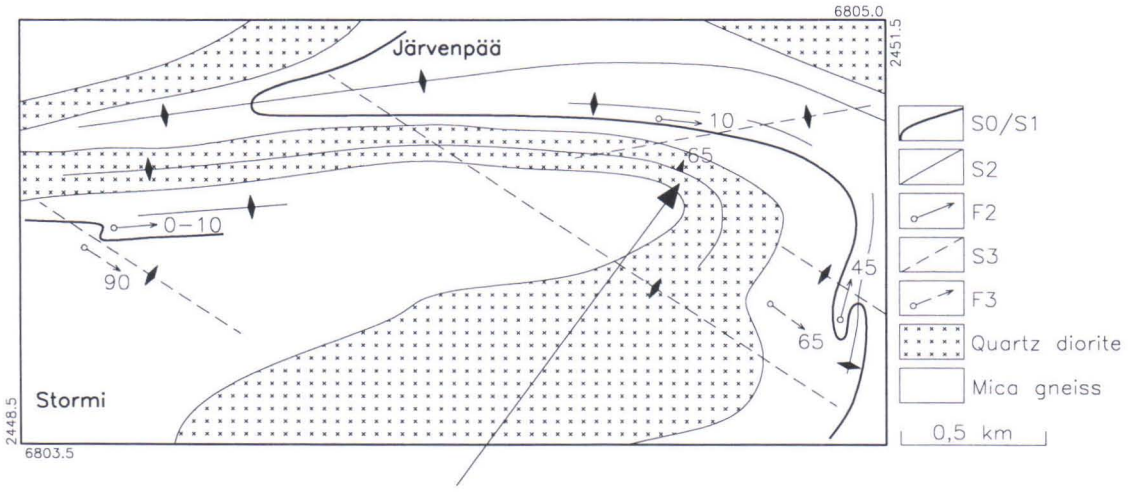

Fig. 18. S_2 oriented and D_3 deformed garnetiferous Järvenpää quartz diorite in Stormi subarea (Fig. 16). Arrow points to sample A1288-Järvenpää. The photograph was taken from the sampling place and covers an area 50 cm wide. North upwards.

Fig. 19a. Mafic dykes fractured by D_2 and D_3 deformations in migmatitic metasedimentary rock of Stormi subarea (Fig. 16). South upwards. X = 6800.10, Y = 2453.00. Code bar 17 cm.

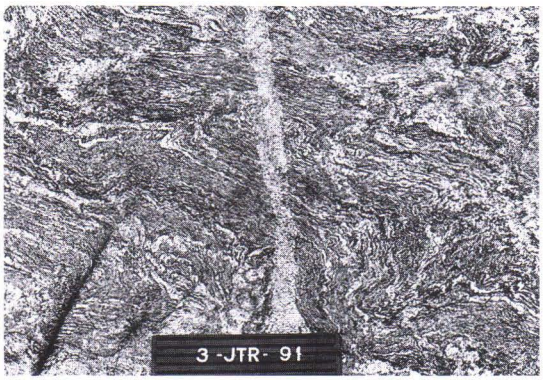

Fig. 19b. Narrow, north-south-striking granite dyke cutting F_3 folding of migmatized metasedimentary rock. North upwards. Stormi subarea (Fig. 16). X = 6797.05, Y = 2451.50. Code bar 17 cm.

and is located in the core of a large F_2 antiform. According to Häkli et al. (1979), its lower contact with the surrounding supracrustal rocks is subconformable. In view of the tectonic location of the intrusion, this probably implies subconformability with the S_1 main schistosity of supracrustal rocks, in which case the ultramafic rocks probably intruded as horizontal sills before D_2 folding. The present bowl shape of the intrusion can be attributed to interference from F_2 and F_3 folding (Kilpeläinen & Rastas 1992).

In the axial planes of the F_3 folds there are equigranular felsic dykes, less than 30 cm wide (Fig. 17b), that are in general plagioclase-dominant but also contain potassium feldspar. Depending on the abundance of potassium feldspar, Kujala (1993) has divided them into tonalitic and granodioritic dykes. Although in composition they resemble the granodioritic plutonic rocks described above, their relative age in the structural succession is different.

Granites or pegmatites are rare in the Stormi subarea. Vertical dykes, which are commonly only a few centimetres wide, almost invariably trend 0-30° (Fig. 19b). They crosscut all the above structures and are fully undeformed. There are also a few small undeformed granite intrusions in the subarea cutting the D_3 structures.

New age data

The garnet-bearing quartz diorite (A1288-Järvenpää) was dated as a part of this study. As mentioned above, this intrusion is synchronous with D_2. Its contacts with supracrustal rocks are in places exposed and it contains abundant zircon in addition to garnet.

The zircon in A1288 is brown and transparent (Fig. 20). Euhedral prismatic and pyramidal crystal faces are common, but almost all the grains were broken in milling, implying an original grain size in excess of 200 µm. Faint oscillatory zoning and some inherited cores could be observed under oil immersion. The zircons were analysed at the Unit for Isotope Geology, GSF, using the analytical methods described by Vaasjoki et al. (1991) with the modification that the data were reduced using the ISOPLOT program (Ludvig 1988).

The zircons exhibit the characteristic features of magmatic zircons: the abraded fractions are the least discordant and the degree of discordancy increases with the increase in

Fig. 20. Magmatic zircons from sample A1288 Järvenpää. Field of view 3 mm wide.

uranium content as the density, owing to the increased metamictization, decreases. The $^{206}Pb/^{204}Pb$ ratio measured is rather high, implying that the exact composition of the common lead correction has no bearing on the age. Moreover, the mean standard error of the weighted deviate (MSWD) is only marginally in excess of 1, indicating that the zircons probably derive from a single source. Thus the upper intercept age, 1881 ± 4 Ma, for the quartz diorite A1288-Järvenpää can be regarded as denoting the time of magmatic emplacement recorded by that sample (Fig. 21, Table 1).

Metamorphism

The arenaceous primary composition of the metasedimentary rocks in the subarea is not very favourable for the crystallization of porphyroblasts. However, in the course of accurate mapping of metamorphism a fairly dense network of outcrops with porphyroblasts was established. In the subarea, metamorphism took place in the equilibrium field of garnet and cordierite, and whenever the composition of the rocks allows, sillimanite, too, seems to be a phase in equilibrium with the above minerals.

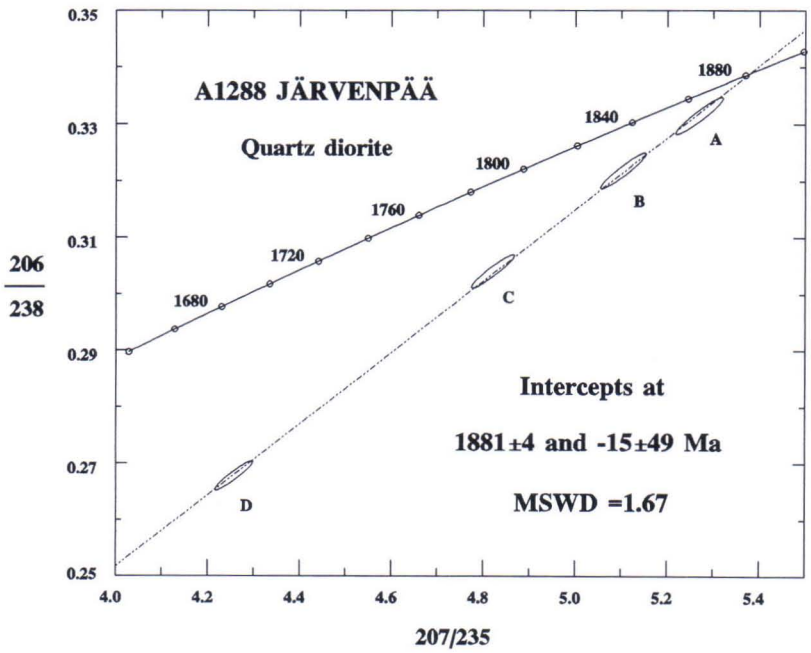

Fig. 21. Concordia diagram of U-Pb zircon data from a syntectonic quartz diorite (Fig. 18) in Stormi subarea. (sample A1288 Järvenpää.)

Table1. U-Pb zircon data on granitoid rocks in the Tampere-Vammala area.

Sample	Fraction	Uconc	Pbconc	206/204	206/238	207/235	207/206	Apparent age in Ma		
	ppm	ppm	meas.	Corrected for blank			6/8	7/5	7/6	
A1288 Järvenpää (Quartz diorite)										
A	+4.5/abr	231.1	77.74	6234	.3315	5.269	.1153	1845	1863	1884
B	+4.5	242.0	78.76	5956	.3218	5.104	.1150	1798	1836	1880
C	4.3-4.5	396.6	122.87	3175	.3040	4.821	.1150	1711	1788	1880
D	4.2-4.3	705.7	200.76	1208	.2678	4.258	.1153	1529	1685	1884
A1290 Aluskylä (Porphyritic granite)										
A	+4.5/abr	229.4	76.75	7089	.3271	5.158	.1144	1824	1845	1870
B	+4.5	257.8	84.98	6495	.3227	5.082	.1142	1803	1833	1867
C	4.3-4.5	367.5	119.66	4799	.3179	4.996	.1140	1779	1818	1863
D	4.2-4.3	700.8	206.41	3249	.2862	4.490	.1138	1622	1729	1860

Common lead correction: $^{206}Pb/^{204}Pb$:15.7; $^{207}Pb/^{204}Pb$:15.3; $^{208}Pb/^{204}Pb$:35.2

Despite the high metamorphic grade, relicts of sillimanite and potassium feldspar that crystallized in the decomposition reaction of muscovite still exist in the Stormi subarea. These sillimanites are oriented parallel to S_1; fibrolite aggregates folded by F_2 occur as relicts in syn-D_2 cordierite porphyroblasts, and potassium feldspars have S_1 relicts as the S_i structure (Fig. 22a). Prograde cordierite started to crystallize syntectonically with D_1, and porphyroblasts continued to crystallize during D_2. The potassium feldspars kept on crystallizing as inclusion-free grains during the crystallization of syn-D_2 cordierite (Fig. 22a).

Garnet crystallized in rocks of the subarea in the course of a long period. The oldest garnet grains probably crystallized during D_1, the S_1/S_2 composite schistosity being deflected around garnet grains (Fig. 22b). Most of the garnets, however, crystallized, at least partly, after D_2 (Fig. 22c). In zones of intense D_3 there are large garnet grains that still continued to grow during that stage, as they are abundant even in migmatizing granite veins associated with D_3.

A feature typical of the migmatites in the Stormi subarea is the alteration of garnet into cordierite along the margins. It has not been possible, however, to connect this reaction, which indicates a drop in pressure, with any definite deformation event. The cordierite porphyroblasts formed in this way are pseudomorphs after garnet and the mutual relationship between the porphyroblast and the matrix thus are also a relict feature. Other retrograde reactions are the biotitization of cordierite and occasional minor crystallization of andalusite. Retrograde muscovite occurs in the north of Stormi as it does in the Ellivuori subarea.

Migmatization

Migmatization started in the area immediately after D_1. As time passed the width of the veins increased and the veins became richer in potassium feldspar. Most of the veins are tonalitic or trondhjemitic in composition and D_1-D_2 in age (Fig. 17b), but in

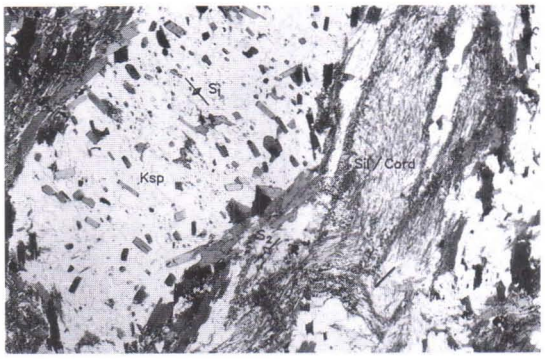

Fig. 22a. Relicts of potassium feldspar-sillimanite metamorphism in migmatitic metasedimentary rock of Stormi subarea (Fig. 16). One nicol. X = 6797.25, Y = 2451.20. Field of view 4 mm wide.

Fig. 22b. Crystallization of pre- or early-D_2 garnet in metasedimentary rock. Stormi subarea (Fig. 16). One nicol. X = 6797.20, Y = 2451.45. Field of view 12 mm wide.

Fig. 22c. Garnet grain partly crystallized on S_2 biotite scales of metasedimentary rock. Stormi subarea (Fig. 16). One nicol. X = 6801.20, Y = 2451.75. Field of view 4 mm wide.

zones of intense D_3 the strongest migmatization did not occur until during D_3 (Figs 17b and 17c). The D_3 veins are distinctly rich in potassium feldspar and occur not only in S_3 axial planes but also by imitating older structures (Figs 17c and 17d). In relation to the temperatures suggested by thermometers, the degree of migmatization is fairly high in the Stormi subarea. As a heat-consuming event migmatization obviously effectively buffered the rise in temperature (Kilpeläinen et al. 1994). As suggested by the isotope ratios of carbon and oxygen measured from the calcite concretions in metasedimentary rocks, the intense migmatization in the area is related to an increase in aqueous fluid flow as well as with a rise in temperature. The ^{18}O compositions are completely homogenized, but the abundance of ^{13}C varies greatly, implying exchange reactions with an hydrous fluid poor in CO_2 (J. Karhu, pers. comm.).

Figure 23 shows a simplified and partly interpreted summary of the crystallization of porphyroblasts and of migmatization stages in migmatic metasedimentary rocks of the Stormi subarea. As a reaction indicating a drop in pressure, the alteration of garnet into cordierite has been interpreted as being associated with F_2 antiforms. The crystallization of andalusite and late muscovite has been attributed to D_3, as suggested by Kilpeläinen et al. (1994). Local S_2 schistosities associated with D_2 shear zones are not included in the figure. The ages of deformation events are based on evidence given elsewhere in the present work.

P-T determinations

In the course of metamorphic detail mapping of the subarea, a total of 830 electron microanalyses were made on 112 samples collected from garnet-bearing outcrops in the central parts of the area and from drill cores (Kilpeläinen & Rastas 1992). Most of the garnets analysed had crystallized pre-syn D_2,

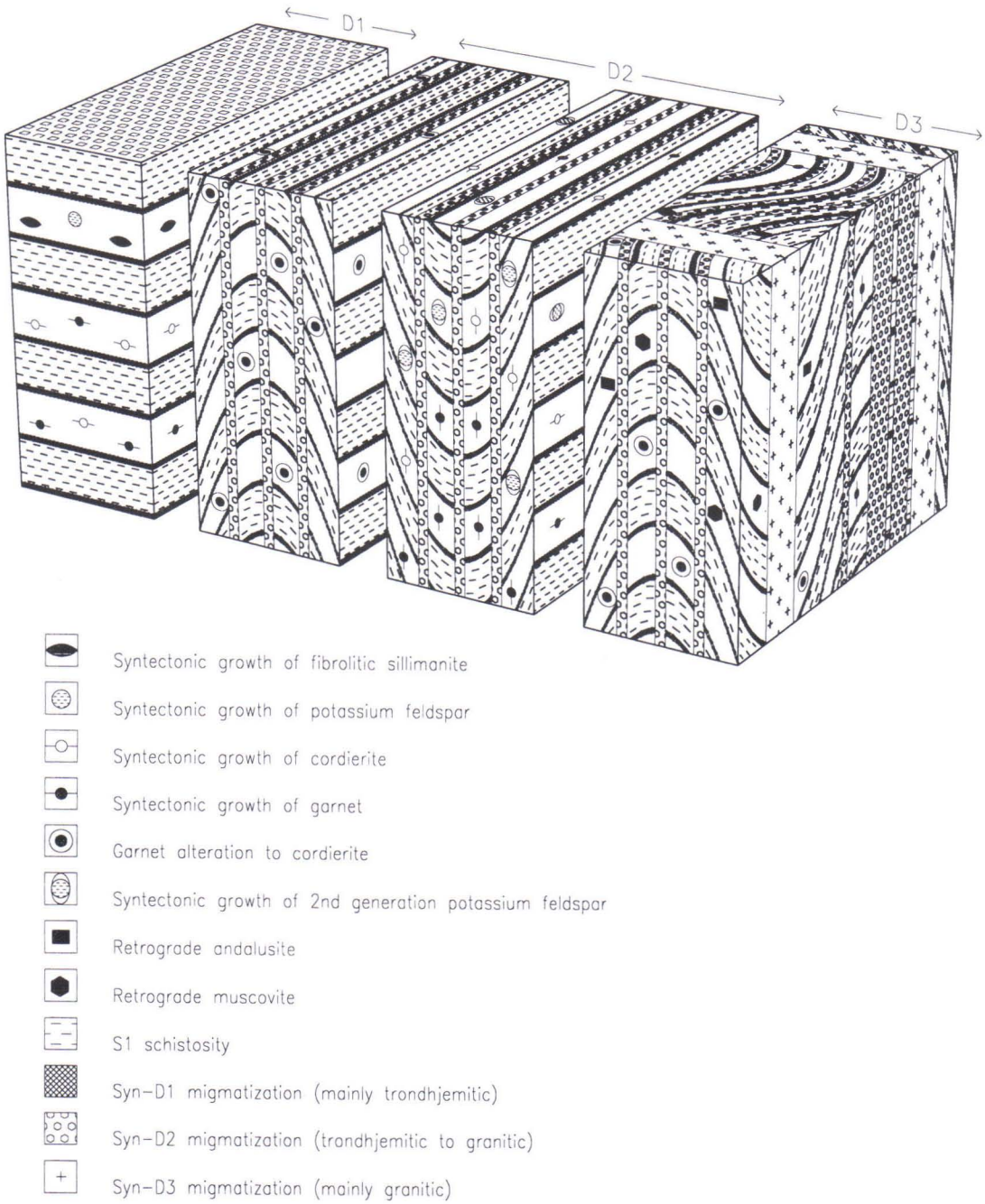

Fig. 23. Simplified summary of relations between crystallization of porphyroblasts, migmatization stages, and tectonic structures in migmatitic metasedimentary rocks of Stormi subarea (Fig. 16).

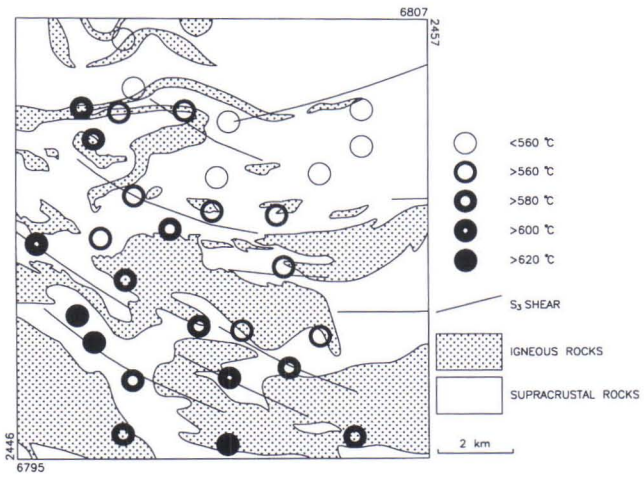

Fig. 24. Garnet-biotite temperatures from central part of Stormi subarea (Fig. 16). Lithology same as in structural maps of Stormi and Ellivuori subareas. Perchuk & Lavrenteva (1983) calibration.

but due to the poor outcrops, the relative crystallization age could not be established for all the garnets. Some samples contained young, syn-D_3 garnets, which yielded temperatures well above the average. Shown in Fig. 24 are garnet-biotite temperatures for regional mapping samples (Append. 1 and 2) of the Stormi subarea calculated as proposed by Perchuk & Lavrenteva (1983). Absolute values calculated with some other calibration method might differ from these, but the mutual relative differences between the observation points would still be similar. The highest temperatures at the southwestern edge of the image were obtained from samples in which garnets were D_3 in age or at least continued to crystallize during D_3.

Garnet chemistry of the supracrustal rocks at the contact of the Stormi ultramafite

During the metamorphic mapping, a set of 19 samples covering 190 m of core length was taken from a hole drilled in the mine from the contact of the ultramafic Stormi formation perpendicularly into the mica gneisses. Neither the mineral compositions analysed from the profile nor the thermometer determinations (Fig. 25) could show a distinct contact effect, the values being fully compatible with those obtained elsewhere in the Stormi subarea (Kilpeläinen & Rastas 1992). We can explain the lacking, or at least unrecognizable, contact metamorphism by assuming that the ultramafites intruded before the peak of regional metamorphism, a concept supporting the estimated pre-D_2 age of the formation based on structural considerations.

Since earlier studies had reported an increase in garnet abundance in mica gneisses towards the contact of the Stormi ultramafite (Häkli et al. 1979), efforts were made to search for the contact effect in a mica gneiss sample taken 2 m from the contact of the ultramafite. A garnet grain poor in inclusions and slightly altered into cordierite along the margins was selected for analysis. The intention was to find the type of zonal composition in garnet that might develop in a grain starting to crystallize in the contact metamorphosis of the intrusion and that might continue to grow during regional metamorphism. Three profiles running in different directions from the centre of the grain towards the margins were analysed at 0.2-mm point intervals. The profiles were chosen in such a manner that the garnet was in contact with a different mineral species at the last

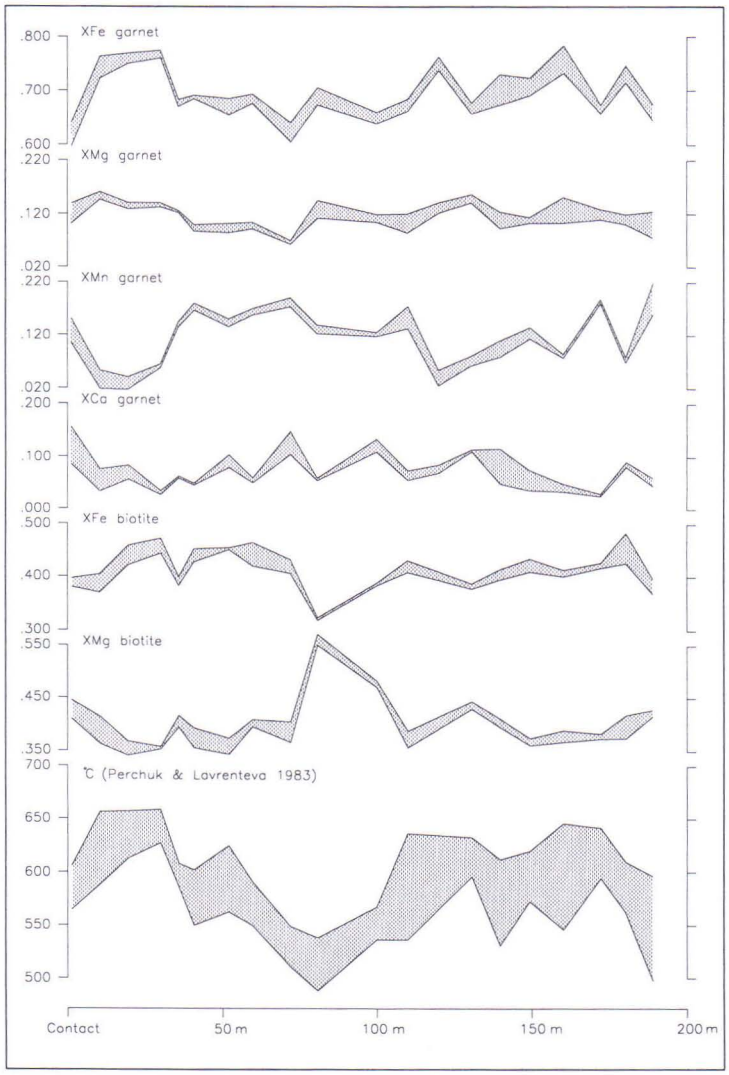

Fig. 25. Compositions of garnets and biotites in mica gneisses and crystallization temperatures calculated from them. Samples taken from a hole VA-925 drilled from contact of Stormi ultramafite directly into mica gneiss. The variation in thickness of composition curves is due to the variation in composition measured at a given point; that in the temperature curve is due to the variation in temperature obtained with different mineral/measurement data combinations.

point on each profile.

Figure 26 shows the location of the profiles and the mole fractions of Fe, Mg, Mn and Ca at each analysis point. Excluding the narrow diffusion seam at the margin of the grain developed during cooling, the composition varied only slightly within the grain. Note that Mg-Fe cation exchange seems also to have happened in the profile ending to plagioclase. The most likely reason is that there was an Mg- and Fe-bearing mineral either above or below the polished section

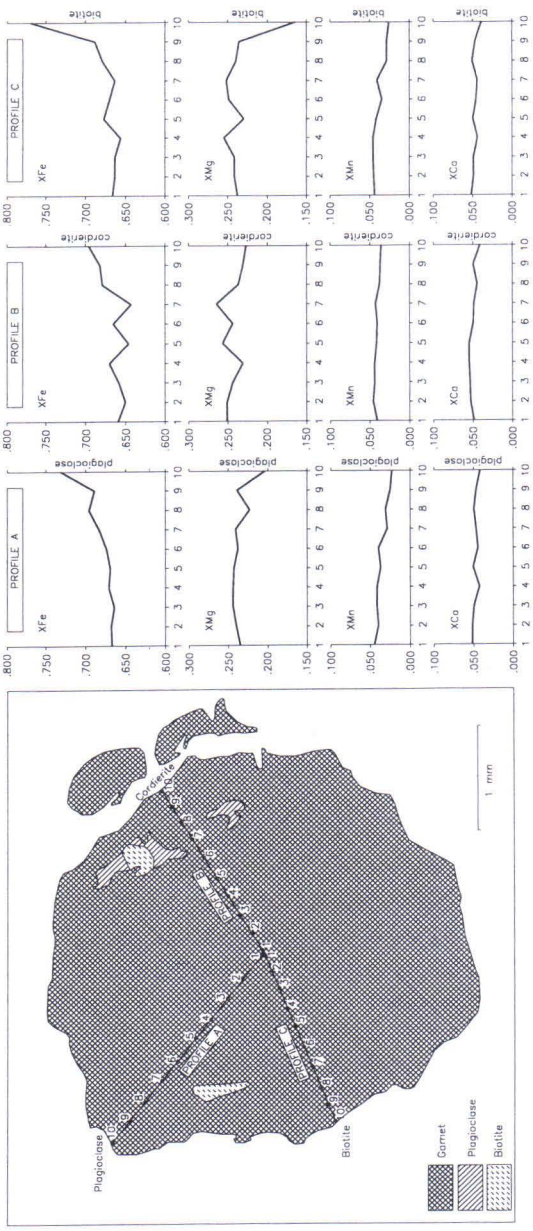

Fig. 26. Composition profiles in a garnet grain in mica gneiss 2 m from contact of Stormi ultramafite. Drill hole VA-408.

used for analysis with which the cation exchange took place. As far as the method applied is concerned, no variation in temperature occurred during the crystallization of garnet and the grain can be interpreted to have crystallized or compositionally homogenized entirely during regional metamorphism.

Koosanmaa subarea

General geology

The Koosanmaa subarea, in the south of the study area, lies at the southern border of the Pori-Vammala-Mikkeli tonalite migmatite zone (Figs 2 and 27). The supracrustal rocks of the area are mostly distinctly layered metasedimentary rocks that have not been migmatized as intensely as those in the Stormi subarea. In structural and metamorphic evolution, however, the area closely resembles the Stormi subarea, although the variation in metamorphic grade is markedly greater. It is the variation in metamorphic grade without tectonic discordances that makes the Koosanmaa subarea appropriate for studying the change in type of deformation structures as a function of metamorphic grade.

As well as supracrustal rocks, the subarea, its southern edge in particular, contains quartz diorite and granodiorite intrusions of various sizes and shapes. None of them have been dated, but in appearance they are typical synkinematic intrusions of the Pori-Vammala-Mikkeli zone, i.e. moderately gneissose and on the whole fairly equigranular plutonic rocks. Mafic and ultramafic intrusions are particularly numerous in the east of the subarea. The best known of them, Kylmäkoski, is a mined-out Ni-bearing, predominantly ultramafic intrusion with a Pb-Pb age on the chalcopyrite fraction of 1856(+177,-203) Ma (Papunen 1980).

Associated with the Kylmäkoski ultramafic intrusion is a small quartz diorite intrusion whose age in relation to structural evolution differs from the ages of other quartz diorites and granodiorites in the area (see later). Microcline granite intrusions are virtually lacking. A potassium feldspar porphyritic, slightly gneissose granite (Matisto 1967) extends to the northern edge of the subarea but it bears a close resemblance to the coarser portions of the porphyric granodiorites at Karkku and Nokia described earlier. There are also microcline granites in the area but they tend to occur as crosscutting dykes less than 1 m wide.

The lowest metamorphic conditions in the western part of the subarea occurred in the equilibrium field of potassium feldspar and sillimanite, but in the more intensely metamorphosed metasedimentary rocks in the east, garnet and cordierite form an equilibrium pair. The amount of migmatization follows roughly the change in metamorphic grade. However, as in the Stormi subarea, migmatization is in places more intense than suggested by the metamorphic grade.

Deformation - D_1, D_2, D_3 and Equal area projections

D_1 - The oldest recognizable deformation and metamorphic structure is the penetrative schistosity (S_1) caused by biotite scales parallel to the layering of the supracrustal rocks. It is visible in all metasedimentary rocks with the appropriate composition but the lower the metamorphic grade, the less well it is developed. In potassium feldspar-sillimanite gneisses, S_1 is just about macroscopically visible (Fig. 28a), but in thin sections it is always recognizable, at least as an S_1 structure of potassium feldspar porphyroblasts (Fig 28b). With the increase in metamorphic grade, S_1 is intensified and in potassium feldspar-cordierite gneisses it is the dominant schistosity (Figs 28c and 28d).

One outcrop in the subarea exhibits the minor hinge of a pre-D_2 fold that is probably related to the same event as the formation of S_1 schistosity. As this fold is the only one observed and is, moreover, fairly modest in size (W~2 cm, A~5 cm), it cannot be used as a basis for interpreting the nature and implication of F_1 folding. The possibility that the structure is synsedimentary is, however, not fully excluded. The present structure of the

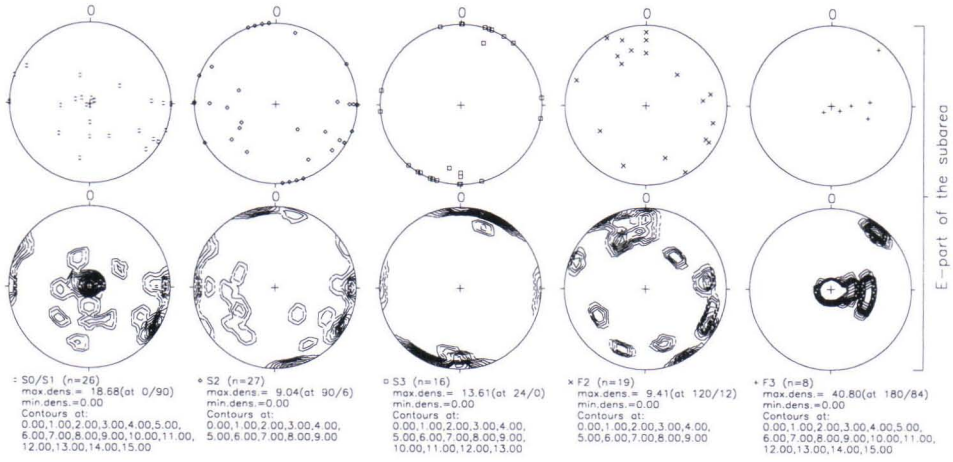
E-part of the subarea
: S0/S1 (n=26)
max.dens.= 18.68(at 0/90)
min.dens.=0.00
Contours at:
0.00,1.00,2.00,3.00,4.00,5.00,
6.00,7.00,8.00,9.00,10.00,11.00,
12.00,13.00,14.00,15.00
* S2 (n=27)
max.dens.= 9.04(at 90/6)
min.dens.=0.00
Contours at:
0.00,1.00,2.00,3.00,4.00,
5.00,6.00,7.00,8.00,9.00
□ S3 (n=16)
max.dens.= 13.61(at 24/0)
min.dens.=0.00
Contours at:
0.00,1.00,2.00,3.00,4.00,
5.00,6.00,7.00,8.00,9.00,
10.00,11.00,12.00,13.00
× F2 (n=19)
max.dens.= 9.41(at 120/12)
min.dens.=0.00
Contours at:
0.00,1.00,2.00,3.00,4.00,
5.00,6.00,7.00,8.00,9.00
+ F3 (n=8)
max.dens.= 40.80(at 180/84)
min.dens.=0.00
Contours at:
0.00,1.00,2.00,3.00,4.00,5.00,
6.00,7.00,8.00,9.00,10.00,11.00,
12.00,13.00,14.00,15.00

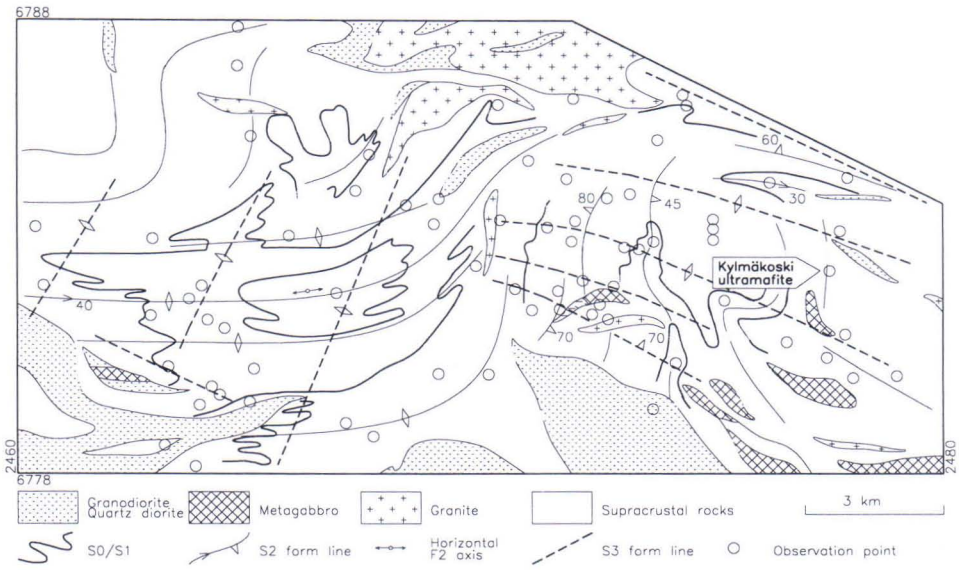
6788
6778
2460
2480
60
80
45
30
40
70
70
Kylmäkoski
ultramafite
Granodiorite
Quartz diorite
Metagabbro
Granite
Supracrustal rocks
3 km
S0/S1
S2 form line
Horizontal
F2 axis
S3 form line
Observation point

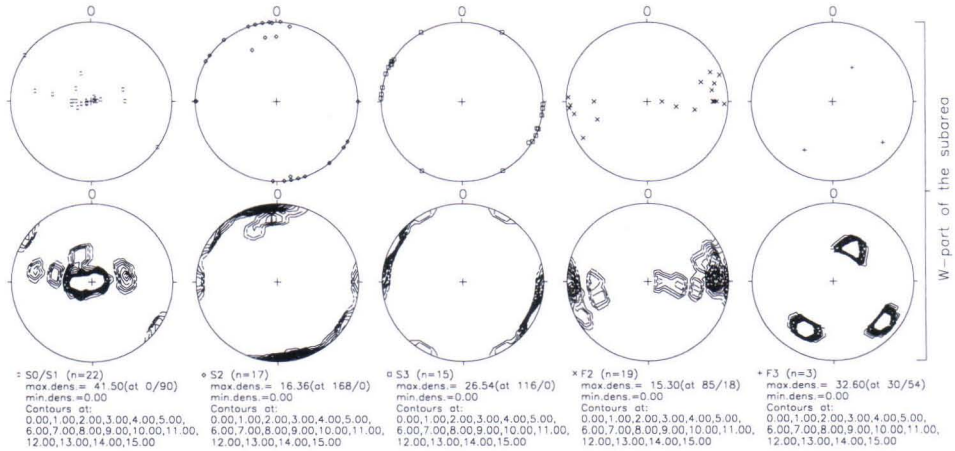
W-part of the subarea
: S0/S1 (n=22)
max.dens.= 41.50(at 0/90)
min.dens.=0.00
Contours at:
0.00,1.00,2.00,3.00,4.00,5.00,
6.00,7.00,8.00,9.00,10.00,11.00,
12.00,13.00,14.00,15.00
* S2 (n=17)
max.dens.= 16.36(at 168/0)
min.dens.=0.00
Contours at:
0.00,1.00,2.00,3.00,4.00,5.00,
6.00,7.00,8.00,9.00,10.00,11.00,
12.00,13.00,14.00,15.00
□ S3 (n=15)
max.dens.= 26.54(at 116/0)
min.dens.=0.00
Contours at:
0.00,1.00,2.00,3.00,4.00,5.00,
6.00,7.00,8.00,9.00,10.00,11.00,
12.00,13.00,14.00,15.00
× F2 (n=19)
max.dens.= 15.30(at 85/18)
min.dens.=0.00
Contours at:
0.00,1.00,2.00,3.00,4.00,5.00,
6.00,7.00,8.00,9.00,10.00,11.00,
12.00,13.00,14.00,15.00
+ F3 (n=3)
max.dens.= 32.60(at 30/54)
min.dens.=0.00
Contours at:
0.00,1.00,2.00,3.00,4.00,5.00,
6.00,7.00,8.00,9.00,10.00,11.00,
12.00,13.00,14.00,15.00

Fig. 27.

Fig. 28a. F_2 folding with east-west-striking axial plane in least metamorphosed metasedimentary rocks of western part of Koosanmaa subarea (Fig. 27). West upwards. X = 6780.35, Y = 2465.05. Code bar 6 cm.

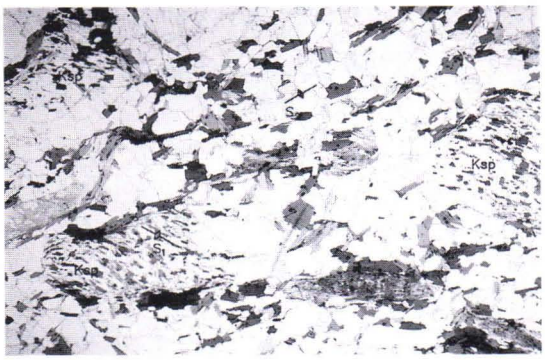

Fig. 28b. S_1 as S_1 structure in potassium feldspar porphyroblasts in metasedimentary rock. Note that the sample is from a limb of F_2. Koosanmaa subarea (Fig. 27). One nicol. X = 6783.05, Y = 2472.00. Field of view 12 mm wide.

Fig. 28c. F_2 folded potassium feldspar-cordierite gneiss. Eastern part of Koosanmaa subarea (Fig. 27). The layering is still recognizable. North upwards. X = 6780.25, Y = 2474.45. Code bar 6 cm.

Fig. 28d. Thin section cut from hinge of F_2 fold in Fig. 28c perpendicular to F_2 axis. Koosanmaa subarea (Fig. 27). One nicol. X = 6780.25, Y = 2474,45. Field of view 12 mm wide.

subarea can best be explained by assuming that even after D_1 the layering and S_1 were still subhorizontal.

D_2 - During the second deformation stage the above structures folded with a horizontal, east-west-striking axis due to a horizontal north-south compression. F_2 axes then assumed a horizontal attitude and the axial planes a vertical one. On the limbs of F_2 folds the layering and S_1 turned from their original position, becoming vertical, with the consequence that the limbs now exhibit S_0, S_1 and S_2 approximately parallel to each other. The subparallelism of the limbs and axial planes implies tight F_2 folding. The size of the F_2 folds can be visualized only on aerogeophysical maps, on which the S_0/S_1 structure of metasedimentary rocks is readily recognizable. On the basis of geophysical maps, the wavelength of the folds is of the order of kilometres, and, due to the tightness of the folding, the amplitude is probably of the same order of magnitude. Depending somewhat on the section, the F_2 structures on the

Fig. 27. Form line map of Koosanmaa subarea and lower hemisphere projections of structures shown on it. Lithology modified from Matisto (1973).

Fig. 28e. F_2 folding with horizontal axes in migmatized metasedimentary rock. Eastern part of Koosanmaa subarea (Fig. 27). East upwards. X = 6780.35, Y = 2474.35. Code bar 6 cm.

Fig. 28f. Fragments of layers of metasedimentary rock (porphyroclasts) containing S_1 schistosity as S_i. Central part of Koosanmaa subarea (Fig. 27). One nicol. X = 6782.50, Y = 2469.90. Field of view 12 mm wide.

Fig. 28g. Incipient crystallization of potassium feldspar in a layer fragment like that in Fig. 28f. Koosanmaa subarea (Fig. 27). One nicol. X = 6780.35, Y = 2465.05. Field of view 4 mm wide.

outcrops are folds with fairly sharp hinges, whose axes are still gently plunging despite post-D_2 deformation (Figs 28a, 28c and 28e).

The axial plane properties of the F_2 folds depend mainly on the M_1 metamorphic grade. As the intensity of S_2 varies zonally across a fold, its character varies considerably from one outcrop to another. In the least intensely metamorphosed metasedimentary rocks, S_2 approaches penetrative biotite schistosity, which, while evolving, fragmented narrow competent layers and their S_1 schistosity. The fragments of these layers occur as rotated porphyroclasts around which S_2 schistosity is deflected and in whose pressure shadows the syn-D_2 recrystallization of minerals occurred under conditions clearly more static that those in the adjacent zones of intense deformation (Figs 28f and 28g).

In potassium feldspar-sillimanite gneisses, S_2 is usually a discrete type of crenulation or in places penetrative biotite schistosity (Fig. 28b). In the potassium feldspar-cordierite gneisses and more intensely metamorphosed metasedimentary rocks, S_2 is a crenulation that does not seem to have been accompanied by substantial biotite crystallization, especially in the fold hinges (Fig. 28d). On the limbs of F_2 folds, S_2 is naturally more intense, but in those cases it is difficult to distinguish between S_1 and S_2 biotites. Even if F_2 structures were invisible in an outcrop, S_2, or most commonly $S_0/S_1/S_2$ composite would be recognizable, at least in thin sections, on the basis of the S_1 biotites in potassium feldspar porphyroblasts (Fig. 28b).

D_3 - The structures described above are deformed in the Koosanmaa subarea by two foldings similar in character but very different in trends. In the west of the area, the axial planes of the cutting folds are vertical and strike about 30°. In general the folds are fairly open, the plunges of fold axes depending on the geometry of the older structures. Folding deformed the plunges of F_2 axes, causing the axial depression of a roughly 5-

km-long F_2 synform to develop in the western part of the area (Fig. 27). The structure is also clearly visible on magnetic maps (Fig. 3), as the current plunge of the F_2 axes may be up to 45° at the ends of the axial depression.

In the east of the subarea, the axial plane of post-D_2 folding strikes about northwest-southeast. The present interference structure is more complicated in the east than in the west, mainly due to the low angle between the axial planes of the F_2 and F_3 folds (Figs 27 and 28c). Owing to the greater homogeneity and more intense metamorphism of the sedimentary rocks, the total structure cannot be interpreted very well from magnetic maps. On the basis of F_2 and F_3 axes measured on outcrops, the large F_2 antiform in the east of the area was deformed during F_3, making the F_2 axes culminate in the middle of the subarea. Associated with D_3 in the east is a distinctly sinistral horizontal component, which further complicates the present total structure.

Only a few observations have been made of the crosscutting relations of these two post-D_2 foldings, as both of them occur almost exclusively in their own areas. There is one outcrop at the western margin of the subarea on which it is seen that the folding with a 30° strike has a northwest-southeast conjugate, too. If this northwest-southeast structure is the same as D_3 in the east, the two D_3's would constitute a conjugate pair, which would explain why both of the S_3 axial strikes occur almost solely in their own areas.

Neither of the above F_3's is accompanied by axial plane schistosity, but instead by intense migmatization in the same way as in the Stormi subarea. As at Stormi, the zones of intense D_3 are broad ductile shear zones and mainly dominated by schollen and schlieren migmatites; no cataclastic D_3 shears have been observed on outcrops.

Equal area projections - Mainly due to the dissimilarity in the mode of occurrence of D_3 structures, the stereograms in Fig. 27 are given separately for the western and eastern parts of the subarea. In the west, the axial planes of F_3 folds almost invariably strike northeast-southwest. However, the effect of D_3 on the older structures was relatively mild, the S_2 planes, for example, having rotated only slightly from their primary east-west attitude. The shallow dips of the layering and the parallel S_1 are shown not only by the S_0/S_1 projection points but also by the low angles of the plunge of the F_2 axes.

In the east, the axial planes of F_3 folds locally strike northwest-southeast. The effect of D_3 was substantially stronger than in the western part, because the projection points of pre-D3 structures show only slight regularity. The S_0/S_1 planes are typically subhorizontal, but some of the F_2 folds are slightly tilted, suggesting some vertical movement associated with D_3.

Igneous rocks

There are several quartz diorite and granodiorite intrusions of various size at the southern edge of the subarea. The majority are equigranular but distinctly gneissose and they commonly contain mafic enclaves elongated along schistosity. The contacts of supracrustal rocks with the above granitoids are not exposed in the area, but quartz diorites and granodiorites do occur as dykes in the metasedimentary rocks, having intruded along the axial planes of F_2 folds. In the gneissic intrusions, the gneissosity was deformed during F_3 folding, from which it is inferred that the intrusions must predate D_3. The potassium feldspar porphyritic granite at the northern edge of the subarea is also clearly gneissose, at least in places, but its age relation to the quartz diorites and granodiorites has not been established.

A small quartz diorite intrusion associated with the mined-out Kylmäkoski Ni deposit

Fig. 29a. Pre- or early-D_1 ultramafic dyke in migmatitic metasedimentary rock. Western part of Koosanmaa subarea (Fig. 27). Viewed towards south. X = 6781.85, Y = 2463.80. Code bar 6 cm.

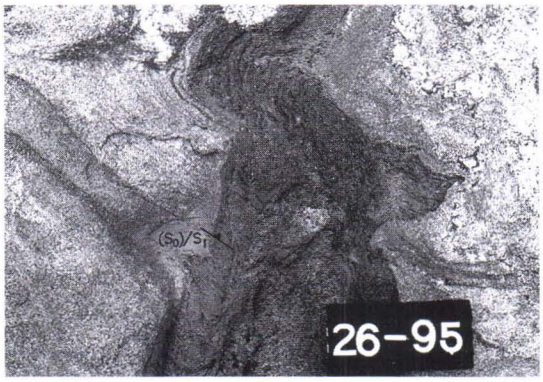

Fig. 29b. Detail of dyke in Fig. 29a. The dyke cuts S_0 in metasedimentary rock and the dyke is cut by S_1. It must therefore have intruded during D_1 at the latest. Code bar 6 cm.

clearly differs from the other quartz diorites in age. The rock is equigranular and fine-grained and, unlike the typical synkinematic plutonites in the area, nonfoliated and in places pinkish. At present it is exposed only at the northern end of the water-filled open pit, but Papunen (1980) maintains that it cuts other structures. Its relations to supracrustal structures cannot yet be established more accurately, but its cutting attitude and nonfoliation suggests that it is younger than other quartz diorites mentioned above.

Pre- or Early-D_2 mafic and ultramafic rocks occur as dykes and sills, particularly in the migmatites of the high-grade metamorphism in the east. In the west of the subarea there is a fairly narrow dyke that was probably originally ultramafic but is now strongly altered by metamorphism and deformation. In places it cuts the layering of the metasedimentary rocks, exhibiting, however, distinct S_1 schistosity (Figs 29a and 29b). According to Papunen (1980), the Kylmäkoski ultramafic intrusion is a trough-shaped formation whose contact with the mica gneisses "curves smoothly and in many places varies surprisingly as small scale folds that vary in axial direction as do folds in migmatite environment". Observations made at the mine show that the trough-shaped structure of the intrusion is a F_2 synform, implying that the contacts of the formation are conformable with S_1 schistosity. The intrusion must, therefore, be either D_1 in age or older still. Small intrusions, mainly gabbros in composition, occur throughout the subarea. Their contacts with the metasedimentary rocks are not exposed, but they are distinctly metamorphosed as will be shown in the next chapter and thus relatively old in terms of structural evolution

Granites commonly occur as dykes less than 1 m wide in the supracrustal rocks of the subarea. They cut all the other deformation structures described above. In the west of the area in particular, their strikes exhibit a clear consistency, trending almost invariable 0-30°, irrespective of the geometry of the host rock structures. In the east of the area their strike is less regular. Minor granite dykes also occur in the east, in the axial planes of F_3 folds.

Metamorphism and migmatization

The least metamorphosed rocks in the subarea are in the western part. Broadly speaking, they occur at the southern part of the local F_2/F_3 interference basin mentioned in the structural description. The most intensely metamorphosed rocks are in the east,

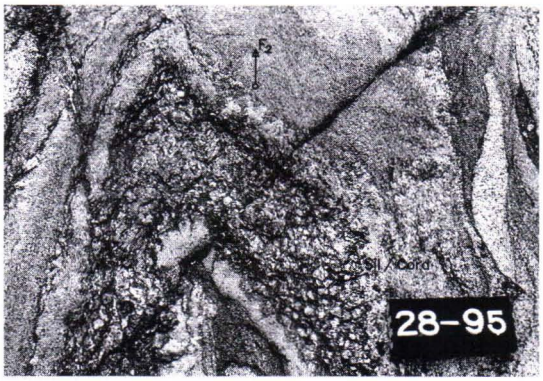

Fig. 30a. Fibrolitic sillimanites deformed by F_2 and altered into cordierite in mica gneiss. Eastern part of Koosanmaa subarea (Fig. 27). Northwest upwards. X = 6780.25, Y = 2474.45. Code bar 6 cm.

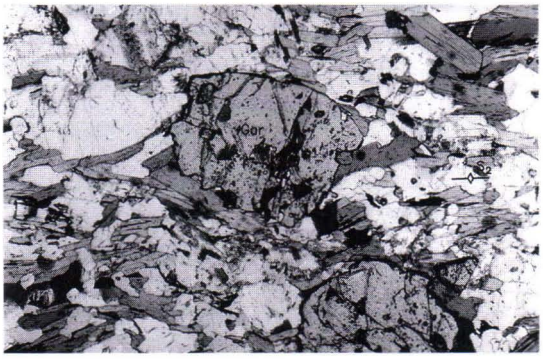

Fig. 30b. Garnets crystallized on S_2 schistosity of metasedimentary rock near closed Kylmäkoski mine. Koosanmaa subarea (Fig. 27). One nicol. X = 6782.85, Y = 2477.65. Field of view 4 mm wide.

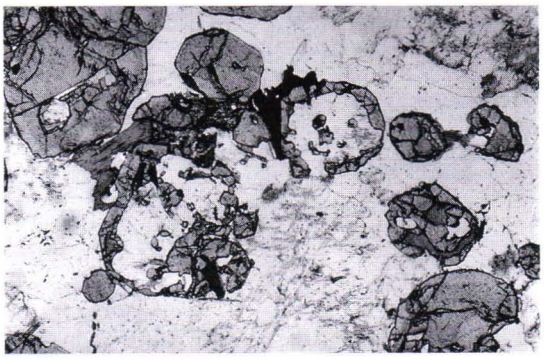

Fig. 30c. Raspberry-structured garnets in metagabbro. Northwestern part of Koosanmaa subarea (Fig. 27). One nicol. X = 6784.30, Y = 2467.35. Field of view 4 mm wide.

which, according to the structural interpretation, represents the deepest section (F_2 antiform). This, together with observations of the crystallization of the earliest porphyroblasts, implies that metamorphism, at least, started before D_2 folding. The situation is not that simple, however, for in many places in the area there are features demonstrating that the temperature increased or remained elevated during D_3.

As shown by the porphyroblasts, the lowest metamorphic grade is represented by the potassium feldspar-sillimanite mica schists in the west. Pseudomorphs, totally altered by retrograde metamorphism, have been encountered in one outcrop. These may have been andalusite grains, but, due to their complete muscovitization, they can no longer be reliably identified. Sillimanite that formed through the decomposition of muscovite crystallized into fibrolite aggregates parallel to S_1, and these in turn deformed during F_2 folding (Figs 28d and 30a). Potassium feldspar crystallized on S_1 schistosity and preserved fine-grained S_1 biotite schistosity as an S_1 structure (Fig. 28b). In places, the potassium feldspar grains have used fragments of the layers mentioned in the description of D_2 structures as their crystal nuclei (Figs 28f and 28g). Not only S_1 biotite schistosity, but also the syn-D_1 recrystallized matrix mainly composed of quartz and feldspars then remained as the S_1 structure of the growing potassium feldspar porphyroblasts. In some places, crystallization of potassium feldspar proceeded so far that, with the exception of the biotite scales, the S_1 structure disappeared.

As the temperature continued to rise, biotite started to decompose and cordierite crystallized on sillimanite grains, sillimanite needles remaining in cordierite as inclusions (Fig. 28d). The margins of cordierite crystallized clearly on S_1 biotites, but were deformed during D_2 (Fig. 28d). A sample taken from the potassium feldspar-cordierite zone

Fig. 30 d. Syn-D_1 and syn-D_2 migmatization in metasedimentary rock. Koosanmaa subarea (Fig. 27). East upwards. X = 6781.55, Y = 2463.20. Code bar 6 cm.

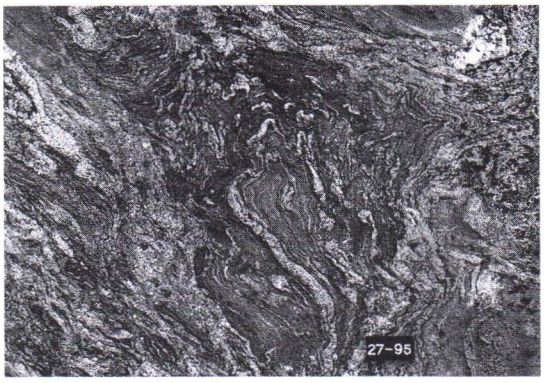

Fig. 30e. Syn-D_3 migmatization cuts F_2 folds and older migmatization in metasedimentary rock. Koosanmaa subarea (Fig. 27). East upwards. X = 6782.15, Y = 2463.95. Code bar 6 cm.

on the limb of an F_2 fold (Fig. 28b) shows how the evolving S_2 controlled the crystallization of cordierite, causing the grains to be elongated parallel to S_2. The S_1 biotite inclusions in the potassium feldspar porphyroblasts that formed in the decomposition reaction of muscovite survived, although new, inclusion-free potassium feldspar grew at the same time as cordierite syntectonically with D_2, the growth commonly having started in the pressure shadows of older potassium feldspar grains.

Garnet crystallized in the supracrustal rocks of the subarea over a long period. The oldest garnets clearly started to crystallize before the "completion" of S_1/S_2 composite schistosity, but some of the garnets, and also the margins of older garnet grains, grew over the S_1/S_2 schistosity (Fig. 30b). Metamorphic garnets occur in some metamorphosed plutonites in the subarea. Because of the coarse matrix, it is difficult to pinpoint when the garnet in them crystallized. The nucleation of the raspberry garnets must, however, have occurred in the triple junctions of already crystallized matrix and so, to minimize surface energy, the small garnets being grown around the matrix grains were later fused into one big grain (Fig. 30c) (Bard, 1987).

The mica gneisses in the subarea were migmatized throughout the structural evolution. The oldest veins are along the S_0/S_1 planes and approximately trondhjemitic in composition. The amount of earliest veining is clearly related to the metamorphic grade and to the decomposition of biotite that began with the increase in temperature, as this process is first encountered in the potassium feldspar-cordierite gneisses or more intensely metamorphosed rocks. Veins are also associated with D_2 but they are potassium feldspar-bearing and do not occur in such abundance as do the veins of syn-D_1 migmatization (Fig. 30d).

Zonal, coarse and potassium feldspar-bearing syn-D_3 migmatization is a conspicuous feature of the Koosanmaa subarea. It cuts older migmatization and F_2 fold structures, although the veins may imitate older, even S_1, structures, to some extent (Fig. 30e). Syn-D_3 migmatization is also encountered in the least metamorphosed rocks, which in view of the metamorphic grade did not undergo *in situ* melting. Owing to the low intensity of F_3 folding, it is difficult to conclude whether a zone of intense syn-D_3 migmatization could also be a zone of intense D_3 deformation. That the migmatization cuts the metamorphic zones, however, implies that deformation was associated with the fluid flow.

Hämeenkyrö subarea

General geology

The Hämeenkyrö subarea is located in the Tampere Schist Belt, no more than 20 km west of the Tampere synform area (Figs 2 and 31) yet differing from it clearly in structure and metamorphic grade. The area, which covers the southern part of the circular formation of supracrustal rocks on the Ikaalinen 1:100 000-scale map sheet, is bounded in the northeast and west by the Central Finland Granitoid Complex and in the south by the Kelhäjärvi synorogenic granitoid pluton. Most of the supracrustal rocks are weakly metamorphosed mica gneisses, in which the layering is commonly visible and which, due to the composition of sedimentary rocks, rarely

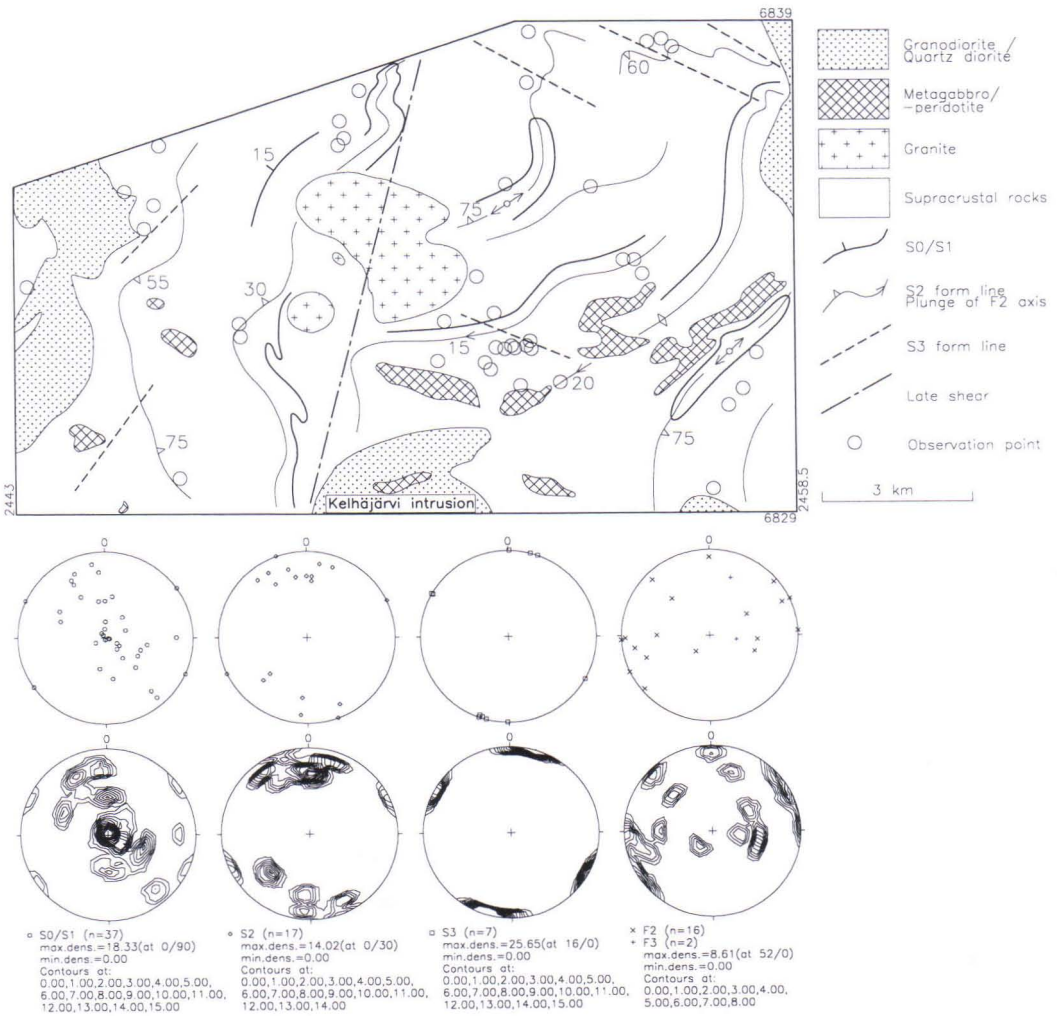

Fig. 31. Form line map of Hämeenkyrö subarea and lower hemisphere projections of structures shown on it. Lithology modified from Virransalo & Vaarma (1993).

contain porphyroblasts. The most intensely migmatized metasedimentary rocks occur at the western margin of the subarea, close to the contact with a metatonalite intrusion. They, too, are virtually devoid of porphyroblasts and in only a few outcrops have small amounts of garnet and cordierite been encountered.

Conglomerates with quartz clasts and very coarse-grained greywackes are particularly well exposed in the northwest of the area. Porphyroblastic metapelites are rare, but drilling conducted in the course of geological remapping at 1:100 000 scale revealed abundant graphite/sulphide-bearing black schist horizons that show up distinctly on magnetic and electromagnetic maps. They are not exposed in the area, but observations made elsewhere suggest that they may be early shear surfaces parallel to the layering. If so, they can be used to advantage in structural interpretations based on geophysical maps.

In addition to the above Kelhäjärvi granodiorite/quartz diorite, there are mafic and ultramafic, layered intrusions in the southeast that, according to Peltonen (1992), are fragments of a single body (sill), initially measuring 7 km x 0.5 km at an unknown depth. This formation is now composed of platy, northward dipping bodies parallel to S_2 planes and according to Peltonen facing northwards. In the south, in particular, the supracrustal rocks contain mafic dykes of various ages in relation to the structural evolution.

In the middle of the subarea there are two granite intrusions, one several square kilometres in size. Granitic dykes occur mainly in the immediate surroundings of the above intrusions only.

Deformation - D_1, D_2, D_3 and Equal area projections

The structure of the subarea and the circular Hämeenkyrö supracrustal area is largely

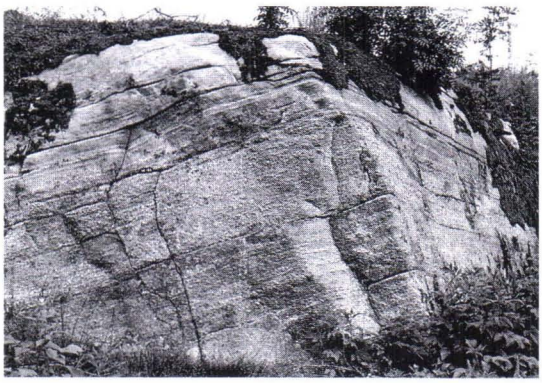

Fig. 32a. Subhorizontal S_0/S_1 in metagreywacke in northwest of Hämeenkyrö subarea (Fig. 31). Viewed towards north. X = 6837.00, Y = 2449.50. Code bar 6 cm.

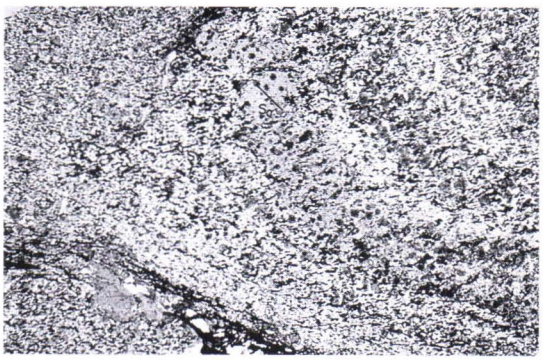

Fig. 32b. Thin section cut from hinge of F_2 fold in layered metasedimentary rock of least metamorphosed southeastern part of Hämeenkyrö subarea (Fig. 31). One nicol. X = 6832.40, Y = 2457.95. Field of view 12 mm wide.

Fig. 32c. Thin section from hinge of F_2 fold in potassium feldspar-sillimanite gneiss. Hämeenkyrö subarea (Fig. 31). One nicol. X = 6837.80, Y = 2453.20. Field of view 12 mm wide.

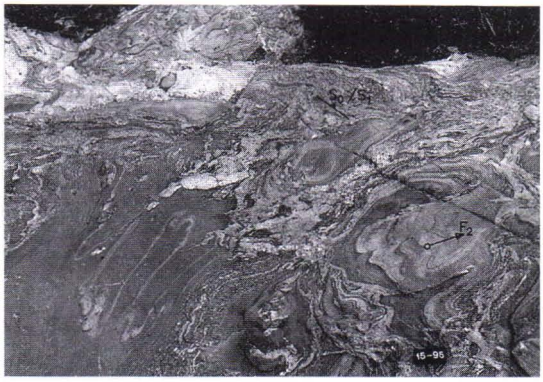

Fig. 32d. Migmatitic metasedimentary rock with intense S_1. Western part of Hämeenkyrö subarea (Fig. 31). Viewed towards north. X = 6835.35, Y 0 2445.80. Code bar 6 cm.

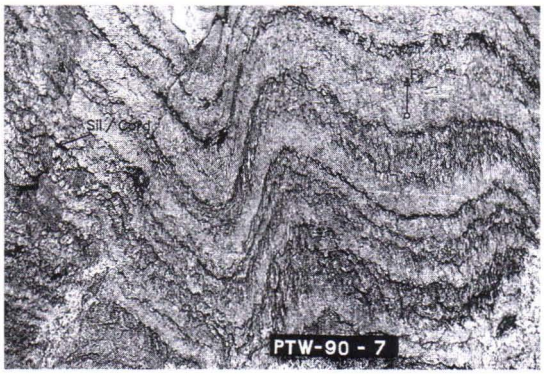

Fig. 32e. F_2 folding deforming S_0/S_1 structure in potassium feldspar-sillimanite gneiss. Hämeenkyrö subarea (Fig. 31). X = 6837.80, Y = 2453.20. Code bar 17 cm.

a result of interference by three deformation events, complicated by differences in the competences of the metasedimentary rocks arising from the marked variation in the composition of the sedimentary rocks. In the course of deformation, which caused intense folding in the finest-grained sedimentary rocks, the thick, coarse-grained metasedimentary rock piles behaved as competent bodies, like felsic plutonic intrusions, whose central parts record hardly any signatures of deformation structures. Instead, they seem to have partitioned the deformation, the finer-grained supracrustal rocks in their surroundings tending to be more intensely deformed than the coarser-grained varieties. For instance, despite the fairly intense regional deformation, the conglomerate-greywacke formations in the northwest of the subarea are almost in their original attitude (Fig. 32a), but the southern continuations of the same formation are clearly more deformed. The more intense deformation in the south may be due to a decline in the total thickness of coarse sedimentary rocks. In other words, the thick northern part of the formation may have caused intense deformation of its own continuations.

D_1 - The oldest structural feature in the subarea is the schistosity parallel to layering the intensity of which varies with the metamorphic grade. The least metamorphosed rocks either lacked S_1 or then it was so weak that later deformations and metamorphism obliterated it altogether (Fig. 32b). However, in potassium feldspar-sillimanite gneisses, S_1 was so intense that it can still be recognized if the composition of the rock is appropriate (Fig. 32c). In garnet-cordierite gneisses or in rocks roughly comparable to them in metamorphic grade as assessed from the amount of migmatization, S_1 is so intense that it can be classified macroscopically as the dominant schistosity in metasedimentary rocks (Fig. 32d).

Folds associated with D_1 have not been recognized in the subarea. As S_1 schistosity is at its strongest in the high-grade rocks, it is possible that the F_1 structures, if there were any, were obliterated by intense metamorphism. Since, however, both S_1 schistosity and even the layering have been largely preserved in the migmatites of the subarea, the obliteration of other D_1 structures is unlikely.

D_2 - The folding associated with the D_2 stage, which deforms S_1 schistosity as well as layering, is the most common deformation structure visible on supracrustal rocks in the subarea (Fig. 32e). The intensity of folding

varies greatly but the shallow plunge of the fold axis is a common feature of all F_2 folds. Excluding the greywackes and conglomerates in the northwest, the layering of the metasedimentary rocks on the limbs of the F_2 folds is now almost vertical. Hence, the F_2 folding as a whole is tight or isoclinal. The strike of axial planes varies, but the axial planes are invariably subvertical. Outcrops are poor, however, and the size of F_2 folds can be visualized only from geophysical maps. If the interpretation that F_2 folds are isoclinal is correct, the wavelength of the folds as measured on the magnetic maps is of the order of hundreds of metres.

In the metasedimentary rocks of lowest metamorphic grade, which lack S_1, S_2 is penetrative schistosity (Fig. 32b). The higher the metamorphic grade the more distinctly S_2 is crenulation, and in the most intensely metamorphosed metasedimentary rocks the S_2 biotite barely grew at all or then only by imitating older structures, with the consequence that no proper S_2 biotite schistosity developed (Fig. 32d). Owing to the tightness of F_2 folding, most of the outcrops in the subarea are located on the limbs of F_2 folds. Thus, in addition to layering, the parallel S_1/S_2 composite is visible.

D_3 - In the third deformation stage, the above structures in the northern and central parts of the subarea were compressed into fairly open folds with axial planes striking northwest-southeast. In the southwest, these folds are lacking, but corresponding folds with axial planes striking northeast-southwest occur instead. No cutting relations have been observed between these two post-D_2 foldings, implying that they may be related to the same event, thus being conjugates. This concept is supported by one observation from the north of the area, where the northwest-southeast-striking F_3 folding has a 30° striking pair in the outcrop. The axial planes of both foldings are vertical or subvertical and their intensity clearly varies zonally.

A post D_3 fault running NNE-SSW cuts the subarea in the middle (Fig. 31). It is not exposed but is clearly visible on magnetic maps and has also been marked on the 1:100 000-scale geological map (Virransalo & Vaarma 1993). Owing to the lack of outcrops, the nature of the fault can only be inferred. As a generalization we can say that the most intensely migmatized rocks in the subarea lie west of the fault. Thus, it is possible that the western side has risen along the fault relative to the eastern side.

Equal area projections - From the projections in Fig. 31, we can deduce that D_3 had considerable influence on the current structure of the subarea. All the projection points of the pre-D_3 structures are distributed on the lower hemisphere without any regularity, excluding the clear maximum of subhorizontal S_0/S_1 structures. This can be attributed to the fact that a substantial proportion of the measurements were made on the conglomerate and greywacke outcrops in the northwest, where D_3 had a minor impact only. Elsewhere, too, the S_0/S_1 structures were originally subhorizontal, as a great number of the F_2 axes still plunge at a low angle.

Igneous rocks

Due to the lack of outcrops, it has not been possible to make observations of the relationship between the Kelhäjärvi granodiorite-quartz diorite and structural evolution in the subarea. The northern part of the Kelhäjärvi intrusion and the synorogenic granitoids at the western edge are, however, distinctly gneissose, the gneissosity being vertical or subvertical. Because of the lack of contact outcrops, all we can say about the gneissosity and the structures of supracrustal rocks is that the gneissosity is correlatable with either S_2 or S_1/S_2 composite schistosity of the metasedimentary rocks. These granitoids must, therefore, be contemporaneous with or older than D_2.

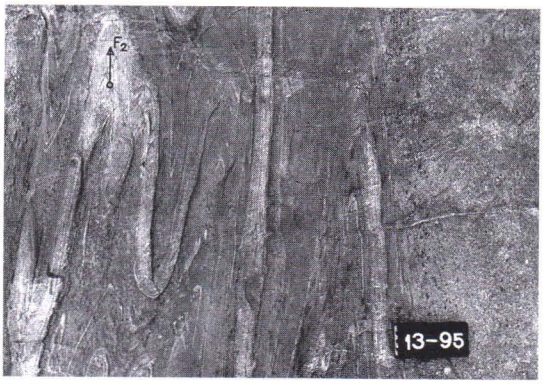

Fig. 33a. Metagabbro dyke (at right-hand margin of picture) in axial plane of F_2 folding in metasedimentary rock. Hämeenkyrö subarea (Fig. 31). Northeast upwards. X = 6832.40, Y = 2457.95. Code bar 6 cm.

Fig. 33b. Mafic dyke fragmented into boudins by D_2. Note F_2 folds of layered metasedimentary rock. Hämeenkyrö subarea (Fig. 31). Southeast upwards. X = 6832.40, Y = 2457.95. Code bar 6 cm.

Fig. 33c. F_2 folded mafic dyke in southwestern part of Hämeenkyrö subarea (Fig. 31). The host rock in migmatitic metasedimentary rock. Viewed towards northwest. X = 6829.60, Y = 2444.85. Code bar 6 cm.

The mode of occurrence of the ultramafic rock formation mentioned above (elongated in the S_2 direction) suggests that it is at least D_2 in age or older, as the fairly open folding at D_3, or even the zonal concentrations of intense D_3, cannot explain the dismembering of the initially coherent ultramafic body (Peltonen 1992).

The age of the mafic dykes in the south of the area in relation to the structures varies. Some of the dykes are parallel to the F_2 axial planes and oriented along S_2 (Fig. 33a). During D_2 these dykes, being more competent than the metasedimentary rocks, broke into boudins in the compression causing also F_2 (Fig. 33b). Therefore, they intruded either during or before D_2. Some of the mafic dykes were already folded in F_2 (Fig. 33c), and since they exhibit F_2-folded schistosity, they must be older than D_2.

Granite dykes cut D_2 structures, but their relation to D_3 is unclear. Granitic and pegmatitic dykes are in places distinctly cutting and in places deformed, but in the latter case tectonization may be due to the above mentioned Post D_3 shear cutting the area. At any rate, this shear cuts the large granite intrusion in the middle of the Hämeenkyrö subarea.

Metamorphism and migmatization

Owing to their composition, the metasedimentary rocks in the Hämeenkyrö subarea only occasionally contain porphyroblasts. The rocks in the central and the southeastern parts are the best preserved, having been metamorphosed in the equilibrium field of potassium feldspar and sillimanite. The sillimanite crystallized into fibrolite aggregates elongated parallel to S_0/S_1 planes, which were further folded during F_2 (Fig. 34a). In the central part of the subarea, and possibly elsewhere, too, the sillimanites have been altered into retrograde muscovite, but even then their crystallization time can be de-

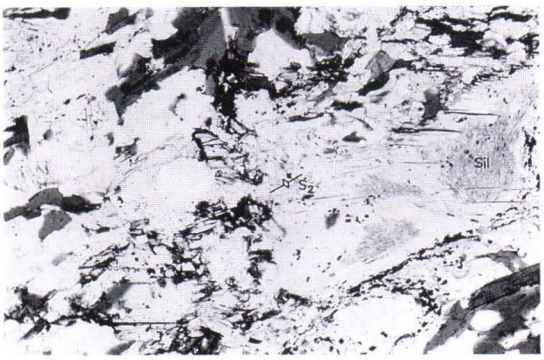

Fig. 34a. D_2 deformed fibrolitic sillimanite aggregates in sillimanite mica gneiss. Hämeenkyrö subarea (Fig. 31). One nicol. X = 6837.80, Y = 2453.20. Field of view 12 mm wide.

Fig. 34b. Garnets crystallized after the development of S_1/S_2 composite schistosity in metasedimentary rock. Western part of Hämeenkyrö subarea (Fig. 31). One nicol. X = 6833.60, Y = 2443.40. Field of view 12 mm wide.

duced from the relicts.

Apart from a couple of outcrops in the east, garnet has been encountered in metasedimentary rocks only in the most intensely migmatized rocks in the west, where garnet and cordierite are in equilibrium. In the garnetiferous supracrustal rocks in the east, S_2 schistosity is deflected around the euhedral garnet grains, implying that the grains crystallized either at or before D_2 (Fig. 32b). In the west, the garnets are slightly younger, some of them having crystallized over the S_1/S_2 composite schistosity (Fig. 34b). These garnets contain abundant fibrolite inclusions, showing that they crystallized in the reaction between biotite and sillimanite. The same reaction produced cordierite, which naturally crystallized at the same time as garnet. As in the sillimanite gneisses, retrograde reactions were also fairly intense in the high-grade rocks in the west. Indicating a drop in pressure, garnets have been altered into cordierite. The relative dating of this reaction is, however, impossible, because the cordierite that formed in this way occurs as pseudomorphs after garnet, and so their relation to the matrix structures is yet another relict feature (Fig. 34b).

Migmatization is strongest in the westernmost part of the subarea. Throughout the area there is at least minor veining in the S_0/S_1 plane (Figs 32d, 33a and 33c), but it is strongest in the garnet-cordierite gneisses in the west. The syn-D_2 migmatization is clearly at its highest adjacent to the contacts of metatonalites in the west. The veins in the S_0/S_1 plane and the syn-D_2 migmatization are tonalitic or trondhjemitic in composition, although part of the latter is already clearly potassium feldspar-bearing. In places, D_3 is accompanied by abundant migmatization, but this is restricted exclusively to zones of intense D_3 (Fig. 32d).

Pirkkala subarea

General geology

The Pirkkala subarea is located south of the Tampere synform area, in a transitional zone (Figs 2 and 35) where the weakly meta-

Fig. 35. Form line map of Pirkkala subarea and lower hemisphere projections of structures shown on it. Lithology modified from Matisto (1961).

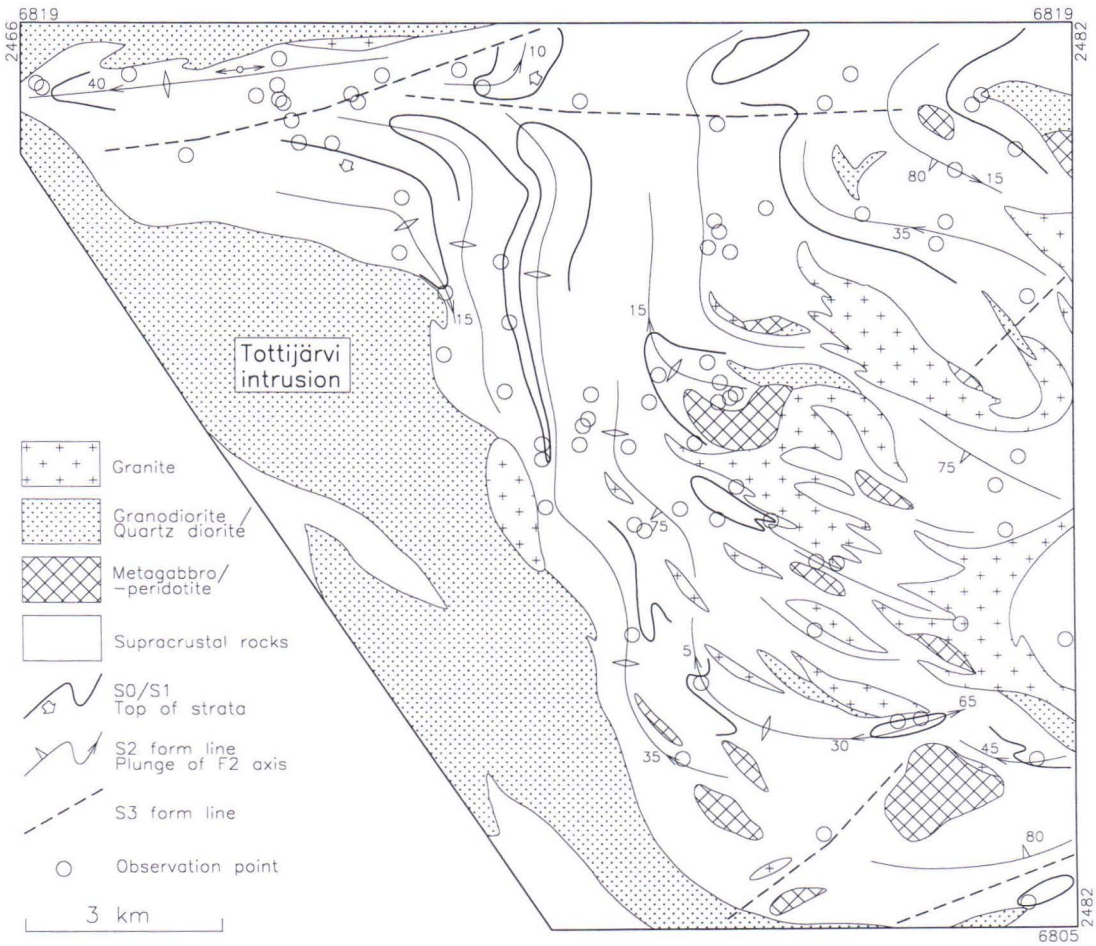

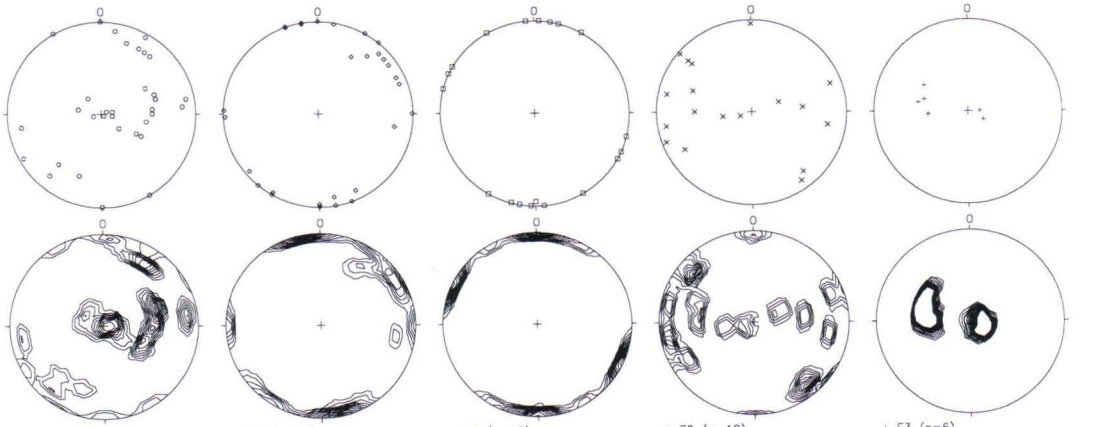

∘ S0/S1 (n=31)
max.dens.=10.01(at 0/90)
min.dens.=0.00
Contours at:
0.00,1.00,2.00,3.00,4.00,5.00,
6.00,7.00,8.00,9.00,10.00

∘ S2 (n=26)
max.dens.=12.56(at 168/0)
min.dens.=0.00
Contours at:
0.00,1.00,2.00,3.00,4.00,
5.00,6.00,7.00,8.00,9.00,
10.00,11.00,12.00

□ S3 (n=13)
max.dens.=14.86(at 116/0)
min.dens.=0.00
Contours at:
0.00,1.00,2.00,3.00,4.00,5.00,
6.00,7.00,8.00,9.00,10.00,
11.00,12.00,13.00,14.00

× F2 (n=18)
max.dens.=9.18(at 310/18)
min.dens.=0.00
Contours at:
0.00,1.00,2.00,3.00,4.00,
5.00,6.00,7.00,8.00,9.00

+ F3 (n=6)
max.dens.=41.46(at 283/48)
min.dens.=0.00
Contours at:
0.00,1.00,2.00,3.00,4.00,5.00,
6.00,7.00,8.00,9.00,10.00,11.00,
12.00,13.00,14.00,15.00

Fig. 35.

Fig. 36a. D_1 shear on limb of F_2 fold with subhorizontal axis. Graphite-bearing schist in Pirkkala subarea (Fig. 35). Viewed towards south. X = 6815. 55, Y = 2476.75. Code bar 6 cm.

morphosed metasedimentary rocks of the synform area grade southwards into the tonalite-veined migmatites typical of the Pori-Vammala-Mikkeli zone. In the west, the subarea is bordered by the Tottijärvi granodiorite/quartz diorite intrusion, but, with the exception of small granodiorite, quartz diorite, metagabbro and granite intrusions, it is composed of metasedimentary rocks varying in composition and metamorphic grade.

The metapelites in the northwest are part of the western continuations of the Tampere synform area in both structure and metamorphic grade. They are distinctly layered, fairly fine-grained metasedimentary rocks with layers usually a few centimetres thick. Intense folding has caused repeated layering, although layering in primary position is also visible in places. Despite their local pelitic composition, no porphyroblasts have been encountered in these metasediments.

In the west, the metamorphic grade is already slightly higher. As a rule, the rocks are still largely unmigmatized metasedimentary rocks that have preserved their primary

Fig. 36b. Tight F_2 folding with subhorizontal axis in layered metasedimentary rock in least metamorphosed northwestern part of Pirkkala subarea (Fig. 35). West upwards. X = 6818.50, Y = 2470.00. Code bar 6 cm.

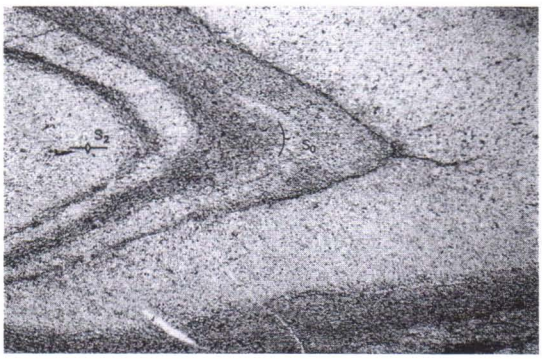

Fig. 36c. Thin section from hinge of F_2 fold in Fig. 36b cut perpendicular to F_2 axis. Pirkkala subarea (Fig. 35). One nicol. X = 6818.50, Y= 2470.00. Field of view 12 mm wide.

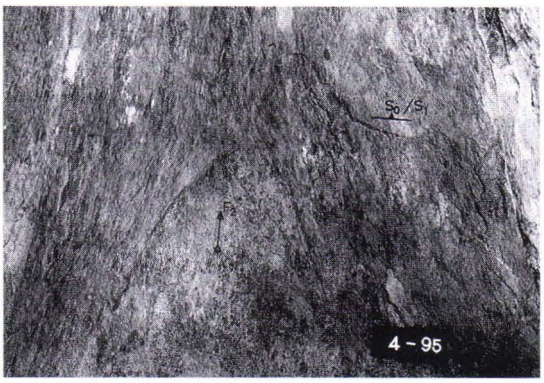

Fig. 36d. Hinge of F_2 fold in layered metasedimentary rock. Western part of Pirkkala subarea (Fig. 35), where S_2 has rotated into north-south direction. South upwards. X = 6814.80, Y = 2472.50. Code bar 6 cm.

Fig. 37. Syn-D_2 intruded granodiorite dykes. Southern part of Pirkkala subarea (Fig. 35). Note migmatization in mica gneiss parallel to S_0/S_1. East-northeast upwards. X = 6805.35, Y = 2481.50. Code bar 6 cm.

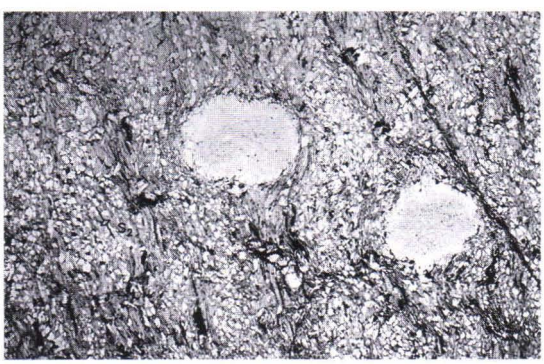

Fig. 38. Retrograde muscovitized pre- or syn-D_2 porphyroblasts in trondhjemite-veined migmatite of Pirkkala subarea (Fig. 35). X = 6805.35, Y = 2481.50. Field of view 12 mm wide.

structures, but their sedimentary material tends to be more sandy than in the northwest. They, too, are poor in porphyroblasts, although here and there small amounts of sillimanite have been met with. Structurally, the northwestern and western parts are correlatable with each other, but in the latter area the earliest deformation structures have been rotated off their primary position.

Migmatites with trondhjemite veins proper occur in the east. They are migmatitic, sandy metasedimentary rocks in which the primary features have commonly been almost totally obliterated. Small, metamorphosed quartz diorite/granodiorite and gabbro intrusions as well as granites cutting deformational and metamorphic structures abound in the area of migmatitic rocks.

Deformation - D_1, D_2, D_3 and Equal area projections

D_1 - The oldest deformation structure in the subarea is the penetrative schistosity, S_1, parallel to the layering of the metasedimentary rocks, the intensity of which is clearly dependent on the metamorphic grade. Although lacking entirely in the northwest, it is the dominant schistosity of the migmatitic metasedimentary rocks in the east. In the western metasedimentary rocks, S_1 is at its strongest in the more pelitic layers and may be lacking entirely in sandy layers or then the S_1 biotites have been recrystallized and reoriented during later deformations. Folds associated with D_1 have not been encountered in the subarea. The present geometry shows, however, that the structures were still subhorizontal after D_1.

Intense shears are also associated with D_1. They are restricted to fine-grained graphite- and sulphide-bearing layers that weather readily and are thus rarely exposed (Fig. 36a). Kinematic indicators have not been found in the D_1 shears and, hence, it has not been possible to determine the direction of movement along them. On the other hand, D_1

shears have been, and, due to the primary low-angle attitude of D_1, probably will be encountered only in places where later deformations have turned the D_1 structures into a vertical position. Reconstruction of the movement during D_1 would, therefore, require the structures caused by post-D_1 events also to be resolved. Owing to the numerous sources of error, we would then have to determine the direction of movement at several places, a task that seems impossible at present.

D_2 - In the second deformation stage the horizontal S_0/S_1 structures were folded with a horizontal, east-west-striking axis in a compression trending roughly north-south (Fig. 36b). The axial planes of F_2 folds then became vertical, striking east-west. The tightness of the F_2 folds varies greatly in the area, but at present the limbs of these folds are usually at least subvertical. Owing to the lack of appropriate continuous horizons, the sizes of the F_2 folds are difficult to assess, but on the basis of the structures visible on aeromagnetic maps the wavelength was probably kilometres.

The nature of the S_1 schistosity depends indirectly on the metamorphic grade; thus, in the least intensely metamorphosed rocks, S_2 developed into penetrative schistosity due to weak or recrystallized S_1 (Fig. 36c), but in rocks where S_1 had already developed into penetrative schistosity, S_2 is currently crenulation. This phenomenon does not directly follow the change in metamorphic grade, for in psammitic, mica-poor layers, S_2 in places developed into penetrative schistosity, even in areas that had already clearly metamorphosed during D_1 (Fig. 36d).

D_3 - The D_2 structures are in their original position only in the northwest. Elsewhere they rotated in the course of dextral, northeast-southwest-striking F_3 folding with a vertical axial plane. During D_3 the rotation occurred in both the horizontal and vertical planes, as the F_2 fold axes that turned into a north-south direction now almost invariably plunge gently northwestwards (Fig. 35). Although the F_3 folding had a decisive effect on the present total structure of the area, D_3 structures are by no means always visible on outcrops due to the large size of the F_3 folds, excluding the F_3 flexures in the southeast and northwest.

At the southern end of the subarea, where the metamorphic grade is higher than in the north, D_3 occurred at a higher grade. Consequently, the D_3 high-strain zones there are zones of plastic deformation and intense migmatization where all structures have rotated into the same direction. In the south, the D_3 high strain zones do not show a change in pre-D_3 metamorphic grade, a marked one at least. At the northwestern edge of the subarea, there is an ENE-WSW-striking shear, which, according to Nironen (1989a), has a vertical component showing that the southern side is uplifted in relation to the northern one. This shear separates the rocks of the Tampere Schist Belt from those of the Vammala migmatite area.

In addition to D_3 above, in places the area exhibits weak folding striking northwest-southeast with a vertical axial plane and crenulation in the axial plane, which deforms the D_2 structures. The relation of this folding to the D_3 structures has not been established, these two post-D_3 structures not being simultaneously visible on any outcrop.

Equal area projections - The projections in Fig. 35 show primarily how strong the influence of D_3 was on the present position of the pre-D_3 structures. Most of the F_2 and S_2 measurements were made east of the Tottijärvi intrusion, where the D_2 structures have been rotated into a northwest-southeast direction.

Igneous rocks

The contacts of the Tottijärvi quartz diorite/granodiorite with the supracrustal rocks are not exposed in the subarea and, hence, its

relation to the structural succession can be deduced only indirectly. The plutonic rock is distinctly metamorphic and the direction of its schistosity close to the contacts is the same as the direction of S_2 in the supracrustal rocks. Moreover, its schistosity was rotated during D_3 in the same way as the S_2 of the metasedimentary rocks. Therefore, the intrusion must be either contemporaneous with or older than D_2. Quartz dioritic and granodioritic plutonic rocks also occur as minor intrusions in various parts of the subarea. In the southeast, in an outcrop several hectares in size, granodioritic dykes up to tens of metres wide intrude along the axial planes of F_2 folds (Fig. 37). This suggests, that the Tottijärvi plutonic rock is also D_2 in age.

Owing to the lack of appropriate outcrops in the subarea, it has not been possible to establish the relation between the ages of the mafic plutonic rocks and the structures of the supracrustal rocks. However, the gabbro/diorite intrusions are metamorphosed and gneissose, suggesting that, like the metatonalites, they are at least D_2 in age. The granites, in contrast, clearly cut the metamorphic structures. They occur as dykes in the axial planes of the post-D_2 folds with axial planes striking northwest-southeast, but they also crosscut all structures.

Metamorphism and migmatization

Porphyroblastic metasedimentary rocks are rare throughout the subarea. In places, the best preserved mica schists at the northwestern edge show muscovitized pseudomorphs similar to those described from the Mauri subarea, but their original mineral species can no longer be recognized. Relatively well preserved rocks continue in the direction of the axial plane of the F_2 folding from the northwest corner of the subarea southwards, following the eastern contact of the Tottijärvi intrusion with a gradual increase in metamorphic grade. At first, the rocks contain small amounts of andalusite in places and also sillimanite further south, but, due to insufficient cross-cutting relationships in the porphyroblast-bearing outcrops, it has been too difficult to establish when the porphyroblasts crystallized. Owing to the sandy composition and retrograde reactions, porphyroblasts are also lacking in the trondhjemite-veined migmatites in the south. Locally, the migmatites contain porphyroblasts that have been muscovitized beyond recognition and whose original mineral species crystallized syntectonically with or before S_2 (Fig. 38).

The metasedimentary rocks in the east started to undergo migmatization during D_1 (Fig. 37). The majority of the veins may, however, be D_2 in age, although their age is not always easy to establish due to their tendency to imitate older structures. At any rate, the amount of migmatization in the subarea seems to be broadly related to changes in the metamorphic grade.

SOME OBSERVATIONS OUTSIDE THE SUBAREAS

Mafic dykes of Tottijärvi area

Metamorphic mafic and ultramafic dykes cutting metasedimentary rocks are characteristic of the study area, the migmatitic areas in particular. The dykes are usually no more than a few decimetres wide and their age in relation to the structural succession can only occasionally be established. They are, however, almost invariably parallel to S_2, but only in the subareas of Hämeenkyrö, Stormi and Koosanmaa have dykes been encountered that were already deformed and foliated during D_1.

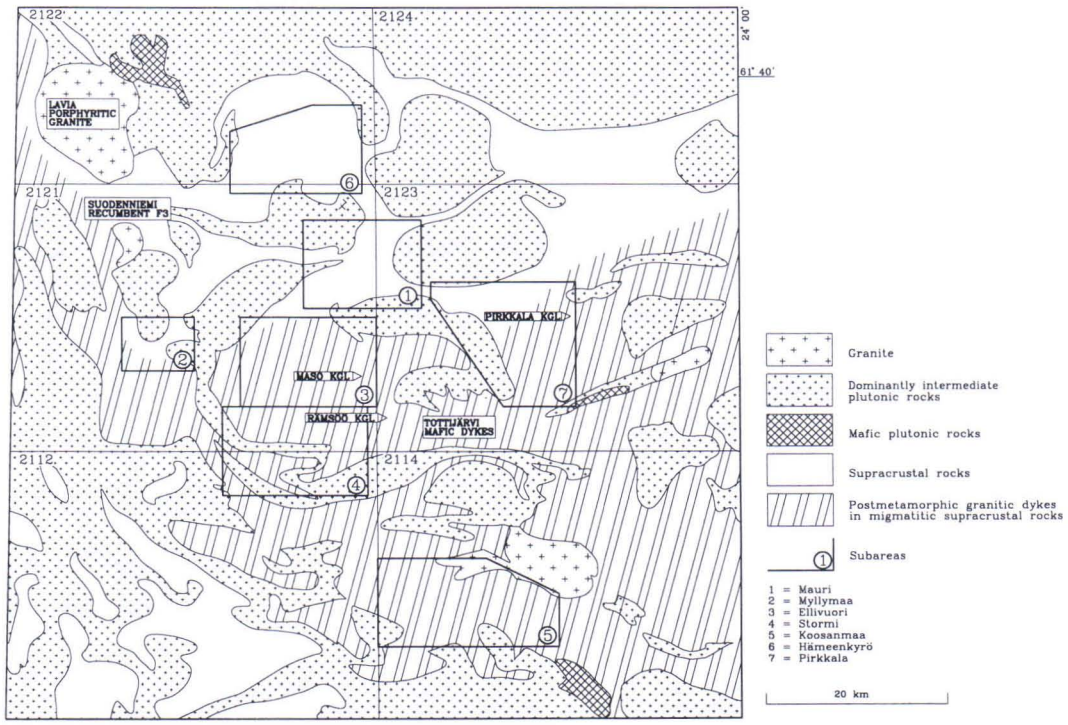

Fig. 39. Location in study area of other observation sites important for present structure and tectono-metamorphic evolution of Tampere-Vammala area.

East of the Stormi subarea, there are a few S_2 oriented, vertical mafic dykes that seem to have intruded along the axial planes of F_2 folding (Figs 39 and 40). Should these dykes be D_2 in age, it would imply that not all the mafic dykes in the area are of the same age in relation to structural evolution and, moreover, that mafic dykes as well as the tonalitic magmatism characteristic of it are associated with D_2. The other alternative is that the dykes are older than D_2 and that since their original position was parallel to the axial plane of the later F_2 folding, they look like syn-F_2 dykes.

Lavia porphyritic granite

The Lavia porphyritic granite in the northwest of the study area (Fig. 39) is a circular intrusion, about 90 km² in area. It is coarse-grained, coarse-porphyritic, nonfoliated or weakly gneissose, grey or pinkish microcline granite. The potassium feldspar megacrysts are usually 2-4 cm long, and biotite is the dominant mafic mineral.

The intrusion is very homogeneous throughout and contains only small amounts of supracrustal fragments. It does not exhibit a significant contact effect on the surrounding supracrustal rocks, but at least at the western contact of the intrusion, apophyses intruded in the supracrustal rocks are common. According to Huhma et al. (1952a, 1952b), the shear zone running southeastwards from Kankaanpää also cuts the Lavia porphyritic granite.

The porphyritic granites at the southern

Fig. 40. Mafic dyke parallel to axial plane of F_2 folding of migmatitic metasedimentary rock east of Stormi subarea (Fig. 39). East-northeast upwards. X = 6801.45, Y = 2470.70. Code bar 6 cm.

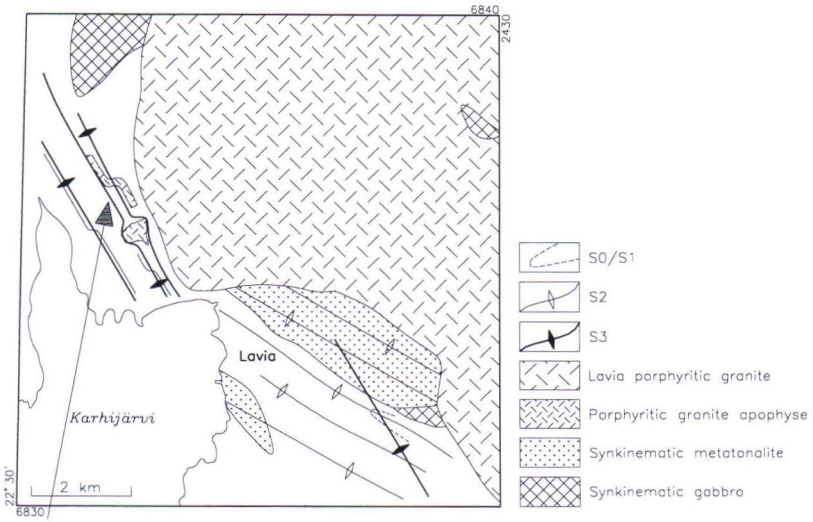

Fig. 41. Relation of Lavia porphyritic granite (Fig. 39) to D_2 and D_3 structures of metasedimentary rock. Code bar 6 cm. North-northeast upwards. Photograph was taken from the point shown by arrow.

edge of the Central Finland Granitoid Complex differ petrologically and geochemically from the synorogenic plutonites, 1890-1880 Ma in age. According to Rämö & Nironen (1996), the similarity between them and the rapakivi granites suggests that the compressional stage of Finland's Svecofennides ended with the emplacement of porphyritic granites.

The supracrustal rocks southwest of the Lavia porphyritic granite are intensely gneissose and only occasionally exhibit primary structures. Depending on the site, the schistosity is either S_2 or S_3 or a composite of the two (Fig. 41). The cutting relations of the structures are best visible east of Lavia village, where in places the S_2 and S_3 planes cut each other at an angle of 30°. Northwest of the village, the macroscopically dominant schistosity in the metasedimentary rocks is the highly evolved S_3 crenulation, in which, however, relicts of S_2 can be recognized in places (Fig. 41). The supracrustal rocks contain abundant porphyrite granite apophyses, which are usually subconformable with the S_3 plane. Some of the dykes, however, intruded D_3 tension cracks and were further deformed during later D_3 (Fig. 41), causing S_3 to deflect around the contacts of the dykes. The structures imply syn- or early-D_3 emplacement for the porphyritic granite.

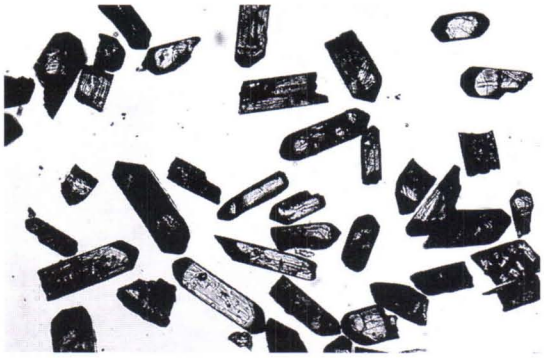

Fig. 42. Magmatic zircons from sample A1290 Aluskylä. Field of view 3 mm wide.

New age data

Porphyritic granite (A1290 Aluskylä) with abundant zircon was selected for age determination. The sample also had titanite, but

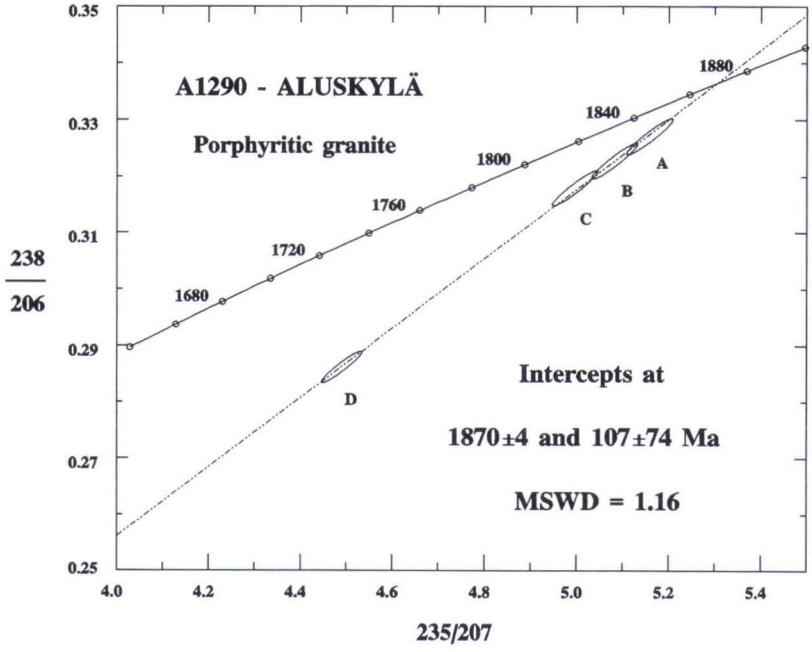

Fig. 43. Concordia diagram of U-Pb zircon data from Lavia porphyritic granite. (Sample A1290.)

this showed very low radioactivity and was not analysed. The zircons are brown, transparent and very fine grained (90% < 70 microns). The crystals exhibit simple prismatic-pyramidal morphology. Under oil immersion, oscillatory zoning is occasionally visible. The grains contain both opaque rounded and transparent needle-like (rutile?) inclusions. The sample was analysed at the Unit for Isotope Geology, GSF, using the analytical methods described by Vaasjoki et al. (1991), with the modification that the data were reduced using the ISOPLOT program (Ludvig 1988).

The zircons of A1290 have the characteristic features of magmatic zircons (Fig. 42), i.e. the abraded fractions are the least discordant and the degree of discordancy increases with the increase in the uranium concentration while the density, due to the increased metamictization, decreases. The $^{206}Pb/^{204}Pb$ ratio measured is rather high, demonstrating that the exact composition of the common lead correction has no bearing on the age. The mean standard error of the weighted deviate (MSWD) only marginally exceeds 1, which implies that the zircons probably derived from a single source. The upper intercept age, 1870 ± 4 Ma, can, then, be regarded as denoting the time of magmatic emplacement for sample A1290 (Fig. 43, Table 1).

From the above it follows that the age of the Lavia porphyritic granite is at least a local maximum age for the D_3 stage in the classification applied here. Porphyritic granodiorite dykes associated with the southern part of the Kelhäjärvi granodiorite and with the Karkku granodiorite as a whole intruded along the axial planes of F_3 folding. The nature of these dykes were described in the context of the Mauri and Myllymaa subareas. Kelhäjärvi and Karkku intrusions have not been dated but, from the above, their ages are probably close to that of the Lavia porphyritic granite.

Granitic dykes of Vammala migmatite area

Granite and pegmatite dykes, a few tens of centimetres wide, commonly pinkish and cutting both D_2 and D_3 structures (Figs 14e, 19b and 44) are common throughout the migmatite area south of the Tampere Schist Belt (Fig. 39). Their mode of occurrence was described in the context of the Myllymaa, Ellivuori, Stormi and Koosanmaa subareas. It is important to note, that the dykes almost invariably strike 0-30°, even at sites structurally different from each other. No specific deformation structure has been found in the study area to which these granites might be tied. Their parallelism in different parts of the area suggests that they intruded the crust when it was already fairly stable.

In the Turku area, south of the study area, the D_4 shear zones of the local classification strike predominantly parallel to the direction of above granite dykes. Although these shears deform the 1830 Ma granites and they have been interpreted as about 1800 Ma old (Väisänen et al. 1994), the Paimio shear

Fig. 44. Cutting, post-tectonic granite dyke in migmatitic metasedimentary rock in Vammala migmatite area. Viewed towards north. X = 6791.05, Y = 2453.70. Code bar 17 cm.

(strike 20°), at least, contains granites as shown by gravity surveys (Seppo Elo, pers. comm.). A great number of 1800 Ma pegmatites have been described from the archipelago of southwestern Finland (Ehlers et al. 1993). It is possible that the granite and pegmatite dykes in the Vammala area also belong to this age group.

Gently dipping axial trace of F_3 folding in Suodenniemi area

The axial planes of F_3 folds were described as vertical in all subareas. The same would seem to apply elsewhere in the study area, except in the northwestern corner where, at Suodenniemi (Fig. 39), the northeast-southwest-striking conjugate of D_3 gradually attains a northwesterly, subhorizontal dip. At its lowest, the axial plane dips at 40° and in the outcrops where an older F_2 with a primarily vertical axial plane is visible, the interference pattern on the erosion level is very complicated (Fig. 45).

According to Pietikäinen (1994), the Pori area is composed of fault blocks within which the structures dip gently towards northwest. In his classification the subhorizontal structures are composed of S_1 and S_2 schistosities, both of which are visible in tonalitic intrusive rocks but S_1 is usually dominant. The blocks in the Pori area contain no metasedimentary rocks (Pietikäinen 1994) at all and thus it has been possible to classify the structures from the emplacement of the tonalites onwards only.

Fig. 45. Interference of F_2 with vertical axial plane and of F_3 with shallowly dipping axial plane in layered metasedimentary rocks at Suodenniemi (Fig. 39). Northwest upwards. X = 6824.20, Y = 2436.50. Code bar 6 cm.

In the Tampere-Vammala area, the metatonalites intruded during D_2 with S_2 as their schistosity. In the Suodenniemi area, too, the metatonalites would first have been oriented in S_2, to be then folded into a subhorizontal position by F_3 with axial planes dipping gently northwestwards. Since the Suodenniemi area is no more than about 10 km from the study area of Pietikäinen, it is possible that, due to the lack of metasedimentary rocks, the Pori area also lacks the D_1 structures of the present work and that the gently dipping structures in the Pori area can be correlated with the D_2/D_3 structures of the Tampere-Vammala area.

On the other hand, Pietikäinen describes the D_3 structures in the Pori area as kilometres in size on a macroscale and as asymmetric folds on a mesoscale. According to him, migmatization occurred during their formation but they are not accompanied by axial plane schistosity; the S_3 plane tends to strike northwest-southeast. These features, too, are very similar to those of the D_3 structures described from the migmatitic rocks in the Tampere-Vammala area, although two schistosities preceding D_3 have not been found in the metatonalites there.

Conglomerates of Vammala migmatite area

On the basis of their maximum ages of deposition and stratigraphic position, the conglomerates in the Tampere synform area can be divided into two groups at least. The

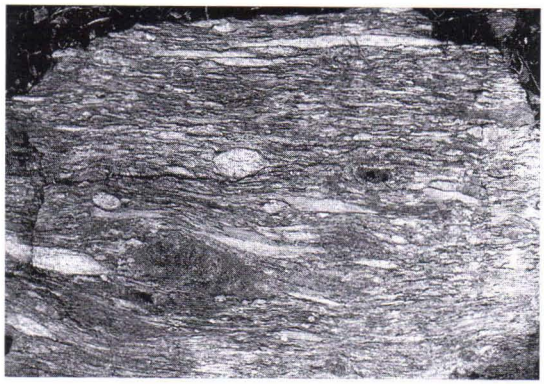

Fig. 46. D_1/D_2 deformed conglomerate with quartz clasts at Maso (Vammala) (Fig. 39). X = 6807.15, Y = 2458.25. Field of view 1.2 m wide.

Fig. 47. Rämsöö polymictic conglomerate (Tottijärvi) (Fig. 39). X = 6803.50, Y = 2460.20. Code bar 17 cm.

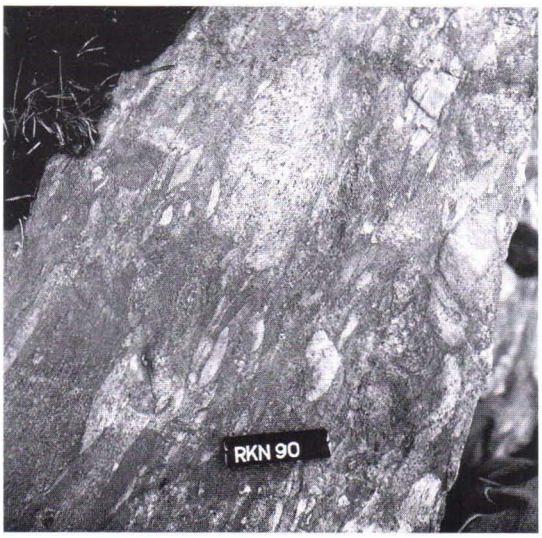

lower conglomerates are stratigraphically correlatable with the Myllyniemi formation, with a maximum deposition age of about 1910 Ma (Huhma et al. 1991, Kähkönen & Leveinen 1994, Kähkönen 1996). This group contains at least the Ahvenlampi conglomerate, which probably represents the proximal part of the Myllyniemi formation (Kähkönen & Leveinen 1994). The conglomerates at Veittijärvi and Tohloppi (upper conglomerates) have been interpreted as being above the Myllyniemi formation in stratigraphy, having been deposited no earlier than 1890 Ma ago (Kähkönen 1994). Yet, the youngest conglomerate clast age obtained from the synclinal area is a mere 1884 ± 3 Ma (Nironen 1989b).

Conglomerates metamorphosed and migmatized like the other metasedimentary rocks also occur in the migmatite zone south of the Tampere synclinal area (Fig. 39). Conglomerates have not been encountered in the southernmost part of the study of the area, possibly because they may have been destroyed beyond recognition in the intensely metamorphic and migmatitic environment.

Maso conglomerate

The Maso conglomerate at the southeastern edge of the Ellivuori subarea (Figs 39 and 46) contains quartz clasts, but as a whole it is so completely deformed that hardly anything can be said about its original appearance or the composition of its clasts. The intense orientation of the conglomerate and the stretching of its clasts are due to both D_1 and D_2 deformations.

Rämsöö conglomerate

The Rämsöö polymictic conglomerate (Figs 39 and 47), a few kilometres northeast of the Stormi subarea, represents formations

Fig. 48. D_1/D_2 deformed Naistenmatka polymictic conglomerate (Pirkkala) (Fig. 39). X = 6817.30, Y = 2481.00. Code bar 10 cm.

of the submarine feeding channel of a delta, but differs from the conglomerates typical of the Tampere synclinal area in the composition of its clasts (Kähkönen 1996). The clasts in the conglomerate have been deformed into elongated cobbles parallel to S_0, implying that it, too, participated in the D_1 deformation.

Pirkkala conglomerate

The Naistenmatka conglomerate (Figs 39 and 48) in Pirkkala is also intensely D_1 deformed. It resembles the conglomerates in the Tampere synclinal area, its clasts, too, being mainly of volcanic origin. The pink feldspar porphyrite clasts typical of the Veittijärvi and Tohloppi conglomerate are, however, lacking (Kähkönen 1996).

According to Lahtinen (1994), the gneisses in the north of the migmatite zone resemble the turbiditic metasedimentary rocks of the Tampere synclinal area geochemically. Since all the above conglomerates occur in the relatively monotonous metaturbidite environment in the northern part of the migmatite zone, they can probably be correlated with the Myllyniemi formation in the lower part of the Tampere synclinal area. On the other hand, Lahtinen (1996) maintains that arc-related sedimentary rocks are encountered in the migmatite area that may be correlatable with the < 1890 Ma sedimentation in the Tampere synclinal area. In that case it would also be possible to correlate the conglomerates in the migmatite area with the Veittijärvi type "upper" conglomerates in the synclinal area.

CORRELATION OF DEFORMATIONAL STRUCTURES BETWEEN SUBAREAS

Introduction

The factors that hamper regional classification in an area of very varied metamorphic grade and degree of deformation, were discussed in the descriptions of subareas. Variation was found not only in the intensity of the older structures within several subareas but also in metamorphic grade and in the relative and absolute ages of peak metamorphism. Owing to the great number of outcrops in the subareas, the change in structures and metamorphism could be followed from one outcrop to the other, which narrowed the likelihood of erroneous interpretations. A similar, gradual regional change can be observed from the Mauri subarea to the Ellivuori and finally the Stormi subarea.

The ages of metamorphic structures in the subareas were compared with deformation structures and referred to as the variation in relative age. However, in correlating the structures in the whole study area, we can use the dated plutonic rocks whose age is known in relation to the local structural succession. The danger then is that the age of a single tectonic structure may vary regionally so much that the magmatism of a given age may show different ages in relation to the structures in different parts of the study area. Since, however, the age relation of the metamorphic structures to the deformation structures and intrusive rocks is taken into account in the correlation, this situation will eventually be noticed.

In the present correlation of structures, use has been made of the synkinematic intrusions at Värmälä (1878 ± 3 Ma), Hämeenkyrö (1885 ± 2 Ma) and Järvenpää (1881 ± 1 Ma) (Nironen 1989b, the present work) because and in spite of the fact that they occur in metamorphically entirely different environments. The reliability of the correlation is further improved by the relations of the Lavia porphyritic granite (1870 ± 4 Ma) (the present work) and the comparable Karkku

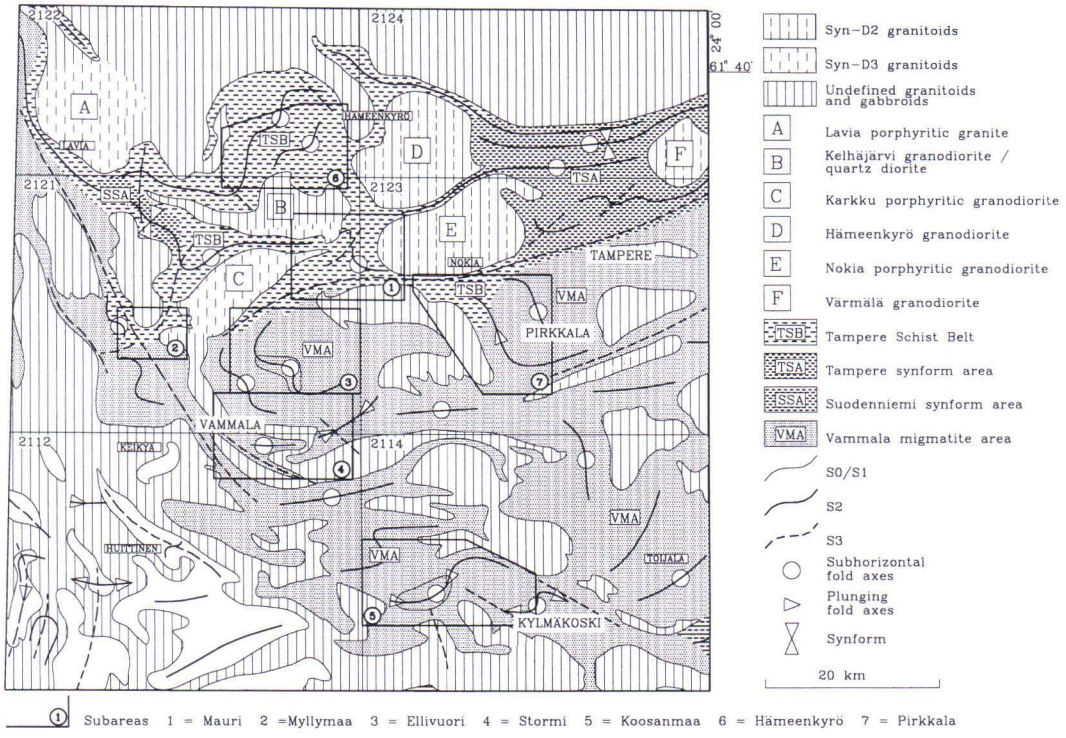

Fig. 49. Deformation structures of study area as form lines, regional correlation and classification of structures and relations of intrusive rocks mentioned in text to structural succession.

porphyritic granodiorite to the structural succession in both the Tampere Schist Belt and the migmatite area (see descriptions of subareas), which differs from that of the above. The final classification covers the whole study area (Fig. 49) and differs from the local classifications (Aarnisalo 1988, Campbell 1978, 1980, Kähkönen & Nironen 1994, Leveinen 1994, Perttula 1982, Pietikäinen 1994) and the classification of the Svecofennian Domain (Koistinen et al. 1996).

Correlation

D_1

The penetrative biotite schistosity parallel to the primary layering in metasedimentary rocks has been mentioned as the oldest recognizable deformational structure in the structural descriptions of all subareas. This structure, called S_1 in every subarea, was, however, found to be lacking in the least metamorphosed parts of the Mauri, Myllymaa and Pirkkala subareas, being, however, the dominant metamorphic schistosity in the more intensely metamorphosed supracrustal rocks in these subareas. It was described as the dominant schistosity in all migmatitic metasedimentary rocks, even though its parallelism to the layering is somewhat unclear in the most intensely metamorphosed rocks, where the primary structures have been almost totally obliterated.

Folds that could be associated indisputably with this oldest deformation event have not been recognized in any subarea. In the description of the Koosanmaa subarea, it was

mentioned that the minor hinge of a fold deformed by F_2 had been found in one outcrop, but no pre-D_2 repetition of layers proper could be found there either. Should there be any F_1 folds in the area, they would be isoclinal, as suggested by the parallelism between S_0 and S_1, and hence difficult to find.

Original position and metamorphic grade

It was further stated that the S_0/S_1 planes were still subhorizontal in all subareas, even after D_1. If there was folding associated with D_1, the folds must have been primarily recumbent. It is therefore possible that the F_1 folds, their axial planes turned into a vertical position in later foldings, cannot be recognized on the limbs of F_2 folds. The only way in which we can distinguish the different fold generations reliably from each other is by determining their cutting relations unambiguously. The size, shape and axial plane properties of the folds depend on either the primary lithology of the rock or the lithology modified by the recrystallization during

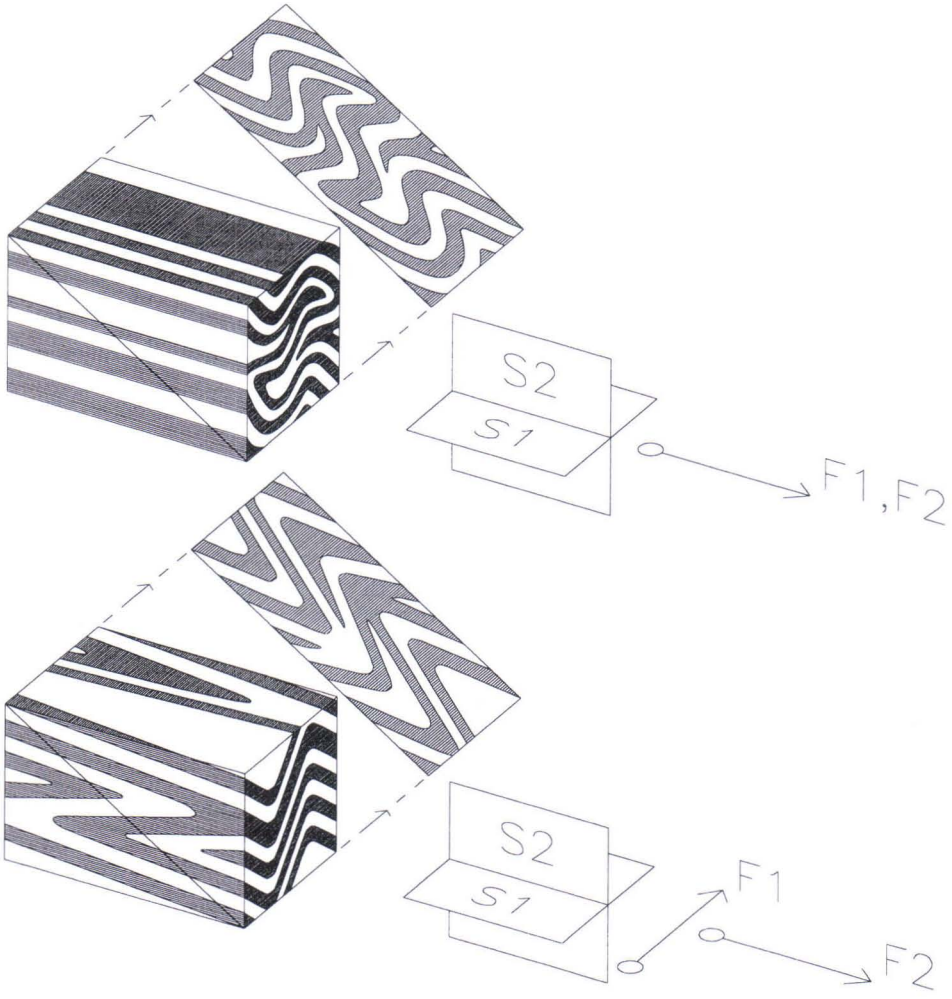

Fig. 50. Effect of angle between F_1 and F_2 axes on interference structure.

metamorphism. The axial plane properties depends also on where and in which part of a larger fold structure the observation outcrop happens to be. More than a hundred observations of the hinges of F_2 folds have been collected from the area. If, therefore, pre-D_2 folds existed, their absence or non-recognition in the hinges of F_2 folds might possibly be explained by assuming that the axes of the recumbent F_1 folds were horizontal and at an angle of about 90° to F_2 axes (Fig. 50).

Since the structure called D_1 here was originally horizontal and thus visible on the present erosion level on the limbs of later folds only as an uplifted and somewhat premetamorphic feature, it is possible that D_1 is composed of several events, which are difficult to distinguish from each other. In addition to the development of S_1 schistosity, early veins parallel to S_0 and layers more competent than their environment were in places fragmented into boudins before D_2. As most of the observation outcrops are on the limbs of F_2 folds and since boudinages was formed in these places during D_2, too, these two similar events are difficult to distinguish from each other, in places even impossible. As all the pre-D_2 structures are such that they could have been formed in one and the same pre-D_2 deformational event and since the risk of misinterpretation in attempts to distinguish pre-D_2 structures from each other is too high, all the pre-D_2 features are here classified collectively as D_1. This classification was retained even though tectonic and metamorphic structures preceding the regional D_2 are totally lacking in the least metamorphosed areas.

The original subhorizontal dip of the S_1 schistosity, its parallelism to the layering and its increase in intensity towards the F_2 antiforms with the increase in the syn-D_1 metamorphic grade imply that, during the D_1 stage, the temperature had increased roughly as a function of depth. If D_1 was not accompanied by folding of rocks or of stratigraphic units or by repetition due to subhorizontal faulting/thrusting, the metamorphic grade of D_1 increased downwards in local stratigraphy, too.

The grade of M_1 metamorphism can be determined only in areas, where M_2 and/or M_3 have not re-equilibrated M_1 metamorphic assemblages. The whole Pori-Vammala migmatite zone have metamorphosed over the equilibrium field of muscovite during M_1 and common stable M_1 assemblage in metasedimentary rocks of pelitic composition is even garnet-cordierite-sillimanite. Andalusite mica schists of the Mauri subarea reached the peak of metamorphism during M_3 and thus the grade of M_1 metamorphism was lower than during M_3.

Age

The ages of the D_1 structures in the study area are somewhat ambiguous. If the turbidites of the Tampere schist belt (Fig. 49), which deposited 1910 Ma ago at their earliest (Huhma et al. 1991), are correlatable with the metasedimentary rocks in the north of the Vammala migmatite area (Fig. 49) (Lahtinen 1994, 1996) where D_1 can be recognized reliably, the above age is probably also the maximum age of D_1. The ages of the volcanic rocks in the Tampere synform area (Fig. 49) vary in the range 1904-1889 Ma (Kähkönen 1987) and the age of the plutonic clasts in the conglomerates above them in stratigraphy in the range 1890-1884 Ma (Nironen 1989b). However, since the D_1 structures are lacking in some parts of the Tampere synform area or were rendered unrecognizable in later deformations, it is not clear whether the above ages are maximum ages of D_1 or whether sedimentation continued in the Tampere synclinal area while the formations lower down in the stratigraphy were already undergoing D_1 deformation.

D_2

Correlation and size of F_2 folds

It was mentioned in the descriptions of all subareas that the S_0/S_1 structures were deformed in the course of folding with subhorizontal axes and vertical axial planes. In some subareas it was noted that the strike of the axial planes of F_2 folds was originally about east-west, although their present position varies greatly due to later folding. With the exception of the Mauri subarea, the size of the F_2 folds can be deduced only from magnetic maps and wavelengths was found to be of the order of at least hundreds of metres or more likely of kilometres. Owing to the tightness of the folding, the amplitude of the F_2 folds is thus probably kilometres throughout the study area.

If the variation in thermometric data given in the description of the Stormi subarea (Fig. 24) is due only to the fact that the sections represent different depths in the different parts of F_2 structures and if we assume that F_2 folding is isoclinal, as suggested by the subverticality of S_0/S_1 structures, the order of magnitude of the amplitude of F_2 folding can be further constrained, at least around Stormi. If it is further assumed that the geothermal gradient was 20°/km during D_1, which can be taken as an average in regional metamorphism (Miyashiro 1987), and that the calibration used in the thermometry gives exactly the correct temperatures, the variation in temperature implies an amplitude of about 1.5-2 km for F_2 folding. If the calibrations of Ferry & Spear (1978) are applied in the thermometry, the estimate of F_2 amplitude would increase by a factor of 1.5. Hence, the estimates based on the variation in metamorphic grade are indicative only. At any rate, the amplitude is probably no more than 2-3 km, for the shears parallel to the F_2 axial planes referred to in the descriptions of subareas probably increased rather than decreased the differences in depth between sections.

S_2 and metamorphic grade

A conspicuous feature is the variation in the nature of S_2 axial plane schistosity as a function of the metamorphic grade in the host rock. This is not due to the metamorphic grade in itself, however, but to the strengthening of the metamorphic structures oldest in relation to structural evolution as the syn-D_1 metamorphic grade increases. In those parts of areas where the metamorphic grade during D_2 was as high as or higher than at D_1, the S_1 biotites, if present, were recrystallized and reoriented, forming the present penetrative S_2 schistosity in the metasedimentary rocks. If, on the other hand, the metamorphic grade during D_1 was not exceeded during D_2 deformation, the S_1 biotites were preserved and S_2 became crenulation cleavage, during which some new biotite crystallized in places. In addition to metamorphic grade, the nature of S_2 is controlled by the general lithology (mainly mica abundance) and the variation in the zonal intensity of S_2 schistosity, for instance, in different parts of F_2 folds. As shown by metapelites, the metamorphic boundary surface, at which the S_1-S_2 relation changes is consistently at the boundary between the stability fields of sillimanite and andalusite .

It is evident from the present work that the synclinal structure of the Tampere Schist Belt described by Nironen (1989a) evolved during the D_2 of the regional classification, even though D_1 structures are lacking in this area. The northwest-southeast-striking synformal structure with a vertical axial plane at Suodenniemi, described by Perttula (1982) and Kähkönen (1996) (Fig. 49), should also be considered an F_2 synform of the classification used here.

Age

According to Nironen (1989b), the granodiorite batholiths in the Tampere synclinal area (Hämeenkyrö and Värmälä) with U-Pb ages on zircon of 1885 and 1878 Ma (Fig. 49) were emplaced during the D_2 stage of this study. In the context of the Mauri subarea, features were dealt with suggesting that the Nokia batholith (Fig. 49) is also syntectonic with D_2. However, the ages measured for the Nokia batholith are clearly older than those of Hämeenkyrö and Värmälä (1898 Ma and 1909 Ma, Nironen 1989b). According to Nironen (1989b), the ages of the Nokia batholith do not necessarily refer to the emplacement event, because even the younger zircons may have inherited some old lead. The Järvenpää granitoid, 1881 Ma in age (the present work), also intruded during the second deformation stage, although, due to the different metamorphic and tectonic environment, it is more intensely foliated than the above batholiths. Since synkinematic granitoids have been observed to exhibit signatures of syn-D_2 emplacement in other subareas, too, it is likely that the age of D_2 in the Tampere-Vammala area as a whole is about 1885-1880 Ma.

D_3

Two conjugates

It was described above, that the D_2 structures are cut by two deformation structures important for the total structure of the study

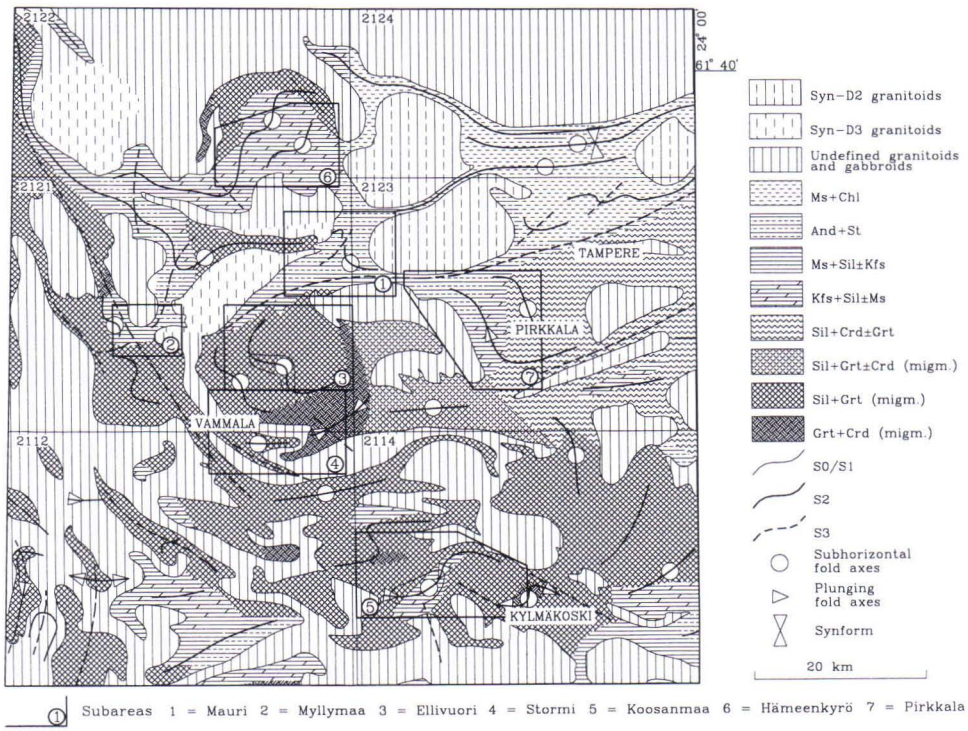

Fig. 51. Tectono-metamorphic map of Tampere-Vammala area. Lithology modified from Koistinen (1994).

area. Both are open folds with vertical axial planes striking either northwest-southeast or northeast-southwest. Since these folds have no unambiguous cutting relation and their metamorphic properties correspond to each other, they are probably conjugates. The existence of a conjugate pair is also suggested by the fact that no significant difference has been observed between the ages of these structures in relation to the plutonic rocks dated.

On outcrop scale, the F_3 conjugate kink bands striking northwest-southeast are usually sinistral and those striking northeast-southwest dextral. From the morphology of the large, regional D_3 high-strain zones (S3 in Fig. 51) on the aeromagnetic map (Fig. 3), however, the displacements would seem to be the other way round.

As discussed in the descriptions of subareas the lithologies in the study area are subhorizontal as a whole (see also closing interference structures on the aeromagnetic map). Since the amounts and commonly even the directions of vertical displacements in D_3 high-strain zones are unknown, the directions of the horizontal movements cannot be reliably determined from the aeromagnetic map. It is also possible that stress field at the D_3 folding stage differed from the stress field that prevailed during the forming of the D_3 high-strain zones. Thus we are here possible dealing with the reactivation of old structures (see also Koistinen 1994, Koistinen et al. 1996).

The metamorphic grade of the D_3 high strain zones and the relations of their ages to peak of regional metamorphism vary within the study area (see descriptions of subareas). They are ductile, usually unexposed zones intensely migmatized in the south of the study area. According to Nironen (1989a), the shear that separates the Tampere Schist belt from the Vammala migmatite area (in Fig. 51 close the name "TAMPERE"), and in which the southern side has risen in relation to the northern side is dominated by a vertical component.

Varying intensity of D_3

S_3 schistosity is best developed in the least metamorphosed areas and even there it is clearly zonal. In some places, as in the southeast of the Mauri area, S_3 is the dominant schistosity, occasionally having obliterated the older schistosities almost totally and during the formation of which andalusite still crystallized. In the areas of high-grade metamorphism, S_3 is invariably lacking for the same reason as is S_2 or crenulation-like mode of occurrence of S_2 described above.

In spite of D_3, the F_2 fold axes are mainly gently plunging in the area. F_2/F_3 interference domes and basins caused by axial culminations and depressions are fairly common. It appears, however, that the F_2 axes rotated in the XY plane more than in a vertical plane, implying that the horizontal component of D_3 was clearly more important than the vertical one. In other words, the differences in depths of sections on the present erosion level seem to be due to F_2 folding rather than D_3.

Since the axial planes of F_2 and F_3 folds were originally vertical, the area can be subdivided into areas where the main schistosity of the metasedimentary rocks is either vertical (S_2 or in places S_3 in the andalusite-staurolite zone or less metamorphosed areas) or gently dipping (S_1 in the potassium feldspar-sillimanite zone and more intensely metamorphosed areas)(Fig. 51). Since sillimanite crystallized syntectonically in relation to S_1 schistosity, these areas, with the exception of some later faults, are still bordered by the originally horizontal surface, in which D_1 metamorphism occurred in pelitic rocks close to the intersection point of the muscovite break down reaction and the stability fields of andalusite-sillimanite.

Age

The Lavia porphyritic granite (1870 ± 4 Ma) (Fig. 49) described above was found to be intruded contemporaneously with D_3. Associated with the porphyritic granodiorites at Karkku and Kelhäjärvi (Fig. 49) are dykes that intruded along the axial planes of F_3 folds in metasedimentary rocks and obtained S_3 schistosity (Figs 10a and 6a) showing that, at least locally, the dykes are contemporaneous with F_3 folding. Although these plutonic rocks have not been dated, it is clear from the structural evolution that in the study area the porphyritic variants of the granodiorites are younger than the equigranular ones.

Migmatization and D_3

Important for metamorphic and tectonic evolution in the area is that the migmatitic rocks, too, exhibit a distinct D_3 migmatization maximum in some places. This migmatization, which is mainly concentrated in zones of intense D_3, cuts the tonalitic or trondhjemitic D_1-D_2 migmatization and, being richer in potassium feldspar, differs from it in composition. The inference is, then, that either in these zones of intense D_3 the temperature tended to remain high longer than elsewhere in the migmatite area or that there was an entirely new thermal pulse restricted to the D_3 zones. Since no discontinuation was found in the crystallization of garnets, for instance, in the description of the Stormi subarea, the first alternative is the more probable.

The post-D_3 deformations are concentrated in some narrow faults and shears of minor importance for the present total structure of the area. They are not therefore discussed here at any length.

GEOMETRICAL 3D MODELLING OF TAMPERE-VAMMALA AREA

Principles and assumptions

Introduction

In the previous chapter it was postulated that although the mode of occurrence of the earliest deformational structures varies with the depth of the section, the same features of structural and metamorphic evolution are recognizable throughout almost the entire Tampere-Vammala area. It has therefore been possible to compile a tectono-metamorphic map covering the whole study area (Fig. 51) in which the form lines of S structures are classified regionally even though the earliest deformation structures are absent in the least metamorphosed F_2 synforms. The scale of the map is such that details dealt with in the description of subareas, but unimportant for the total structure, are not included. Form lines are, however, also drawn outside the subareas studied in detail. All the structures marked on the map are based on the field observations made on the area covered by the map.

Form lines

To make them easier to read, the form lines of S structures are not provided with dips, but the plunges of the fold axes are shown. The map can be read by assuming that all S_2 and S_3 planes are vertical, the only exception being the northwestern part of the area at Suodenniemi, where the S_3 plane locally dips northwest. The low angle of the dip of the S_0/S_1 planes is evident without any markings owing to their closing patterns. When the type of a closed F_2/F_3 interference pattern is known (dome/basin), it manifests itself in the directions of plunge of F_2 axes. The plunge of the axes of F_2 folds is not

given numerically, as it is only the strike of the axis that matters. The S_3 form lines represent the high-strain zones at D_3, which in many cases separate areas of dissimilar pre-D_3 structures differing in geometry from each other.

Metamorphic assemblages

Marked on the map in Fig. 51 are the variations in metamorphic grade based on stable, diagnostic mineral assemblages, without, however, taking a stand on the crystallization time of the metamorphic minerals in relation to structural evolution. This mode of representation is, of course, a generalizing one as in reality each assemblage is stable within a certain P/T field, the size of which varies case by case. More illustrative would be a map showing the variation in metamorphic temperature as on the map in the description of the Stormi subarea (Fig. 24). Compiling a map to cover an area as large as the present one would, however, require thousands of samples with the appropriate mineral composition and tens of thousands of mineral analyses and so is totally impracticable. Essential for the tectono-metamorphic structure and its evolution is not only the metamorphic grade but also the age of the metamorphism, which will be discussed later.

Intrusions

The map (Fig. 51) also shows the ages of granitoids in relation to structures in cases in which there is information available, either from the literature or from work done for this study. More comprehensive grounds for each intrusion are given in the descriptions of the subareas and in the context of the Lavia porphyritic granite. Most of the plutonic rocks are classified as undefined. In reality they are mainly gneissose granodiorites and quartz diorites, and so could have been included with good reason among the S_2 oriented plutonic rocks. Since, however, there are no unambiguous contact observations of them from structurally appropriate outcrops, their relative ages are not given here.

Geometrical modelling

General

To enhance the perspicuity of the three-dimensionality of the structures and to test the correctness of the interpretation of the total structure, 3D models, mainly dealing with postmetamorphic folding of metamorphic isograds, were developed for the Tampere-Vammala area as the work proceeded (Kilpeläinen & Rastas 1992, Kilpeläinen et al. 1994). One of the objectives was to compile a 3D structural model for the entire Tampere-Vammala area using as parameters when applicable all the structural and metamorphic data on the area presented both here and in the literature. The model was thus to display the present structure of the area without taking into account interpretations of the structural evolution. The idea was that understanding of 3-dimensional geometry of the structure (tectonic and metamorphic) would make it easier to understand and interpret also the processes that generated the present structure.

It has been possible to produce geological 3D models with PCs for less than a decade (see also Pflug & Harbaugh 1992). Most of the software was originally planned and tailored for mines and quarries and so could not be used directly here. Another problem was earlier the presentation of arched surfaces, and the repetition of a plane due to folding with the horizontal axial plane. A plane can then have several points with the same X- and Y- coordinates, only the value of Z varying. With the increase in the capacity of PCs, however, the programs have improved and they are now more useful for complex geological modelling.

The models and their sections presented

here were made using the 3D modelling part of AutoCad. The surfaces describing layering, metamorphic isograds or other planar structures form a matrix composed of nodal points, the density of which can be set to meet the requirements of the user. The grid surface can be produced in different ways. The first and simplest way is to provide each nodal point of the grid with three coordinates. Depending on the command, the grid surface is either rectangular or its topology can be chosen freely. Another, more useful, way is to define the forms of the edges of the surface to be constructed and to fit the surface with the aid of these forms. The third possibility is to fit the desired surface with the guiding points. These together with the preliminary framework of the surface can then be produced as in the previous alternative.

The second technique was mainly used here, and the surfaces obtained were not refitted even if this would have improved the visualization, because the fitting of surfaces has adverse consequences, the effect of original parameters controlling the shape of the surfaces being reduced. The fitting surface was usually produced with the edgesurf command, which creates a Coon´s (saddle) surface between four 3D polylines that touch each other at their ends. The edge of the Coon´s surface joins the determined edges and runs through their corner points, thus making it possible to create very complicated 3D surfaces.

Building a 3D geometrical model

A 3D model for an area as large as this can be compiled in two ways. Either a total image can be built from small detailed images, in which case all, even local and specific, features can be included. A disadvantage is that the model may then be so detailed that its readability and informativeness will suffer. Another factor restricting the use of this approach is the limited capacity of computers: the greater the number of details the harder it is to run the system. The second alternative is to build up the model for the whole area at once. In this case, the scale of the image is such that local details cannot be included; the starting point must then be structures correlated for the whole area.

The approach used here is a compromise between these two. Simplified lithological data, the same as in other maps of this work, were used as the base map. The lithological map was simplified to emphasize the fact that it is a model and cannot be read in the same way as the form line maps based on field observations. The whole study area was first divided into three parts differing from each other in the mode of occurrence of D_3 structures and in metamorphic properties (see the description of subareas and structural correlation) (Fig. 52a). The possible F_1 folding with a primarily recumbent axial plane was not included in the modelling, because the information about its existence, and especially about the amount and importance of D_1 repetitions, is ambiguous. The model must, then, be read in such a manner that its surfaces display originally horizontal planes, which are either layering exclusively, post-D_1 recumbent but repeated layering, or metamorphic isotherms and/or isobars parallel to S_0/S_1 plane(s).

Subareas

The northern part (Fig. 52.a.1) covers mainly the Tampere Schist Belt and its western continuations bounded in the south by the S_3 shear marked in Fig. 51. In this area, D_3 occurs typically as dextral folding with a northeast-southwest-striking axial traces and a wavelengths of up to tens of kilometres.

The central part (Fig. 52.a.2) contains strongly metamorphosed migmatites of the Pori-Vammala type, although in western Pirkkala there is a small area of relatively

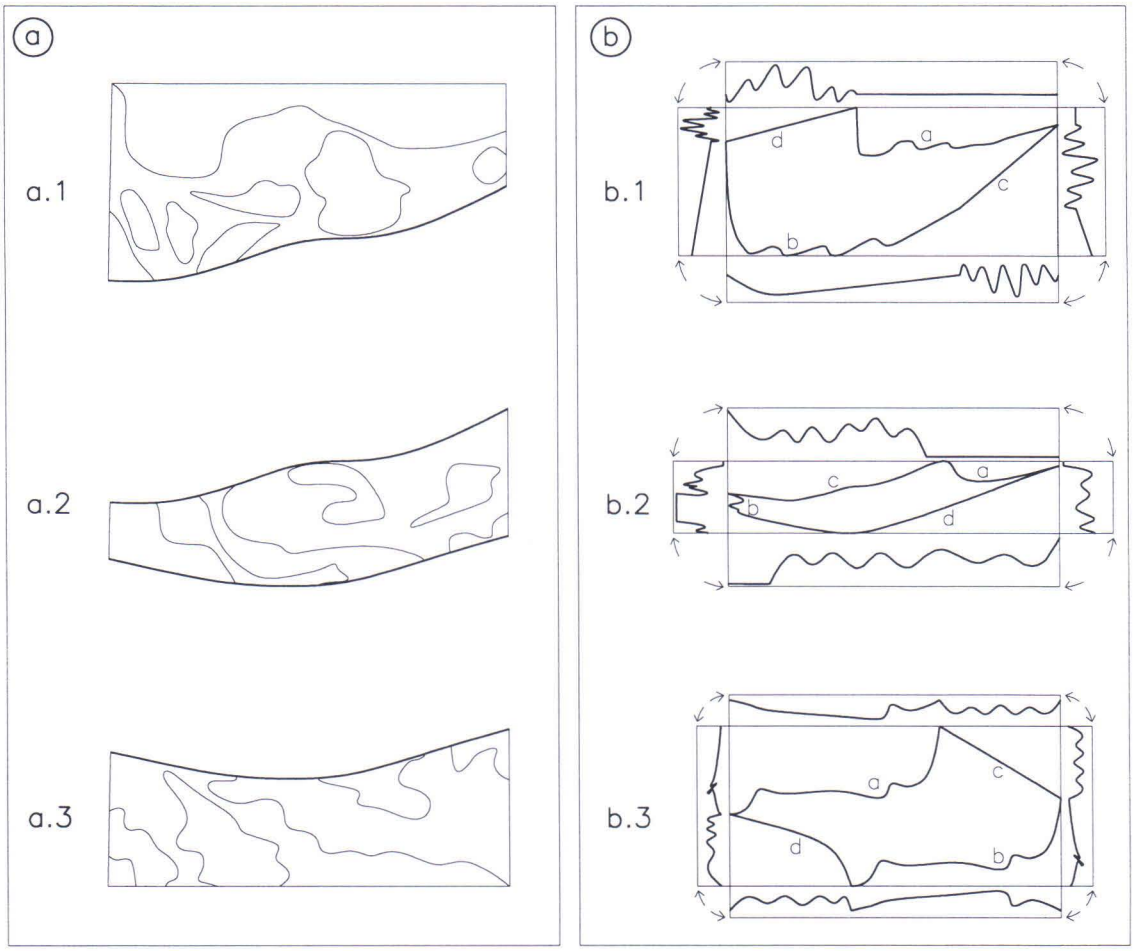

Fig. 52. a.1-a.3: Division of study area into three parts on basis of mode of occurrence of D_3 structures and metamorphic properties. The northern part comprises mainly the Tampere Schist Belt. The central part is composed of intensely metamorphosed migmatites of the Pori-Vammala-Mikkeli type. In both areas the axial plane of the dextral F_3 folding strikes northeast-southwest. The southern part covers an area where rocks vary in metamorphic grade from andalusite-mica schists to garnet-cordierite gneisses and where sinistral F_3 with a northwest-southeast-striking axial plane dominates. Also shown are heavily simplified lithological contacts in the study area.
b.1-b.3: The form lines controlling the shapes of the grid surfaces used in 3D modelling for each area.

well preserved metasedimentary rocks. Typical of the central part is that S_2 and S_3 planes cut each other at a high angle. In the north and south this part is bordered by S_3 shears, and D_3 occurs mainly as dextral folding, its axial plane striking northeast-southwest.

In **the southern part** (Fig. 52.a.3), the metamorphic grade varies greatly, the supracrustal rocks being in places andalusite-mica schists and in places migmatitic garnet-cordierite gneisses. This part differs from the others in that D_3 occurs predominantly as sinistral folding, its axial plane striking northwest-southeast.

The areas are thus composed of parts bordered by D_3 shears, each with its own D_3 and pre-D_3 characteristics. The F_3 asymmetry and the strike of the axial planes are the same

in the northern and central parts but the metamorphic grade is different. In the southern part, on the other hand, the metamorphic grade resembles that of the central part but the strike and asymmetry of the D_3 structures are different. The borders could be defined also another way, maybe by subdividing the study area into a greater number of parts on the basis of the above criteria. However, this would defeat the key purpose of the areal division, which was to make it easier for the reader to understand the criteria and parameters used to calculate the grid surfaces of the 3D model.

Figure 52.b shows separately for each part the 3D polylines that control the forms of the grid surfaces. Since these are lines winding in 3D space, they first had to be projected onto the XY plane and also four vertical planes, which were then rotated into the XY plane. The images can, thus, be understood as inverted boxes, with the structural elements visible on the erosion level drawn on the bottom, and the sides, once the form lines of the vertical planes had been drawn, cut open along the edges and spread onto the same plane as the bottom. Since the lines on the XY plane are curvilinear, the vertical planes cannot be parallel to the intersection line of the form lines and the XY plane. In other words, all four vertical sections are needed to outline the nature of the Z direction of the form lines. Note that the presentation of form lines is not provided with a scale, as it is the shape of the intersection lines of the XY, XZ and YZ planes that is essential, not their scale. This point is particularly strongly emphasized in the lines projected onto vertical planes, as numerical Z values would require a greater number of accurate pressure determinations on the present erosional level than would be feasible within the error limits of current geological barometers.

Northern subarea

The form lines of the northern part (Fig. 52.b.1) were drawn on the basis of the works of Nironen (1989a,b), Perttula (1982), Kähkönen (1996), Leveinen (1994) and Kilpeläinen et al.(1994) and the description of subareas given here. Of the lines on the XY plane, a and b display the intersection lines of the S_2 plane and the erosion level, and c and d the intersection of the S_3 plane and the erosion level. The winding of the S_2 form lines is thus due to F_3 folding. It is known that the S_2 schistosities in the northwest of the Tampere-Vammala area first strike northwest-southeast (Perttula 1982) and further west almost north-south. In the east, the S_2 schistosities strike about east-west as a whole, but are distinctly deformed by dextral F_3 folding, its axial plane striking northeast-southwest. The size and shape of the F_3 folds are directly visible on the present erosion level due to the vertical S_2 planes. In the lithology this is seen in the hooked form of the Mauri meta-arkose and on the tectonic maps of Nironen (1989a,b) (D_2 in the local classification of Nironen).

According to Nironen (1989a,b), the F_2 axes of the present work are subhorizontal in the Tampere synform area. Leveinen (1994) points out that the Mauri arkose is located stratigraphically in the upper or middle part of the Tampere schist belt. In the description of the Mauri subarea, it was mentioned that the andalusite-mica schists south of the meta-arkose are located stratigraphically even higher than the arkose. Hence, it is likely that, at the Mauri arkose, there is at least a minor F_2 axial depression in the Tampere Schist Belt. Its existence was inferred when the vertical intersection of line b was determined. Note, however, that the vertical intersection of line a has been assumed horizontal over its whole length due to the scarcity of observations of plunges of F_2 axes close to the contact of the Central Finland Granitoid

Complex.

Nironen (1989a,b) maintains that the structure of the central part of the Tampere schist belt is due to the large syncline, near the northern edge, on both limbs of which there are smaller synclines and anticlines. Here, the structures must be considered as syn- and antiforms, but their forms can be understood as similar to those described by Nironen. Drawing on his structural and stratigraphic studies he further maintains that the wavelength of the synclinal folding must be of the order of > 1 km. The stratigraphy in the Mauri subarea suggests that the wavelength of F_2 folds is of the order of kilometres there, too (the present work).

In the Tampere synform area and the Mauri and Myllymaa subareas, the layering on the limbs of the F_2 folds is vertical and the S_2 schistosity approximately parallel to the layering. We can then assume that, at least in the part of the Tampere Schist Belt covered by the present study, the F_2 folding is tight, as also reported by Nironen (1989a) from the synclinal area. The nature of the F_2 folding in the Z dimension is visible on all the vertical planes in Fig. 52.b.1, but since the S_2 direction is assumed to be east-west in the east, only the north-south-striking vertical section at the far right can be considered approximately perpendicular to the F_2 axis. This section shows that, on the basis of the above descriptions, the F_2 folding has been assumed to be tight with a vertical axial plane and an amplitude more than W/2.

Central subarea

The form lines of the central part (Fig. 52.b.2) are based on the structural interpretations presented here in the descriptions of the Ellivuori, Pirkkala, Stormi and, partly, Myllymaa subareas. In the central part the S_3 planes still strike about northeast-southwest but, unlike in the northern part, the S_2 planes are more strongly D_3 rotated, especially when compared with the Tampere synclinal area, and S_2 and S_3 tend to cut each other at a high angle. The structural elements in Fig. 51 also show that the intensity of F_3 folding increases westwards. Of the form lines in the XY plane, a and b refer to the intersection line of the S_2 planes and the erosion level, as in the northern part, and c and d to the intersection of the S_3 planes and the erosion level.

The form of the easternmost S_2 line on the XY plane (line a) has been copied directly from the form line map of the Pirkkala subarea. Thus, the ends of line a mainly represent S_2 in a primary position, whereas the middle part of line a has been deformed almost into a north-south direction. S_2 has been deformed even more strongly at the western margin of the central subarea. The style and amount of deformation of line b is a combination obtained from the form line maps of the Myllymaa and Ellivuori subareas and thus represents the style of intense F_3 folding on the erosion level. Since the F_3 folding in the central part is dextral, the asymmetry of both of the S_2 form lines on the XY plane is dextral.

In the chapter dealing with the correlation of the structures of subareas, it was suggested that the horizontal displacement component of D_3 shears was considerably more important than the vertical one. Owing to the vertical position of the S_2 planes, the horizontal displacement is directly visible on the erosion level, but the magnitude of the vertical movement cannot be determined accurately. That this movement was minor is suggested by the fact that the F_2 axes are invariably gently plunging, although the strike varies, and that the variation in syn-D_1 metamorphic grade along the S_2 planes is slight. To prevent the model from taking a stand on vertical displacement, the intersections of the S_2 planes and vertical planes are horizontal lines.

Lines c and d on the XY plane represent the intersection lines of the S_3 planes and the

erosion level. Line c has the same shape as the boundary line between the northern and central parts, which runs along the S_3 line shown in Fig. 51. The shape of line d on the XY plane was determined in such a manner that the strike of its eastern end was obtained from the S_3 line south of Pirkkala in Fig. 51 and that of the western end from the S_3 form lines on the tectonic map of the Stormi subarea. Owing to the high angle between S_2 and S_3, the effect of F_2 folding is visible in the projections of lines c and d in vertical sections. We are not here concerned with deformation of F_3 axes but with the apparent influence of the geometry of older structures on the measured axes of younger folds. Since the model assumes the vertical displacement of D_3 to be zero, the F_3 axis must be vertical in the model.

It was mentioned above, that the F_2 axes have a gentle plunge in the area but that their strike varies. In the description of the Pirkkala subarea it was pointed out, however, that the axes of F_2 folds, which were rotated into a north-south direction, mainly plunge gently northwards. This exception to the general regional geometry was taken into account when the model was compiled, the synform at the eastern end being made shallower in the vertical section of line d than in that of line c. The same could have been done by giving line a a gentle plunge northwards in the vertical section. The operation, although adding little more than a cosmetic touch to the modelling, produces F_2 fold patterns on the erosion level in the final model.

Southern subarea

The form lines of the southern part (Fig. 52.b.3) differ conspicuously from the above due to the different strike of S_3 planes. The lines were drawn largely on the basis of the tectonic map of the Koosanmaa subarea. Since this subarea, which was mapped in detail, covers only a portion of the southern part of the study area, observations from outside it were also used. As in the northern and central subareas, lines a and b represent the intersection line of the S_2 planes and the erosion level and lines c and d the intersection line of the S_3 planes and the erosion level. Note that lines a and b are identical. This is because detailed structural mapping could not be conducted in the northwest of the southern subarea owing to the lack of appropriate supracrustal outcrops. Form line b was therefore copied as such to be used as line a in the model. Another alternative would have been to present line a as a neutral straight line but, as shown by Fig. 51, enough observations have been made in the northwest to show that the structure resembles, at least to a certain extent, that of the Koosanmaa subarea.

The form line map of the Koosanmaa subarea shows that the sinistral F_3 folding with a northwest-southeast-striking axial plane has locally rotated S_2 planes into a north-south direction. This feature was copied as such into lines a and b, as was the feature in the west of the southern part, and visible in Fig. 51, where local F_3 with an almost north-south axial plane intensely deforms the S_2 planes. As elsewhere in the study area, the S_2 planes are vertical, and the horizontal component of D_3 is directly visible on the present erosion level. The southern part differs distinctly from the northern and central parts in that here the changes in M_1 metamorphic grade along S_2 planes are characteristic and fairly intense (see the description of the Koosanmaa subarea).

The relative crystallization time of porphyroblasts suggest, that metamorphism occurred before D_2. The explanation must be in the strong F_2 axial culminations and depressions. It appears, then, that a distinct vertical movement occurred in the D_3 conjugate with a northwest-southeast-striking axial plane. Over a distance of about 5 km, the supracrustal rocks of the Koosanmaa subarea change

in the direction of S_2 from potassium feldspar-sillimanite gneisses into garnet-cordierite gneisses, implying that the fold axis plunges at about 45° on the hinge of the axial culmination/depression. This was assumed to be the case when the Z values were determined for S_2. Note that the vertical sections are not perpendicular to the intersection lines of S_2/erosion level, and angles cannot therefore be measured from the vertical sections. Moreover, there is some repetition of S_2 in the eastern and western vertical projections.

The shape of lines c and d on the XY plane derives from the structural elements in Fig. 51. Line c is straight, trending northwest-southeast, as do S_3 lines in the Kylmäkoski area in Fig. 51, but line d turns into a north-south position in its southern part reflecting the local north-south-striking S_3 (see above). Since S_2 and S_3 cut each other in the southern part at an angle of almost 90°, the Z values of F_2 folds are visible directly in the vertical intersections of lines c and d. Note again that nowhere are the vertical projections in Fig. 52.b.3 parallel to lines c and d. Nevertheless, the vertical sections show that lines c and d, like lines a and b, are identical to each other in their Z properties.

3D geometry of tectonic structures

Perspective models

Based on the above criteria, grid surfaces were made that reflect S_0/S_1 planes as well as syn-D1 metamorphic isotherms. The node distance of the grid pattern in this model is about 500 m, and so the fitting of the grid surface follows the shapes of the border lines accurately enough without making the size of the final image unnecessarily large. In the perspective model in Fig. 53, where the area is viewed from SSW at an angle of 20°, sev-

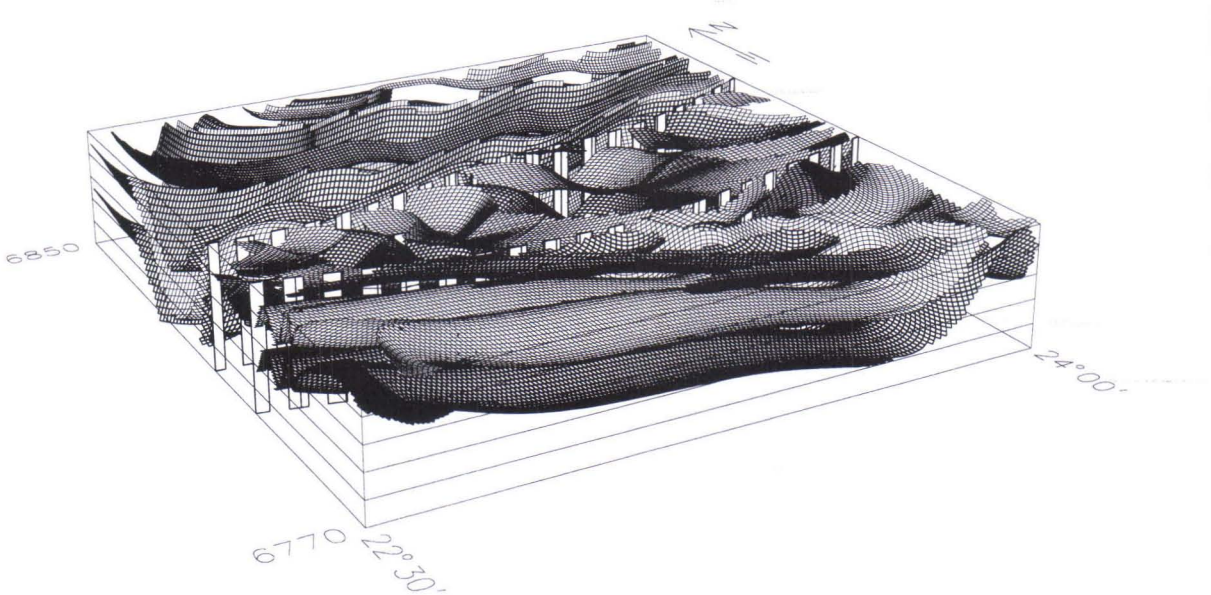

Fig. 53. Grid surfaces produced with the aid of the form lines inviewed obliquely from SSW. Note that borders of 3D boxes correspond to borders of study area (Fig. 2). To ease perspicuity, the northern, central and southern parts have been provided with "fences" that represent D_3 high-strain zones.

eral planes were copied onto different Z planes for the sake of clarity, after which an artificial erosion level was cut on the Z_0 plane. To enhance perspicuity, the margins of the northern, central and southern subareas were also marked in the image. As shown by Fig. 53, the direction from which perspective pictures is viewed is always a compromise as it only exhibits structures striking in a certain direction. Visualization of the whole structure thus requires several viewing angles from different directions, and for this, the model offers unlimited possibilities. On the other hand, due to the difficulties of visualization, the informative value of even a slightly more complicated 3D perspective image is rather poor. 3D modelling can, thus, be considered as a tool of geometric structural analysis that produces 3D images as by-products. These images can then be further elaborated into a more visual form.

Before 3D perspective models like those in Fig. 53 are worth displaying, we have to test how compatible the model is with structural interpretations made from the erosion level with traditional methods. In an interpretation of the total structure of a larger area, such as the present study area, we can use geophysical maps reflecting the surficial geology; aeromagnetic low-altitude maps are probably the most useful, and so they can also be used to test the correctness of the 3D models.

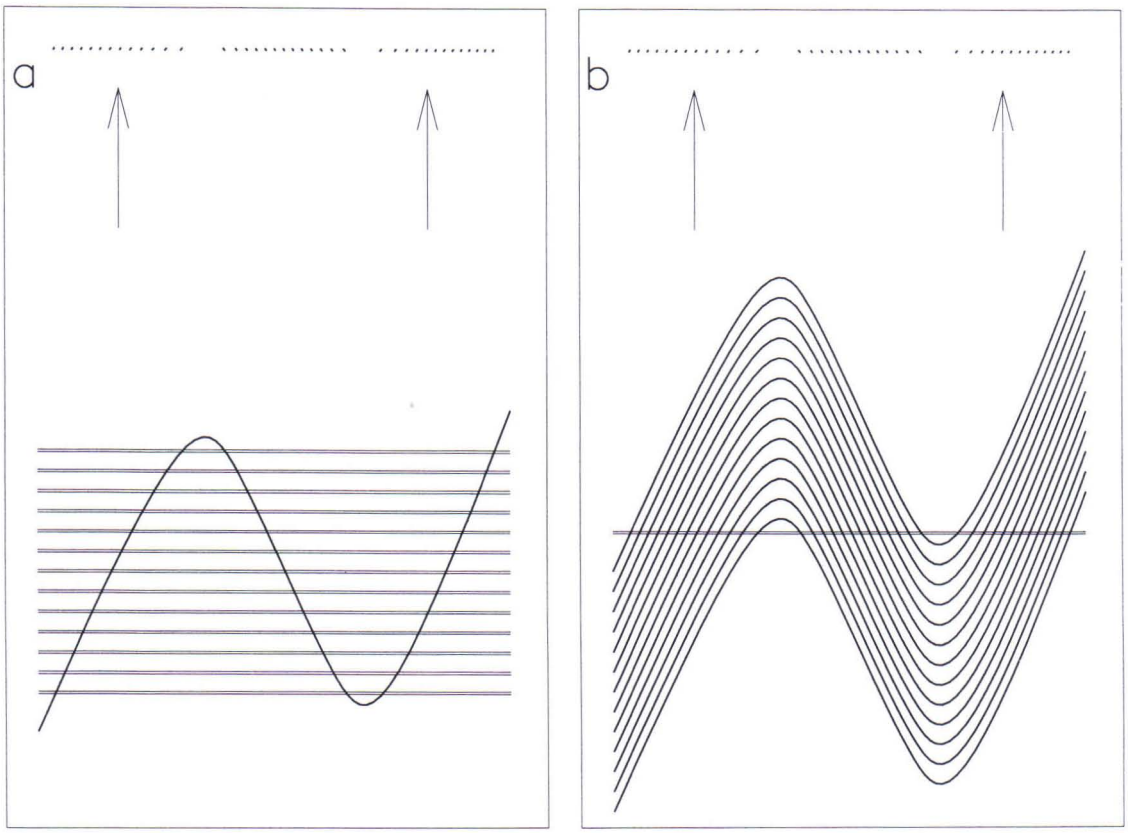

Fig. 54. Ways in which the interference pattern is cut from 3D grid surface model. At left, sections cut from one grid surface at different depths are projected on an XY plane. At right, one XY section is cut from the grid surface multiplied in Z direction.

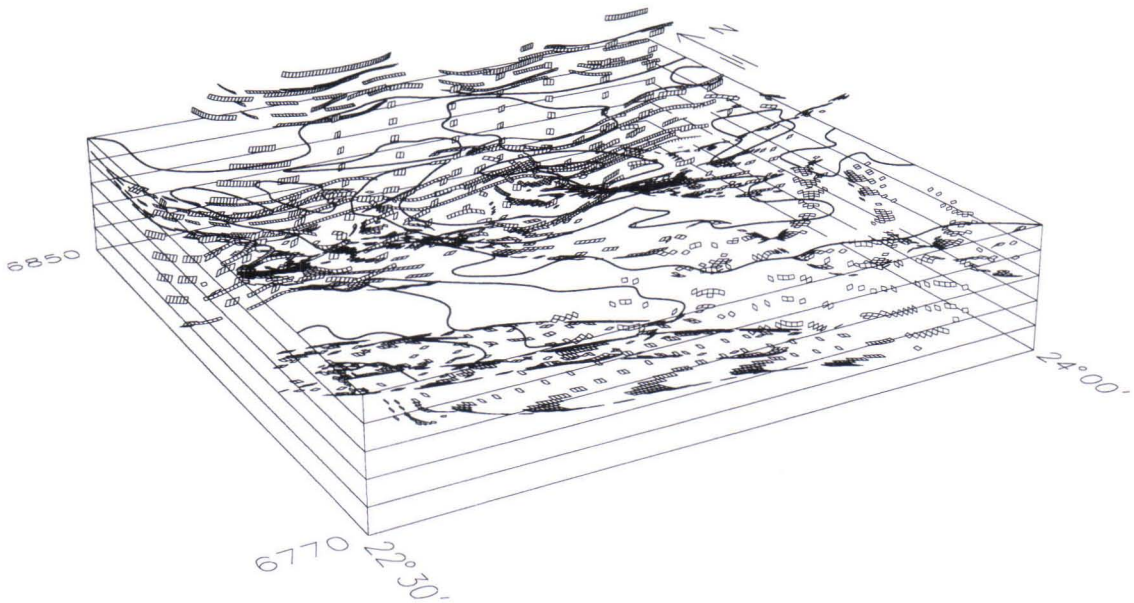

Fig. 55. Surfaces produced using first cutting option of Fig. 54 before being projected onto same XY plane. The borders of the 3D box correspond to those of the study area (Fig. 2). Also drawn on Z=0 plane are the simplified lithological contacts of Fig. 52.

However, we are in danger of getting into a vicious circle here, as the erosion level cut from a 3D structural model built up solely from the structural interpretation of a magnetic map, for instance, perforce resembles the starting material. If, however, 2D maps and thus the model, too, are compiled using several techniques the danger of unintentional self-steering is reduced. The danger is also reduced by the fact that erosion levels cut from even slightly complicated surfaces folding in 3D spaces are difficult to imagine beforehand. If structures that cannot be measured geophysically are to be modelled, the models must be tested with methods other than geophysical maps.

2D interference patterns

The desired erosion level can be cut from the model in several ways. If only the interference pattern of a folding surface is required, the easiest way to get it, and with the least computer capacity, is to handle only one grid surface and to cut several sections from it at different depths and project them onto one plane (Fig. 54a). The alternative is to multiply the surface in the Z direction and then take one section (Fig. 54b). If the multiplied surfaces are equal, both approaches give identical results. However, it is often necessary to identify each surface, for example, with colour, on the erosion level; in that case, the latter approach is practical. One way is to examine a model like that in Fig. 53 from a direction perpendicular to the section plane and not to display the surfaces behind (under) each surface. An image is then obtained in which the uppermost grid surface at each place fills up the spaces between the intersection lines of the cutting plane and the cutted surfaces.

Whichever of the two ways we use to create the interference pattern of the erosion level, it can still be presented using several techniques. If only the intersection lines of the surfaces and the erosion level are presented, we obtain closed structures, exclud-

ing the lines extending to the margin, from which it is possible in principle to identify the intersection line of each grid surface by counting them (without colour). The weakness of this presentation is that dips are difficult to interpret from a surface projection without the original data. Another approach is to cut a thin slice rather than a surface from the model, and to display only the whole meshes in the XY plane projection. Then, the shape of the meshes, if originally quadrate, reveals directly the angle of the dip although not its direction. When a section of a 3D model of a refolded fold is examined, the shape of the mesh is also indicative of the plunges of the fold axes. These elements can, however, be interpreted only when there is no need for a perspective presentation, as, for instance, when viewing one section alone.

The section in Fig. 55 was made mainly using the first approach. A surface was fitted for each area with the aid of the border lines in Fig. 52. The grid surface was then sliced in the Z direction into segments 500 m thick (the size of meshes in the whole model was 500 m x 500 m) and every other segment was removed. In a perspective image, the model then looks like that in Fig. 55. The meshes in Fig. 55 have not yet been projected onto one plane, but this is not necessary if the image is viewed directly from above without perspective presentation, as in Fig. 56. The intersection lines in Fig. 57 were obtained from the same data, but all the slices of Fig. 55 were first transferred onto the Z_0 plane,

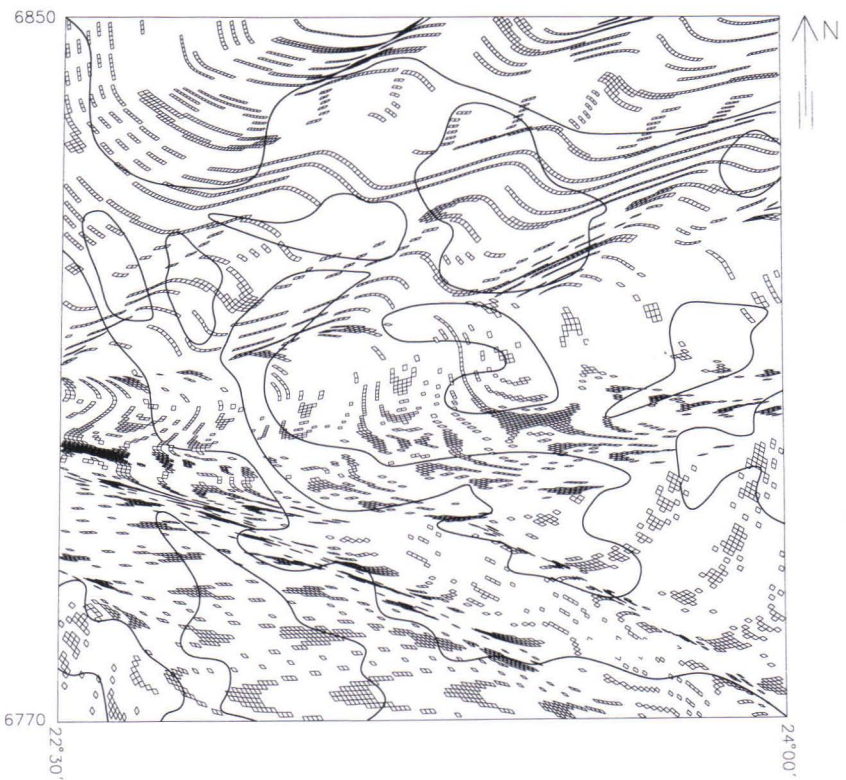

Fig. 56. Figure 55 viewed from above. The shape of meshes can be used to estimate the magnitude of dip but not its direction. Image borders correspond to those of study area (Fig. 2) but lithological contacts are simplified.

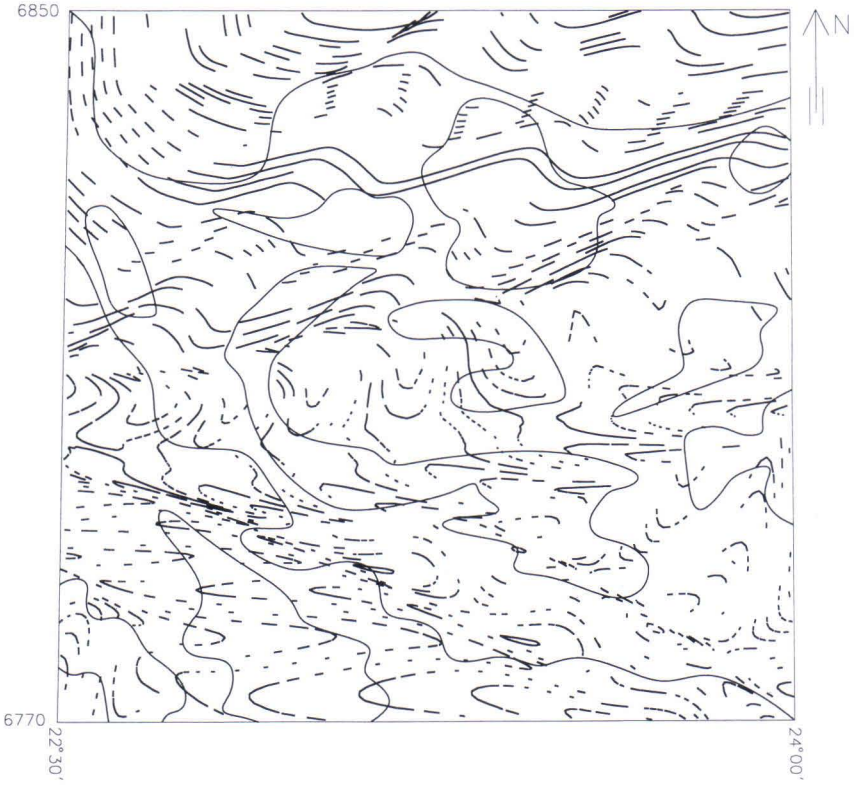

Fig. 57. Intersection lines of Z=0 plane and sections of Fig. 56 projected on Z=0 plane. The borders of the image correspond to those of the study area (Fig. 2) but the lithological contacts are simplified.

and the interference patterns are the intersection lines of the meshes and the Z_0 plane. The intersection lines are not coherent here, neither do they form closed structures, because the starting material was not the original whole network surfaces of Fig. 53 but the cutted surfaces shown in Fig. 55.

Limitations

With the completed model, it must be remembered that when the form of the surfaces is calculated in 3D space it is assumed that the folding surface is homogeneous everywhere. But this is never the case in reality, no matter what geological properties the surfaces are supposed to show, such as layering, isograds, isotherms and so on. First, the inhomogeneity increases with the increase in the size of the area and, second the increase in temperature with depth alters the physical properties of deposits and formations, controlling the shape of folds (plasticity of rocks). Another point to be remembered when examining the model, and which is difficult to take into account with when it is being built, is the effect of intrusive rocks. In principle, the effect of postorogenic intrusions can be eliminated if the form of the intrusion is known in the Z direction, too. Synorogenic plutonic rocks, however, make the starting material even more heterogeneous, controlling the partitioning of strain during deformation. What is more, the 3D shape of the synorogenic intrusions is difficult to outline. The effect of the intrusions is, however, taken indirectly into account in

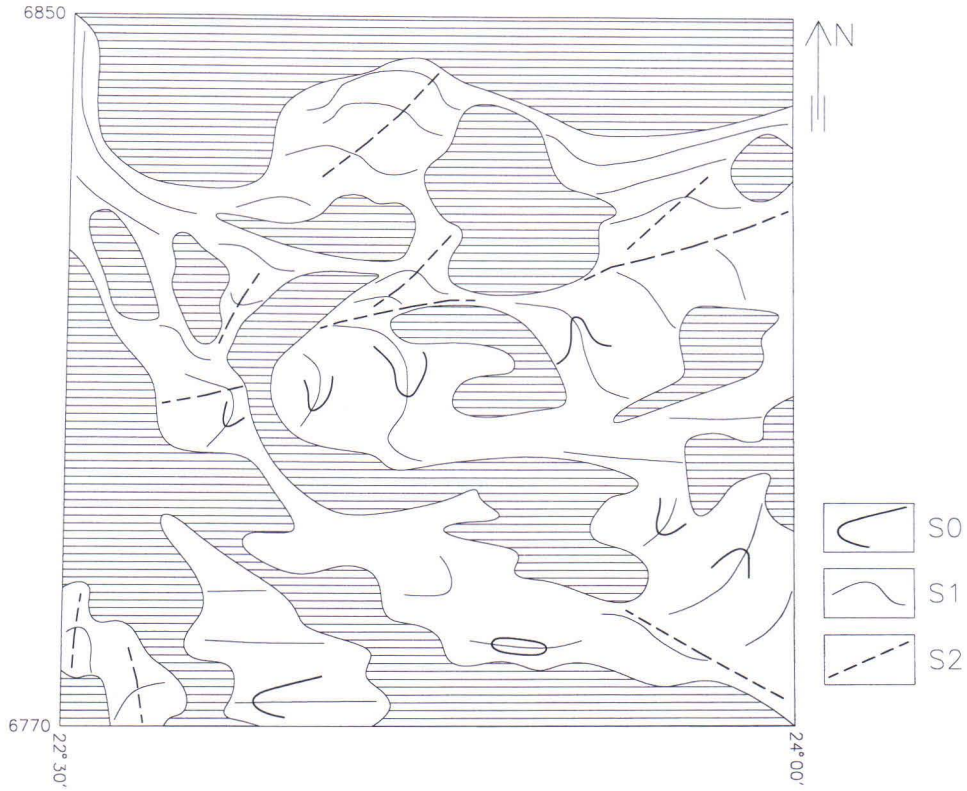

Fig. 58. "Second generation form line map". Hatched plutonite areas drawn in accordance with simplified lithology in Fig. 52. Unhatched areas refer to supracrustal rocks. Area shown in figure corresponds to study area (Fig. 2).

modellings, such as that applied here, the shape of the 3D curves that mark the fitted surfaces having been interpreted from the structural data affected by the intrusions. The problem is, however, that the effect of the intrusions on the geometry of the structures is visible only on the erosion level. In the erosion level images of Figs 56 and 57 the contacts of plutonic rocks were drawn without classifying them on the basis of their relative ages.

Although the erosion levels of Figs 56 and 57 were deduced from generalized data, and so local details were omitted, they still exhibit clear similarities with the magnetic map of the same area (Fig. 3). A "second generation form line map" (Fig. 58) can be drawn on the basis of Figs 53, 56 and 57. The similarities with the form line map in Fig. 51 are evident.

3D geometry of syn-D_2 and syn-D_3 isotherms

Geometry of D_3 conjugates

Many structural studies on the Tampere-Vammala area (Nironen 1989a,b, Kilpeläinen & Rastas 1992, Kilpeläinen et al. 1994) maintain that the D_2 structures of the present work were formed as a result of north-south shortening. Nironen (1989b) further suggest-

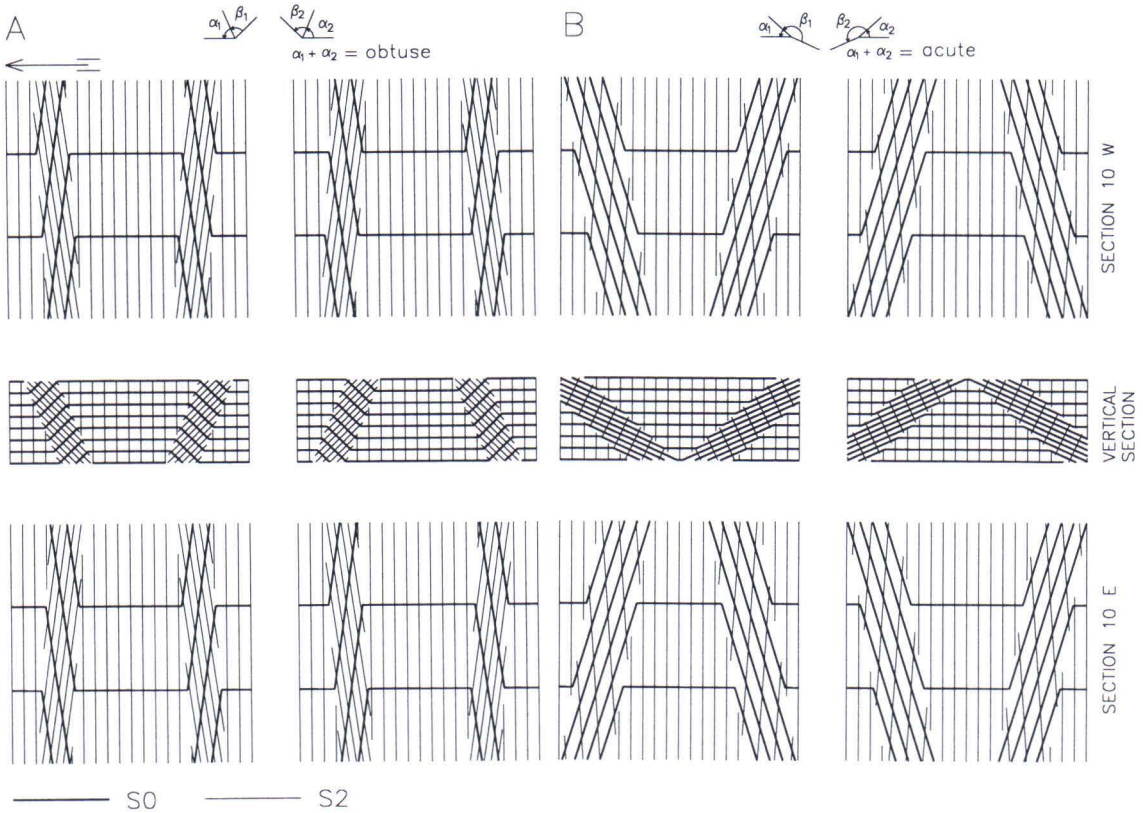

Fig. 59.3D geometry of conjugate F_3 pair and effect of section on pattern on erosion level. A = compressional alternative, B = extensional alternative. Section 10 W = section dipping 10°W. Section 10 E = section dipping 10°E. Modified after Ramsay & Huber 1989.

ed that the F_3 structures of the present work in the Tampere synclinal area are due to a dextral, horizontal shear striking east-west. It is here proposed, however, that D_3 occurs as two conjugates differing in asymmetry. If it is assumed that compression during D_2 acted in a north-south direction, the D_3 structures can be explained as having formed in the same stress field. Figure 59 shows what a conjugate fold pair that deforms a gently dipping (S_0/S_1) planal structure and a vertical one perpendicular to it (S_2) at the same time would look like in a gently dipping section. For the sake of simplification, it is assumed in the figure that the maximum shortening was exactly horizontal (symmetrical structures) and exactly perpendicular to the vertical S_2 schistosity.

Figure 59 shows both a contractional (A, $\alpha_1+\alpha_2$ = obtuse) and an extensional (B, $\alpha_1+\alpha_2$ = acute) alternative (Ramsay & Huber, 1989), which differ from each other in that the former is caused by compression and the latter by stretching. The gently E and W dipping sections show that, in these cases, both the contractional and extensional models result in similar interference structures if the section in the first model dips gently eastwards and that in the second model gently westwards. In other words, the D_3 structures in the Tampere-Vammala area can be understood as conjugates, but we cannot tell

from the interference patterns visible on the erosion level whether D_3 is associated with compression or extension.

Isotherms, their folding and metamorphic overprinting

In those parts of the Tampere-Vammala area where metamorphism occurred above the break down reaction of muscovite, the originally subhorizontal S_1 schistosity dominates and the porphyroblasts started to crystallize syntectonically in relation to the S_1 schistosity. We can therefore assume that the isograds, too, were originally gently dipping and that the metamorphic grade increased downwards. If the isograds throughout the area were still parallel to S_0/S_1, the metamorphic grade on the present erosion level would vary in direct correlation with D_2/D_3 interference structures, i.e. the synforms would have the lowest-grade and the antiforms the highest-grade rocks. However, as it is seen from the relatively late crystallization of the porphyroblasts in weakly metamorphosed areas, things are not that simple. In the least metamorphosed areas the porphyroblasts crystallized during D_2 and D_3 and in places even over S_3. Moreover, features were found in migmatitic subareas implying that the temperature remained high for a long time in the zones of intense D_3, or that these zones even experienced a new thermal pulse. The association of the late, high temperature with the D_3 zones in the migmatite areas is unlikely to be due to the D_3 itself, but to the possibility that the D_3 zones were favourable to the movement of water-rich fluids transporting heat, as is also reflected in the syn-post-D_3 migmatization maximum in these zones.

That the temperature remained high for a long time is suggested by the fact that garnet continued to crystallize in the above zones of the Vammala high-grade migmatites - without interruption - from D_1 right through to the final stages of D_3 or even up to post-D_3 (large garnets also crystallized in undeformed neosome imitating the existing structures). Since the late thermal effect is restricted to certain structural places only and since the syn-D_1 and syn-D_3 crystallizations differ clearly in age, it is arqued to speak about a new thermal pulse, depending on the part of the Tampere-Vammala area referred

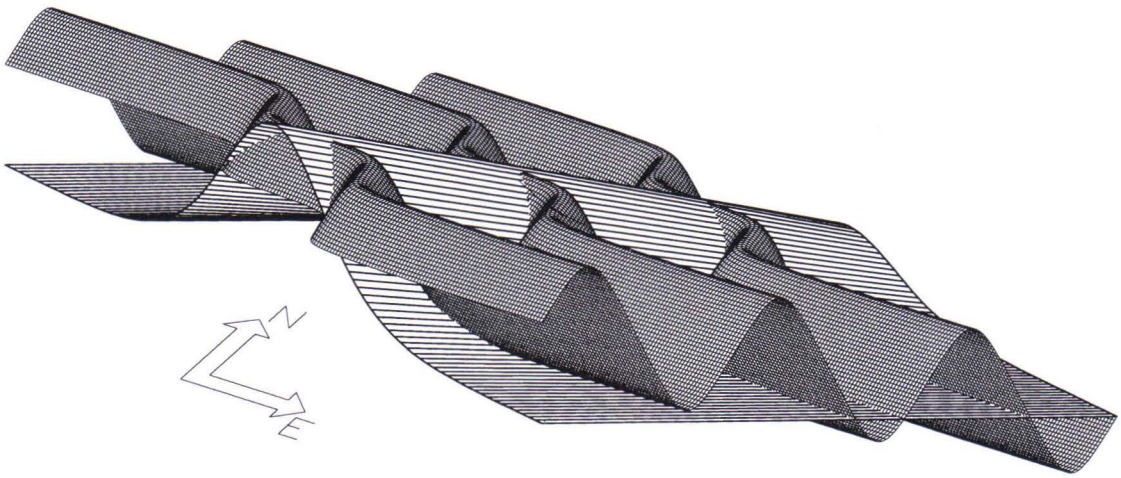

Fig. 60. Dependence of the culmination age of metamorphism on 3D geometry of syn-D_1 and syn-D_3 isotherms. Cross-hatched surface = M_1 isotherm, hatched surface = M_3 isotherm. Note oblique view from above.

to. Direct evidence of the age of the younger thermal pulse in the Tampere-Vammala area does not exist; it probably, however, reflects the metamorphic pulse of southwesternmost Finland, 1850-1830 Ma (Korja et al. 1994, Väisänen et al. 1994).

We can best explain the manifestation of the new thermal effect mainly in F_2 synforms and zones of intense D_3 by assuming that the pre-D_2 and syn-D_3 isotherms of the same temperature in the Tampere-Vammala area are close to each other in a vertical direction. Figure 60 shows how the geometry of syn-D_1 and syn-D_3 isotherms of the same temperature can cause the above variation in the age of peak metamorphism in the Tampere-Vammala area. The cross-hatched surface presents a syn-D_1 isotherm folded by F_2, which forms a metamorphic synform in the north of the area. The younger isotherm (hatched surface) is assumed to represent high grade metamorphism of southwestern Finland. Therefore it cuts the D_2 structures, dipping gently northwards. The concentration of fluidal activity in D_3 zones is displayed in the upward bending of the younger isotherm in this zone. If a horizontal section is cut from the surfaces in Fig. 60 to present the erosion level, the temperature of the younger metamorphism in the northern synforms exceeds the temperature of the old metamorphism, causing the old structures to recrystallize. In the south, on the other hand, the new thermal pulse exceeds the conditions of the old metamorphism only in D_3 zones.

Age of metamorphism

The map in Fig. 61 shows the age of metamorphism as the time of crystallization of the porphyroblasts in relation to the structural elements. The oldest syn-D_1 metamor-

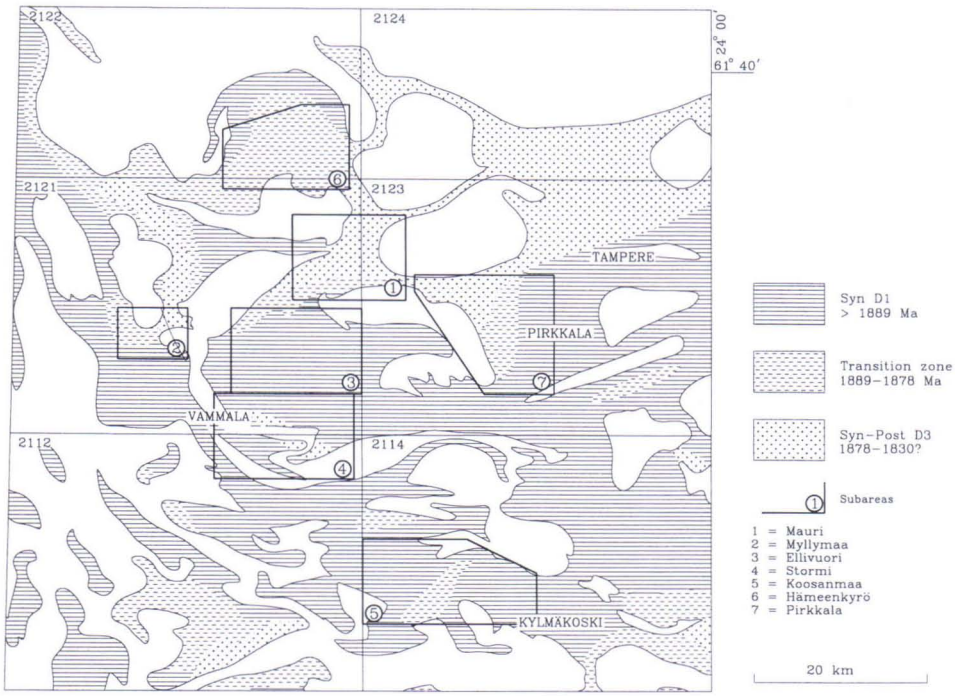

Fig. 61. Age of peak metamorphism in Tampere-Vammala area. Based on the relations between crystallization of porphyroblasts and development of deformation structures.

phism is represented by almost all the migmatitic rocks (Fig. 51). The rocks of the transitional zone are potassium feldspar-sillimanite and potassium feldspar-cordierite gneisses, in which some of the porphyroblasts are clearly older than D_2, whereas some cut the D_2 structures. The effect of the young metamorphism is mainly visible in migmatites south of Vammala. In the migmatite area the borders of the area affected by young metamorphism are gradual and thus the shading denoting the young metamorphism should in reality have a halo describing the transitional zone. Due to the scale used, however, it is not marked on the map. Porphyroblasts are virtually lacking in the core of the Tampere synclinal area, but all andalusite-bearing mica schists of the Tampere schist belt have S_2 or S_1/S_2 composite schistosity as andalusite inclusions, irrespective of whether the F_3 folding or the S_3 schistosity is visible on outcrops or not.

Also shown in Fig. 61 are the probable ages of metamorphism based on the age relations between the deformation structures and dated plutonic rocks. Since the emphasis is on the time of crystallization of the porphyroblasts in metasedimentary rocks, the shading does not cover the area of distinctly metamorphosed plutonic rocks.

Summary

The geometric 3D modelling was based on the intersection lines of S structures and the erosion level, the plunges of the fold axes and the mutual age relations of the metamorphic assemblages and the structural elements in the different parts of the study area. The starting point of the modelling was a simplified lithological map and the study area was divided into subunits on the basis of the metamorphic grade and the geometry of the pre-D_3 structures. Possible pre-D_2 fold structures were omitted and thus the 3D grid surface obtained can be considered to represent originally horizontal planes, which could be layering, repeated post-F_1 layering or metamorphic isotherms/isobars.

3D network surfaces can be presented as perspective models. Their informative value is, however, rather low due to their lack of perspicuity. The 3D modelling, can, therefore, be considered as a structural-analytic tool for testing the correctness of structural interpretations, i.e. whether or not the assumed 3D geometry will produce the features observed on the outcrops on the erosion level.

A weak point in the modelling is that the deforming objects must be assumed homogeneous, and the capability of the intrusive rocks to partition the deformation cannot be taken fully into account.

From the model we can conclude that both D_2 and D_3 structures could have been produced in a north-south stress field, but the geometry of the D_3 structures on the erosion level does not reveal whether these structures were generated by a compressional or an extensional tectonic event.

The modelling also demonstrates that the 3D geometry of M_1 and M_3 isotherms and their evolution as a function of time explain the syn-D3 culmination of metamorphism in both the Tampere synform area and the D_3 high-strain zones of the Vammala migmatite area.

EVOLUTIONARY MODEL OF TAMPERE-VAMMALA AREA

Problems with identifying and correlating pre-D_2 structures

Metamorphic patterns and pre-D_2 structures

For many reasons it is difficult to establish the nature and importance of pre-D_2 structures on the outcrops of the study area. Wherever the primary structures of the

metasedimentary rocks can still be identified, M_2 and M_3 metamorphisms have obliterated older metamorphic structures either totally or at least to such an extent that the earlier stages can no longer be distinguished from each other. In the areas of highest-grade metamorphism, D_1 structures are the most intense structural and metamorphic features, but then the primary layering has been destroyed, making it impossible to recognize possible F_1 fold structures or outline their geometry.

In the above structural model, all the pre-D_2 structures were collectively classified as D_1, which, typically, occurs as primarily gently dipping schistosity that increases in intensity with metamorphic grade. In the least metamorphosed areas, S_1 is lacking altogether and becomes recognizable only due to the break down reaction of muscovite. As also pointed out above, the variation in metamorphic grade in the area can be satisfactorily explained by post-D_1 events. Hence, it was not necessary to subdivide the D_1 structures when the present tectono-metamorphic structure was modelled.

The above D_2 and D_3 structures alone cannot, however, explain why some of the formations comparable to each other were already metamorphosed at the D_1 stage under conditions requiring depths of over 15 km but others remained almost unmetamorphosed. One explanation put forward by Kilpeläinen et al. (1994) is early thrusting. This notion is supported by observations of Kähkönen (1996) from the Tampere Schist Belt, where the synclinal structure described by Nironen (1989a) is not fully compatible with the age data. Thrusting would explain the rapid burial of formations at 15-km depth, i.e. the minor age difference between deposition and metamorphism. If, however, the intensely metamorphosed and migmatized conglomerate at Naistenmatka, Pirkkala, and the conglomerates in the Tampere synclinal area are the same formation, as suggested by Kähkönen (1996), the tectonic thickening of the crust caused by thrusting cannot explain the difference. As well as the conglomerates, the turbiditic metasedimentary rocks in the Tampere synclinal area and the Vammala migmatite area are comparable to each other in geochemistry (Lahtinen 1994), despite a substantial difference in metamorphic grade. The difference in metamorphic grade is even greater between the arc-related metasedimentary rocks of the Vammala migmatite area and the < 1890 Ma metasedimentary rocks of the synclinal area (Veittijärvi), which, according to Lahtinen (1996) are also possibly correlatable.

Key role of stratigraphy in Tampere Schist Belt

Although the Tampere Schist Belt is the best-preserved part of the Tampere-Vammala area and, for the reasons mentioned above, the deformational and metamorphic structures of the D_1 stage are largely lacking, it is in a key position in efforts to clarify the early deformations in the whole study area owing to its well-known stratigraphy. The whole of the Tampere Schist Belt formed in a developing island arc environment, the lowest formations (Haveri) representing an early rifting stage, and the youngest conglomerates having deposited during D_2, as shown by the dates of their clasts.

The whole rock Pb-Pb age, 1990 ± 25 Ma (Vaasjoki & Huhma 1987), of the formations around Haveri, which represent the lowest part in the stratigraphy, differs substantially from the age of the arc volcanic rocks in the Tampere Schist Belt (1904-1889 Ma) (Kähkönen et al. 1989), but structural-geological studies do not support the concept that Haveri represents an exotic relict markedly older than the Tampere arc volcanic rocks (Kähkönen & Nironen 1994). The geochemistry of even the lowermost metaturbidites of the Myllyniemi formation implies that they deposited in a distinctly volcanic

arc environment (Kähkönen & Leveinen 1994) and, according to Lahtinen (1994), subduction under the Tampere Schist Belt started at least 1905 Ma ago. According to Lahtinen (1994), subduction did not last long, because the last subduction related formations (Takamaa) deposited 1889 Ma ago (Kähkönen et al. 1989, Lahtinen 1994). According to Nironen (1989b), the synkinematic, 1885-1878-Ma-old granitoids were emplaced syntectonically in relation to synclinal folding in the Tampere synclinal area, that is, not until the collisional stage following subduction. Divergent opinions have been expressed concerning the direction of subduction. According to Nironen (1989a), the vergences of the structures in the schist belt suggest southward subduction, whereas Lahtinen (1994) bases his evolutionary model on assumed northward subduction under the Tampere Schist Belt.

Correlation between Tampere schists and Vammala migmatites

If the turbiditic gneisses in the Vammala migmatite area are correlatable with the lowest turbiditic metasedimentary rocks in the Tampere Schist Belt, the D_1 stage must be younger than the minimum age of the clastic zircons in the turbidites of the schist belt, 1910 Ma. D_1 structures are also visible in the andalusite-mica schists above the 1.9 Ga old Mauri meta-arenite. The D_1 structures of the present work are lacking in the core areas of the Tampere synform (Nironen 1989a), where the uppermost parts of the schist belt stratigraphy are exposed on the present erosion level. Since, however, the intensity of the D_1 structures declines upwards in the stratigraphy, their absence does not necessarily imply that the youngest metasedimentary rocks of the Tampere schist belt are younger than D_1. The synkinematic Hämeenkyrö and Värmälä metagranodiorites (1885 ± 2 Ma and 1878 ± 3 Ma) (Nironen 1989b) intruded in the following deformation stage, and so the age of the Hämeenkyrö intrusion is also the minimum age of D_1. On similar grounds it can be argued that the conglomerates with tonalite clasts as young as 1884 Ma in age (Nironen 1989b) deposited after D_1.

Subduction tectonics and pre-D_2 structures

The D_1 structures therefore evolved during the subduction stage but, at least partly, only towards its end, as they affect the horizons in the upper part of the stratigraphy of the Tampere Schist Belt (the andalusite-mica schists above the Mauri meta-arkose). The subduction stage was fairly short (15-20 Ma, Lahtinen 1994) but, as shown by the dates, the time in which the D_1 structures had to evolve was probably shorter. As mentioned earlier, during that period, and associated with D_1, marked level differences developed. As a result, some of the rocks of a certain stratigraphic horizon underwent syn-D_1 metamorphism at a depth of over 15 km while others remained unmetamorphosed or their syn-D_1 metamorphic grade was lower than the currently visible metamorphism, which occurred in the equilibrium field of muscovite and chlorite in association with $D_{2\text{-}3}$.

In the context of subareas, a few shears were described that were associated with D_1 and turned by F_2 into a vertical position from their original gently dipping or subhorizontal position. They are now graphite-bearing and, in places, sulphide-bearing, fine-grained schists and, being highly susceptible to weathering, are exposed mainly in road and railway cuts. Kinematic indicators that could be used to determine the direction of displacement have not been found in them and due to their more or less premetamorphic nature, it has been difficult to establish the conditions under which they were formed. Gentle dips may equally well refer to overthrusts and extensional events.

Extension in orogenic belts

Extensional events in orogenic belts are due to isostatic changes associated with shortening of the crust and the tendency towards equilibrium. Isostatic disequilibrium is caused among other things by thickening of the crust in collision zones. Extension then starts when isostatic forces finally nullify the horizontal compression caused by collision (Tapponnier & Molnar 1976, England & McKenzie 1982, 1983, Houseman & England 1986). According to this interpretation, the intensity of extension is proportional to the elevation of the area above sea level. Platt & England (1993) have presented a model in which the potential energy is reduced at the initial stage of thickening if the original thickness of the crust is less than 40 km, because the lithospheric mantle is denser than the surrounding asthenosphere, thus cancelling the tendency of the thickened crust to uplift. Isostatic disequilibrium, rapid uplift and extensional events do not start until the lower part of the thickened lithosphere has been convectively replaced by asthenosphere. The process is thought to last from a few million to a few tens of millions of years, counting from the beginning of the thickening process. Hence, the model states that the amount of potential energy depends on the original thickness of the crust and cannot be deduced from the elevation above sea level.

According to Malavieille (1993), extensional events can be divided into two categories: extension during the shortening stage of the crust and late-orogenic extension. The best known examples of the latter are the Cenozoic Basin and Range area in North America (Wernicke 1992) and the late-Palaeozoic, Variscan French Massif Central (Maluski et al. 1991, Malavieille et al. 1990, Echtler & Malavieille 1993). The first type is best represented by the Himalayas (Burchfiel & Royden 1985), where extensional events are still going on, and by the Alpine orogeny, which started in the late Jurassic and terminated about 30 Ma ago (Ratschbacher et al. 1989).

Extension during subduction has been described from southeastern China, where the HT-LP metamorphic extensional Wugongshan massif formed in an active-margin environment before the Cretaceous collision of the China and West Philippines microcontinents (Faure et al. 1996). The extension of arc and back-arc environments has been described from the vicinity of the Mediterranean (Jolivet et al. 1994), where in the Aegean and Tyrrhenian back-arc areas the metamorphic rocks are being exposed in extensional processes, whilst the crust is continuing to thicken in the thrust front zone. Jolivet et al. (1994) maintain that the thrust front and the areas dominated by extensional events migrate in the opposite direction to the subducting plate. The compressional structures of the thrust front therefore migrate into an extensional environment and are reoriented as subduction proceeds.

Gentle dipping shear surfaces exhibiting all the transitional stages from deep ductile to shallow brittle shears are among the most typical deformational structures formed in the course of extension. Also fairly common are boudinages on various scales, folds with axes parallel to the stretching lineation and subvertical brittle faults (Malavieille 1993). Not only do the structures formed in extension rework the existing structures caused by compression, but many of them are identical with the latter and so are very difficult to distinguish from each other after reorientation.

Evolutionary model

Basic ideas, components and simplifications

Figures 62 and 63 show a scaleless model of D_1 evolution dominated by extensional structures during subduction (1910-1889 Ma) and the subsequent D_2 compression (1889-1878 Ma) in the Tampere-Vammala area. In Fig. 62 the D_1 structures start to evolve immediately after the 1.93-1.91-Ga rifting stage of the model of Lahtinen (1994, Fig. 29), and in Fig. 63 the structures correlate with the collision of the Tampere Schist Belt/Central Finland Granitoid Complex-Hämeenlinna-Somero Volcanic Belt/Kemiö-Mäntsälä Belt, which started about 1.89 Ga ago as presented by Lahtinen (1994) and Kähkönen et al. (1994). The model does not take a stand on the occurrence of 1.9-2.0-Ga-old Palaeoproterozoic crust (Lahtinen 1994), except that all the metaturbidites of the Vammala migmatite area are assumed to correlate with the turbidites in the lower part of the Tampere Schist Belt, and thus do not represent, even partly, the older crust, as suggested by Kähkönen (1994).

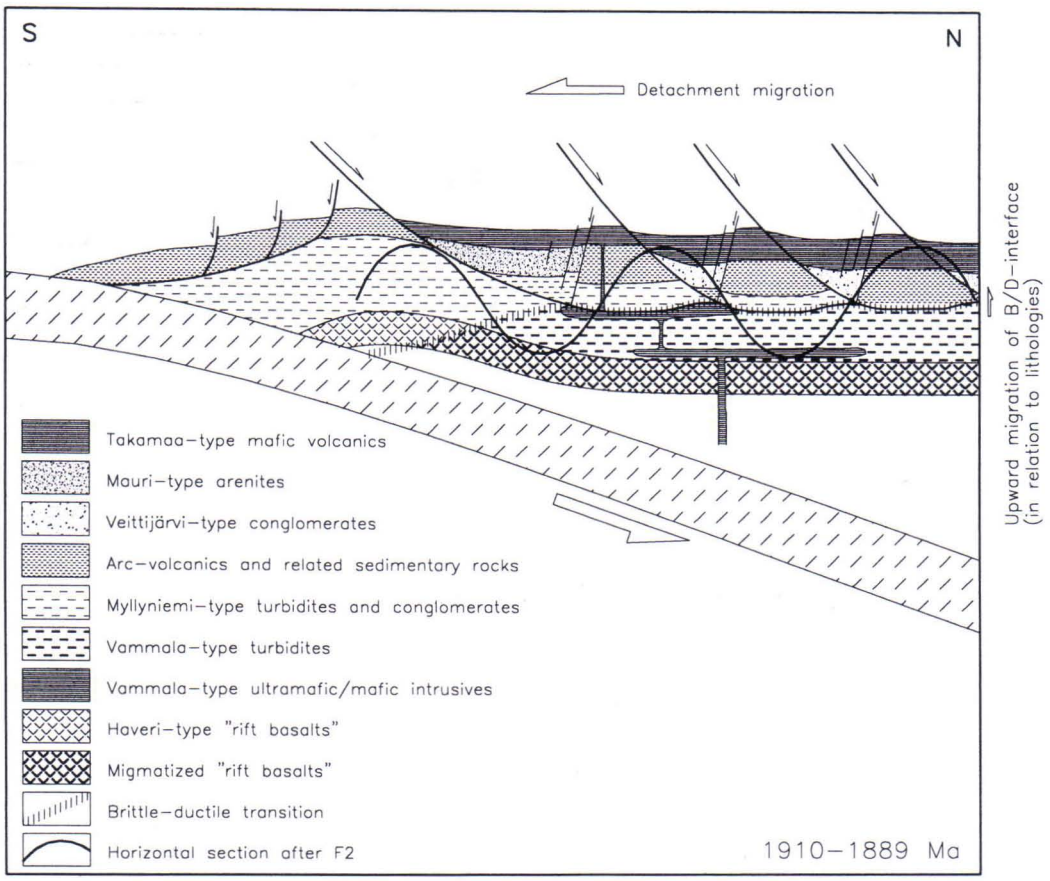

Fig. 62. Schematic model of D_1 and M_1 evolution during subduction dominated by extensional structures in Tampere-Vammala area. Not to scale. For details, see text. Note, that Takamaa-type mafic volcanic rocks and Vammala-type ultramafic/mafic intrusive rocks are considered as comagmatic.

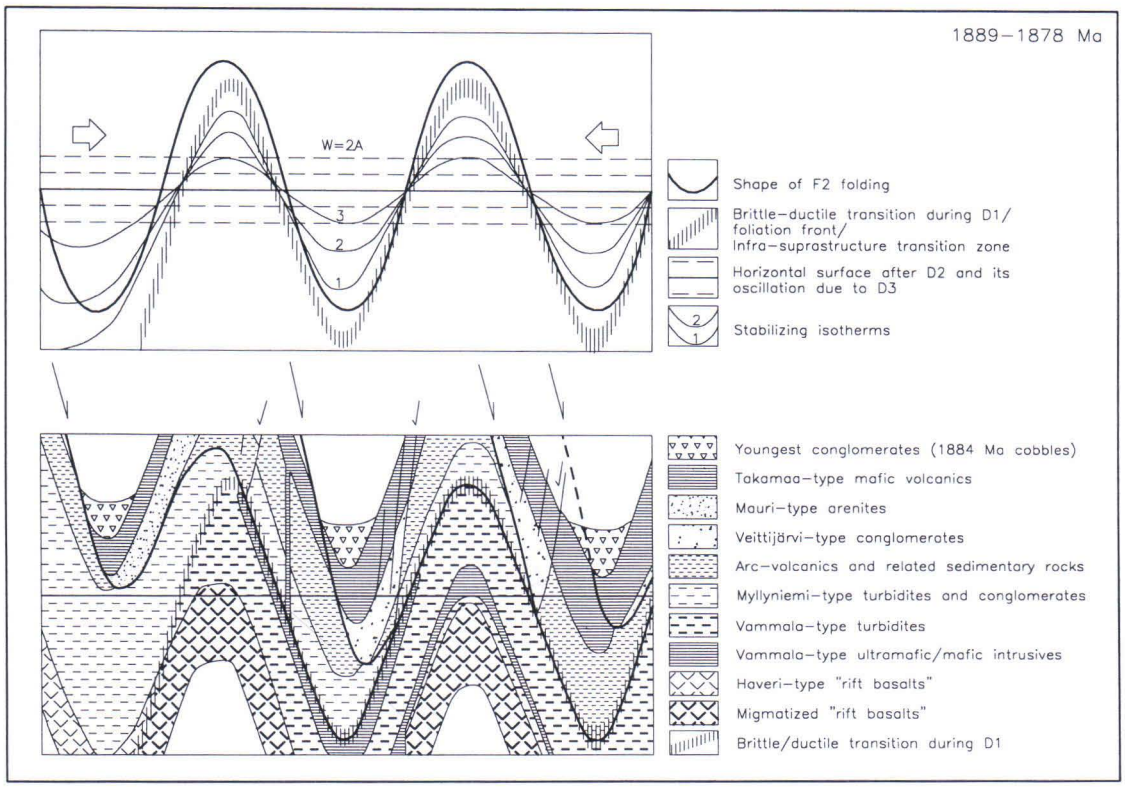

Fig. 63. Effect of F_2 folding on geometry of D_1 and M_1 structures in Fig. 62 in north-south-striking vertical section. For details, see text.

The assumed evolution and geometry of the D_1 structures are mainly based on models published by Jolivet et al. (1994), Ratschbacher et al. (1989) and Faure et al. (1996). In their models, extension is triggered by the gravitative instability caused by a subducting plate (Ratschbacher et al. 1989), thermal and gravitative instability due to arc magmatism (Faure et al. 1996), and thrust front migration in the opposite direction to the movement of the subducting plate, as a result of which the thickened part of the upper plate gradually moves towards a hotter arc environment. The brittle/ductile transitional zone rises upwards in the thickened crust and the whole mass becomes more plastic and easier to deform (Jolivet et al. 1994).

Figures 62 and 63 show the most important stratigraphic units (Kähkönen et al. 1989, Kähkönen & Leveinen 1994, Kähkönen & Nironen 1994, Mäkelä 1980, Matisto 1968, Ojakangas 1986, Peltonen 1995a), omitting the thicknesses of the formations and assuming that they occur throughout the area covered by the model. Essential for the model is the depositional order, the geometry of the structures and the evolution of the structures as subduction proceeds, and the reorientation of D_1 structures in F_2 folding. The movement direction of D_1 normal faults visible on the limbs of F_2 folds on the current erosion level may thus strike in any direction; the same applies to other D_1 structures whose asymmetry allows deductions to be made of the direction of movements during D_1. The model also simulates thermal evolution, which,

with a lag, tends to equilibrate the disturbances caused by the folding of isograds.

The model does not include synkinematic or latekinematic granitoids as it is intended to be as simple as possible yet sufficiently comprehensive to explain the features visible on the current erosion level. Of course, the emplacement of granitoids syntectonic in relation to D_2 affected the geometry of F_2 folds at least locally but in modelling the effect is difficult to simulate because each intrusion is unique in shape and size, and their uniqueness is further enhanced by the position of the intrusion in the total structure.

The direction of subduction in the model is that of the interpretation of Lahtinen (1994), whilst the geometry (tightness) of F_2 folding was taken from the interpretations of Nironen (1989a) and those presented here. The erosion level after F_2 folding in Fig. 63 is copied directly into the model in Fig. 62. Consequently, its attitude in relation to the F_2 form line is as much gentler as is the shortening caused by F_2. The F_2 synforms in Fig. 63 are shown as an "antiform" structure in the form line describing the post-D_2 horizontal section in Fig. 62, and vice versa. Since the images do not show the Tampere-Vammala area as such, the position of the F_2 form line and the post-D_2 horizontal section in the model are imaginary. However, for the model to match the observations made on the current erosion level, it is essential that the folds should have sufficient amplitude relative to the thickness of the layers and the D_2 geometry.

Stratigraphy and D_1 evolution

Haveri rift basalts

The rocks of the Haveri formation, which is lowermost in the stratigraphy, have been interpreted as representing marginal basin basalts associated with rifting of the pre-1910 Ma Palaeoproterozoic crust, and those of the Osara formation immediately above it as indicating a change towards an evolving island arc environment (Kähkönen and Nironen 1994, Lahtinen 1994). The "Haveri-type rift basalts" in Fig. 62 represent both formations, and since at least the lowest part of the former deposited before the subduction stage, that part can be taken as the "zero point" of evolution in the image. According to Kähkönen & Nironen (1994), the Harhala formation south of Haveri can probably be correlated with the arc volcanic rocks of the Tampere synclinal area proper.

The metamorphic grade of the Haveri formation on the present erosional level is higher west than east of Lake Kyrösjärvi. Schistosity parallel to layering is the oldest metamorphic feature on both sides of the lake. On the eastern shore, the porphyroblasts (garnet and muscovite pseudomorphs) crystallized before the end of the D_1 stage, but on the western shore the migmatization is in all likelihood D_1 in age (Kähkönen & Nironen 1994). It is uncertain whether the structures can be correlated with the classification applied here, for fold structures correlatable with the Tampere synform folding have not been encountered in that area. According to Kähkönen & Nironen (1994), the facing, which is invariably southwards implies, however, that the area is located on the northern limb of the Tampere syncline (here, F_2 synform). Hence, the schistosity subconformable with the layering is either S_1 or S_2 or a combination of the two, depending on the depth of the syn-D_1 section represented by the present erosion level. In any case, the retrograde alteration of the porphyroblasts differs from the features typical of the Tampere Schist Belt, where the prograde stage of metamorphism clearly cuts the synclinal folding. If S_1 and the peak of metamorphism correlate with the D_1 stage in Fig. 62, the present section could refer to a situation in which the difference in the metamorphic grade on opposite shores of Kyrösjärvi was

D_1 in age and the retrograde features were due to a local F_2 antiform.

Lowermost units of Tampere Schist Belt

The turbiditic metasedimentary rocks in the lower part of the Tampere Schist Belt and the metaturbidites of the northern part of the Vammala migmatite area are displayed as the same formation in Figs 62 and 63, which, depending on the place and time, may have been either only slightly metamorphosed, not metamorphosed until during or after D_2 (Myllyniemi-type turbidites) or metamorphosed so intensely in syn-D_1 that the temperature never exceeded it thereafter (Vammala-type turbidites). Owing to syn-D_2 metamorphism, vertical axial plane schistosity, such as that in the Tampere synclinal folding, would develop in formations above the brittle/ductile transitional zone without signatures of earlier metamorphism or, for that matter, earlier deformation either. In the local classification, this schistosity should then be referred to as S_1 in the same way as the originally subhorizontal schistosity in the migmatite area. The above concerns not only these turbiditic metasedimentary rocks but also all the other lithological units, of which some could have reached a depth capable of causing metamorphic reactions during D_1.

Kähkönen (1994) maintains that a single synclinal folding episode cannot explain the discrepancy between the stratigraphic information and age data at the southern edge of the synclinal area, and suggests thrust before the synclinal folding as a possible explanation. Alternative explanations could be the D_1 gently dipping detachment surfaces of Fig. 62 or the brittle, more vertical faults that developed at the same time. Both, although normal faults, might have caused the formations to get locally older towards the centre of the syncline. Reconstruction of the original positions of any pre-D_2 faults, and thus that of vergence, after the F_2 folding (synform folding) is not possible here, as the faults are not exposed and conclusions must be drawn from the stratigraphy only.

Arc-related metavolcanic and metasedimentary rocks

The rocks in the central part of the Tampere synform area are mainly medium-K, high-K and shoshonitic arc volcanic rocks and the associated sedimentary rocks (Kähkönen 1989, Ojakangas 1986, Kähkönen et al. 1994). According to Lahtinen (1994), some of the turbiditic gneisses in the Vammala migmatite area also contain substantial amounts of components indicative of these volcanic rocks. Like the above metaturbidites, the arc-related volcanic rocks in the model of Fig. 62, deposited before D_1. The total thickness of these formations therefore declines northwards in the model even though originally there was a formation of constant thickness. We see this particularly clearly in the basins bordered by D_1 faults, of which the northernmost has no arc-related volcanic rocks at its bottom at all. The phenomenon illustrates the trend of D_1 evolution. In the model, some of the arc-related volcanic rocks are buried so deep into the crust during D_1 that they undergo distinct syn-D_1 metamorphism, as suggested by the above interpretation of Lahtinen according to which, some of the rocks south of the Tampere schist belt could also be correlated with the arc-related volcanic rocks of the TSB.

Uppermost units of Tampere Schist Belt stratigraphy

Conglomerates of the Veittijärvi type and arenites of the Mauri type are displayed in the model in Fig. 62 as having deposited in basins bordered by D_1 faults. The age of the clastic zircon in the Mauri arenite, 1.9 Ga (Matisto 1968), has been generally thought to show that the arenite is located relatively high in the stratigraphy of the Tampere

Schist Belt. In the model, the Mauri rocks have deposited in the southernmost basin, implying that they are probably slightly younger than the Veittijärvi-type conglomerates. In the northernmost basins of the model, the basal parts of the conglomerate formations metamorphosed and deformed by a gently dipping D_1 shear, whilst the surficial parts remained undeformed, suggesting that some of the formations of this age may be strongly metamorphosed (the Naistenmatka conglomerate at Pirkkala) but others only weakly so, metamorphism having occurred after D_1 in them (conglomerates in the synform area).

The ages measured from the tonalitic clasts of the conglomerates are problematic; the oldest U-Pb zircon age thus determined is 1890 ± 3 Ma (Nironen 1989b), which is somewhat older than the ages of the Hämeenkyrö and Värmälä intrusions, which are synkinematic in relation to the synclinal folding, but the youngest conglomerate clast age is 1884 ± 3 Ma. It is possible, therefore, that at least some of the conglomerates deposited after D1. Figure 63 illustrates a case in which some of the conglomerates deposited after the intrusion of the synkinematic tonalites. According to the model, however, it is impossible for conglomerates of this age to occur in the migmatite area south of the Tampere Schist Belt.

Uppermost in the stratigraphy are the Takamaa mafic volcanic rocks, 1889 Ma in age (Kähkönen et al. 1989). In the model of Figs 62 and 63, formations of the Takamaa type deposited during D_1 and thus changes in their theoretical thicknesses in a north-south direction are the reverse of those of the pre-D_1 arc volcanic rocks. The model assumes that the Vammala ultramafic intrusions are comagmatic with the uppermost Tampere (Takamaa) volcanic rocks. This assumption is based on the ideas of Peltonen (1995a), according to whom, the subsolidus reactions connected with cooling and metamorphism in the Vammala intrusion and the age of the intrusion, 1890 Ma (Häkli et al. 1979), provide yet further support for the concept. In line with the reasoning of Elo (1994), the intrusions are depicted in the model as subhorizontal plates whose ages, in theory, get slightly younger upwards. The change in age, however, is so minor that all the intrusions are syntectonic in relation to D_1. For the sake of simplicity, the probable fragmentation of the intrusions into boudins at D_1 is not shown in the images. The horizontal and platy intrusions that fragmented into boudins at D_1 are then folded at F_2 (Fig. 63), generating bowl-shaped formations such as the intrusions of Stormi and Kylmäkoski. In principle, the fragments that once formed a single intrusion show on the present erosion level the horizontal palaeoplane on which the intrusion originally crystallized.

Syn-D_1 dykes

Figure 63 also shows how the originally vertical dykes associated with the above magmatism remain vertical despite F_2 folding. If the strike of a dyke was parallel to the developing S_2 axial plane the dykes may seem to be syn-D_2 intruded in a post-F_2 horizontal section. If, on the other hand, the primary strike of the dykes deviated from S_2, they are still vertical, but F_2 folded (mafic dykes of Tottijärvi, the Ellijärvi subarea, the Hämeenkyrö subarea and the Herttuala sill, Peltonen 1992).

Ductile shears

It is also possible that the boundary between the well-preserved rocks of the Tampere Schist Belt and the Vammala migmatite area was initially D_1 in age. In places where the boundary is sharp it might represent a D_1 detachment surface; such surfaces tend to run along the boundary between plastic and brittle rocks. Should this assumption be valid, the boundary was probably reactivated during D_2 and D_3 and hence any kinematic

indicators would no longer represent the D_1 stage. In places, however, the boundary is gradual (Pirkkala) and the brittle/ductile transitional zone cannot represent a detachment (see the limb of the left-hand synform in Fig. 63). Elsewhere, too, in the Tampere-Vammala area the changes in metamorphic grade are gradual in places but in others associated with faults, of which some at least are ductile (Koistinen 1994, Koistinen et al. 1996) and probably had already developed during D_1.

Importance of amplitude of F_2 and F_3 folds

If the amplitude of F_2 folding is half of the wavelength, as assumed in Fig. 63, the shortening caused by folding is about 57%. Almost everywhere in the study area the layering and/or S_1 planes are subvertical on the limbs of F_2 folds, suggesting even greater shortening. According to Jolivet et al. (1994), the distance between the "detachment front" and the thrust front in the Aegean and Tyrrhenian areas is about 100 km. If the same holds in the present study area, the Tampere-Vammala/Hämeenlinna-Somero suture (Lahtinen 1994, 1996) would be no more than 40 km south of the southernmost detachment surface after F_2 (the southernmost detachment has not been defined). Lahtinen (1994, 1996) suggests that the MORB-type volcanic rocks in the southern part of the Vammala migmatite area and the younger mafic/ultramafic intrusions spatially connected with them might indicate the above suture. On the basis of all structural and metamorphic features, the ultramafic intrusions of Stormi and Kylmäkoski, at least, are older than D_2 (Kilpeläinen & Rastas 1992, Peltonen 1995a, Marshall et al. 1995, the present work), and thus already existed before the collision. If the location of the suture is assumed to be where suggested by Lahtinen (1996), we could expect signatures of syn-D_1-HP-LT metamorphism to be visible on the current erosion level immediately north of the suture.

The upper part of Fig. 63 shows how the culminations and depressions of F_2 axes caused by F_3 folding affect the location of the post-D_3 erosion level in the model. Since the F_2 axes may plunge at any angle the amount of D_3 oscillation cannot be established through structural analysis. And since the metamorphic zones in the study area still trend roughly in east-west direction, i.e. parallel to the original strike of S_2 planes, it is evident that the effect of D_3 on the variation in metamorphic grade was weaker than that of D_2. On the other hand, the syn-D_1 metamorphism in the migmatite area varies, even in the direction of S_2 planes, from the potassium feldspar and sillimanite equilibrium field to that of garnet and cordierite, implying that locally the differences caused by D_3 may be of the same order of magnitude as the F_2 amplitudes assessed on the basis of structural criteria.

The model in Figs 62 and 63 does not take into account the influence of syn-D_3 metamorphism, which is comonly strongest in the deepest F_2 synforms. Since, however, D_3 metamorphism occurs zonally it cannot be presented in images that show only one vertical section striking N-S (see the geometry of syn-D_1 and syn-D_3 isotherms).

Interfering $D_1/D_2/D_3$

If we assume F_3 to be open, dextral folding, its axial plane striking 45° and its vertical component parallel to the post-D_3 erosion levels shown in Fig. 63, the variations in lithology seen in Fig. 64 will be obtained on a horizontal plane when the model in Fig. 63 is folded. In Fig. 64 the wavelength of F_3

Fig. 64. Effect of $D_1/D_2/D_3$ interference on lithology in horizontal section of Fig. 63. For details, see text.

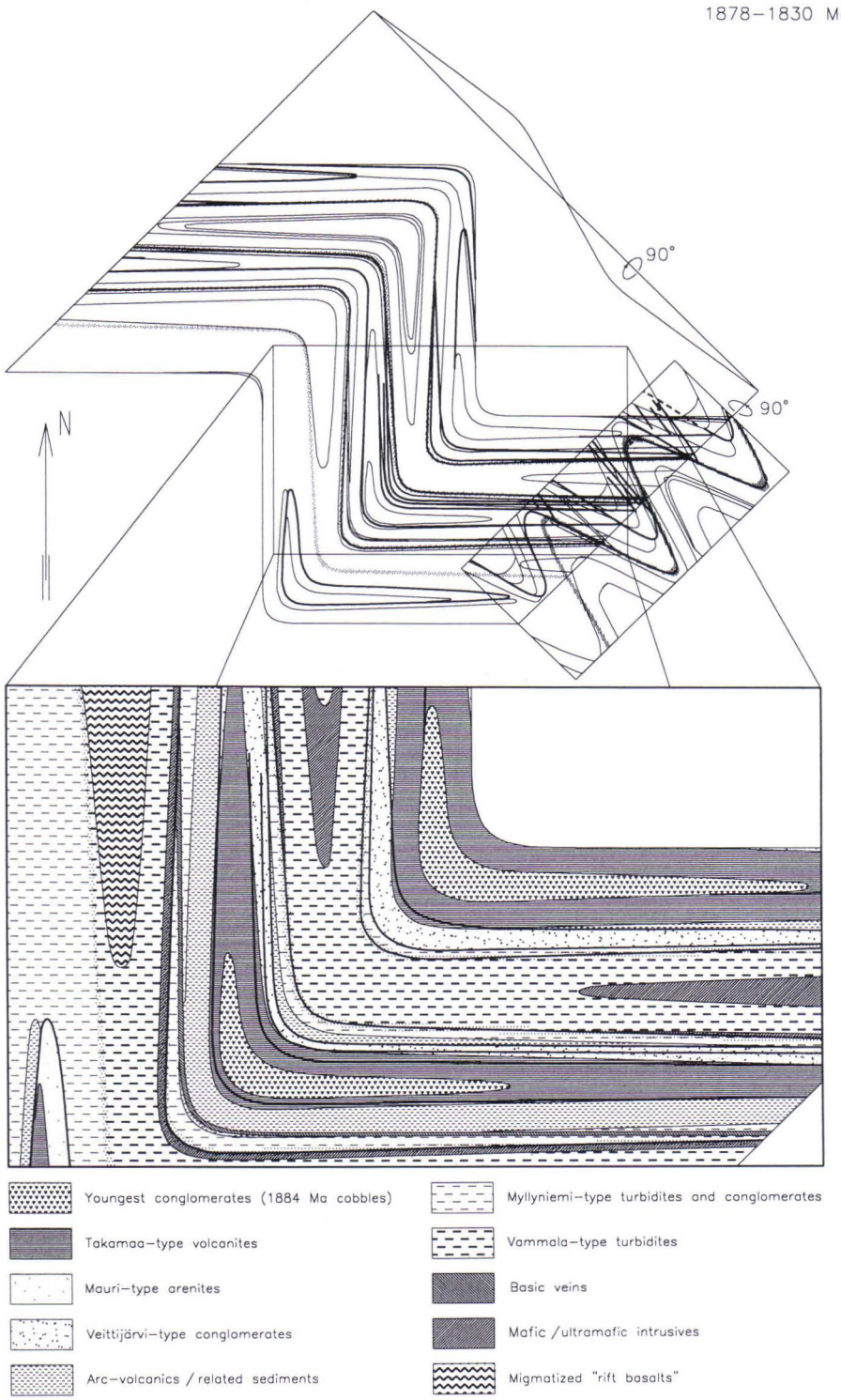
1878–1830 Ma
90°
90°
N
Youngest conglomerates (1884 Ma cobbles)
Takamaa–type volcanites
Mauri–type arenites
Veittijärvi–type conglomerates
Arc–volcanics / related sediments
Myllyniemi–type turbidites and conglomerates
Vammala–type turbidites
Basic veins
Mafic / ultramafic intrusives
Migmatized "rift basalts"

Fig. 64

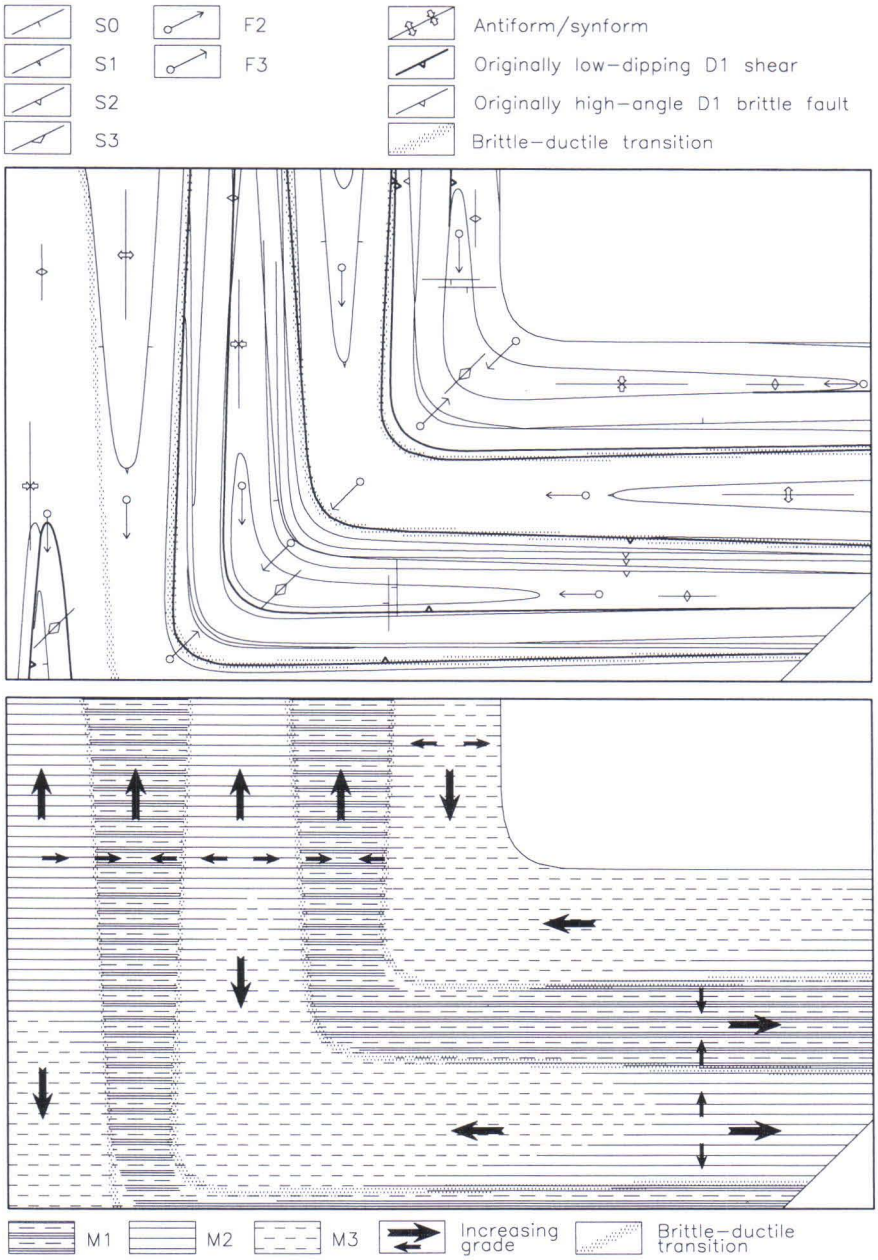

Fig. 65. Structural elements and variation in metamorphic grade in horizontal section of evolution model of Figs 62-64. For details, see text.

is thus many times that of F_2, as indeed is true in the Tampere-Vammala area. Since Figs 62 and 63 are not provided with a scale, the horizontal sections in Figs 64 and 65 are also without a scale. Some of the features illustrated in the images are visible only on out-

crops in the Tampere-Vammala area, some mainly on mesoscale. The form lines of F_3 are shown both in the XY plane and the Z dimension in the upper part of Fig. 64. We see that the F_3 flexures contain both an F_2 axial culminations (F_3 antiforms) and an F_2 axial depressions (F_3 synforms). Since in the model the dips on the different limbs of F_3 are symmetric in the vertical section perpendicular to the vertical section describing F_2, F_3 is asymmetric, the east-west limbs in the model being longer than the north-south limbs. This feature is shown in the Tampere-Vammala area by, for instance, the S_2 planes and metamorphic zones that still largely strike east-west despite F_3 folding. As the model endeavours to describe the form lines of folded structures, two adjacent vertical sections of an imaginary cube are shown as a compromise. The vertical sections show only the direction of the dips, not their magnitude. For it to be possible to read also the numeric values of the dips from the vertical sections, it would be necessary to present as many sections as there are fold limbs differing in plunge. Since the numeric values of the dips have no importance *per se* in this model, the model has been converted into a more perspicuous, rectangular form.

To illustrate more graphically the effect of the $F_1/F_2/F_3$ interference in horizontal sections, the southern F_3 flexure of the model with the F_2 axial depression is examined in greater detail in Figs 64 and 65. The corresponding interference patterns are, of course, visible in the other F_3 flexure, too, although, due to the F_3 antiform, they are different in symmetry. The variation in lithology is marked with the same symbols as in Fig. 63. Thus, syn-D_2 conglomerates are highest in the stratigraphy and migmatized rift basalts lowermost. The numeric values of the plunges and dips are not marked on the tectonic model of Fig. 65, as the mutual relations between the lithology and tectonic structures of different ages do not depend on the angle of plunges in the model. The intensity of both D_2 and D_3 structures in the model is indeed a compromise between the perspicuity of the structures (in image) and observations made in the area. Were the F_2 folding depicted as tight and isoclinal in the model and were, at the same time, all the most important stratigraphic units presented, the lithology would vary in horizontal section so much that the model would be difficult to read.

Evolution of isotherms

The metamorphic map in the lower part of Fig. 65 shows the age of metamorphism and the direction of the variation in metamorphic grade in a horizontal section, since, due to the lack of a scale in the model, metamorphic grade cannot be presented on the map of metamorphism. The mutual relation of M_1 and M_2 metamorphisms is taken directly from Fig. 63 (stabilizing isotherms 1 and 3), but the Z elevation of the M_3 isothermal surface was selected to show the syn-D_3 metamorphism observed in the Tampere synclinal area. In the light of the features described here from the Vammala migmatite area, D_3 metamorphism is assumed to be zonal in the model. The M_3 isothermal surface is horizontal, except in the southern F_3 flexure, where it bends upwards as a mirror image of the Z component of the F_3 synform.

Earlier in this work it was assumed that the isotherm surfaces of the D_3 metamorphism dip gently northwards. In the model this property would show only in a downsizing of the M_3 subareas northeastwards, and so was omitted for the sake of simplicity. When reading the metamorphic model, we should, however, remember that, although it shows areas of metamorphisms of different ages, all three metamorphic stages may be visible in one area, provided that the younger metamorphism did not exceed the previous one in intensity, as that would re-equilibrate the

metamorphic structures. Therefore, the metamorphic grade of the metamorphisms of different ages may vary in different directions in a given subarea.

In the model, M_1 exists everywhere except in the youngest conglomerates, but in places its intensity may be almost nil, as in the central part of the Tampere synform area. Similarly, M_2 covers the whole area, including the above conglomerates, but, depending on the site, it may be stronger or weaker than M_1. This is most conspicuous in the age difference between the main metamorphisms of the Tampere Schist Belt and the migmatite area south of it. Likewise, M_3 may be the dominant feature, as in parts of the Tampere Schist Belt, or then it may manifest itself in retrograde reactions in migmatites dominated by M_1 metamorphism.

Since D_3 occurs in both the migmatite area and the well-preserved Tampere Schist Belt, M_3 must also cut the syn-D_1 brittle/ductile transition, as seen in the horizontal section of the model. By combining horizontal sections of the model showing different properties, we can draw conclusions about the tectonic positions of the observation sites from the style of metamorphism. For example, for the temperature to remain high throughout the structural evolution as described from the Vammala migmatite area requires, according to the model, the outcrops where such a property has been observed to be located in an area of horizontal syn-D_1-B/D transition, on the limb of an F_2 fold, and in an area where intense D_3 has promoted the flow of fluids and thus the upward bending of the M_3 isothermal surface.

Further assumptions based on modelling

Although S_0 and S_1 were originally subhorizontal in the model the same does not always hold for the contacts of rock types, and the fold-like shapes of the rocks in the horizontal section do not directly indicate the style of F_2 folding. This is most clearly visible in the southwestern part of the lithological (Fig. 64) and tectonic map (Fig. 65), where there is a flexure of the F_2 synform at the side of both lithological and D_1 detachment folds. Owing to the geometry of the D_1 structures, the age order of lithologies on the limbs of F_2 synforms may in places be reversed, without, however, any change in facing in rock types and formations. This is the situation on the southern limb of the Tampere synclinal area.

The lithologies form closed structures in the horizontal section of the model, but should AF_3:AF_2 be high enough in relation to the surface area of the horizontal section and should the erosion level be at an appropriate elevation, the D_1 shear surfaces may also be ring-shaped. Most probably, however, they occur approximately parallel to the S_2 plane and so are difficult to distinguish from possible D_2 shears. In principle, their dip should differ from that of S_2, but this is not easy to verify on outcrops. Examples of D_2-deformed shears were given in the descriptions of the Pirkkala and Mauri subareas.

The syn-D_2 deposition of the youngest conglomerate in the model cut the initially vertical and brittle D_1 fault. Such a situation has not, however, been encountered in the Tampere-Vammala area. Moreover, the contact between the Takamaa volcanic rocks and conglomerate should differ from the layering of the conglomerate (Figs 64 and 65). These features would be visible only if the youngest conglomerates were, like the synkinematic metatonalites, D_2 in age.

Another essential feature of the model is that all deformation structures could have developed due to north-south compression (see also chapter 7, pp. 93-95). Thus the time difference between D_1 and D_2 structures need not be substantial, a concept in harmony with the evolution model of Lahtinen (1994). In a similar manner, M_1 and M_2 are direct continuations of each other, although, due to post-

D_1 folding, the age of metamorphism in relation to structures may change on the erosion level, even over a short distance. Kilpeläinen et al. (1994) proposed that M_3 might be a reflection of the metamorphism that culminated in southwesternmost Finland 1830-1840 Ma ago. Since D_3 probably started as early as 1878 Ma ago (the present work), D_3 either lasted longer than D_1 and D_2 or, preferably, the finished D_3 structures controlled the fluid activity associated with the youngest metamorphic pulse and, thus, also the heat transfer. Observations of the metamorphism associated with D_3 zones in the Vammala migmatite area, however, imply that the temperature remained high in these zones throughout M_1-M_3 evolution.

DISCUSSION

The main objective of this work was to construct an evolutional model that would explain as accurately yet as simply as possible the lithology and structural and metamorphic signatures visible on the current erosion level. The variation in lithology and metamorphic features in the study area and efforts to unravel the structures backwards in time led to a number of initial situations of which those best in harmony with the accepted evolutional models had to be chosen. The final model is thus a synthesis of observational data and of information gleaned from the literature and so contains many generalizations but also details that were not encountered, or at least recognized, in the study area.

Problematic infra-/suprastructure

The *overbau* and *unterbau* structures presented by Wegmann (1935) to describe the change in the style of structures with depth were later called infrastructure and suprastructure in works published from the Pyrenees (de Sitter & Zwart 1960, Zwart 1963a, 1963b). In the Axial Zone of the Variscan (Hercynian) orogeny, Cambrian and older formations represent the deeper section. These areas, which are characterized by gently dipping structures, occur as dome-like or anticline/antiform structures. Characteristic of the younger formations between them, and representing an upper section, are vertical fold structures with vertical axial plane schistosity. The infra-/suprastructure boundary in the Pyrenees is in places gradual, but in places these structures are bordered sharply by a lime-rich schist that acted as a décollement plane (Zwart 1963a,b, Oele 1966). Corresponding zonality indicating the depth of the section of structures has later been described from many other areas (Holland & Lambert 1969, Campbell 1970, Fyson 1971, Sanderson 1979, Murphy 1987, Matte & Xu Zi 1988). The infra-/suprastructure boundary has been located, for instance, in the transitional zone between low- and medium-grade metamorphism (Carreras & Capella 1994) or in rocks of the greenschist facies (Holland & Lambert 1969).

Different opinions have been expressed concerning the relative ages of the vertical and gently dipping structures and their evolution in the Pyrenees. De Sitter & Zwart (1960) considered the current geometry of the structures a primary feature, and assumed that the structures had been produced simultaneously by the same geotectonic process. According to them, the dissimilar

attitudes of the structures were due to an increase in plasticity with depth. Possible synchroneity of the structures was also suggested by Soula et al. (1986), although on different grounds. Seguret & Proust (1968a, 1968b) and Matte (1969) assumed that the suprastructures had originally been gently dipping but had been turned into a vertical position by later, disharmonic folding.

More recent works from the Pyrenees, however, have assumed that the vertical and gently dipping structures are of different ages, in most cases the infrastructures being described as older than the suprastructures. The gently dipping infrastructures may then have developed either in the shortening of the crust (Carreras & Cappella 1994) or in the extension that preceded the shortening (Soula et al. 1986). Zwart (1986) and Vissers (1992) have further proposed that the gently dipping structures in deep sections are due to postorogenic extension.

Depending on the evolutional model, the infra-/suprastructure boundary is either determined in the first deformation stage or it is assumed to slide vertically in the course of evolution as folding moves rocks either higher or lower than during D_1 in the crust (Fyson 1971, Carreras & Capella 1994).

In the light of the example from the Pyrenees, several models are available to solve the infra-/suprastructure problem in the Tampere-Vammala area. However, the area differs from the Pyrenees in that the boundary between the gently dipping and vertical structures is not tied to the stratigraphy in the same way; for instance, the turbiditic metasedimentary rocks in the lower part of the Tampere Schist Belt correlate with the metaturbidites in the Vammala migmatite area. On the basis of the mutual relations between the plutonites and deformation structures we can be conclude that the gently dipping schistosity in the migmatite area is older than the vertical schistosity in the Tampere Schist Belt (Kilpeläinen et al. 1994). No indications have been found suggesting that the main schistosity in the Tampere Schist Belt was originally gently dipping (Nironen 1989a). The gently dipping structures in the migmatite area were not folded into a vertical position until horizontal compression took place during D_2. Hence, the gently dipping pre-D_2 structures associated with either compression or extension explain satisfactorily the present structures in the Tampere-Vammala area. The latter option is suggested by the fact that the difference in crystallization pressure between the Tampere Schist Belt and the migmatite area seems to have been slight in relation to the difference in temperature.

Simplifications or oversimplifications?

Perhaps the greatest shortcoming in the model presented here is that it ignores the compressional structures that develop in an accretion wedge in association with subduction. Even if the compressional structures in the model were later to move into an extensional environment, there to be destroyed beyond recognition, they still affect the present total structure of the area and the position and manner in which the rocks and lithological complexes are located on the present erosion level. Unless we can recognize the compressional structures and reconstruct their geometry, we cannot accurately assess the "zero" situation before the D_1 stage of the model, particularly because the compressional and extensional structures evolve at the same time, but at different sites, in the model. Furthermore, the compressional structures of the thrust front do not concern all formations and formations of all ages, even in theory. Thus, as simultane-

ous events, the D_1 stage should include both the evolution of compressional structures and the reorientation of corresponding structures in extension together with sedimentation. One way of establishing the importance of the compressional structures would be to analyse those structural and metamorphic features recorded from the area that the model cannot explain. That would, however, require the model to be accurate down to the smallest detail. This would be very complicated and, due to the large number of parameters, difficult to control.

The model is firmly based on the well-known stratigraphy of the Tampere synform area, but it also contains a deliberate generalization: since the original thicknesses and lateral extensions of the synform area formations or stratigraphic units are not fully known, they were all assumed to have been plates of equal thickness and extension. In reality, this is not the case, but as a starting point it is not only neutral but also easy to visualize.

Associated with the perspicuity of the model is the presentation of the subducting plate in Fig. 62. With the means available here it was not possible to establish either the direction or place of subduction and these are therefore based on previously published papers from the area. In terms of the objective of the model, that is, to explain the tectono-metamorphic phenomena on the erosion level, the direction of subduction or even its exact site is immaterial. As to the geometry of the model, it is possible that the D_1 structures are related to the southwestward subduction at the boundary between the Archaean craton and the Svecofennian domain (the Savo Schist Belt), in which case the rocks of the Vammala migmatite area would be the lower members of the back arc basin formations. Since, however, the collision of the Archaean craton with the Proterozoic island arc system started 1.91 Ga ago (Lahtinen 1994), the ages of the formations in the Tampere synclinal area are not compatible with this interpretation.

Conglomerates and rapid tectono-metamorphic evolution

The ages of the synkinematic (syn-D_2) granitoids in the Tampere synclinal area are 1885-1878 Ma (Nironen 1989b) and in the Vammala migmatite area 1881 Ma (here). No matter with which conglomerates of the Tampere synclinal area the conglomerates of the migmatite area correlate, soon after their deposition they were metamorphosed at a depth of at least 15 km, as the synclinal sedimentary rocks correlatable with them were metamorphosed at the same time under conditions of greenschist facies. On the basis of the crystallization of porphyroblasts in the migmatites, this metamorphism can be related to D_1, which, due to the low syn-D_1 temperature, is usually absent from the Tampere synclinal area.

Should the conglomerates correlate with the Myllyniemi formation, they were migmatized, D_1 deformed and at least partly F_2 folded at 1910-1885 Ma. If the conglomerates in the migmatite area correlate with the Veittijärvi type of conglomerates, the depositional maximum of which occurred 1890 Ma ago, D_1 deformation and metamorphism occurred even more rapidly. In the context of the Mauri subarea, D_1 structures were described from the andalusite-mica schists located stratigraphically above the meta-arkose, <1.9 Ga old. Should the interpretation of the location of the Mauri meta-arkose in the upper part of the stratigraphy of the Tampere schist belt be valid, it means that the D_1 stage was probably shorter than suggested by the model or, alternatively, that sedimentary rocks deposited in the synclinal area during

D_1.

Rapid evolution implies either tectonic thickening of the crust due to an overthrust or the bringing of some of the sedimentary rocks deeper into the crust by extensional processes. In either case, the proximity of the sedimentary rocks on the current erosion level requires a post-D_1 event, in which rocks that had migrated into entirely different PT conditions during D_1 were brought back in a vertical direction to approximately the same level. The event might have been post-D_1 faulting or folding with sufficient frequency and approximately horizontal axis.

The high-temperature and low-pressure metamorphism typical of the Svecofennian domain is related temporally to magmatism in the central and northern parts of the domain (Korsman et al., in press). The thick high-velocity layer of the lower crust, which makes the Svecofennian crust abnormally thick, extends over the whole area of the high-grade Svecofennian crust. Thus the metamorphism could have been caused by the magmatic underplating about 1885Ma ago connected with the extension of the lower crust (Korsman et al., in press).

As already pointed out, the mode of occurrence of the metamorphic and tectonic structures visible on the current erosion level can best be explained by syn-D_1 normal faults. Therefore, the above magmatic underplating should have occurred before the formation of the D_1 structures visible today. The tectonic pre-D_1 thickening of the crust and subsequent replacement of the lower part of the lithosphere by the asthenosphere, as outlined by the model of Platt & England (1993), could then offer an explanation for the extensional D_1 structures. In that case, the D_1 structures would not be associated with northward subduction under the Tampere Schist Belt, as proposed by the model here.

Relative age of intrusive rocks and structures

Many papers published from the area discuss the age of the Ni-bearing intrusions in the Vammala migmatite area in relation to structural and metamorphic evolution (Kilpeläinen & Rastas 1992, Peltonen 1995, Marshall et al. 1995). According to the present model, we cannot solve the problem by studying the properties of one formation alone. Although the intrusions in the model are syntectonic in relation to D_1 - an interpretation permitted by all the above authors - their relation to deformation and metamorphism depends on the depth at which and how far from the thrust front they originally crystallized. Since the B/D transition moves vertically during D_1, the intrusions of the same age in the migmatite area, too, may be pre-, syn- or post-tectonic in relation to D_1. This is especially clearly seen in the formations that intruded above the "final" syn-D_1-B/D boundary (the present unmigmatized environment). In theory, they should have a distinct contact aureole, even if cut later by S_2 and M_2. On the same grounds, it is possible that, because the age of the metamorphic and tectonic structures varies both with depth and laterally, as shown by the model, the contact relations of dykes of the same age with the host rocks vary markedly (mafic dykes in the Tottijärvi, Ellivuori, Koosanmaa, Hämeenkyrö and Stormi areas). The issue is further complicated by the primary direction of the dykes in relation to N-S compression during D_2.

The above also holds for the age relation of the synkinematic metatonalites to structures and metamorphism. Since the intrusion rate of a felsic magma is substantially lower than that of a mafic magma, the age difference in relation to the structures between the intru-

sions of the same magmatic pulse may be real, depending on the crystallization depth, considering the rapidity of evolution in the Tampere-Vammala area (Paterson & Tobisch 1992).

With the exception of the beginning of D_1, we know the ages of the D_1 and D_2 stages in the Tampere-Vammala area fairly accurately. On the basis of the porphyritic granites, we also know when D_3 began, but its duration is still somewhat ambiguous. Even though the youngest metamorphic pulse is associated with zones of intense D_3, we do not know whether D_3 was active throughout M_3 or not. The crystallization of younger garnets in neosomes in S_3 planes suggests that it was, but it is possible that these neosomes are only imitating structures that were present while they crystallized. Despite their narrowness and fragmentation, the plagioclase porphyry dykes that intruded syntectonically in relation to F_3 folding in the Mauri subarea could probably be dated, thus offering a way of resolving the issue.

If the D_2 and D_3 structures were created in the course of north-south compression, the structures classified as D_2 and D_3 may have formed simultaneously in adjacent areas. Inversely, this also means that D_3 structures are not necessarily of the same age everywhere. Hence, the syntectonic relation of the Lavia porphyritic granite to D_3 structures may indicate the age of D_3 only in the northwestern part of the Tampere-Vammala area. Consequently, the granitic migmatization and metamorphism, 1840-1830 Ma in age, in the southern part of the area may be a syntectonic event in relation to D_3, without D_3 having to be interpreted as a long-lasting deformation stage. This idea is also applicable to the evolution of D_2 structures, even though the ages and syn-D_2 nature of the synkinematic intrusions in the Tampere Schist Belt and at Stormi indicate synchronism of D_2, at least in these parts of the study area.

CONCLUSIONS

Several explanatory models, in which the emphasis is on establishing the age relations between the tectonic structures of migmatitic areas and better preserved rocks, can be presented to solve the infra-/suprastructure issue in the Tampere-Vammala area. The present work is based on a geometric analysis of tectonic and metamorphic structures and on the stratigraphy of the Tampere synclinal area.

In the Tampere-Vammala area:

- The syn-D_1 metamorphic grade varies with section depth, and S_1 is the main schistosity in rocks that were below the B/D transition at the end of D_1. The brittle/ductile transition corresponds approximately to the Muscovite+Quarz=Potassium Feldspar+Sillimanite+H_2O isograd of the metasedimentary rocks. Locally, the syn-D_1 metamorphic grade also increased downwards in stratigraphy.
- The geometry of both the tectonic and metamorphic structures on the current erosion level implies normal faults at D_1.
- The D_1 structures can be explained by north-south compression associated with simultaneous extension, at least locally. A D_1 evolution is presented here, in which the extension occurs in an arc and back arc environment during subduction from the south to under the Tampere Schist Belt. Alternatively, the extensional D_1 structures may be due to the isostatic disequilibrium caused by pre-D_1 thickening of the crust and magmatic underplating.
- The variations in syn-D_1 metamorphic grade on the current erosion level are explained with the aid of D_2-D_3 modelling. The D_2 structures were produced in north-south

compression and the D_3 structures can also be attributed to this stress field.

- The D_1 metamorphic structures are cut by syn-D_2 and syn-D_3 metamorphic structures concentrated on F_2 synforms, F_2/F_3 interference basins and D_3 shear zones.
- The subhorizontal D1 structures are estimated to be over 1889 Ma in age. The D_2 syn- and antiforms with horizontal axes and vertical axial planes developed at 1889-1878 Ma. The last folds to significantly rework the current structure of the area were the plastic, mesoscale ones that developed during D_3 (1878-1830 Ma). The ages of the D_2 and D_3 stages vary in the area and the D_2 and D_3 structures could have evolved partly synchronously. The age estimates are based on the relations between the dated intrusive rocks and tectonic structures of supracrustal rocks.
- The nature and composition of migmatization changes broadly with time. The D_1 leucosomes are trondhjemitic, narrow veins striking parallel to S_0/S_1. The D_2 veins cut or imitate older structures and are richer in potassium feldspar. The D_3 dykes are cutting granites, which, in high-grade D_3 zones, contain garnet.
- The nature of magmatism changed with time. The pre- and syn-D_1 dykes and intrusions are mafic and ultramafic. The synorogenic granitoid intrusions at D_2 constitute the major part of the magmatism. At least some of the porphyritic granitoids were emplaced during D_3. However, small amounts of mafic and intermediate dykes intruded throughout the structural evolution period.

FURTHER WORK

Should a more detailed picture of the 3D geometry of the Tampere-Vammala be desired than that provided by the present model, we should attempt to clarify the kinematics of the D_3 high strain zones in particular. Unfortunately, these shear zones are poorly exposed and, even then, due to the intensity of metamorphic overprinting, kinematic indicators may be difficult to find. Although some of the shears may represent reactivated older high-strain surfaces, it is indisputable that movements occurred along them, at least after M_1 metamorphism.

The area is known to contain post-D_3 brittle faults, and they, too, may have had a local impact on the depth of the section now visible on the erosion level. The fault marked on the map of the Hämeenkyrö subarea, at least, strikes in the same direction as the postmetamorphic and post-tectonic granite dykes common in the migmatite area. It would be worthwhile establishing whether the fault and dykes belong to the same east-west-trending extension, i.e. the Svecofennian postcollisional extension.

ACKNOWLEDGEMENTS

This study forms a part of the Finland´s Global Geoscience Transect Project (GGT) being carried out jointly by Geological Survey of Finland, Department of Geology at the University of Turku, Institute of Seismology at the University of Helsinki and the Institute of Geophysics at the University of Oulu. My work in GGT-project was financially supported by GSF, Academy of Finland and University of Turku.

First I would like to express my gratitude to the leader of the GGT-project, Dr. Kalevi Korsman, whos interest and support during my work was conclusive. I wish to thank also Professor Heikki Papunen for his interest during this prolonged study.

I owe thanks to Pekka Wasenius and Reijo Niemelä, who have made a great number of

useful field observations from the study area, and also to all other co-workers from the Unit of Thematic Studies at the GSF. I also thank my colleagues and co-workers at Turku University, especially Jyri Rastas, with whom I started my work in Tampere-Vammala area. Special thanks to Dr. Matti Vaasjoki for the new age data published in this paper.

My supervisor, Dr. Tapio Koistinen helped me during field work and discussions with him were very simulating. The manuscript was officially reviewed by Drs. Raimo Lahtinen and Juhani Ojala and unofficially by Dr. Jarmo Kohonen. All the comments and corrections are acknowledged with great gratitude.

The manuscript was translated into English by Mrs. Gillian Häkli.

I express my thanks to the Director of the GSF, Professor Raimo Matikainen and Professor Matti Saarnisto, for approving the publication of this thesis in the GSF´s Bulletin series.

And last but not least, I want to thank my life-companion Suvi and my little son Antta for their forbearance and understanding.

REFERENCES

Aarnisalo, J. 1988. Etelä-Suomen Ni-vyöhykkeen kartoitus, raportti vuosilta 1982-1987. Outokumpu Oy Malminetsintä, julkaisematon tutkimusraportti, 230 p. (unpublished, in Finnish).

Bard, J.P. 1987. Microtextures of igneous and metamorphic rocks. Dordrecht, Holland: D. Reidel Publishing Company. 264 p.

Bell, T.H. 1985. Deformation partitioning and porphyroblast rotation in metamorphic rocks: a radical reinterpretation. Journal of Metamorphic Geology 3, 109-118.

Bell, T.H. & Rubenach, M.J. 1983. Sequential porphyroblast growth and crenulation cleavage development during progressive deformation. Tectonopysics 92, 171-194.

Bell, T.H., Rubenach, M.J. & Fleming, P.D. 1986. Porphyroblast nucleation, growth and dissolution in regional metamorphic rocks as a function of deformational partitioning during foliation development. Journal of Metamorphic Geology 3, 37-67.

Burchfiel, B.C. & Royden, L.H. 1985. North-south extension within the convergent Himalayan region. Geology 13, 679-682.

Campbell, D.S. 1978. Structural and metamorphic studies in the Svecokarelides, Tampere, Finland. Unpublished Ph.D. thesis, Glasgow University, 146 p.

Campbell, D.S. 1980. Structural and metamorphic development of migmatites in the Svecokarelides, near Tampere, Finland. Transactions of Royal Society Edinburgh, Earth Science 71, 185-200.

Campbell, R.B. 1970. Structural and metamorphic transitions from infrastructure to suprastructure, Cariboo Mountains, British Columbia. In: Wheeler, J.D. (ed.) Structure of the Southern Canadian Cordillera. Geological Association of Canada, Special Paper 6, 67-72.

Carreras, J. & Capella, I. 1994. Tectonic levels in the Palaeozoic basement of the Pyrenees: a review and a new interpretation. Journal of Structural Geology 16 (11), 1509-1524.

Claesson, S., Huhma, H., Kinny, P.D. & Williams, I.S. 1993. Svecofennian detrital zircon ages - implications for the Precambrian evolution of the Baltic Shield. Precambrian Research 64, 109-130.

Colley, H. & Westra, L. 1987. The volcano-tectonic setting and mineralization of the early Proterozoic Kemiö-Orijärvi-Lohja belt, SW Finland. In: Pharaoh, T.C., Beckinsale, R.D. & Rickard, D. (eds.) Geochemistry and Mineralization of Proterozoic Volcanic Suites. Geological Society Special Publication 33, 95-107.

Dietworst, E.J.L. 1982. Prograde metamorphic zoning in amphibolite facies pelitic gneisses from Kemiö, southwest Finland. Geologische Rundschau 71, 245-262.

van Duin, J.A. 1992. The Turku granulite area, SW Finland: a fluid absent Svecofennian granulite occurrence. Academisch Proefschrift. Amsterdam: Vrije Universiteit. 234 p.

Echtler, H. & Malavieille, J. 1990. Extensional tectonics, basement uplift and Stephano-Permian collapse basin in a late Variscan metamorphic core complex (Montagne Noire, Southern Massif Central). In: Matte, P. (ed.) Terranes in the Variscan Belt of Europe and Circum-Atlantic Paleozoic Orogens. Tectonophysics 177, 125-138.

Ehlers, C., Lindroos, A. & Selonen, O. 1993. The late Svecofennian granite-migmatite zone of southern Finland - a belt of transpressive deformation and granite emplacement. Precambrian Research 64, 295-309.

Elo, S. 1994. Preliminary notes on gravity anomalies

and mafic magmatism in Finland. In: Pajunen, M. (ed.) High temperature-low pressure metamorphism and deep crustal structures. Meeting of IGCP project 304 "Deep Crustal Processes" in Finland, September 16-20, 1994. Geological Survey of Finland, Guide 37, 49-55.

England, P.C. & McKenzie, D.P., 1982. A thin viscous sheet model for continental deformation. Geophysical Journal of the Royal Astronomical Society 70, 295-332.

England, P.C. & McKenzie, D.P., 1983. Correction to: A thin viscous sheet model for continental deformation. Geophysical Journal of the Royal Astronomical Society 73, 523-532.

Eskola, P. 1963. The Precambrian of Finland. In: Rankama, K. (ed.) The Precambrian 1. New York: Wiley, 145-263.

Faure, M., Sun, Y., Shu, L., Monié, P. & Charvet, J. 1996. Extensional tectonics within a subduction-type orogen. The case study of the Wugongshan dome (Jiangxi Province, southeastern China). Tectonophysics 263, 77-106.

Ferguson, C.C. & Harte, B. 1975. Textural patterns at porphyroblast margins and their use in determining the time relations of deformation and crystallization. Geological Magazine 112, 467-480.

Ferry, J.M. & Spear, F.S. 1978. Experimental calibration of the partitioning of Fe and Mg between biotite and garnet. Contributions to Mineralogy and Petrology 66, 113-117.

Front, K. & Nurmi, P. 1987. Characteristics and geological setting of synkinematic Svecokarelian granitoids in southern Finland. Precambrian Research 35, 207-224.

Fyson, W.K. 1971. Fold attitudes in metamorphic rocks. American Journal of Science 270, 373-382.

Gaál, G. & Gorbatschev, R. 1987. An outline of the Precambrian evolution of the Baltic Shield. Precambrian Research 35, 15-52.

Hakkarainen, G. 1994. Geology and geochemistry of the Hämeenlinna-Somero Volcanic Belt, southwestern Finland: a Paleoproterozoic island arc. In: Nironen, M. & Kähkönen, Y. (eds.) Geochemistry of Proterozoic supracrustal rocks in Finland. Geological Survey of Finland, Special Paper 19, 85-100.

Häkli, T.A. & Vormisto, K. 1985. The Vammala nickel deposit. In: Papunen, H. & Gorbunov, G.I. (eds.) Nickel-copper deposits of Baltic Shield and Scandinavian Caledonides. Geological Survey of Finland, Bulletin 333, 273-286.

Häkli, T.A., Vormisto, K. & Hänninen, E. 1979. Vammala, a nickel deposit in layered ultramafite, Southwest Finland. Economic Geology 74, 1166-1182.

Haudenschild, U. 1988. K-Ar age determination on biotite and muscovite in the Pihtipudas-Iisalmi and Joroinen-Sulkava areas, Eastern Finland. In: Korsman, K. (ed.) Tectono-metamorphic evolution of the Raahe-Ladoga zone. Geological Survey of Finland, Bulletin 343, 33-50.

Haudenschild, U. 1995. The Vaaraslahti pyroxene granitoid intrusion and its contact aureole: isotope geology. In: Hölttä, P. (ed.) Relationship of granitoids, structures and metamorphism at the eastern margin of the Central Finland Granitoid Complex. Geological Survey of Finland, Bulletin 382, 81-89.

Heikkilä-Harinen, R. 1975. Stormin alueen kallioperästä. Unpublished M.Sc. Thesis, University of Turku. 112 p. (in Finnish).

Helovuori, O. 1979. Geology of the Pyhäsalmi ore deposit, Finland. Economic Geology 74, 1084-1101.

Hobbs, B.E., Means, W.D. & Williams, P.F. 1976. An outline of structural geology. New York: Wiley. 571 p.

Holland, J.G. & Lambert, R.St.J. 1969. Structural regimes and metamorphic facies. Tectonophysics 7, 197-217.

Hölttä, P. 1986. Observations on the metamorphic reactions and PT conditions in the Turku granulite area. In: Korsman, K. (ed.) Development of deformation, metamorphism and metamorphic blocks in eastern and southern Finland. Geological Survey of Finland, Bulletin 339, 43-58.

Hölttä, P. 1988. Metamorphic zones and the evolution of granulite grade metamorphism in the Early Proterozoic Pielavesi area, central Finland. Geological Survey of Finland, Bulletin 344. 50 p.

Hölttä, P. 1995. Contact metamorphism of the Vaaraslahti pyroxene granitoid intrusion in Pielavesi, Central Finland. In: Hölttä, P. (ed.) Relationship of granitoids, structures and metamorphism at the eastern margin of the Central Finland Granitoid Complex. Geological Survey of Finland, Bulletin 282, 27-79.

Hopgood, A.M., Bowes, D.R., Kouvo, O. & Halliday, A.N. 1983. U-Pb and Rb-Sr isotopic study of polyphase deformed migmatites in the Svecokarelides, southern Finland. In: Atherton, M.P. & Gribble, C.D. (eds.) Migmatites, Melting and Metamorphism. Nantwich: Shiva, 80-92.

Houseman, G.A. & England, P.C. 1986. Finite strain calculations of continental deformation. I. Method and general results for convergent zones. Journal of Geophysical Research 91, 3651-3663.

Huhma, A., Salli, I. & Matisto, A. 1952a. Ikaalinen. Geological map of Finland 1 : 100 000, Pre-Quaternary rocks, Sheet 2122. Geological Survey

of Finland.

Huhma, A., Salli, I. & Matisto, A. 1952b. Ikaalinen. Kallioperäkartan selitys. Summary: Explanation to the map of rocks. Geological Map of Finland 1 : 100 000, Explanation to the Map of Pre-Quaternary Rocks, Sheet 2122. Geological Survey of Finland. 75 p.

Huhma, H. 1986. Sm-Nd, U-Pb and Pb-Pb isotopic evidence for the origin of the Early Proterozoic Svecokarelian crust in Finland. Geological Survey of Finland, Bulletin 337. 48 p.

Huhma, H., Claesson, S., Kinny, P.D. & Williams, I.S. 1991. The growth of Early Proterozoic crust: new evidence from Svecofennian detrital zircons. Terra Nova 3, 175-179.

Jolivet, L., Daniel, J.M., Truffert, C. & Goffé, B. 1994. Exhumation of deep crustal metamorphic rocks and crustal extension in arc and back-arc regions. Lithos 33, 3-40.

Kähkönen, Y. 1987. Geochemistry and tectonomagmatic affinities of the metavolcanic rocks of the early Proterozoic Tampere Schist Belt, southern Finland. Precambrian Research 35, 295-311.

Kähkönen, Y. 1989. Geochemistry and petrology of the metavolcanic rocks of the early Proterozoic Tampere Schist Belt, Southern Finland. Geological Survey of Finland, Bulletin 345. 104 p.

Kähkönen, Y. 1994. Shoshonitic and high-K metavolcanic rocks in the southern parts of the Palaeoproterozoic Tampere Schist Belt, southern Finland; evidence for an evolved arc-type setting. In: Nironen, M. & Kähkönen, Y. (eds.) Geochemistry of Proterozoic supracrustal rocks in Finland. Geological Survey of Finland, Special Paper 19, 101-115.

Kähkönen, Y. 1996. Stratigraphy and evolution of the Palaeoproterozoic supracrustal rocks in the Tampere area, southern Finland: a preliminary review. In: Ekdahl, E. & Autio, S. (eds.) Global Geoscience Transect/SVEKA - Proceedings of the Kuopio Seminar, Finland 25.-26.11.1993. Geological Survey of Finland, Report of Investigation 136, 9-12.

Kähkönen, Y. & Huhma, H. 1993. An Archaean cobble in a Svecofennian conglomerate near Tampere, southern Finland. In: Autio, S. (ed.) Geological Survey of Finland, Current Research 1991-1992. Geological Survey of Finland, Special Paper 18, 31-36.

Kähkönen, Y. & Leveinen, J. 1994. Geochemistry of the metasedimentary rocks of the Palaeoproterozoic Tampere Schist Belt, southern Finland. In: Nironen, M. & Kähkönen, Y. (eds.) Geochemistry of Proterozoic supracrustal rocks in Finland. Geological Survey of Finland, Special Paper 19, 117-136.

Kähkönen, Y. & Nironen, M. 1994. Supracrustal rocks around the Palaeoproterozoic Haveri Au-Cu-mine, southern Finland: evolution from a spreading center to a volcanic arc environment. In: Nironen, M. & Kähkönen, Y. (eds.) Geochemistry of Proterozoic supracrustal rocks in Finland. Geological Survey of Finland, Special Paper 19, 141-159.

Kähkönen, Y., Huhma, H. & Aro, K. 1989. U-Pb zircon ages and Pb-Sr whole rock isotope studies of early Proterozoic volcanic and plutonic rocks near Tampere, southern Finland. Precambrian Research 45, 27-43.

Kähkönen, Y., Lahtinen, R. & Nironen, M. 1994. Paleoproterozoic supracrustal belts in southwestern Finland. Geological Survey of Finland, Guide 37, 43-47.

Kilpeläinen, T. 1988. Evolution of deformation and metamorphism as a function of time in the Rantasalmi-Sulkava area, Southeastern Finland. In: Korsman, K. (ed.) Tectono-metamorphic evolution of the Raahe-Ladoga zone. Geological Survey of Finland, Bulletin 343, 77-87.

Kilpeläinen, T. & Rastas, J. 1992. Vammalan Stormin Ni-malmin ympäristön metamorfisista ja rakennegeologisista tutkimuksista. Turun yliopisto, geologian ja mineralogian osaston julkaisuja 30, 18 p. (in Finnish)

Kilpeläinen, T., Korikovsky, S., Korsman, K. & Nironen, M. 1994. Tectono-metamorphic evolution in the Tampere-Vammala area. In: Pajunen, M. (ed.) High temperature-low pressure metamorphism and deep crustal structures. Meeting of IGCP project 304 "Deep Crustal Processes" in Finland, September 16-20, 1994. Geological Survey of Finland, Guide 37, 27-34.

Kohonen, J. 1995. From continental drifting to collisional crustal shortening - Paleoproterozoic Kaleva metasediments of the Höytiäinen area in North Karelia, Finland. Geological Survey of Finland, Bulletin 380. 79 p.

Koistinen, T.J. 1981. Structural evolution of an Early Proterozoic strata-bound Cu-Co-Zn deposit, Outokumpu, Finland. Transactions of Royal Society Edinburgh, Earth Science 72, 115-158.

Koistinen, T. (ed.) 1994. Precambrian basement of the Gulf of Finland and surrounding area, 1:1 mill. Geological Survey of Finland, Espoo.

Koistinen, T., Klein, V., Koppelmaa, H., Korsman, K., Lahtinen, R., Nironen, M., Puura, V., Saltykova, T., Tikhomirov, S. & Yanovskiy, A. 1996. Paleoproterozoic Svecofennian orogenic belt in the surroundings of the Gulf of Finland. In: Koistinen, T., 1996. (ed.) Explanation to the Map of Precambrian Basement of the Gulf of Finland and Surrounding area 1 : 1 mill. Geological Sur-

vey of Finland, Special Paper 21, 21-57.

Korja, A. 1995. Structure of the Svecofennian crust-growth and destruction of the Svecofennian orogen. Institute of Seismology, University of Helsinki, Report S-31. 36 p.

Korja, A. & Heikkinen, P. 1995. Proterozoic extensional tectonics of the central Fennoscandian Shield: results from the Baltic and Bothnian echoes from the Litosphere experiment. Tectonics 14 (2), 504-517.

Korja, T., Luosto, U., Korsman, K. & Pajunen, M. 1994. Geophysical and metamorphic features of Palaeoproterozoic Svecofennian orogeny and Palaeoproterozoic overprinting on Archaean crust. In: Pajunen, M. (ed.) High temperature-low pressure metamorphism and deep crustal structures. Meeting of IGCP project 304 "Deep Crustal Processes" in Finland, September 16-20, 1994. Geological Survey of Finland, Guide 37, 11-20.

Korsman, K. 1977. Progressive metamorphism of the metapelites in the Rantasalmi-Sulkava area, southeastern Finland. Geological Survey of Finland, Bulletin 290. 82 p.

Korsman, K., Hölttä, P., Hautala, T. & Wasenius, P. 1984. Metamorphism as an indicator of evolution and structure of the crust in eastern Finland. Geological Survey of Finland, Bulletin 328. 40 p.

Korsman, K., Niemelä, R. & Wasenius, P. 1988. Multistage evolution of the Proterozoic crust in the Savo schist belt, eastern Finland. In: Korsman, K. (ed.) Tectono-metamorphic evolution of the Raahe-Ladoga zone. Geological Survey of Finland, Bulletin 343, 89-96.

Korsman, K., Koistinen, T., Kohonen, J., Wennerström, M., Ekdahl, E., Honkamo, M., Idman, H. & Pekkala, Y. (eds.) 1997. Suomen kallioperäkartta - Berggrundskarta över Finland - Bedrock map of Finland 1 : 1 000 000. Geological Survey of Finland, Espoo, Finland.

Korsman, K., Korja, T., Pajunen, M., Virransalo, P. and the GGT/SVEKA Working Group. The GGT/SVEKA Transect - Structure and evolution of the continental crust in the Palaeoproterozoic Svecofennian orogen in Finland (Precambrian Research, in press).

Kousa, J., Marttila, E. & Vaasjoki, M. 1994. Petrology, geochemistry and dating of Paleoproterozoic metavolcanic rocks in the Pyhäjärvi area, central Finland. In: Nironen, M & Kähkönen, Y. (eds.) Geochemistry of Proterozoic Supracrustal Rocks in Finland. Geological Survey of Finland, Special Paper 19, 7-27.

Kouvo, O. & Tilton, G.R. 1966. Mineral ages from the Finnish Precambrian. The Journal of Geology 74, 421-442.

Kujala, H. 1993. Vammalan Stormin ultramafisen intruusion ja siihen liittyvän Ni-Cu-malmin muuttumisilmiöistä. Unpublished M.Sc. thesis, University of Turku, 104 p. (in Finnish)

Lahtinen, R. 1994. Crustal evolution of the Svecofennian and Karelian domains during 2.1-1.79 Ga, with special emphasis on the geochemistry and origin of 1.93-1.91 Ga gneissic tonalites and associated supracrustal rocks in the Rautalampi area, central Finland. Geological Survey of Finland, Bulletin 378. 128 p.

Lahtinen, R. 1996. Geochemistry of Palaeoproterozoic supracrustal and plutonic rocks in the Tampere-Hämeenlinna area, southern Finland. Geological Survey of Finland, Bulletin 389. 113 p.

Lahtinen, R. & Huhma, H. 1997. Isotopic and geochemical constraints on the evolution of the 1.93-1.79 Ga Svecofennian crust and mantle in Finland. Precambrian Research 82, 13-34.

Leveinen, J. 1994. Sedimentary petrology of the Mauri metasandstone and adjacent supracrustal rocks of the early Proterozoic Tampere Schist Belt, southern Finland. Geological Survey of Finland, unpublished report. 22 p.

Ludvig, K.R. 1988. ISOPLOT - A plotting regression program for radiogenic isotope data for IBM-PC-compatible computers. U.S. Geological Survey Open File Report 88-557. 32 p.

Luosto, U. 1991. Moho depth map of the Fennoscandian Shield based on seismic refraction data. In: Korhonen, H. & Lipponen, A. (eds.) Structure and Dynamics of the Fennoscandian Lithosphere. Proceedings of the Second Workshop on Investigation of the Lithosphere in the Fennoscandian Shield by Seismological Methods, Helsinki, May 14-18, 1990. University of Helsinki, Institute of Seismology. Report S-25, 43-49.

Mäkelä, K. 1980. Geochemistry and origin of Haveri and Kiipu, Proterozoic stratabound volcanogenic gold-copper and zinc mineralizations from southwestern Finland. Geological Survey of Finland, Bulletin 310, 1-79.

Mäkinen, E. 1914. Ytterligare om kontakten vid Naarajärvi i Lavia. Geologiska Föreningens i Stockholm Förhandlingar 36, 185-203.

Mäkinen, E. 1915. Ein archäisches Konglomeratvorkommen bei Lavia in Finnland. Geologiska Föreningens i Stockholm Förhandlingar 37, 385-421.

Malavieille, J. 1993. Late orogenic extension in mountain belts: insight from the Basin and Range and the late Paleozoic Variscan belt. Tectonics 12, 1115-1130.

Malavieille, J., Guihot, P., Costa, S., Lardeaux, J.M. & Gardien, V. 1990. Collapse of the thickened Variscan crust in the French Massif Central: Mont Pilat extensional shear zone and St Etienne

Late Carboniferous basin. Tectonophysics 177, 139-149.

Maluski, H., Costa, S. & Echtler, H. 1991. Late Variscan tectonic evolution by thinning of earlier thickened crust: An ^{40}Ar-^{39}Ar study of the Montagne Noire, southern Massif Central, France. Lithos 26, 287-304.

Mancini, F. 1996. A petrographic, mineralogical and geochemical study of the regional metamorphic Svecofennian Sääksjärvi and Stormi ultramafic-mafic intrusions, southwest Finland: implications for petrogenesis. Turun yliopiston julkaisuja, sarja A II (89). 321 p.

Mancini, F., Marshall, B. & Papunen, H. 1996a. Petrogenetic and tectonic interpretations of ultramafic bodies in the Vammala Nickel belt, southwest Finland, from the study of the Sääksjärvi ultramafic-mafic complex. International Geology Review 38, 268-283.

Mancini, F., Marshall, B. & Papunen, H. 1996b. Petrography and metamorphism of the Sääksjärvi ultramafic body, southwest Finland. Mineralogy and Petrology 56, 185-208.

Marshall, B., Smith, J.V. & Mancini, F. 1995. Emplacement and implications of peridotite-hosted leucocratic dykes, Vammala Mine, Finland. Geologiska Föreningen i Stockholm Förhandlingar 117, 199-205.

Matisto, A. 1961. Tampere. Geological map of Finland 1 : 100 000, Pre-Quaternary rocks, Sheet 2123. Geological Survey of Finland.

Matisto, A. 1967. Vammala. Geological map of Finland 1 : 100 000, Pre-Quaternary rocks, Sheet 2121. Geological Survey of Finland.

Matisto, A. 1968. Die Meta-Arkose von Mauri bei Tampere. Bulletin de la Commission géologique Finlande 235. 21 p.

Matisto, A. 1971. Vammala. Kallioperäkartan selitys. Summary: Explanation to the map of rocks. Geological map of Finland 1 : 100 000, Explanation to the Maps of Pre-Quaternary Rocks, Sheet 2121. Geological Survey of Finland. 44 p.

Matisto, A. 1973. Toijala. Geological map of Finland 1 : 100 000, Pre-Quaternary rocks, Sheet 2114. Geological Survey of Finland.

Matisto, A. 1976a. Toijalan kartta-alueen kallioperä. Summary: Precambrian rocks of the Toijala map-sheet area. Geological map of Finland 1 : 100 000, Explanation to the map of Pre-Quaternary Rocks, Sheet 2114. Geological Survey of Finland. 26 p.

Matisto, A. 1976b. Huittinen. Geological map of Finland 1 : 100 000, Pre-Quaternary rocks, Sheet 2112. Geological Survey of Finland.

Matisto, A. 1977. Tampereen kartta-alueen kallioperä. Summary: Precambrian rocks of the Tampere map-sheet area. Geological map of Finland 1 : 100 000, Explanation to the Maps of Pre-Quaternary Rocks, Sheet 2123. Geological Survey of Finland. 50 p.

Matisto, A. 1978. Huittisten kartta-alueen kallioperä. Summary: Precambrian rocks of the Huittinen map-sheet area. Geological map of Finland 1 : 100 000, Explanation to the map of Pre-Quaternary Rocks, Sheet 2112. Geological Survey of Finland. 30 p.

Matte, Ph. 1969. Le problème du passage de la schistosité horizontale à la schistosité verticale dans le dôme Garonne (Paléozoïque des Pyrénées centrales). Comptes Rendus Hedomadaires des Seances de l´Academie des Sciences, Serie D: Sciences Naturelles 268, 1841-1844.

Matte, P. & Xu Zhi, Q. 1988. Décollements in slate belts, examples from the European variscides and Qin Ling Belt of Central China. Geologische Rundschau 77, 227-238.

Miyashiro, A. 1987. Metamorphism and metamorphic belts. London: Allen & Unwin. 492 p.

Murphy, D.C. 1987. Suprastructure/infrastructure transition, east-central Cariboo Mountains, British Columbia: geometry, kinematics and tectonic implications. Journal of Structural Geology 9, 13-29.

Nironen, M. 1989a. The Tampere Schist Belt: Structural style within an Early Proterozoic volcanic arc system in Southwestern Finland. Precambrian Research 43, 23-40.

Nironen, M. 1989b. Emplacement and structural setting of granitoids in the Early Proterozoic Tampere and Savo Schist Belts, Finland - implications for contrasting crustal evolution. Geological Survey of Finland, Bulletin 346. 83 p.

Nironen, M. & Front, K. 1992. The 1.88 Ga old Mäntylä complex central Finland: emplacement and deformation of mafic to felsic plutonic rocks and associated Mo mineralization. Bulletin of the Geological Society of Finland 64, 75-90.

Nironen, M. 1997. The Svecofennian orogen: a tectonic model. Precambrian Research 86, 21-44.

Nurmi, P. & Haapala, I. 1986. The Proterozoic granitoids of Finland: Granite types, metallogeny and relation to crustal evolution. Bulletin of the Geological Society of Finland 58, 203-233.

Oele, J.A. 1966. The structural history of the Vall Ferrera Area, the Aston Massif and the Salat-Pallaresa anticlinorium (Central Pyrenees, France, Spain). Leidse Geologische Mededelingen 38, 129-164.

Ojakangas, R.W. 1986. An Early Proterozoic metagraywacke-slate turbidite sequence: the Tampere schist belt, southwestern Finland. Bulletin of the Geological Society of Finland 58, 241-261.

Papunen, H. 1980. The Kylmäkoski nickel-copper deposit in southwestern Finland. Bulletin of the Geological Society of Finland 52, 129-145.

Parras, K. 1958. On the charnockites in the light of a highly metamorphic rock complex in SW Finland. Bulletin de la Commission geologique Finlande 181. 137 p.

Patchett, P.J. & Kouvo, O. 1986. Origin of continental crust of 1.9-1.7 Ga age: Nd isotopes and U-Pb ages in the Svecokarelian Terrain of South Finland. Contributions to Mineralogy and Petrology 92, 1-12.

Paterson, S.R. & Tobisch, O.T. 1992. Rates of processes in magmatic arcs: implications for the timing and nature of pluton emplacement and wall rock deformation. Journal of Structural Geology 14 (3), 291-300.

Peltonen, P. 1992. Alustavia havaintoja Herttualan kerrosjuonen (Hämeenkyrö) petrologiasta ja malmiutumisesta.Geological Survey of Finland, Report K/31.4/2122/92/1. (in Finnish) 18 p.

Peltonen, P. 1995a. Petrogenesis of ultramafic rocks in the Vammala Nickel Belt: Implications for crustal evolution of the early Proterozoic Svecofennian arc terrane. Lithos 34, 253-274.

Peltonen, P. 1995b. Magma-country rock interaction and the genesis of Ni-Cu deposits in the Vammala Nickel Belt, SW Finland. Mineralogy and Petrology 52, 1-24.

Perchuk, L.L. & Lavrenteva, I.V. 1983. Experimental investigation of exchange equilibria in the system cordierite-garnet-biotite. In: Saxena, S.K. (ed.) Kinetics and Equilibrium in Mineral Reactions, Advances in Physical Geochemistry 3. New York: Springer Verlag, 199-239..

Perttula, J.P. 1982. Suodenniemen geologiasta. Unpublished M.Sc. Thesis, Univ. Turku, 78 p. (in Finnish)

Pflug, R. & Harbaugh, J.W. 1992. Computer graphics in geology. Three-dimensional computer graphics in modeling geologic structures and simulating geologic processes. Lecture Notes in Earth Sciences 41. Berlin: Springer Verlag. 298 p.

Pietikäinen, K. 1994. The geology of the Paleoproterozoic Pori Shear Zone, Southwestern Finland, with special reference to the evolution of veined gneisses from tonalitic protoliths. Unpublished Ph.D. thesis, Michigan Technological University. 130 p.

Platt, J.P. & England, P.C. 1993. Convective removal of lithosphere beneath mountain belts: thermal and mechanical consequences. American Journal of Science 293, 307-336.

Powell, C. Mc. A. 1979. A morphological classification of rock cleavage. Tectonophysics 58, 21-34.

Rämö, T., Haapala, I. & Salonsaari, P. 1994. Rapakivi granite magmatism: implications for lithospheric evolution. In: Pajunen, M. (ed.) High temperature-low pressure metamorphism and deep crustal structures. Meeting of IGCP project 304 "Deep Crustal Processes" in Finland, September 16-20, 1994. Geological Survey of Finland, Guide 37, 61-68.

Rämö, T. & Nironen, M. 1996. Petrogenesis of a 1.87 Ga post-tectonic bimodal granite suite in the Central Finland Granitoid Complex: the end of an orogenic cycle. The 22nd Nordic Geological Winter meeting, Turku, Åbo. (abstract) 1 p.

Ramsay, J.G. & Huber, M.I. 1989. The techniques of modern structural geology. London: Academic Press. 700 p.

Ratschbacher, L., Frisch, W., Neubauer, F., Schmid, S.M. & Neugebauer, J. 1989. Extension in compressional orogenic belts: The eastern Alps. Geology 17, 404-407.

Sanderson, D.J. 1979. The transition from upright to recumbent folding in the Variscan fold belt of southwest England: a model based on the kinematics of simple shear. Journal of Structural Geology 1, 171-180.

Schreurs, J. 1984. The amphibolite-granulite facies transition in West Uusimaa, S.W. Finland. A fluid inclusion study. Journal of Metamorphic Geology 2, 327-341.

Schreurs, J. & Westra, L. 1985. Cordierite-orthopyroxene rocks: the granulite facies equivalents of the Orijärvi cordierite-antophyllite rocks in West Uusimaa, southwest Finland. Lithos 18, 215-228.

Schreurs, J. & Westra, L. 1986. The termotectonic evolution of a Proterozoic, low pressure, granulite dome, West Uusimaa, SW Finland. Contributions to Mineralogy and Petrology 93, 236-250.

Sederholm, J.J. 1897. Über eine archäische Sedimentformation im Südwestlichen Finnland und ihre Bedeutung für die Erklärung der Entstehungsweise des Grundgebirges. Bulletin de la Commission géologique Finlande 6. 254 p.

Sederholm, J.J. 1913. Tampere. General Geological Map of Finland 1:400 000. Explanation to the Map of Rocks, Sheet B2. Commission géologique de Finlande. 122 p. (in Finnish)

Sederholm, J.J. 1931. On the sub-Bothnian unconformity and on Archaean rocks formed by secular weathering. Bulletin de la Commission géologique Finlande 95. 81 p.

Sederholm, J.J. 1932. On the geology of Fennoscandia with special references to the Pre-Cambrian. Bulletin de la Commission géologique Finlande 98. 30 p.

Sederholm, J.J. 1934. On migmatites and associat-

ed pre-Cambrian rocks of southwestern Finland III. The Åland islands. Bulletin de la Commission géologique Finlande 107. 68 p.

Seitsaari, J. 1951. The schist belt northeast of Tampere in Finland. Bulletin de la Commission géologique Finlande 153. 120 p.

Seguret, M. & Proust, F. 1968a. Contribution à l'étude des tectoniques superposées dans la chaïne hercynienne: l'allure anticlinale de la schistosité à l'Ques du massif de l'Aston (Pyrénées centrales) n'est pas originelle mais due à un replissement. Comptes Rendus Hedomadaires des Seances de l´Academie des Sciences, Serie D: Sciences Naturelles 266, 317-320.

Seguret, M. & Proust, F. 1968b. Tectonique hercynienne des Pyrénées centrales: signification des schistosités redressées, chronologie des déformations. Comptes Rendus Hedomadaires des Seances de l´Academie des Sciences, Serie D: Sciences Naturelles 266, 984-987.

Simonen, A. 1948. New evidence of the origin of Pre-Cambrian carbon. Geological Society of America, Bulletin 59, 389-416.

Simonen, A. 1952. Viljakkala-Teisko. Kallioperäkartan selitys. Summary: Explanation to the map of rocks. Geological map of Finland 1 : 100 000, Explanation to the Maps of Pre-Quaternary Rocks, Sheet 2124. Geological Survey of Finland. 74 p.

Simonen, A. 1953a. Viljakkala-Teisko. Geological Map of Finland 1 : 100 000, Pre-Quaternary Rocks, Sheet 2124. Geological Survey of Finland.

Simonen, A. 1953b. Stratigraphy and sedimentation of the Svecofennidic, early Archean supracrustal rocks in southwestern Finland. Bulletin de la Commission géologique Finlande 160, 64 p.

Simonen, A. 1971. Das finnische grundgebirge. Geologische Rundschau 60 (4), 1406-1421.

Simonen, A. 1980. The Precambrian of Finland. Geological Survey of Finland, Bulletin 304. 58 p.

De Sitter, L.U. & Zwart, H.J. 1960. Tectonic development in supra and infra-structures of a mountain chain. Proceeding 21st, International Congress Copenhagen 18, 248-256.

Soula, J.C., Debat, P., Déramond, J. & Pouget, P. 1986. A dynamic model of the structural evolution of the Hercynian Pyrenees. Tectonophysics 129, 29-51.

Stel, H., Veenhof, R., Huizenga, J.M., Timmerman, M. & Hartsink, J. M. H. 1989. Infra-supra structure relations of a microcline-granite dome in the Somero area, Svecofennides, SW Finland. Geological Survey of Finland, Bulletin 61 (2), 131-134.

Suominen, V. 1991. The chronostratigraphy of southwestern Finland, with special reference to Postjotnian and Subjotnian diabases. Geological Survey of Finland, Bulletin 356. 100 p.

Tapponnier, P. & Molnar, P. 1976. Slip-line field theory and large scale continental tectonics. Nature 264, 319-324.

Tiainen, M. & Viita, H. 1994. Determination of ore potential areas in the Häme belt, southwestern Finland, by integration of geological, geophysical and till geochemical data. Geological Survey of Finland, Report of Investigation 125. 49 p.

Törnroos, R. 1982. Sphalerite geobarometry of some metamorphosed sulphide ore deposits in Finland. Geological Survey of Finland, Bulletin 323. 42 p.

Vaasjoki, M. 1977. Rapakivi granites and other postorogenic rocks in Finland: their age and the lead isotopic composition of certain associated galena mineralizations. Geological Survey of Finland, Bulletin 294. 71 p.

Vaasjoki, M. & Huhma, H. 1987. Lead isotopic results from metabasalts of the Haveri formation, southern Finland: an indication of early Proterozoic mantle derivation. Terra Cognita 7, 159.

Vaasjoki, M. & Sakko, M. 1988. The evolution of the Raahe-Ladoga zone in Finland: isotopic constraints. In: Korsman, K. (ed.), Tectonometamorphic evolution of the Raahe-Ladoga zone. Geological Survey of Finland, Bulletin 343, 7-32.

Vaasjoki, M., Huhma, H. & Karhu, J. 1994. Evolution of the continental crust in Finland with special reference to the Svecokarelian orogeny. Geological Survey of Finland, Guide 37, 21-26.

Vaasjoki, M., Pietikäinen, K. & Vaarma, M. 1996. U-Pb zircon determinations from the Keikyä breccia and other cites in the Svecofennides: indications of a Svecokarelian protocrust. Bulletin of the Geological Society of Finland 68 (1), 3-10.

Vaasjoki, M., Rämö, T. & Sakko, M. 1991. New U-Pb ages from the Wiborg rapakivi area: constraints on the temporal evolution of the rapakivi granite-anorthosite-diabase dyke association of southeastern Finland. Precambrian Research 51, 227-243.

Väisänen, M., Hölttä, P., Rastas, J., Korja, A. & Heikkinen, P. 1994. Deformation, metamorphism and the deep structure of the crust in the Turku area, southwestern Finland. Geological Survey of Finland, Guide 37, 35-41.

Vernon, R.H. 1977. Relations between microstructures and metamorphic assemblages. Tectonophysics 39, 439-452.

Vernon, R.H. 1978. Porphyroblast-matrix microstructural relationships in deformed metamorphic rocks. Geologische Rundschau 67, 288-304.

Virransalo, P. & Vaarma, M. 1993. Ikaalinen. Geological Map of Finland 1 : 100 000, Pre-Qua-

ternary Rocks, Sheet 2122. Geological Survey of Finland.

Vissers, R.L.M. 1992. Variscan extension in the Pyrenees. Tectonics 11, 1369-1384.

Wahl, W. 1936. The granites of the Finnish part of the Svecofennian Archaean mountain chain. Bulletin de la Commission géologique Finlande 115, 489-505.

Ward, P. 1987. Early Proterozoic deposition and deformation at the Karelian craton margin in southeastern Finland. In: Gaál, G. & Gorbatschev, R. (eds.) Precambrian geology and evolution of the central Baltic Shield: 1st Symposium on the Baltic Shield. Precambrian Research, 35, 71-93.

Wegmann, C.E. 1935. Zur Deutung der Migmatite. Geologische Rundschau 26, 305-350.

Welin, E. 1987. The depositional evolution of the Svecofennian supracrustal sequence in Finland and Sweden. Precambrian Research 35, 95-113.

Wernicke, B. 1992. Cenozoic extensional tectonics of the U.S. Cordillera. In: Burchfiel et. al. (eds.) The geology of North America, G3, The Cordilleran Orogen: Coterminous United States G-3. Geological Society of America, 553-581.

Williams, F.F. & Schoneweld, Chr. 1981. Garnet rotation and the development of axial plane crenulation cleavage. Tectonophysics 78, 307-334.

Zwart, H.J. 1963a. The structural evolution of the Paleozoic of the Pyrenees. Geologische Rundschau 53, 170-205.

Zwart, H.J. 1963b. Metamorphic history of the Central Pyrenees, Part II. Valle de Aran, sheet 4. Leidse Geologische Mededelingen 28, 321-376.

Zwart, H.J. 1986. The Variscan geology of the Pyrenees. Tectonophysics 129, 9-27.

Appendix 1/ 1. Microprobe analyses of garnets in the Stormi subarea.

SAMPLE	1A-TTK-91	1B-TTK-91	1C-TTK-91	1D-TTK-91	2A-TTK-91	2B-TTK-91	2C-TTK-91	2D-TTK-91	3A-TTK-91	3B-TTK-91	3C-TTK-91	3D-TTK-91	3E-TTK-91	3F-TTK-91	10A-TTK-91	10B-TTK-91
X-COORD	2453900	2453900	2453900	2453900	2455000	2455000	2455000	2455000	2454900	2454900	2454900	2454900	2454900	2454900	2451000	2451000
Y-COORD	6802600	6802600	6802600	6802600	6804500	6804500	6804500	6804500	6803300	6803300	6803300	6803300	6803300	6803300	6801400	6801400
SiO_2	34,51	35,59	36,04	37,11	37,46	37,30	37,18	36,90	37,91	37,92	37,56	37,17	37,22	38,02	37,28	36,94
TiO_2	0,06	0,13	0,00	0,04	0,94	0,26	0,00	0,03	0,00	0,00	0,00	0,10	0,05	0,00	0,15	0,17
Al_2O_3	19,07	19,80	19,89	19,90	20,34	19,56	19,74	19,54	20,15	20,55	19,78	20,11	19,65	20,63	20,34	20,04
FeO(tot.)	28,51	29,25	33,67	34,69	32,88	30,70	33,18	31,84	33,12	32,55	33,71	34,23	33,47	34,62	35,24	34,79
MnO	9,14	9,65	3,29	3,07	1,41	1,25	2,54	2,26	1,31	1,52	1,96	1,56	1,47	2,25	4,02	3,83
MgO	1,70	1,55	2,47	2,75	1,37	1,20	0,70	0,43	2,71	3,51	2,15	2,34	2,24	2,00	2,17	2,39
CaO	1,10	1,33	1,61	1,69	6,50	6,96	6,39	6,20	4,34	4,35	3,97	4,53	4,40	3,55	1,70	1,56
Na_2O	0,00	0,00	0,00	0,00	0,00	0,00	0,00	0,00	0,00	0,00	0,00	0,00	0,00	0,00	0,00	0,00
K_2O	0,03	0,00	0,00	0,04	0,10	0,01	0,04	0,04	0,10	0,08	0,00	0,00	0,13	0,08	0,04	0,04
Total	94,26	97,44	96,96	99,46	101,00	97,24	99,82	97,33	99,92	100,47	99,19	100,09	98,69	101,15	101,00	99,75

SAMPLE	10C-TTK-91	10D-TTK-91	11A-TTK-91	11B-TTK-91	11C-TTK-91	11D-TTK-91	12A-TTK-91	12B-TTK-91	12C-TTK-91	12D-TTK-91	12E-TTK-91	12F-TTK-91	16A-TTK-91	16B-TTK-91	16C-TTK-91	16D-TTK-91
X-COORD	2451000	2451000	2450300	2450300	2450300	2450300	2448300	2448300	2448300	2448300	2448300	2448300	2451700	2451700	2451700	2451700
Y-COORD	6801400	6801400	6801200	6801200	6801200	6801200	6800800	6800800	6800800	6800800	6800800	6800800	6804200	6804200	6804200	6804200
SiO_2	39,00	35,44	38,40	38,38	37,50	37,13	38,77	37,77	37,40	38,16	37,66	37,02	34,87	35,39	37,09	36,80
TiO_2	0,00	0,10	0,07	0,26	0,10	0,00	0,00	0,00	0,00	0,00	0,02	0,00	0,05	0,00	0,00	0,07
Al_2O_3	22,24	19,18	20,64	21,45	20,31	20,36	20,52	20,49	20,13	20,84	20,18	20,35	19,04	19,13	19,84	19,60
FeO(tot.)	37,97	34,33	36,58	36,35	35,13	34,32	35,89	35,17	36,08	35,15	34,33	36,49	31,81	32,27	32,09	34,74
MnO	3,89	3,53	2,05	2,06	2,23	1,77	1,90	1,54	1,88	1,89	1,58	1,87	1,06	0,79	0,95	1,09
MgO	2,64	2,30	4,19	3,81	3,35	3,79	2,60	2,75	3,07	3,63	2,92	2,46	1,54	1,55	2,28	1,68
CaO	1,75	1,61	1,56	1,56	1,71	1,98	3,05	2,90	1,24	3,06	2,90	1,35	4,93	5,43	6,38	4,65
Na_2O	0,00	0,00	0,00	0,00	0,00	0,10	0,00	0,00	0,00	0,00	0,00	0,00	0,00	0,00	0,00	0,00
K_2O	0,00	0,00	0,00	0,13	0,07	0,07	0,05	0,00	0,00	0,01	0,05	0,05	0,00	0,02	0,09	0,00
Total	107,62	96,52	103,54	103,99	100,69	99,51	103,07	100,76	99,96	102,74	99,70	99,72	93,47	94,62	98,75	98,74

SAMPLE	17A-TTK-91	17B-TTK-91	17C-TTK-91	17D-TTK-91	18A-TTK-91	18B-TTK-91	18C-TTK-91	18D-TTK-91	19A-TTK-91	19B-TTK-91	19C-TTK-91	19D-TTK-91	20A-TTK-91	20B-TTK-91	20C-TTK-91	20D-TTK-91
X-COORD	2451200	2451200	2451200	2451200	2448700	2448700	2448700	2448700	2448900	2448900	2448900	2448900	2449000	2449000	2449000	2449000
Y-COORD	6804200	6804200	6804200	6804200	6804200	6804200	6804200	6804200	6804900	6804900	6804900	6804900	6802000	6802000	6802000	6802000
SiO_2	35,68	34,82	35,38	35,39	34,51	34,02	34,68	34,46	39,26	36,90	37,68	36,32	36,73	36,63	36,98	36,77
TiO_2	0,03	0,00	0,19	0,12	0,00	0,00	0,00	0,00	0,04	0,00	0,14	0,00	0,04	0,00	0,19	0,06
Al_2O_3	19,15	18,83	18,26	19,16	18,31	18,27	19,07	18,55	20,81	19,85	20,66	19,91	21,34	20,78	19,58	19,27
FeO(tot.)	30,27	30,39	30,12	30,01	30,99	30,11	31,14	31,37	29,62	28,19	28,82	28,21	33,44	32,11	32,53	32,40
MnO	1,73	2,21	1,87	1,89	4,79	4,93	4,56	4,79	10,89	10,71	11,27	10,59	2,49	2,50	2,33	2,74
MgO	0,84	0,75	1,01	1,37	1,72	1,72	2,16	2,09	0,80	0,63	1,35	1,28	2,85	2,76	2,83	2,73
CaO	7,62	7,45	7,79	7,08	1,50	1,43	1,25	1,34	2,47	2,46	2,58	2,48	2,33	2,25	2,41	2,14
Na_2O	0,00	0,00	0,00	0,00	0,00	0,00	0,00	0,00	0,00	0,00	0,00	0,00	0,00	0,00	0,00	0,00
K_2O	0,00	0,08	0,00	0,10	0,00	0,00	0,00	0,00	0,07	0,03	0,04	0,04	0,01	0,10	0,03	0,00
Total	95,32	94,66	94,72	95,32	91,82	90,47	92,87	92,61	104,07	98,85	102,59	98,82	99,40	97,15	96,94	96,13

SAMPLE	21A-TTK-91	21B-TTK-91	21C-TTK-91	21D-TTK-91	27A-TTK-91	27B-TTK-91	27C-TTK-91	27D-TTK-91	28A-TTK-91	28B-TTK-91	28C-TTK-91	28D-TTK-91	29A-TTK-91	29B-TTK-91	29C-TTK-91	29D-TTK-91
X-COORD	2446500	2446500	2446500	2446500	2452800	2452800	2452800	2452800	2453000	2453000	2453000	2453000	2451200	2451200	2451200	2451200
Y-COORD	6800700	6800700	6800700	6800700	6801400	6801400	6801400	6801400	6800100	6800100	6800100	6800100	6802300	6802300	6802300	6802300
SiO_2	35,12	35,00	35,48	35,86	36,43	36,87	37,14	36,93	37,40	38,13	37,51	38,03	38,65	38,00	35,27	37,56
TiO_2	0,04	0,00	0,00	0,04	0,00	0,04	0,04	0,05	0,00	0,10	0,08	0,00	0,00	0,11	0,04	0,02
Al_2O_3	19,10	19,00	19,60	19,80	20,07	19,45	20,71	20,05	20,27	20,55	21,33	21,27	20,92	20,39	19,16	20,22
FeO(tot.)	34,36	34,92	34,78	35,10	26,46	26,48	26,30	25,96	35,49	35,21	35,14	34,48	35,56	34,58	32,73	35,00
MnO	2,04	1,97	1,41	1,27	7,58	8,33	8,50	9,28	2,30	2,57	3,37	3,49	3,35	3,14	2,99	2,94
MgO	2,32	2,50	2,94	2,78	1,24	0,89	2,33	1,62	3,12	3,09	3,00	4,00	2,46	2,59	2,80	2,66
CaO	1,00	1,08	1,10	1,03	5,79	6,29	6,21	5,56	1,35	1,40	1,34	1,57	1,05	1,20	1,21	1,32
Na_2O	0,00	0,00	0,00	0,00	0,00	0,00	0,38	0,00	0,71	0,00	0,00	0,06	0,00	0,00	0,00	0,00
K_2O	0,00	0,00	0,01	0,00	0,00	0,03	0,02	0,01	0,02	0,05	0,00	0,00	0,02	0,00	0,01	0,06
Total	94,00	94,49	95,37	96,14	97,85	98,40	101,63	99,59	100,70	101,25	101,87	103,06	102,07	100,05	94,28	99,99

Appendix 1/ 2. Microprobe analyses of garnets in the Stormi subarea.

SAMPLE	40A-TTK-91	40B-TTK-91	40C-TTK-91	40D-TTK-91	41A-TTK-91	41B-TTK-91	41C-TTK-91	41D-TTK-91	41E-TTK-91	41F-TTK-91	1A-JTR-91	1B-JTR-91	1C-JTR-91	1D-JTR-91	3A-JTR-91	3B-JTR-91
X-COORD	2447300	2447300	2447300	2447300	2447600	2447600	2447600	2447600	2447600	2447600	2454650	2454650	2454650	2454650	2451200	2451200
Y-COORD	6804600	6804600	6804600	6804600	6803500	6803500	6803500	6803500	6803500	6803500	6795550	6795550	6795550	6795550	6797250	6797250
SiO_2	37,06	37,61	37,54	36,40	36,52	35,45	35,59	37,52	38,22	37,39	34,13	35,34	38,61	35,82	38,01	37,76
TiO_2	0,14	0,00	0,00	0,00	0,01	0,04	0,06	0,01	0,00	0,07	0,00	0,00	0,15	0,13	0,00	0,00
Al_2O_3	20,54	20,59	20,29	19,82	20,69	20,21	20,13	20,41	21,37	20,34	18,64	19,53	21,42	20,47	20,80	20,28
FeO(tot.)	30,06	29,96	31,68	30,74	27,23	27,33	26,69	25,87	26,30	26,43	31,91	33,47	35,64	33,73	38,18	37,55
MnO	5,77	6,01	5,34	5,36	5,84	6,24	6,26	5,81	5,91	5,81	5,37	5,65	7,68	5,85	0,63	0,74
MgO	2,98	2,47	1,96	2,55	3,10	2,93	3,06	2,82	2,95	2,55	1,29	1,69	1,78	2,03	3,56	3,06
CaO	1,32	1,44	1,48	1,63	2,97	3,01	2,80	4,93	5,20	5,21	0,88	0,90	1,15	1,00	1,21	1,21
Na_2O	0,00	0,00	0,00	0,00	0,00	0,03	0,28	0,00	0,10	0,00	0,00	0,00	0,00	0,00	0,00	0,00
K_2O	0,08	0,14	0,03	0,04	0,12	0,02	0,00	0,05	0,16	0,00	0,00	0,00	0,05	0,00	0,03	0,01
Total	98,03	98,22	98,33	96,65	96,48	95,40	95,02	97,49	100,74	97,87	92,27	96,89	106,61	99,34	102,43	100,65

SAMPLE	3C-JTR-91	3D-JTR-91	4A-JTR-91	4B-JTR-91	4C-JTR-91	4D-JTR-91	6A-JTR-91	6B-JTR-91	6C-JTR-91	6D-JTR-91	11A-JTR-91	11B-JTR-91	11C-JTR-91	11D-JTR-91	11E-JTR-91	12A-JTR-91
X-COORD	2451200	2451200	2449100	2449100	2449100	2449100	2448700	2448700	2448700	2448700	2451300	2451300	2451300	2451300	2451300	2453100
Y-COORD	6797250	6797250	6797100	6797100	6797100	6797100	6795450	6795450	6795450	6795450	6795400	6795400	6795400	6795400	6795400	6797650
SiO_2	38,26	37,64	36,71	36,38	35,94	35,85	36,73	36,32	34,77	36,40	39,11	39,06	37,21	37,25	36,42	37,92
TiO_2	0,07	0,00	0,00	0,00	0,00	0,00	0,02	0,07	0,02	0,02	0,07	0,16	0,06	0,00	0,00	0,00
Al_2O_3	20,48	21,07	20,07	19,51	19,00	19,30	19,96	19,52	18,50	19,69	21,76	21,42	20,05	20,90	20,15	21,00
FeO(tot.)	36,40	37,91	35,17	35,19	34,26	34,75	32,93	32,56	31,36	33,28	36,05	35,03	32,71	34,32	33,84	36,56
MnO	0,87	0,67	1,31	1,04	1,19	1,15	2,96	2,72	2,74	3,09	1,90	2,13	3,28	2,22	1,99	2,65
MgO	3,69	3,24	2,83	3,02	2,50	2,72	2,72	2,98	2,17	2,03	4,48	3,82	3,08	4,53	4,31	2,61
CaO	1,20	1,13	1,38	1,11	1,87	1,43	2,48	2,53	2,25	2,47	1,39	1,38	1,80	1,50	1,40	1,27
Na_2O	0,00	0,00	0,00	0,00	0,00	0,00	0,00	0,00	0,00	0,00	0,31	0,00	0,00	0,29	0,00	0,00
K_2O	0,00	0,00	0,02	0,04	0,10	0,04	0,00	0,03	0,08	0,05	0,00	0,02	0,01	0,02	0,05	0,05
Total	101,20	101,67	97,60	96,38	94,87	95,34	97,83	96,90	92,00	97,05	105,08	103,17	98,31	101,20	98,30	102,05

SAMPLE	12B-JTR-91	12C-JTR-91	12D-JTR-91	12E-JTR-91	13A-JTR-91	13B-JTR-91	13C-JTR-91	13D-JTR-91	14A-JTR-91	14B-JTR-91	14C-JTR-91	14D-JTR-91	14E-JTR-91	16A-JTR-91	16B-JTR-91	16C-JTR-91
X-COORD	2453100	2453100	2453100	2453100	2451850	2451850	2451850	2451850	2448750	2448750	2448750	2448750	2448750	2447250	2447250	2447250
Y-COORD	6797650	6797650	6797650	6797650	6798300	6798300	6798300	6798300	6799850	6799850	6799850	6799850	6799850	6799150	6799150	6799150
SiO_2	37,38	37,91	38,52	37,69	37,77	37,34	35,20	36,85	37,85	37,02	36,39	38,18	38,14	36,97	37,49	36,33
TiO_2	0,00	0,06	0,04	0,00	0,03	0,15	0,26	0,00	0,00	0,00	0,08	0,12	0,00	0,00	0,00	0,00
Al_2O_3	20,29	20,72	20,77	20,61	20,56	20,19	20,94	20,31	21,15	20,09	20,38	20,55	20,38	19,91	20,02	19,44
FeO(tot.)	36,04	35,89	35,97	35,36	34,16	33,59	35,00	34,56	36,00	34,28	33,00	35,83	35,47	35,06	33,95	33,60
MnO	2,66	4,49	3,23	3,46	5,45	5,55	4,76	4,26	2,44	2,45	3,94	2,16	2,12	1,22	1,30	1,51
MgO	2,71	1,44	2,67	2,22	2,18	1,94	2,06	2,07	3,70	2,84	2,45	3,03	3,13	3,54	3,84	3,37
CaO	1,42	1,27	1,31	1,38	1,35	1,35	1,28	1,15	1,35	1,50	1,64	1,65	1,81	1,30	1,45	1,43
Na_2O	0,00	0,00	0,00	0,00	0,00	0,00	0,00	0,00	0,06	0,00	0,00	0,00	0,00	0,00	0,00	0,00
K_2O	0,00	0,00	0,03	0,03	0,03	0,05	0,03	0,02	0,00	0,00	0,04	0,11	0,12	0,00	0,02	0,09
Total	100,56	101,85	102,70	100,86	101,58	100,42	101,52	99,30	102,56	98,19	98,19	101,63	101,34	98,06	98,33	95,90

SAMPLE	16D-JTR-91	16E-JTR-91	17A-JTR-91	17B-JTR-91	17C-JTR-91	17D-JTR-91	18A-JTR-91	18B-JTR-91	18C-JTR-91	18D-JTR-91	18E-JTR-91	22A-JTR-91	22B-JTR-91	22C-JTR-91	22D-JTR-91	22E-JTR-91
X-COORD	2447250	2447250	2447600	2447600	2447600	2447600	2450800	2450800	2450800	2450800	2450800	2453950	2453950	2453950	2453950	2453950
Y-COORD	6799150	6799150	6798100	6798100	6798100	6798100	6798600	6798600	6798600	6798600	6798600	6798250	6798250	6798250	6798250	6798250
SiO_2	37,24	36,75	36,55	37,90	38,39	37,98	38,07	36,26	37,03	37,85	37,64	37,70	37,44	37,56	36,83	36,96
TiO_2	0,00	0,00	0,00	0,12	0,00	0,00	0,00	0,03	0,00	0,06	0,00	0,12	0,00	0,00	0,29	0,08
Al_2O_3	20,41	19,55	20,51	20,79	21,39	20,82	20,94	19,23	19,63	20,54	19,65	20,93	20,54	20,48	19,55	19,82
FeO(tot.)	35,41	34,46	32,60	34,50	32,76	32,29	34,76	31,96	33,03	33,21	33,40	37,37	37,56	36,87	36,35	36,68
MnO	0,95	1,18	1,39	1,68	1,10	1,82	4,09	3,85	3,88	6,28	6,45	2,28	2,27	1,91	1,68	3,54
MgO	3,86	3,32	3,47	3,19	4,22	3,93	3,71	2,33	2,53	2,87	2,35	2,73	2,48	3,37	2,06	1,44
CaO	1,26	1,30	1,25	1,08	1,01	0,93	1,56	1,54	1,58	1,70	1,60	1,12	1,14	1,18	1,15	1,26
Na_2O	0,00	0,00	0,24	0,00	0,65	0,00	0,00	0,00	0,00	0,00	0,00	0,00	0,00	0,00	0,00	0,12
K_2O	0,00	0,00	0,00	0,00	0,00	0,03	0,06	0,00	0,01	0,00	0,13	0,00	0,03	0,00	0,00	0,00
Total	99,24	96,61	96,10	99,44	99,79	98,11	103,29	95,43	97,95	102,59	101,20	102,47	101,62	101,38	97,91	100,07

Appendix 2/ 1. Microprobe analyses of biotites in the Stormi subarea.

SAMPLE	1E-TTK-91	1F-TTK-91	1G-TTK-91	1H-TTK-91	2E-TTK-91	2F-TTK-91	2G-TTK-91	2H-TTK-91	3G-TTK-91	3H-TTK-91	3I-TTK-91	3J-TTK-91	10E-TTK-91	10F-TTK-91	10G-TTK-91	10H-TTK-91
X-COORD	2453900	2453900	2453900	2453900	2455000	2455000	2455000	2455000	2454900	2454900	2454900	2454900	2451000	2451000	2451000	2451000
Y-COORD	6802600	6802600	6802600	6802600	6804500	6804500	6804500	6804500	6803300	6803300	6803300	6803300	6801400	6801400	6801400	6801400
SiO_2	35	35,04	35	35,43	35,51	34,89	35,11	34,56	37,55	36,83	36,38	37,14	35,43	35,30	35,13	35,18
TiO_2	2,69	2,73	2,45	2,56	2,9	2,76	2,71	2,80	2,98	2,79	3,14	2,87	3,01	2,71	3,09	2,64
Al_2O_3	17,68	17,79	18,01	17,88	15,36	15,31	15,58	15,85	15,65	14,79	14,99	15,03	15,83	15,88	15,55	15,58
FeO(tot.)	20,15	20,53	20,26	20,03	25,73	25,13	24,18	24,54	21,60	21,81	21,78	21,86	21,07	20,35	20,58	20,40
MnO	0,44	0,36	0,24	0,39	0,24	0,08	0,34	0,44	0,06	0,22	0,12	0,10	0,01	0,32	0,25	0,09
MgO	7,62	8,14	7,77	7,85	7,04	6,74	6,62	6,93	10,49	10,37	10,73	10,01	9,32	9,62	9,30	8,58
CaO	0,00	0	0,04	0	0,12	0,01	0,00	0,02	0,00	0,00	0,13	0,04	0,00	0,06	0,06	0,05
Na_2O	0,00	0,00	0,00	0,00	0,03	0,00	0,00	0,00	0,33	0,48	0,55	0,00	0,00	0,00	0,19	0,00
K_2O	10,34	10,10	10,50	10,04	9,80	9,57	9,84	9,87	9,76	9,83	9,42	9,46	10,06	10,05	9,69	9,84
Total	94,21	94,74	94,35	94,3	96,72	94,63	94,36	95,01	98,49	97,20	97,29	96,59	94,73	94,44	93,99	92,54

SAMPLE	11E-TTK-91	11F-TTK-91	11G-TTK-91	11H-TTK-91	12G-TTK-91	12H-TTK-91	12I-TTK-91	12J-TTK-91	16E-TTK-91	16F-TTK-91	16G-TTK-91	16H-TTK-91	17E-TTK-91	17F-TTK-91	17G-TTK-91	17H-TTK-91
X-COORD	2450300	2450300	2450300	2450300	2448300	2448300	2448300	2448300	2451700	2451700	2451700	2451700	2451200	2451200	2451200	2451200
Y-COORD	6801200	6801200	6801200	6801200	6800800	6800800	6800800	6800800	6804200	6804200	6804200	6804200	6804200	6804200	6804200	6804200
SiO_2	35,24	36,14	35,25	35,40	35,26	35,37	35,11	35,10	34,30	33,91	34,10	32,46	32,04	32,65	33,05	32,71
TiO_2	3,00	3,40	3,24	3,23	2,45	2,55	2,53	2,33	2,60	2,75	3,40	3,32	4,05	3,73	3,89	3,08
Al_2O_3	16,36	18,01	16,43	16,71	17,63	17,84	17,44	18,18	14,60	15,16	14,86	14,54	12,87	12,63	13,41	13,15
FeO(tot.)	17,95	19,10	17,03	17,76	18,60	18,94	19,17	19,13	23,14	23,04	23,57	21,89	25,46	26,22	25,66	26,13
MnO	0,13	0,11	0,00	0,03	0,05	0,03	0,12	0,18	0,10	0,03	0,06	0,00	0,10	0,16	0,32	0,11
MgO	9,28	11,17	10,05	9,52	10,04	9,23	9,47	9,55	7,83	7,87	7,35	6,83	4,87	5,43	5,29	5,26
CaO	0,00	0,00	0,00	0,01	0,03	0,03	0,02	0,00	0,08	0,00	0,00	0,02	0,00	0,05	0,00	0,00
Na_2O	0,00	0,00	0,00	0,00	0,00	0,00	0,17	0,00	0,00	0,02	0,00	0,00	0,00	0,00	0,11	0,00
K_2O	9,15	9,58	9,70	9,81	10,14	9,84	10,06	9,74	9,13	8,94	9,38	8,90	9,53	9,04	9,20	8,99
Total	91,28	97,71	91,77	92,65	94,47	93,87	94,21	94,25	91,97	91,75	92,80	88,00	89,13	89,97	91,04	89,70

SAMPLE	18E-TTK-91	18F-TTK-91	18G-TTK-91	18H-TTK-91	19E-TTK-91	19F-TTK-91	19G-TTK-91	19H-TTK-91	20E-TTK-91	20F-TTK-91	20G-TTK-91	20H-TTK-91	21E-TTK-91	21F-TTK-91	21G-TTK-91	21H-TTK-91
X-COORD	2448700	2448700	2448700	2448700	2448900	2448900	2448900	2448900	2449000	2449000	2449000	2449000	2446500	2446500	2446500	2446500
Y-COORD	6804200	6804200	6804200	6804200	6804900	6804900	6804900	6804900	6802000	6802000	6802000	6802000	6800700	6800700	6800700	6800700
SiO_2	32,57	32,88	32,72	31,81	34,60	34,07	35,14	34,33	34,26	33,88	33,55	33,78	33,86	33,52	32,51	32,70
TiO_2	2,23	2,26	2,58	2,74	3,06	3,03	3,14	2,89	2,54	2,50	2,70	2,22	2,94	3,15	3,04	3,21
Al_2O_3	17,21	17,07	16,82	16,78	17,72	16,58	16,86	16,19	16,75	16,54	16,50	16,06	17,33	17,38	17,46	17,11
FeO(tot.)	17,94	17,45	18,33	18,82	20,54	20,48	21,26	21,61	18,16	17,98	18,16	18,24	19,24	19,60	19,63	19,88
MnO	0,31	0,00	0,25	0,00	0,39	0,43	0,30	0,31	0,07	0,12	0,30	0,16	0,20	0,21	0,20	0,06
MgO	7,32	6,75	7,25	6,79	8,57	7,03	7,17	7,62	9,92	10,05	9,62	9,40	7,53	7,63	7,69	7,81
CaO	0,13	0,00	0,06	0,08	0,00	0,06	0,07	0,00	0,03	0,02	0,00	0,00	0,00	0,00	0,00	0,00
Na_2O	0,00	0,00	0,00	0,00	0,21	0,00	0,00	0,00	0,17	0,04	0,00	0,00	0,00	0,00	0,00	0,00
K_2O	9,36	9,50	9,25	9,01	10,06	10,09	10,07	9,99	9,95	9,94	9,60	9,67	10,04	9,94	9,84	9,81
Total	87,40	85,96	87,35	86,08	95,43	91,77	94,37	92,96	91,97	91,28	90,79	89,76	91,23	91,58	90,48	90,75

SAMPLE	27E-TTK-91	27F-TTK-91	27G-TTK-91	27H-TTK-91	28E-TTK-91	28F-TTK-91	28G-TTK-91	28H-TTK-91	29E-TTK-91	29F-TTK-91	29G-TTK-91	29H-TTK-91	40E-TTK-91	40F-TTK-91	40G-TTK-91	40H-TTK-91
X-COORD	2452800	2452800	2452800	2452800	2453000	2453000	2453000	2453000	2451200	2451200	2451200	2451200	2447300	2447300	2447300	2447300
Y-COORD	6801400	6801400	6801400	6801400	6800100	6800100	6800100	6800100	6802300	6802300	6802300	6802300	6804600	6804600	6804600	6804600
SiO_2	36,33	36,96	35,90	35,72	35,71	35,57	35,16	35,90	33,60	33,78	34,97	35,63	34,56	35,37	34,78	35,17
TiO_2	3,03	3,05	3,25	3,07	2,77	2,86	3,07	2,83	2,33	2,29	2,28	3,01	2,26	2,21	1,83	2,17
Al_2O_3	16,12	16,44	16,37	16,06	17,68	17,92	17,81	18,22	18,13	18,57	18,86	18,16	17,92	17,54	18,91	18,24
FeO(tot.)	19,87	19,62	20,47	20,12	18,22	18,31	18,07	17,36	16,91	15,80	18,40	18,89	18,46	18,49	17,70	17,90
MnO	0,33	0,34	0,42	0,35	0,00	0,22	0,01	0,19	0,06	0,16	0,00	0,22	0,33	0,16	0,13	0,27
MgO	9,80	9,54	9,71	9,31	9,38	10,24	9,73	10,65	8,27	8,09	9,59	9,14	9,38	9,19	9,85	9,83
CaO	0,11	0,03	0,00	0,00	0,00	0,01	0,00	0,00	0,01	0,15	0,09	0,00	0,00	0,01	0,10	0,00
Na_2O	0,00	0,00	0,00	0,00	0,00	0,00	0,00	0,00	0,00	0,00	0,00	0,00	0,38	0,00	0,38	0,00
K_2O	10,00	10,03	10,29	10,14	10,15	10,05	10,32	10,24	9,54	8,82	10,33	10,47	9,62	9,69	9,45	9,78
Total	95,78	96,13	96,46	94,96	94,11	95,50	94,22	95,38	88,88	88,19	94,63	95,62	92,91	92,75	93,24	93,38

Appendix 2/ 2. Microprobe analyses of biotites in the Stormi subarea.

SAMPLE	41G-TTK-91	41H-TTK-91	41I-TTK-91	41J-TTK-91	41K-TTK-91	1E-JTR-91	1F-JTR-91	1G-JTR-91	1H-JTR-91	1I-JTR-91	3E-JTR-91	3F-JTR-91	3G-JTR-91	3H-JTR-91	3I-JTR-91	4E-JTR-91
X-COORD	2447600	2447600	2447600	2447600	2447600	2454650	2454650	2454650	2454650	2454650	2451200	2451200	2451200	2451200	2451200	2449100
Y-COORD	6803500	6803500	6803500	6803500	6803500	6795550	6795550	6795550	6795550	6795550	6797250	6797250	6797250	6797250	6797250	6797100
SiO_2	36,07	36,04	38,02	38,23	37,84	34,63	33,31	35,33	35,01	35,30	34,75	35,12	34,87	35,14	36,36	34,23
TiO_2	2,94	3,13	2,98	3,75	3,59	2,24	2,01	1,68	2,02	1,84	3,58	3,54	3,39	3,25	3,26	3,23
Al_2O_3	16,50	16,76	17,89	18,70	18,72	18,32	16,60	18,43	18,15	18,86	16,78	17,62	17,43	17,23	18,31	17,11
FeO(tot.)	16,98	16,78	17,89	17,27	17,17	21,53	21,50	22,33	21,62	21,60	20,94	20,84	20,67	19,73	19,70	18,73
MnO	0,19	0,17	0,21	0,22	0,15	0,19	0,26	0,23	0,33	0,48	0,00	0,00	0,00	0,06	0,10	0,02
MgO	10,16	10,86	11,28	10,42	10,37	6,76	6,51	6,89	7,25	6,89	8,57	7,86	8,34	9,23	9,46	8,79
CaO	0,02	0,00	0,00	0,00	0,00	0,00	0,00	0,00	0,00	0,15	0,07	0,07	0,00	0,00	0,00	0,10
Na_2O	0,07	0,00	0,85	0,43	0,00	0,06	0,00	0,00	0,00	0,00	0,00	0,00	0,00	0,00	0,00	0,00
K_2O	9,79	9,85	10,02	10,34	10,37	9,85	10,34	10,15	10,25	10,31	10,21	10,37	10,10	10,17	10,21	9,70
Total	92,75	94,02	99,34	99,51	98,24	93,79	90,90	95,39	94,65	95,53	95,30	95,54	95,04	94,96	97,43	92,12

SAMPLE	4F-JTR-91	4G-JTR-91	4H-JTR-91	6E-JTR-91	6F-JTR-91	6G-JTR-91	6H-JTR-91	11F-JTR-91	11G-JTR-91	11H-JTR-91	11I-JTR-91	12F-JTR-91	12G-JTR-91	12H-JTR-91	12I-JTR-91	13E-JTR-91
X-COORD	2449100	2449100	2449100	2448700	2448700	2448700	2448700	2451300	2451300	2451300	2451300	2453100	2453100	2453100	2453100	2451850
Y-COORD	6797100	6797100	6797100	6795450	6795450	6795450	6795450	6795400	6795400	6795400	6795400	6797650	6797650	6797650	6797650	6798300
SiO_2	34,32	33,80	34,14	34,45	34,76	34,38	34,04	37,28	36,32	34,51	38,77	36,22	35,34	35,42	34,88	35,20
TiO_2	3,03	2,84	3,23	2,57	2,57	2,96	3,11	3,34	3,57	3,16	3,92	2,49	2,57	1,97	1,96	1,40
Al_2O_3	16,74	16,31	16,54	17,70	17,16	17,16	17,22	17,87	17,15	15,74	18,85	19,08	18,98	19,61	19,54	18,96
FeO(tot.)	18,58	17,96	18,15	19,09	19,14	19,25	19,37	19,36	19,29	18,61	20,08	20,11	20,23	21,26	19,71	20,03
MnO	0,20	0,02	0,14	0,30	0,11	0,14	0,15	0,27	0,13	0,05	0,09	0,08	0,11	0,06	0,14	0,24
MgO	8,82	8,61	8,68	8,89	7,86	8,46	8,84	10,90	10,35	9,23	10,49	7,72	8,35	8,19	8,21	8,00
CaO	0,00	0,00	0,00	0,01	0,00	0,00	0,03	0,00	0,00	0,01	0,00	0,00	0,01	0,00	0,00	0,14
Na_2O	0,00	0,00	0,00	0,00	0,00	0,00	0,00	0,00	0,00	0,00	0,00	0,00	0,15	0,00	0,00	0,00
K_2O	9,90	9,57	9,90	9,76	10,01	9,91	10,09	10,33	10,55	9,86	10,69	10,59	10,04	10,08	10,27	9,93
Total	91,74	89,31	90,99	92,94	91,65	92,33	92,96	99,45	97,39	91,28	103,05	96,55	95,77	96,81	94,97	93,95

SAMPLE	13F-JTR-91	13G-JTR-91	13H-JTR-91	14F-JTR-91	14G-JTR-91	14H-JTR-91	14I-JTR-91	16F-JTR-91	16G-JTR-91	16H-JTR-91	16I-JTR-91	17E-JTR-91	17F-JTR-91	17G-JTR-91	17H-JTR-91	18F-JTR-91
X-COORD	2451850	2451850	2451850	2448750	2448750	2448750	2448750	2447250	2447250	2447250	2447250	2447600	2447600	2447600	2447600	2450800
Y-COORD	6798300	6798300	6798300	6799850	6799850	6799850	6799850	6799150	6799150	6799150	6799150	6798100	6798100	6798100	6798100	6798600
SiO_2	35,00	35,35	34,28	35,27	36,41	35,99	35,70	34,80	35,10	35,46	35,72	34,43	35,39	34,64	36,38	34,61
TiO_2	1,25	2,85	2,55	2,51	2,63	2,70	2,76	3,05	2,99	3,60	3,35	3,20	2,91	3,20	3,66	2,72
Al_2O_3	19,09	18,95	18,21	17,28	17,95	17,67	16,73	16,57	17,29	17,06	17,32	17,20	17,40	17,52	18,14	17,94
FeO(tot.)	19,98	19,64	20,06	19,32	20,29	19,52	19,59	18,01	18,69	17,80	18,28	17,13	17,23	16,07	17,88	18,60
MnO	0,28	0,44	0,24	0,38	0,09	0,15	0,00	0,20	0,14	0,02	0,27	0,00	0,07	0,07	0,08	0,25
MgO	8,17	7,77	8,55	8,76	9,40	9,73	9,02	9,38	9,12	9,58	9,26	9,42	10,10	9,50	9,91	8,61
CaO	0,00	0,18	0,06	0,05	0,05	0,09	0,00	0,00	0,12	0,00	0,00	0,09	0,00	0,03	0,11	0,02
Na_2O	0,30	0,00	0,00	0,00	0,00	0,00	0,00	0,00	0,00	0,04	0,00	0,00	0,00	0,00	0,00	0,00
K_2O	10,41	10,42	9,93	10,21	10,52	10,08	10,15	9,60	9,95	9,87	10,08	9,77	10,43	9,65	10,48	9,81
Total	94,49	95,64	93,88	93,82	97,41	95,93	93,97	91,63	93,44	93,80	94,62	91,40	93,88	90,81	96,82	92,67

SAMPLE	18G-JTR-91	18H-JTR-91	18I-JTR-91	18J-JTR-91	22F-JTR-91	22G-JTR-91	22H-JTR-91
X-COORD	2450800	2450800	2450800	2450800	2453950	2453950	2453950
Y-COORD	6798600	6798600	6798600	6798600	6798250	6798250	6798250
SiO_2	35,65	34,85	34,51	34,93	34,49	34,29	35,70
TiO_2	2,59	2,85	2,39	2,30	3,76	3,63	3,59
Al_2O_3	18,31	18,20	18,80	18,03	17,84	18,35	18,55
FeO(tot.)	19,30	19,41	18,47	19,18	19,46	19,51	19,22
MnO	0,03	0,10	0,13	0,26	0,31	0,21	0,07
MgO	8,89	8,37	8,48	8,93	8,20	8,50	7,94
CaO	0,00	0,02	0,01	0,10	0,02	0,04	0,00
Na_2O	0,00	0,00	0,00	0,00	0,36	0,00	0,00
K_2O	9,76	10,38	10,07	9,87	9,99	10,21	10,51
Total	94,54	94,40	93,03	94,02	94,49	94,83	95,60

Tätä julkaisua myy

GEOLOGIAN
TUTKIMUSKESKUS (GTK)
Julkaisumyynti
PL 96
02151 Espoo
☎ 0205 50 11
Telekopio: 0205 50 12

GTK, Väli-Suomen
aluetoimisto
Kirjasto
PL 1237
70211 Kuopio
☎ 0205 50 11
Telekopio: 0205 50 13

GTK, Pohjois-Suomen
aluetoimisto
Kirjasto
PL 77
96101 Rovaniemi
☎ 0205 50 11
Telekopio: 0205 50 14

Denna publikation säljes av

GEOLOGISKA
FORSKNINGSCENTRALEN (GFC)
Publikationsförsäljning
PB 96
02151 Esbo
☎ 0205 50 11
Telefax: 0205 50 12

GFC, Distriktsbyrån för
Mellersta Finland
Biblioteket
PB 1237
70211 Kuopio
☎ 0205 50 11
Telefax: 0205 50 13

GFC, Distriktsbyrån för
Norra Finland
Biblioteket
PB 77
96101 Rovaniemi
☎ 0205 50 11
Telefax: 0205 50 14

This publication can be obtained
from
GEOLOGICAL SURVEY
OF FINLAND (GSF)
Publication sales
P.O. Box 96
FIN-02151 Espoo, Finland
☎ +358 205 50 11
Telefax: +358 205 50 12

GSF, Regional office for
Mid-Finland
Library
P.O. Box 1237
FIN-70211 Kuopio, Finland
☎ +358 205 50 11
Telefax: +358 205 50 13

GSF, Regional office for
Northern Finland
Library
P.O. Box 77
FIN-96101 Rovaniemi, Finland
☎ +358 205 50 11
Telefax: +358 205 50 14

ISBN 951-690-701-6
ISSN 0367-522X

9 789516 907010

E-mail: info@gsf.fi
WWW-address: http://www.gsf.fi